TECHNISCHE UNIVERSITÄT MÜNCHEN

Lehrstuhl für Raumfahrttechnik

Visual Augmentation Methods for Teleoperated Space Rendezvous

Dipl.-Ing. Univ. Markus Wilde

Vollständiger Abdruck der von der Fakultät für Maschinenwesen der Technischen Universität München zur Erlangung des akademischen Grades eines

Doktor-Ingenieurs (Dr.-Ing.)

genehmigten Dissertation .

Vorsitzender: Univ.-Prof. Dr.-Ing. habil. Boris Lohmann

Prüfer der Dissertation:

1. Univ.-Prof. Dr. rer. nat. Dr. h.c. Ulrich Walter
2. Univ.-Prof. Dr.-Ing. Berthold Färber

(Universität der Bundeswehr München)

Die Dissertation wurde am 27.06.2012 bei der Technischen Universität München eingereicht und durch die Fakultät für Maschinenwesen am 13.12.2012 angenommen.

ABSTRACT

Rendezvous & docking is a quintessential capability for all on-orbit servicing and space debris removal activities. Considerable research and development effort has been expended to develop automated or even autonomous rendezvous & docking systems for these applications. Nonetheless, uncooperative targets which are not equipped with docking interfaces and sensor targets, and which might be rotating or tumbling, still require the involvement of a human operator to be captured successfully.

This doctoral thesis investigates the two-pronged hypothesis that (1) a human operator is able to successfully conduct final approach and docking maneuvers of a generic, rotating target object, using a joystick, live video feedback, and a support suite consisting of a spacecraft attitude head-up display (HUD), and a trajectory prediction display; and (2) the operator's performance is increased when the chaser spacecraft is equipped with a robotic camera arm called the *ThirdEye*, providing an auxiliary, flexible vantage point, and a graphical user interface integrating the HUD, trajectory prediction and multiple camera views into an accessible and intuitive operator interface. These approach and docking maneuvers are to be conducted under the impact of time delays representative of space communication links using a single geostationary relay satellite.

The system components' design and implementation is described, with their requirements being developed from existing human-machine interfaces in the underwater, ground and air vehicle teleoperation domains. This description is accompanied by a number of user studies testing and evaluating single system components in order to identify the most usable system configuration. The results of the development process are an attitude HUD based on the outside-in principle in an orbital-plane based coordinate reference system; a three-dimensional (3D) trajectory prediction display in the chaser spacecraft body coordinate system; the *ThirdEye*, a five degrees of freedom robotic camera arm with a virtual, 3D status display, controlled by means of a single joystick; and an operator interface integrating these features with two monoscopic video streams.

Using this operator support system, a series of final approach and docking experiments was conducted. The experiments showed that even inexperienced operators could successfully dock to rotating target objects using the combination of attitude HUD, trajectory prediction display and a single monoscopic video stream. With the introduction of the robotic camera arm and the auxiliary camera view, the success rates and the precision of the docking maneuvers was increased along with operator situation awareness, albeit at the cost of increased propellant and time consumption. Operator task load and docking safety were not influenced by use of the *ThirdEye*.

Human operators can therefore be enabled to successfully complete the challenging approach and docking maneuvers of rotating, uncooperative targets. Teleoperation of this mission phase is thus an alternative to automated or autonomous systems, either as a contingency backup or as the nominal approach.

ZUSAMMENFASSUNG

Rendezvous & Docking ist eine essentielle Fähigkeit für alle On-Orbit Servicing und Space Debris Removal-Missionen. Daher wurde beträchtlicher Forschungs- und Entwicklungsaufwand im Bereich automatischer und autonomer Rendezvous & Docking-Systeme betrieben. Dennoch erfordern unkooperative Ziele, die nicht mit Docking-Schnittstellen und Sensorzielen ausgestattet sind, und eventuell rotieren oder taumeln, die Miteinbeziehung eines menschlichen Operators.

Diese Dissertation untersucht die zweiteilige Hypothese, dass (1) ein Operator in der Lage ist, nur unter Verwendung eines Joysticks, Live-Videos, einem Lage-Head-Up-Display (HUD), und einer Flugpfadprädiktion erfolgreich Dockinganflüge eines generischen, rotierenden Zielobjekts durchzuführen; (2) die Leistung des Operators wird verbessert, wenn der anfliegende Satellit mit dem *ThirdEye* ausgerüstet ist, einem robotischen Kameraarm, der einen zusätzlichen, flexiblen Blickpunkt bietet, sowie einer grafischen Nutzerschnittstelle, die das HUD, die Flugpfadanzeige und die beiden Kamerabilder integriert. Die Anflug- und Dockingmanöver sollen dabei unter dem Einfluss der Signallaufzeitverzögerungen stattfinden, die für Kommunikationstrecken übern einen geostationären Relaissatelliten repräsentativ sind.

Das Design und die Umsetzung der Systemkomponenten werden beschrieben, wobei die Systemanforderungen aus vergleichbaren Mensch-Maschine-Schnittstellen der Unterwasser-, Luft-, und Fahrrobotik entwickelt werden. Diese Systembeschreibung wird durch eine Reihe von Nutzerstudien begleitet, die einzelne Komponenten testen und evaluieren, um die geeignetste Systemkonfiguration zu identifizieren. Dier Ergebnisse der Entwicklung sind ein Lage-HUD, welches auf dem „Inside-Out"-Prinzip und einem Orbitebenen-basierenden Koordinatensystem basiert; eine dreidimensionale (3D) Flugpfadprädiktion im Körperkoordinatensystem des anfliegenden Satelliten; das *ThirdEye*, ein robotischer Kameraarm mit fünf Freiheitsgraden welcher über eine virtuelle, 3D Statusanzeige und einen einfachen Joystick gesteuert wird; und eine Mensch-Maschine-Schnittstelle, die diese Komponenten mit zwei monoskopischen Videos kombiniert.

Eine Reihe von Dockingexperimenten wurde durchgeführt. Die Experimente zeigten, dass auch unerfahrene Operatoren in der Lage sind, unter Verwendung des HUD, der Flugpfadanzeige, und Mono-Video an rotierende Zielobjekte anzudocken. Die Verwendung des Kameraarms und der zusätzlichen Kamera erhöht die Erfolgsraten, die Andockpräzision, sowie das Situationsbewusstsein der Operatoren, jedoch zu dem Preis erhöhten Treibstoff- und Zeitbedarfs. Die Arbeitsbelastung des Operators und die Sicherheit der Anflüge wurden durch das *ThirdEye* nicht beeinflusst.

Bodenoperatoren können daher in die Lage versetzt werden, die herausfordernden Anflüge unkooperativer, rotierender Ziele erfolgreich durchzuführen. Die Teleoperation dieser Anflüge ist daher eine Alternative zu automatischen oder autonomen Systemen, entweder als Ausweichmöglichkeit für Systemfehlverhalten, oder auch als nominaler Operationsansatz.

ACKNOWLEDGMENTS

Although only the author receives credit and deserves criticism, a complex and technically challenging project like an experimental doctoral thesis cannot be accomplished without considerable support of students, colleagues, friends and family.

I'd therefore like to thank the students who through their research theses and assistant jobs expended considerable effort into implementing the hard- and software used throughout the experiment series, and who also came up with a number of excellent ideas that greatly improved individual system components. A special thanks is owed to Ludwig Friedman, who went way beyond duty to help solve numerous technical problems with the robotic camera arm and its control software.

Then there is also Zarrin Chua, at the time of writing a Ph.D. student at Georgia Institute of Technology. She assisted me in designing the evaluation experiments and lent me invaluable advice in running the experiments and the statistical analysis. Without her guidance I might have got lost in an ocean of statistics.

All of my colleagues at LRT contributed substantially to this thesis, by either patiently listening to my complaints and doubts, or by helping me solve the innumerable problems I had with the details of the system components and the evaluation and test setup. Great morale-boosters in times of doubt and black holes swallowing all motivation were Philipp Hager, Claas Olthoff, Dr. Alex Hoehn, and Dr. Martin Rott who on numerous occasions convinced me to press on when I wanted to close the shop and go home. I'd also especially like to acknowledge the technical genius Andreas Fleischner, who never failed to come up with solutions for electronics and software problems, and Jan Harder, who helped greatly in finalizing the video-transmission component of the *ThirdEye* user interface and who took it upon him to read through the whole thesis and providing me with invaluable feedback.

But above all, my gratitude is owed to my family and friends, first and foremost my wife Sonja, who had to live with my frustration, doubts and panic attacks for four long years and who never ceases to support me.

TABLE OF CONTENTS

FIGURES

TABLES

ACRONYMS AND ABBREVIATIONS

3dSVK	3d Stereo Visualization Kit
AFSCN	Air Force Satellite Control Network
ANOVA	Analysis of Variance
AOCS	Attitude and Orbit Control System
APAS	Androgynous Peripheral Attachment System
API	Application Programming Interface
approx.	approximately
AR	Augmented Reality
ASTRO	Autonomous Space Transfer and Robotic Orbiter
ATV	Automated Transfer Vehicle
AVGS	Advanced Video Guidance System
BOL	Begin of Life
bps	Bits per Second
CAD	Computer Aided Design
CBM	Common Berthing Mechanism
CCTV	Closed-Circuit Television
CEV	Crew Exploration Vehicle
cm	centimeter
COAS	Crew Optical Alignment Sight
CompactRIO	Compact Realtime Input/Output
COTS	Commercial off-the-Shelf
CRV	Crew Rescue Vehicle
CW	Clohessy-Wiltshire
DARPA	Defense Advanced Research Projects Agency
DART	Demonstration of Autonomous Rendezvous Technology
DC	Direct Current
DCM	Direction Cosine Matrix
DDS	Data Distribution Service
DEOS	Deutsche Orbitale Servicing Mission
DOF	Degree of Freedom
DRM	Design Reference Mission
DRS	Data Relay Satellite
DSRV	Deep Submergence Rescue Vehicle
ECI	Earth Centered Inertial
e.g.	example given
EOL	End of Life
EPS	Electrical Power System
ETS	Engineering Test Satellite
EVA	Extra-Vehicular Activity
FOV	Field of View
fps	frames per second
GEI	Geocentric Ecliptic Inertial
GEO	Geostationary Earth Orbit
GNC	Guidance, Navigation and Control
GNSS	Global Navigation Satellite System
GPS	Global Positioning System
GSV	Geostationary Servicing Vehicle
GUI	Graphical User Interface
HDRM	High Data Rate Modem
HIL	Hardware in the Loop
HMD	Head-Mounted Display
HMI	Human-Machine Interface

HSD	Honestly Significant Difference
HTV	H-II Transfer Vehicle
HUD	Head-Up Display
I^2C	Inter-Integrated Circuit
IEEE	Institute of Electrical and Electronics Engineers
in.	inch
IP	Internet Protocol
IR	Infrared
ISS	International Space Station
JAXA	Japanese Space Agency
JEM	Japanese Experiment Module
JPEG	Joint Photographics Experts Groups
JPL	Jet Propulsion Laboratory
kbps	kilobits per second
LCD	Liquid Crystal Display
LDEF	Long Duration Exposure Facility
LED	Light Emitting Diode
LEO	Low Earth Orbit
lidar	Light Detection and Ranging
LIDS	Low Impact Docking System
LISA	Lightweight Intersatellite Antenna
LRT	Lehrstuhl für Raumfahrttechnik
LVLH	Local Vertical Local Horizontal
m	meter
MCC	Mission Control Center
MEO	Medium Earth Orbit
MFD	Multi-Function Display
MiTEx	Micro-Satellite Technology Experiment
MLI	Multi-Layer Insulation
mm	millimeter
MMU	Manned Maneuvering Unit
MPLM	Multi-Purpose Logistics Module
ms	millisecond
MSL	Mars Science Laboratory
n/a	not applicable
NASA	National Aeronautics and Space Administration
NEO	Near Earth Object
NEXTSat	Next Generation Satellite and Commodities Spacecraft
NFIR	Natural Feature Image Recognition
NRL	Naval Research Laboratory
OECS	Orbital Express Capture System
OMV	Orbital Maneuvering Vehicle
OOS	On-Orbit Servicing
OpenGL	Open Graphics Library
ORU	Orbit Replacement Unit
PC	Personal Computer
RACOON	Realtime Attitude Control and On-Orbit Navigation
RCS	Reaction Control Thruster
RDS	Russian Docking System
RF	Radio Frequency
RMS	Remote Manipulator System
ROKVISS	Robotikkomponentenverifikation auf der ISS
ROTEX	Robotics Experiment
ROV	Remotely Operated Vehicle
RPOP	Rendezvous and Proximity Operations Program
RTI	Real-Time Innovations
RVD	Rendezvous and Docking
s	second
SA	Situation Awareness
SAGAT	Situation Awareness Global

	Assessment Technique
SAINT	Satellite Interceptor
SART	Situation Awareness Rating Technique
SCAMP	Secondary Camera and Maneuvering Platform
SCM	Soft Capture Mechanism
SD	Spatial Disorientation
SIS	Space Infrastructure Servicer
Smart-OLEV	Smart Orbital Life Extension Vehicle
SMM	Solar Maximum Mission
SSRMS	Space Station Remote Manipulator System
SUMO	Spacecraft for the Universal Modification of Orbits
TCP	Transmission Control Protocol
TDRSS	Tracking and Data Relay Satellite System
TFX	Telerobotic Flight Experiment
TLX	Task Load Index
TPI	Terminal Phase Initiation
TROV	Telepresence Remotely Operated Vehicle
TSX	Telerobotic Shuttle Experiment
U.S.	United States
UAV	Unmanned Aerial Vehicle
UDP	User Datagram Protocol
UGV	Unmanned Ground Vehicle
USAF	United States Air Force
UUV	Unmanned Underwater Vehicle
VEVI	Virtual Environment Vehicle Interface
VGS	Video Guidance System
Vis-STAR	Vision-based Software for Track, Attitude and Ranging
VR	Virtual Reality
WAN	Wide Area Network
WiiMote	Wii Remote Control
WinGDI	Windows Graphical Device Interface
XSS	Experimental Satellite System

MATHEMATICAL SYMBOLS

Symbol	Description
a	orbit semimajor axis
$\boldsymbol{a} = (a_x, a_y, a_z)^T$	linear acceleration vector
a_i	translation along *x* axis of joint *i*
$\boldsymbol{A_i}$	direction cosine matrix
$\boldsymbol{A_i^j}$	transformation matrix from reference system *i* to *j*
α	general angle
α_i	DH rotation about *x* axis of joint *i*
B	index for Body coordinate system
$\boldsymbol{c}$	auxiliary vector
D	index for docking
d_i	translation along *z* axis of joint *i*
δ_D	docking angle
Δt	time step
$\boldsymbol{\Delta v}$	impulsive velocity change
$\boldsymbol{e}$	normalized base vector
	orbit inclination
i	index number
	index for inertial coordinate system
j	index number
l_i	link length
O	index for Orbit coordinate system
ω	argument of periapsis
	orbit mean motion
$\boldsymbol{\omega} = (\dot{\varphi}, \dot{\vartheta}, \dot{\psi})^T$	rotation rate vector
Ω	right ascension of the ascending node
$\boldsymbol{P}$	point coordinates for HUD drawing
φ	roll angle
ψ	yaw angle

$\boldsymbol{r} = (x, y, z)^T$	position vector
$\boldsymbol{R_{i,j}}$	homogenous rotation matrix about axis *i* by angle *j*
s	trajectory display target symbol size
S_{corr}	correction factor for HUD drawing
T	task completion time
$\boldsymbol{T_{i,j}}$	homogenous translation matrix along axis *i* by distance *j*
τ	trigger angle
θ	orbit true anomaly
ϑ	pitch angle
ϑ_i	joint angle
$\boldsymbol{v} = (\dot{x}, \dot{y}, \dot{z})^T$	velocity vector
v_c	circular orbit velocity
v_Δ	velocity deviation from circular orbit velocity

THESIS SCOPE

1. INTRODUCTION

Rendezvous & docking of spacecraft has been one of the principal challenges of spaceflight. The capability of having one spacecraft perform what is essentially a controlled collision with another, establish a secure connection, and disengage after the completed mission has been quintessential for the Moon missions of the *Apollo* program, the servicing flights of the *Space Shuttle*, as well as assembly and supply of the space stations. It will furthermore be an enabling capability for future missions like satellite servicing, space debris removal, missions to Near Earth Objects (NEOs), sample return missions, as well as any crewed exploration of the other planets in the solar system.

While the approach of cooperative objects like the *ISS* or the *Hubble Space Telescope* has been mastered by both crewed and automated space systems, the advent of robotic on-orbit servicing (OOS) and space debris removal missions presents a new set of challenges for rendezvous & docking systems. The majority of servicing clients and debris objects are of uncooperative nature, meaning that they are not equipped with sensor targets and docking mechanisms and will in many cases rotate or tumble around their axes. The approach of such targets is a major challenge to any rendezvous & docking system and is currently at the edge of the capability of automated robotic systems.

This doctoral thesis therefore proposes to put a human operator into the control loop of the final approach and docking to increase the teleoperation system's capabilities of motion recognition, docking point identification, path planning, and problem solving. The operator will thus perform the maneuvers in direct realtime teleoperation. Whether this approach is taken during nominal operations or as a last-ditch measure to rescue a mission is not of concern to this research. This is a decision to be taken by program managers and mission controllers.

In order to enable the operator to perform this demanding task, two systems are developed and tested regarding their effect on operator situation awareness and teleoperation system performance. One is a head-up display (HUD) designed to intuitively display the chaser spacecraft attitude and a projection of its flight path into the near future. This serves to enable the operator to understand the motion of his own craft and thus to establish a baseline for estimation of all relative motion. The second system is the so-called *ThirdEye*. This system is to provide the operator with multiple, freely positionable vantage points that enable him to understand the relative motion between the involved spacecraft during final approach and docking. The system consists of a robotic arm carrying a camera, and an operator interface integrating the HUDs both with the primary and secondary camera views, as well as with a virtual representation of the camera arm.

This doctoral thesis develops the necessity and the requirements for an operator support system facilitating teleoperated final approach and docking. It then describes the development of the

ThirdEye Situation Awareness Enhancement System, as well as the experiment campaign aimed at evaluating the system and verifying its functionality.

2. WORKING HYPOTHESES

Presuppositions

The docking approach to be simulated shall be a stable orbit approach from a distance of below 10 meters, thus representing the final minutes in a rendezvous & docking scenario.

The research hypothesis behind this doctoral thesis is two-pronged.

Teleoperator Hypothesis

A human operator, relying on video data and supported by an attitude HUD and a trajectory prediction display, is able to accomplish safe and efficient final approach and docking of an uncooperative, rotating target spacecraft under the system limitations typical for space teleoperation. These limitations concern the roundtrip time delay in the communication chain, which shall assume values demonstrated in literature, the quality and frame rates of available video data, as well as the quantity and quality of other available sensor data.

Requirements

The roundtrip time delay in the test setup shall be around 700 ms, with the jitter associated with Wide Area Network (WAN) transmissions. This reflects the measurements made for single-DRS communication chains in preceding research activities as detailed in sections 3.1 and 3.2.

ThirdEye Hypothesis

A robotic camera arm (so-called *ThirdEye*), guided independently of other manipulators and the satellite platform, enhances the operator's awareness of the chaser satellite's position and orientation relative to the target spacecraft sufficiently to improve his performance compared to the baseline.

Requirements

The available sensor information shall only include attitude and position information about the chaser spacecraft and the amount of relative position and velocity information that would be available using laser rangefinders. It shall not include any information about target object orientation and motion. This will ensure that the system and the verification and evaluation experiments represent a realistic use case applicable to current robotic space systems capabilities and operational limitations.

These hypotheses are to be investigated in mission simulations and experiments utilizing an experimental setup specifically designed for this doctoral research. The results of these experiments shall prove or refute the hypotheses.

3. OBJECTIVES AND APPROACH

Research Gap

The survey of OOS applications and tasks in Chapter 1 shows that the **prerequisite for any operational OOS and space debris removal system is the capability of rendezvous & docking** with potentially uncharacterized and uncooperative target objects. Such rendezvous & docking systems must be adaptable and flexible in order to be usable on a wide range of missions and for a multitude of different targets, as well as being able to react to unforeseen events like unknown or unexpected target geometries or chaser subsystem failures. This places demanding requirements on robotic systems.

The **demonstrator missions flown thus far have all been limited in their realism** in that the targets were all equipped with dedicated docking targets facilitating sensor acquisition and tracking. The targets furthermore were fully cooperative, i.e. expecting to be captured, equipped to be captured, and remaining in a stable position to be captured. It is explained in Chapters 1 and 4 why this behavior is not likely to be encountered on operational OOS and debris removal missions.

For future operations in the context of OOS and space debris removal, the uncertain environment and anomalies encountered during rendezvous missions [1] will lead to a **need for faster responses and more adaptability, flexibility and innovation** [2]. Supported by the computer system, the operator will be asked to make critical decisions based on the data available [3]. So a human operator monitoring or guiding the robotic system is necessary or at least desirable.

NASA conducted a number of risk assessment studies as part of the *Exploration System Architecture Study* [4]. In this study, based on historical data of U.S. and Russian rendezvous & docking missions, the probability of the failure of a rendezvous on a mission to Moon or Mars is given as 1 in 97 for an automated rendezvous & docking system like *Kurs*, and between 1 in 230 and 1 in 369 for human-piloted rendezvous & docking [4]. NASA operations procedures therefore require that a human pilot be able to assume manual command over a vessel even for flight operations which will nominally be executed in automated control modes [5]. The assumption of human control is especially valuable in the OOS scenario with uncooperative targets, since **astronaut pilots have repeatedly demonstrated their capability of successfully guiding spacecraft based on visual cues**, even visually distinguishing tumbling motions [6].

Removing the pilot from the spacecraft and having him teleoperate the maneuvers will certainly increase the man-in-the-loop failure rates over an actual astronaut pilot. Nonetheless, **teleoperated final approach and docking is expected to increase system flexibility and performance** over automated or even autonomous systems, and thus to be a viable compromise between human spaceflight and fully automated systems.

As is shown in the short survey of telerobotic systems in Chapter 2, teleoperation tasks of comparable complexity and difficulty can be successfully achieved by robotic air, ground and sea systems. Technology demonstrator missions like *ETS-VII* have also **proven the general feasibility of tele-**

operated docking, albeit **with a cooperative target**. There thus exists no reason to conclude that teleoperated final approach and docking should not be feasible within the limitations of teleoperation in space.

Control-loop simulations conducted for teleoperated docking have shown that the control performance of the operator under the impact of time delay was within the requirements of safe proximity operations and docking [2]. These simulations however did **not involve actual human-in-the-loop experiments**.

Experiments for teleoperated docking of *Gemini* spacecraft showed that docking based on camera images alone is feasible, with no resulting change in operator technique and workload, and little degradation in vertical and lateral accuracy in docking [7]. These experiments were **limited to fully cooperative targets**.

Further teleoperated experiments conducted in dive tanks showed that while teleoperated docking under time delay is fully feasible, adding some automated closed-loop functionality like attitude hold or autonomous trajectory following improves docking performance [8]. Facilitating the use of these automated systems would be a full 3D positioning sensor suite [8], as used in many high performance robotic systems and virtual reality laboratories (see Section 2.4). While this kind of setup is readily available in a confined laboratory environment, it cannot be realized in space. There, **only the sensors mounted on the chaser are available** to the operator. These sensors are of course subject to the same limitations restricting the effectiveness of automated systems.

The key challenges of teleoperated orbital rendezvous are the accumulated time delay between successive ground-commanded maneuvers, navigation errors, maneuver execution accuracy, and environment modeling error [9]. Of these, the **time delay is the major factor**, albeit influenced by the other three. Time delay between telemetry data reception and a responding command uplink is on the one hand due the roundtrip signal travel delay between the ground station and the spacecraft (refer to Section 3). On the other hand, the time required by the operators to interpret the telemetry data, pass it up the command hierarchy, get a decision approved, pass this down the hierarchy and uplink it to the spacecraft is the dominating component [10]. Since the minimum safe approach distance is predetermined by the fact that in order to avoid a collision the station-keeping uncertainties must be less than the distance to the target multiplied by a safety factor [9], this time delay must be reduced so that correction commands are uploaded frequently enough to maintain a safe condition. If this is not possible, an automated system must be introduced for quicker response times.

While the signal travel delay cannot be significantly reduced apart from some optimization in the data processing components of the communication chain, the status perception and decision-making loop can be accelerated by immersing the operator in the remote environment and allowing him to directly guide the spacecraft on his own, without having to wait for approval for each maneuver command to be executed. This requires the **formatting and display of telemetry data** so that the operator can **more intuitively understand** what is happening on orbit and **rapidly issue**

commands using intuitive man-machine interfaces. The lessons learned for HMI design in the other fields of telerobotics (see Section 2.4) can be applied to space teleoperation interfaces and thus lead to highly intuitive and efficient HMI designs.

Objectives

The objectives of this doctoral thesis are to design such a suite of space teleoperation displays using Head-Up Displays (HUDs) and virtual representations of the remote environment, as well as a robotic camera arm system providing flexible vantage points of the remote situation. This system, called the *ThirdEye Situation Awareness Enhancement System*, is to augment the operator's inherent capabilities of image processing, pattern and motion recognition, and thus allow the operator to safely and efficiently control orbital rendezvous maneuvers with uncooperative targets under time delay.

This system is to be **tested in human-in-the-loop mission simulations**. These simulations will have the operators control the **final approach and docking of uncooperative, rotating target objects**. The teleoperation control chain will be **under the impact of a roundtrip delay of 700 ms**, which is representative of communication chains via a single geostationary data relay satellite (DRS).

Situation Awareness

The *ThirdEye Situation Awareness Enhancement System* is meant to enhance the operator's situation awareness (SA). Following the general definition of SA (Section 2.4), SA for proximity operations is in this thesis defined as

- knowledge of ownship position, attitude and motion
- prediction of ownship state into the future for maneuver planning and time delay compensation
- knowledge of target object relative position, attitude and motion

ThirdEye System

These SA requirements will be addressed by the *ThirdEye Situation Awareness Enhancement System* as shown in Table 1-1.

Table 1-1: Information requirement for operator SA during proximity operations and the corresponding ThirdEye system components.

Proximity operations SA requirement	ThirdEye System component
knowledge of ownship position, attitude and motion	ThirdEye Proximity Operations HUD
prediction of ownship state into the future for maneuver planning and time delay compensation	
knowledge of target object relative position, attitude and motion	ThirdEye Robotic Camera Arm System

Knowledge of ownship position, attitude and motion will be provided to the operator by means of a *ThirdEye Proximity Operations HUD*. This HUD will convey information about ownship attitude in an intuitively accessible format. The HUD will furthermore contain a **realtime trajectory prediction display** showing the chaser vehicle's flight path in relation to the target object based on current user commands.

Knowledge of target object relative position, attitude and motion will be provided by the *ThirdEye Robotic Camera Arm System*. This system will be mounted on the chaser satellite and provide visual information about the proximity operations maneuver from a **flexible vantage point**. This allows the operator to "look around the corner" and so observe the docking approach from above or the sides in addition to a first-person view. The camera views provided by this system will be integrated with the attitude and trajectory prediction HUDs in the *ThirdEye Proximity Operations Graphical User Interface* (GUI).

These systems are designed to increase operator SA and thus performance during the critical phase of rendezvous & docking, allowing safe and efficient teleoperation of proximity operations and docking maneuvers.

4. THESIS STRUCTURE

This doctoral thesis is organized in three chapters and fourteen sections, plus an appendix providing supplementary information.

Chapter A serves to summarize the **state of the art in research and technology** in the fields relevant to teleoperated rendezvous & docking in the context of on-orbit servicing. First, the different applications of on-orbit servicing are discussed, as well as the planned, completed and cancelled missions in order to demonstrate the relevance of rendezvous & docking research to this emerging field (Section 1). The reader is then introduced to the applications in other fields of telerobotics and to the various interface design principles and lessons learned for human-machine interaction in realtime teleoperation (Section 2). The discussion is then continued in Section 3 with an overview of both the special considerations deriving from space communications and the resulting signal time delays, and the challenges of teleoperation in the orbital environment. Section 4 then proceeds to provide the basics of rendezvous & docking of spacecraft, as well as the limitations of current systems in the on-orbit servicing context.

Chapter B covers the description of the **research program**. It starts in Section 5 with the description of the simulation environment used for testing the working hypothesis. Section 6 then describes the requirements for a proximity operations head-up display, its design and implementation, as well as the experiments evaluating the system and identifying the most beneficent system configuration. This treatment is repeated for the *ThirdEye* robotic camera arm system in Chapter 7. Section 8 closes the chapter with the discussion of the *ThirdEye* evaluation experiments and the analysis of the experiment data. Chapter B therefore covers the technical contributions achieved over the course of this doctoral thesis, as well as the measurements and statistical analyses made.

Chapter C finalizes the thesis with a discussion of the experimental **results and the confirmation of the hypothesis** (Section 9). Section 10 describes a number of technical issues which must be considered before teleoperated rendezvous & docking and a system like the *ThirdEye* can be employed in operational missions, and provides pointers to future research directions in the field of spacecraft teleoperation. Finally, the thesis is summarized and concluded in Section 11.

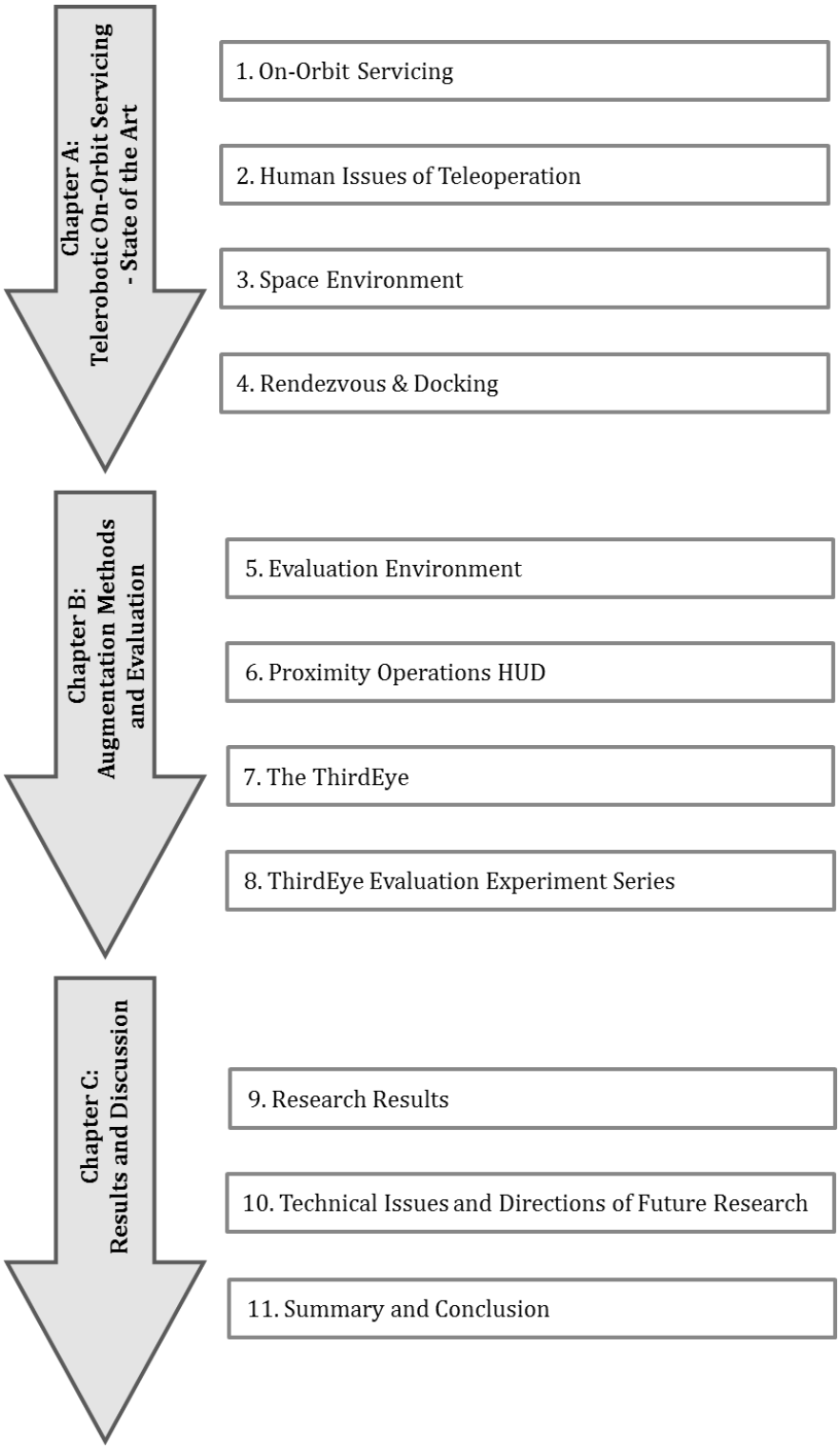
Chapter A:
Telerobotic On-Orbit Servicing
- State of the Art
1. On-Orbit Servicing
2. Human Issues of Teleoperation
3. Space Environment
4. Rendezvous & Docking
Chapter B:
Augmentation Methods
and Evaluation
5. Evaluation Environment
6. Proximity Operations HUD
7. The ThirdEye
8. ThirdEye Evaluation Experiment Series
Chapter C:
Results and Discussion
9. Research Results
10. Technical Issues and Directions of Future Research
11. Summary and Conclusion

CHAPTER A:
TELEROBOTIC ON-ORBIT SERVICING – STATE OF THE ART

If I have seen further than others,

it is by standing upon the shoulders of giants.

Isaac Newton

1 On-Orbit Servicing

Telerobotic on-orbit servicing and space debris removal are considered the main application fields for the systems developed within this thesis, as well as for the research results generated. This section therefore serves to describe the state-of-the art in OOS systems, as well as their current limitations. Section 1.1 describes the main motivation factors behind the general idea of OOS and takes a critical look at the business case of OOS systems. Section 1.2 discusses the different tasks to be accomplished by operational OOS systems and provides examples of space systems that have demonstrated individual or multiple subtasks. The achievements and limitations of the major operational and demonstration systems are then discussed in Section 1.3. Section 1.4 serves to derive the requirements for operational OOS systems which are relevant for the *ThirdEye Situation Awareness Enhancement System* to be developed and evaluated in this doctoral thesis

1.1 Motivation and Business Case

Spacecraft are very expensive articles that must be operated for a long time in order to justify the investment by the owner/operator or to earn a profit [11]. A geostationary Earth orbit (GEO) communications satellite costs around 100 million Euros [12, 13]. It is equipped with 60 – 80 [13, 14] radio frequency (RF) transponders that are leased to customers like TV stations or internet service providers. As a rule of thumb, each leased transponder earns an operator like Astra, Intelsat or Eutelsat around €1 million per year [13].

Spacecraft Lifetime Trends

During the 1980s and 1990s, the design life of GEO telecom satellites increased from an average of 7 years to 15 years [15, 16]. Such long lifetimes increase the risk of system failure [17]. In the absence of an orbital servicing infrastructure this spawns a requirement for high system reliability [14]. High reliability can be achieved by a combination of redundancy in the system design and highly reliable and proven components [12]. Redundant components increase procurement cost, spacecraft mass, and thus launch cost and propellant requirements for on-orbit operations. The launch mass of a spacecraft is also increased by the higher propellant usage during a longer life, as well as increased demand on power generation and storage capabilities [11, 16]. Increasing the reliability of individual spacecraft components entails long and expensive testing and qualification processes. This makes it difficult to introduce modern, often cheaper commercial off-the-shelf (COTS) components [14], and thus limits the design capability and flexibility and increases the risk of technology obsolescence [12, 17]. The long design lives of spacecraft also increase the risk of commercial obsolescence, when the market the satellite was designed for disappears or new opportunities emerge that the spacecraft is unable to serve [16, 17].

Spacecraft Failures

In spite of the efforts spent in increasing satellite reliability and lifetime, on-orbit failure rates have increased substantially over the past decades, to 1-2 orbit insertion failures per year and 5-10 failures per year during begin of life (BOL) and initial operations of a satellite [14]. Overall, approximately 9% of all satellites experience critical failures before their planned end of life (EOL), with another 4-5% falling victim to launcher failures [12].

The loss of a typical GEO telecom satellite costs $150 million for the spacecraft, plus $80 million for the launch [13], apart from the lost revenue. With on average 7.4 failures occurring per year, the economic cost caused by these failures has in the past been $748 million per year [13]. Satellite insurance rates have therefore also been rising steadily [14].

The most common failure types encountered by spacecraft are launcher failures, orbit insertion failures, mechanism deployment failures, attitude and orbit control system (AOCS) failures, as well as depletion of propellants or cryogens, degradation of power generation and storage capabilities towards EOL [14]. 40% of all failures are fatal for the spacecraft and/or the mission, while 65% resulted in a degradation of the spacecraft capabilities [18]. The majority of failures are caused by the AOCS and power subsystems, with the solar array deployment mechanisms being responsible for almost half of power failures [18].

One total satellite loss per year occurs on average in the active GEO constellation [19]. About 40% of all failures occur during the first year of operations [18]. This number clearly shows the potential for saved revenue if some of the malfunctioning satellites could be restored to operating condition. This is furthermore emphasized by the fact that many failure modes are shared by a number of satellites of the same satellite bus, which in the past caused economic losses and thus insurance claims of up to $1400 million due to a single failure mode afflicting multiple satellites [13].

Repair Options

In the current engineering and business approach, satellite operators address in-orbit failures most commonly with software workarounds, if the communication system is still functioning [14]. This countermeasure succeeds in restoring about 17% of all failed spacecraft [14]. Alternatively, orbiting spares or unused payload capacity on other spacecraft can be used [20]. In severe cases the operator can be forced to reconfigure a complete satellite constellation [17].

An on-orbit servicing (OOS) infrastructure would increase the number of options available to owners/operators. The term OOS describes activities like inspection, replenishment, repair or modifications to a satellite's position and orientation, which serve to improve a space-based capability [12]. The driving consideration behind OOS is to attain superior cost efficiency of space systems by extending their operational lifetimes, with lower cost than by replacing a satellite [21]. This can be achieved by correcting malfunctions, exchange defective units, or replenish depleted consumables, such as propellants [22, 23]. OOS capabilities could thus reduce lifecycle cost, increase payload availability, extend a spacecraft's capabilities and orbital lifetime, as well as provide enhanced

mission flexibility and operational readiness [24]. OOS could also provide a measure of flexibility for satellite designer and operators [12, 24]. This could lead to a paradigm shift in the space business towards shorter-lived satellites which can be upgraded or replaced as required by the market [12].

Technical and Programmatic Impact

Due to this potential, OOS was studied as early as the 1960s [22, 25] and was the central idea behind the *Space Shuttle* and the planned *Space Station Freedom* [23], which eventually evolved into the *International Space Station (ISS)*. It is likely to be an important part in future architectures for sustainable activities in Earth orbits, as well as for space exploration [26]. Research & development activities for OOS systems have therefore not only be taken up in Europe and the U.S., but also by China [27].

In order for any of the servicing tasks defined above to be performed on a spacecraft, it must be "serviceable". In general, a spacecraft is considered to be serviceable, if the benefits of OOS outweigh the associated cost [15]. To drive down servicing costs and to increase the performance gain by servicing operations, a number of novel system design requirements must be introduced [22–25]. These design changes result in additional design complexity and considerable volume, mass and cost penalties of up to 20% [12, 22]. *Hubble* is a prime example for a serviceable space system [12].

The decision whether to opt for OOS for a given mission must therefore be made before the prospective client satellite is designed, and is based on a number of programmatic, financial and operational parameters, as well as the technical feasibility of an OOS system [23] .

Business Studies

These considerations have been the subject of multiple government and industry studies [13, 15, 26, 28–30]. The results of these studies are not conclusive. They mostly agree on the feasibility and general benefits of OOS and on the availability of a market [13, 20, 26, 30], but there exists a wide spread of conclusions on the economic viability of OOS for particular OOS tasks, systems and orbital ranges [13]. Most studies tend to ignore the risk of failure of the OOS mission and the uncertainty thus created in the cost-benefit models [13]. It was shown that for most LEO satellites, the cost advantages of OOS are smaller than the cost uncertainties of the venture, making longer design lifetimes more attractive than provisions for refueling [31]. For GEO, on the other hand, current satellite reliability is so high that even a single servicing vehicle would be underutilized [12].

Space System Flexibility

The real value of OOS seems therefore not to be in reduced cost or increased revenue, but in the flexibility it allows system and mission designers concerning market demands, technology levels, and satellite functionality [30, 31]. With OOS available, the uncertainties in these areas need not be addressed in the initial satellite design. Designers can therefore pursue the design considered the

optimum solution, and in case of malfunctions, technical obsolescence or changing market demands, the operated spacecraft can be restored or adapted accordingly [31]. This could lead to a new paradigm in space business, meaning more flexible satellite designs with shorter lifetimes that are continuously being repaired, upgraded or replaced as necessary, using the rapid launch capabilities offered by new generations of responsive commercial and military launchers [12, 20, 31, 32].

Government Customers

The prime customer for more flexible space systems and thus OOS would obviously be the military. A major military application for OOS is in-orbit refueling, increasing the maneuverability of spacecraft and thus making them more survivable and their ground tracks less predictable [23, 33]. In-orbit refueling could also serve to overcome launch vehicle constraints, allowing the launch of partially fueled satellites with a larger payload mass, thus making the system more capable [23]. In total, these measures would increase the utility of military space systems, which is the parameter to be optimized for military applications, as opposed to revenue in the commercial world [32]. In LEO, a large part of all servicing opportunities is thus formed by the refueling and upgrade of military satellites, in addition to other government-owned Earth observation and astronomy missions [14]. The OOS customer base in Medium Earth Orbit (MEO) is also formed by government (mostly military) systems like the U.S. Global Positioning System (GPS) satellite fleet, its European counterpart *Galileo*, as well as the Russian and Chinese navigation satellites [14]. Servicing these systems in orbit could be more economical than continuously replacing them, albeit the concerning studies have not been conclusive [15].

Commercial Customers

The only viable commercial customer base seems therefore to exist in GEO. About 70% of the 398 GEO satellites operational as of August 2011 are owned and operated by commercial companies [34]. All these satellites are potential OOS customers, with the most required OOS activity being refueling [14], but also in-orbit maneuvering and positioning, as well as deployment assist and mechanism repair being a possible market, as was shown before.

1.2 OOS Tasks

The tasks of an OOS system can be categorized in a number of groups [14, 20, 22, 23]:

- Inspection
- Assembly
- Maintenance / Repair
- Replenishment
- Upgrade
- Maneuvering

With combinations of these tasks all major contingencies arising during orbital operations of a client spacecraft can be addressed. Servicing missions can be performed based on a servicing schedule, comparable to the automotive or aviation sectors, for systems or components with a quasi-deterministic and thus predictable time between failures or time before depletion [31]. Other kinds of failures, either by components with a probabilistic behavior, or by unpredictable occurrences such as a micro-meteorite strike or solar flares must be addressed by on-demand servicing missions [31].

The following paragraphs provide details for the servicing tasks mentioned above, as well as for past and future demonstrator missions addressing the required capabilities.

1.2.1 Inspection

To conduct an inspection, an OOS satellite performs a fly-around of a target object while scanning it with cameras or other imaging sensors such as a laser scanner. During the initial deployment phase an inspection could confirm the proper deployment of spacecraft appendages like solar arrays and antennas [13]. Periodical health inspections could monitor the external condition of the spacecraft and check for solar array degradation or micro-meteorite damage [13]. In case of system failures, a visual inspection could help to identify the nature and cause of a failure. It could also be used by insurance companies to visually verify insurance claims [13]. In addition, inspection flights could be used to determine the physical state of a space object and its motion, in preparation for other OOS missions requiring rendezvous & docking/capture (RVD). For military purposes, a visual inspection of a foreign spacecraft serves to determine its tasks and capabilities. It can also set the ground for other, more hostile missions.

Inspection craft must be able to safely and efficiently circumnavigate the target object. They must therefore be **capable of teleoperated or autonomous orbital rendezvous, proximity operations** and formation flight. The demonstration of this critical capability has therefore been the prime objective of the majority of demonstration missions.

NASA in 1997 tested *AERCam Sprint*, a teleoperated small satellite designed to inspect the *Space Shuttle* and *ISS* for external damages [35]. A similar purpose had *Mir-Inspector*, a failed German inspection satellite intended to perform an external survey of space station Mir [13]. A military inspection vehicle was first studied in the 1960s in project *SAINT* (Satellite Interceptor) [19]. In the recent past the United States Air Force (USAF) tested two spacecraft specifically designed for autonomous formation flight and inspection missions, called *Experimental Space System (XSS) 10* and *XSS-11* [13, 19, 36]. The lessons learned on these experimental missions probably influenced the operations of the unmanned space plane *X-37* [37]. Little is known about the purpose and tasks of *X-37*, although on-orbit inspection is assumed to be one of its applications. In addition, the U.S. also operate the two spacecraft of the Micro-satellite Technology Experiment (*MiTEx*) in GEO [19], which have been used in 2009 to inspect a non-responding and drifting U.S. surveillance satellite [38].

1.2.2 Assembly

In-space assembly is the process of joining, construction or fabrication of spacecraft, space systems or space structures [23]. To date, this capability is realized by having self-contained modules rendezvous & dock in orbit to form larger structures, as was done for space station *Mir* and the Russian components of *ISS*, or have modules be transported to orbit in a *Space Shuttle* and be joined to one another by means of robotic manipulators and extra-vehicular activities (EVAs). The highest possible level of space assembly would be to construct large space structures from component parts, or even to manufacture components from unique materials in the space environment [23]. In addition to crewed space stations, there are also visions to have robots construct large space-based solar power generators [39, 40] in GEO, as well as plans to assemble future crewed Mars spaceships in Low Earth Orbit (LEO) [41]. In most of these visions or plans, robots play a major role in assembly operations [35].

Assembly operations require highly dexterous robotic manipulators. These have to be carried by spacecraft capable of very precise formation flight, positioning and maneuvering. **Robotic rendezvous & docking is therefore considered a critical design driver** in future space exploration systems [41].

1.2.3 Maintenance / Repair

Maintenance is generally defined as the upkeep of facilities or equipment, either when necessary or by schedule [23]. In the context of OOS, maintenance describes any kind of repair, realignment, replacement of components, contamination removal or surface restoration [13, 23].

Scheduled and unscheduled on-orbit repair and maintenance activities have been a necessary part of running the space stations *Skylab*, *Salyut*, *Mir* and *ISS* [23, 23] . Many of these repair missions were only possible due to astronaut/cosmonaut daring and improvisation [23].

The prime example for the benefits of in-orbit satellite maintenance and repair are the repair missions accomplished by the *Space Shuttle*, most notably to the *Hubble Space Telescope*. When *Hubble* was afflicted by numerous critical system malfunctions after its launch, the *Space Shuttle* and its crew performed an unprecedented repair mission which saved the spacecraft [21, 42]. On four further occurrences, *Hubble* servicing calls by *Space Shuttle* orbiters succeeded in restoring or replacing critical systems, thus extending the telescope's lifetime substantially at lower cost than a replacement spacecraft. The cost for the first servicing mission was $500 million, while the spacecraft had cost $1 billion [17].

Apart from *Hubble*, the *Space Shuttle* was also deployed to repair a number of government and commercial satellites [43, 44]. These repairs were either accomplished by the *Shuttle* crews on-orbit, or by the manufacturers on ground, after the satellites were recovered by the *Shuttle* and returned within its payload bay [43].

Studies show that up to one third of all spacecraft components could practically be repaired or replaced in case of a failure [24]. A higher percentage would be possible, if more modular bus architectures and payload designs were adopted [24]. This approach of course requires satellites to be designed for on-orbit maintenance or repair, which current spacecraft are not. In the near future, repair missions will therefore always be very complex missions, requiring a high dexterity of the robotic systems and human involvement. Servicer spacecraft **must be able to rendezvous with and dock to mostly uncooperative client satellites** and must be able to safely and effectively navigate around and on the client.

Since the required level of robotic capabilities also entails high cost of servicing missions, client spacecraft will most likely be high-value space assets, such as expensive scientific spacecraft, valuable military and intelligence-gathering missions, and commercial spacecraft suffering failures in the early years of their lives. Another repair opportunity with high impact and a lower level of complexity is deployment support for spacecraft appendages, i.e. the mechanical deployment of solar arrays and antennas stuck in their folded launch configuration. In 2011 alone, there were multiple occurrences of such mechanism failures, degrading the performance of the afflicted spacecraft [45, 46].

1.2.4 Replenishment

The term replenishment summarizes the replacement of spent spacecraft consumables [23]. The consumable mostly mentioned in OOS business studies is spacecraft propellants [13, 23, 32, 44, 47]. The majority of GEO satellites reach the end of their station-keeping propellants before other subsystems fail [13]. An on-orbit refueling system could therefore extend the life and revenue-generation of these spacecraft. The duration of this extended lifetime is however uncertain, since failures in other critical subsystems beyond the design life cannot be predicted. Apart from lifetime extension, a refueling capability could allow a decrease of the initial fuel reserves, thereby allowing the launch of more payload and thus increased mission capability [44] or the launch of less mass on highly reliable and thus expensive launchers [47], with fuel being subsequently launched with cheaper launch vehicles. This basic idea has over the years spawned a number of technology development and demonstration programs, most recently the German *Smart Orbital Life Extension Vehicle* (Smart-OLEV) [48, 49], the Canadian *Space Infrastructure Services* (SIS) program [50, 51], with Intelsat as initial customer[1], and the NASA *Robotic Refueling Mission* on ISS [53, 54]. The requirements of such systems regarding rendezvous & docking and proximity operations are the same as for the repair and maintenance missions.

Refueling also offers benefits for military space activities. A refueling system would allow spacecraft to actually spend more fuel in orbit. This would allow operators to adjust or optimize satellite ground coverage for given requirements [14, 44] and it would also enable military spacecraft to

[1] The agreement between Intelsat and MDA Canada was scrapped in January 2012. The stated reason was that the lack of interest in an orbital refueling concept by U.S. government agencies removed the biggest potential customer and destroyed the economic viability of the SIS concept [52]. As of June 2012, the future of SIS is unclear.

employ evasion maneuvers to counter hostile action or to change their orbits to throw off adversary activity scheduling [55]. This application was one of the main motivations behind the U.S. Defense Advanced Research Projects Agency (DARPA) *Orbital Express* OOS demonstration in 2007 [47].

The exchange of cryogenics [23] used in cooling space-based instruments is also a possible approach for extending the lifetime of high-value astronomy or Earth observation missions [13], or to reduce their launch mass and thus cost. In the case of *Spitzer* [56], the liquid Helium used to cool the main instrument was spent after 2.5 years, while the spacecraft bus and the instruments are still functioning [57]. A capability to replenish coolants in space could thus substantially increase the value of some space-based assets.

1.2.5 Upgrade

On-orbit satellite upgrade is a way to react against performance degradation and technological or commercial obsolescence [17]. New hardware utilizing technologies not yet mature at time of launch can be added to the space system to increase its capability, such as more capable sensors, instruments or other payloads [13]. This approach would reduce the time-to-market of new technology in space business, and thus improve mission performance in a more economical way than the replacement of whole satellites or even constellations [55]. This was demonstrated by the multiple servicing missions of the *Space Shuttle* to *Hubble*, during which the space telescope was upgraded with state-of-the-art scientific instruments, thus vastly improving its science output [17, 42].

1.2.6 Maneuvering

Upgrades of space-based capabilities can not only be achieved by upgrading individual satellites, but also by changing the architecture of a system of satellites. This entails a reconfiguration of a satellite constellation, changes of altitudes or inclinations, or the addition of new satellites [17]. Such space system architecture changes could be enabled by a capability of in-orbit refueling, which would however come at the cost of a change in spacecraft design and some mass penalty [22]. The alternative is to have dedicated in-orbit maneuvering spacecraft, also referred to as “space tugs”, rendezvous and dock with client satellites and position them in orbit as required, or take over station-keeping functions in order to save on-board fuel [49].

Rephasing or relocation maneuvers are common during the operational phases of GEO satellites [13]. During the orbit injection phase, a space tug could be used to transfer satellites from its initial launch orbit to its operational orbit [14], either in nominal operations as a cost-saving measure, or to salvage a mission after malfunctions of the launcher or the orbit transfer stage.

At the end of their design life or after a malfunction, many spacecraft remain in orbit uncontrolled and thus become space debris objects [19], threatening the operational spacecraft in their vicinity [58]. In collisions with other debris objects or operational spacecraft [59], large clouds of minuscule

debris objects are created, which in turn form a collision hazard for other spacecraft [60]. This creates the potential for a runaway chain reaction, the so-called Kessler Syndrome, which could make Earth orbit inhospitable for spacecraft [61]. The reduction and removal of space debris [13] is therefore a priority mission for the spaceflight community in order to allow future use of space-based assets [59]. One approach to achieve this task is to repair spacecraft in orbit and thus to reduce the number of failed satellites [14] becoming debris objects. In addition, spacecraft must be removed from the operational orbits after they become inoperable. For LEO satellites, this means a controlled de-orbit into the Earth's atmosphere, for GEO an orbit transfer to a "graveyard" orbit 200 km above the GEO belt [13]. Such maneuvers, especially de-orbit burns, require substantial amounts of fuel [31], which drives mass and cost of any debris removal system.

Orbit maneuvering and debris removal have high significance for operators and legislators of space operations. With the *Orbital Maneuvering Vehicle* (*OMV*), a space tug was a component of the original *Space Shuttle/Space Station Freedom* OOS program, until cancelled by budget cuts [23, 23]. ESA also in the early 1990s formulated plans for a *Geostationary Servicing Vehicle* (*GSV*), facilitating inspection, repair and maneuvering of GEO satellites [62]. Several recent technology development programs also have had the goal of demonstrating such capability, most notably the Naval Research Laboratory's (NRL) *Spacecraft for Universal Modification of Orbits* (*SUMO*) [63, 64]. Germany is currently also pursuing a demonstration mission for the **capture of uncooperative debris objects**, called *Deutsche Orbital Servicing* (DEOS) missions [48, 65].

A possible space debris removal spacecraft called *Leopard* was furthermore studied in two Master's theses contributing to this doctoral research, identifying the main accumulations of discarded rocket stages and inoperable satellites in orbit and the maneuvers required to reaching them [66], as well as designing the removal spacecraft itself [67].

1.3 Lessons Learned

Above sections show that there have been numerous technology demonstration mission related to OOS research. However, only a small number of them have addressed actual final approach, docking & capture of two spacecraft and are therefore of interest for the research presented in this doctoral thesis. These systems are the NASA *Space Shuttle*, the University of Maryland *Ranger*, the Japanese *ETS-VII*, as well as DARPA's *Orbital Express*. These spacecraft are considered to be full-spectrum OOS systems in that they are capable to approach and capture client spacecraft, and perform a wide array of repair, upgrade and replenishment tasks. The USAF *X-37* is not included in this chapter, due to the uncertainties about the nature of its mission [37].

The above-mentioned systems and their missions shall be briefly described in more detail and henceforth be used to derive requirements for future operational telerobotic OOS systems.

1.3.1 Space Shuttle

As of June 2012, the *Space Shuttle* had been the only operational OOS system. OOS requirements were the core of its design. Its three design reference missions (DRMs) were (1) rendezvous with a space tug returning GEO satellites for servicing, (2) servicing of an orbital science platform (*Skylab*), and (3) short-notice launch or retrieval of military reconnaissance satellites from LEO [43]. In order to achieve the flexibility in rendezvous and proximity operations required for this variety of missions, the *Shuttle* relied on **manual piloting** by its crew. For satellite deployment and retrieval, in-space assembly, as well as support of astronauts on EVAs, the Shuttle was equipped with the remote manipulator system (RMS), also called Canadarm [68]. The RMS has six degrees of freedom (DOF) and is controlled by a crew member from the aft flight deck, using a combination of hand controllers, video cameras and the view out of the aft flight deck and overhead windows. This arm proved a highly reliable and flexible tool and subsequently evolved into the Space Station RMS (SSRMS) aboard *ISS*. However, the RMS had to be supported by free-flying astronauts using manned maneuvering units (MMUs) to successfully capture spinning or tumbling satellites [13].

Using the RMS and also extensively relying on the flexibility and ingenuity of the astronaut crew (see Figure 1-1), the *Shuttle* was able to successfully repair, reboost or return to Earth a number of scientific and commercial satellites [23, 43, 44]. It also conducted experiments addressing future options of in-orbit refueling, as well as in-orbit construction and space telerobotics [13]. These led to the successful assembly and maintenance of the ISS [43].

Figure 1-1: Astronauts working on the Hubble Space Telescope *fixated in shuttle* Discovery*'s payload bay [69].* Hubble *is supported by a rotating table in the payload bay. The RMS supports the astronauts in their repair tasks. This view shows the complex coordination between* Shuttle*, RMS and astronauts to accomplish servicing missions*

Projections early in the *Shuttle* program assumed that space program costs could be reduced by up to 50% if spacecraft were designed to be refurbishable and modular [23]. This philosophy was successfully demonstrated with the *Hubble Space Telescope* [21]. The *Hubble* design was to create a space-equivalent of an observatory on Earth, at a price of $1.5 billion (1993) [23] . Its spacecraft bus and instrument suite was therefore designed and required to be serviced by astronauts in three-year intervals [21], to modernize the science instruments and restore and update short-lived bus components in order to reach a design life of fifteen years [23] , at servicing costs of about 50% that of a replacement spacecraft [17]. To allow effective servicing operations, *Hubble* was designed and built with standardized and EVA-compatible component interfaces, standardized access doors, electrical connector maps, instruction labels, sockets for foot restraints, as well as hand rails [42]. The associated cost and mass penalties paid off when four of six gyroscopes failed shortly after commissioning [21], a flaw was discovered in the primary mirror, and a solar array did not fully extend and lock [23] . These catastrophic component failures and a number of less-critical malfunctions were addressed on the first *Hubble* servicing mission by the *Space Shuttle* [42, 70], thus saving the spacecraft and the mission. Four subsequent servicing missions continuously upgraded the science instrument suite, replaced bus components and reboosted the telescope in order to extend the original design life of fifteen years to over twenty years [42, 70]. Over the years, a number of technical problems were encountered that were not considered during the initial design of the telescope, including accelerated degradation of thermal blankets, disturbance of observations due to oscillations of the flexible solar panels, and the premature failure of gyroscopes [21]. Without the provisions for OOS, the space telescope would not have fulfilled its design life.

The complexity of OOS is demonstrated that for each of the servicing missions typically 150 different tools were carried aboard the *Space Shuttle* [42]. In order to prevent fitting problems in orbit, more than 3500 flight tool fit-checks were conducted prior to a mission [42]. In addition to the preplanned servicing tasks, the Shuttle crews were also confronted by previously unknown technical problems. Instrument covers and thermal insulation patches had to be fabricated and installed, Multi-Layer Insulation (MLI) was repaired [42]. Even a power unit box never designed to be serviced was repaired successfully [21]. This clearly demonstrated the **value of human ingenuity, flexibility and improvisation** for complex OOS operations.

1.3.2 Ranger

Ranger is an OOS robotics system developed at the Space Systems Lab at the University of Maryland. It was originally conceived as a competitor to NASA's Flight Telerobotic Servicer concept [23] and was thus designed to increase the *Space Station Freedom*/*Space Shuttle* servicing resources by providing a relatively low-cost, lightweight, **free-flying satellite servicing robot** [71]. On-orbit experience indicated that the most important servicing tasks were not the ones planned for during mission preparations [8]. Since all spacecraft are built by humans on ground, a servicing robot must therefore have human-sized components, human levels of strength and dexterity, and human-equivalent visual acuity to be able to reach into constrained spaces and successfully repair or re-

place satellite components [8]. *Ranger* design goals were therefore for the robot to be as capable as an astronaut in a pressure suit, to be able to use standard EVA interfaces, and for the design to incorporate the lessons learned during HST servicing missions [72]. The resulting system was equipped with two dexterous manipulator arms, a grappling arm, and a video arm carrying a stereo camera pair and providing the motion envelope of a human torso and neck [72]. The original *Ranger* Telerobotic Flight Experiment (TFX) mission concept (illustrated in Figure 1-2) called for a robot mounted on a propulsion module to perform visual inspections, rendezvous and grappling operations on its launcher's third rocket stage, while being teleoperated from the ground via the NASA ground station network or the Tracking and Data Relay Satellite System (TDRSS) [71, 73]. For budgetary reasons this plan was then modified into the *Ranger* Telerobotic Shuttle Experiment (TSX), with the manipulator suite being mounted in the Shuttle payload bay and the robot being operated either remotely from the ground or by the Shuttle crew [74].

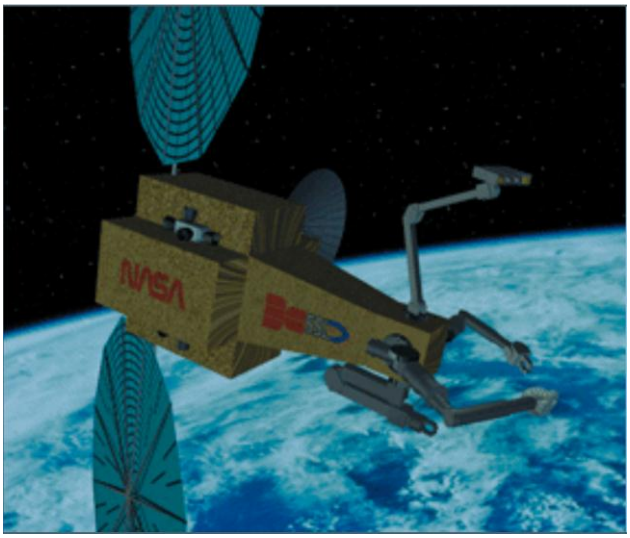

Figure 1-2: Concept art of the Ranger Telerobotic Flight Experiment (TFX) [75]

In the reorientation of NASA after the loss of *Columbia*, *Ranger* was removed from the Shuttle manifest. Nonetheless, it represents a major step in the development of dexterous space robotics systems and resulted in numerous publications which laid the ground work for later OOS research, including the fields of interface design [74, 76] and teleoperation under time delay. An interesting system tested in a neutral buoyancy facility as part of *Ranger* experiments is the Secondary Camera and Maneuvering Platform (SCAMP), which is a small free-flying camera platform used for external views of the worksite for *Ranger* control and monitoring [72]. It is used to increase operator and observer situation awareness and has been utilized to verify object alignment during docking tasks [8]. The research results generated with this system therefore laid the foundation for some of the research contributions of this thesis.

1.3.3 ETS-VII

The Engineering Test Satellite (ETS) VII was launched in 1997 by the Japanese Space Agency (JAXA). Its mission was to develop and verify automated rendezvous & docking and space robotics technologies needed for the HTV and the Japanese Experiment Module (JEM) manipulator aboard ISS, as well as for future OOS missions [77]. The space segment of the mission consisted of the chaser satellite *Hikoboshi* and client satellite *Orihime* [48]. *Hikoboshi* had a mass of 2500 kg and was equipped with a 2 m manipulator arm, a docking mechanism, as well as an inter-satellite link antenna for communication via a GEO data relay satellite (DRS) [77] (refer to Figure 1-3).

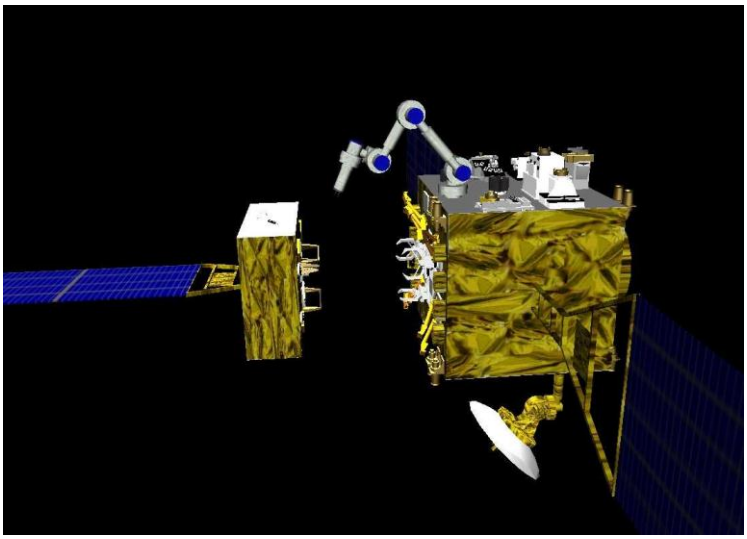

Figure 1-3: Representation of ETS-VII mission. Chaser Hikoboshi *extends manipulator to capture target* Orihime *[78]*

Orihime, with a mass of 400 kg, was usually docked to the chaser when not in use as target for rendezvous & docking experiments [77]. The experiments accomplished during the mission included **remote piloting during final approach and docking** [77], autonomous and ground controlled capture of the target satellite [13, 77], visual target inspection, ORU exchange, manipulator tool exchange, liquid and gas transfer, as well as experiments addressing the dynamics of the coupled multi-body system [77]. The teleoperation experiments were conducted under a time delay of up to 7 s [77], which was accomplished by using techniques such as shared control, predictive displays and visual operator guidance [48]. The mission also encountered problems which can be considered characteristic for teleoperated space robotics systems. There were computer malfunctions, loss of attitude control, and subsequent loss of DRS communications [77]. One incidence demonstrated the effects of operating a manipulator system on a small servicing platform, when the torque induced on the chaser vehicle overwhelmed the AOCS and manipulator movement had to be terminated in order to prevent the antenna to lose contact with the DRS [79].

The accomplishments of ETS-VII are most relevant for this research, since the mission demonstrated the **general feasibility of teleoperated final approach and docking** [77].

1.3.4 Orbital Express

DARPA envisions an OOS infrastructure with satellites being equipped with standard mechanical and electrical interfaces, enabling the automated transfer of fuel and cryogens as well as upgraded electronics components by unmanned servicing vehicles [55]. The *Orbital Express* program was launched to demonstrate the ability to autonomously approach, rendezvous and capture a spacecraft, and then service the target robotically [80]. The servicing tasks were the initiation of electrical and fluid couplings, the transfer of hydrazine fuel between the spacecraft, as well as the autonomous transfer of one battery and one high-speed computer ORU using a robotic manipulator [80]. The space segment consisted of the *Autonomous Space Transfer and Robotic Orbiter* vehicle (ASTRO), equipped with an antenna for contact with the Air Force Satellite Control Network (AFSCN) and TDRSS and a 3.3 m manipulator, and the target *Next Generation Satellite and Commodities Spacecraft* (NEXTSat), carrying passive docking reflectors, a passive docking mechanism and a capture fitting [55] (see Figure 1-4). The orbit was selected to maximize communications time via the AFSCN [47].

Figure 1-4: Artwork of Orbital Express. ASTRO (left) is approaching NEXTSat with the manipulator in stowed configuration [81]

Orbital Express successfully demonstrated automated system capabilities crucial for OOS missions. These include automated approach, soft capture and mating, autonomous circumnavigation of the target, the first autonomous capture of a satellite by another satellite exclusively using a robotic manipulator, autonomous removal and re-insertion of a sensor flight computer, autonomous exchange of a battery, as well as pressure-fed and pump-fed hydrazine transfer from one satellite to another [82].

While the emphasis was placed on system autonomy, *Orbital Express* still required the services of approximately 50 ground-support personnel performing mission planning, orbit analysis, subsystem management, rendezvous and proximity operations planning and execution, arm berthing and grappling operations, as well as the hydrazine propellant transfer [47]. The extensive ground sup-

port team was elementary in recovering the system from a number of failures in the AOCS, flight computer, guidance and sensor subsystems [47, 83].

This exemplifies the fact that autonomous space systems, especially robotic systems, have to rely on the **human ground controllers' flexibility, adaptability and ingenuity** to enable mission success. The fact that such a substantial commitment of ground support was required for a mission as thoroughly scripted and tested as *Orbital Express* leads to reason that a similar effort will be required for any operational OOS mission, and that contingencies during the mission will require **continuous monitoring and also commanding by ground operators** during critical mission phases. The ground operators therefore must be enabled to **know and understand the state of the chaser vehicle** and the situation in the remote orbital environment [83]. They must furthermore be provided with **the interface devices necessary to quickly and efficiently interact with the spacecraft** in case of off-nominal system behavior and situations.

1.4 OOS Requirements

The servicing missions of the *Space Shuttle* have demonstrated repeatedly that **OOS of complex space systems is feasible** and that it also is a valuable proposition for high-value space assets, such as expensive scientific satellites or commercial satellites with BOL failures. These missions also showed the **immense complexity of OOS missions**. On the first Space Shuttle servicing mission, the *Solar Maximum Mission* (SMM) satellite was the client. In order to prepare for the mission, a high-fidelity model of SMM was set up on the ground and astronauts practiced on it for one year prior to mission launch [23] . And even after this extensive preparation, the mission plan had to be adapted on orbit to reflect actual circumstances. On *Hubble* servicing missions, the actual situation encountered on orbit also required the servicing astronauts to **adapt, improvise and overcome technical and operational challenges** that were not anticipated during mission preparation. However, the *Space Shuttle* with its combination of capable rendezvous & docking systems, robotic components and a well-trained human crew was able to successfully complete all its servicing missions to commercial and scientific satellites, as well as the ISS.

Cost of Manned OOS

While this clearly demonstrated the capabilities of a crewed OOS system, it also showed the cost associated with it. Apart from the lives lost with *Challenger* and *Columbia*, the *Space Shuttle* program was too expensive for any long-term OOS effort. The servicing cost for the SMM mission was reported as $60 million, in order to restore a $230 million satellite [23] . The typical repairing cost for *Hubble* is set at $70 million for every four years of operation of the $1.6 billion telescope [21]. However, if all the factors contributing to the cost of a *Space Shuttle* mission are included in the cost model, each *Hubble* servicing mission carried a price tag of $2.3 billion [21]. These high costs arise from the increased complexity of a crewed spacecraft over an unmanned vehicle, resulting from

requirements for a life-support system, radiation protection, crew-training, increased reliability, etc. [24], which makes a **crewed OOS servicing system impractical, while also highly capable**.

Limitations of Robotic Demonstrator Systems

ETS-VII and *Orbital Express*, as well as the research & development flowing into *Ranger*, have demonstrated that **telerobotic and supervised autonomous systems can accomplish basic OOS tasks**. Due to the current limitations of any robotic system, highly-automated robotic OOS missions are only efficient for servicing operations that have been planned in advance and for which both the client and the servicer have been specifically designed [21]. If any failure or problem occurs that has not been anticipated during mission preparation and indeed satellite design, a robotic system will have difficulties in accomplishing its mission [21]. The technologies demonstrated on *ETS-VII* and *Orbital Express* are **limited to capturing satellites that are cooperative and attitude-stabilized** [84]. The majority of **client satellites or space debris objects will however be of uncooperative nature**, meaning that their body rotation rates will not be available a priori (albeit the measurement and estimation by ground-based radar is possible [60]) and that they will not carry equipment to support relative navigation and attitude estimation, such as reflectors or beacons [85], not to mention docking or capture interfaces. **Human operators will therefore be a critical part of an OOS system**, in order to augment the robotic systems in areas of challenged capabilities. This will obviously be the case **in unexpected situations and for non-routine tasks during rendezvous & docking** and well as servicing [86, 87], but might also be necessary in the fields of visual object recognition and pattern discrimination in the challenging visual environment of space, where human capabilities might be a valuable addition to computer vision.

Size and Mass of Servicing Targets

Another aspect in which the OOS demonstrations so far lacked realism is the mass and size ratio between servicer and client. An important measure for the disturbance created by the manipulator and the captured client is the vehicle-to-arm mass ratio, which is between 200 : 1 (RMS only) and 7.8 : 1 (*Hubble* extended on RMS) for the *Shuttle*, and 6.25 : 1 for *ETS-VII* [79]. On *ETS-VII*, *Orbital Express*, as well as the planned *DEOS*, the **client has always been significantly smaller than the servicer**. This facilitates computer vision tasks such as edge detection, allows the use of a relatively compact robotic manipulator, and reduces the disturbance torque enacted upon the servicer by the motion of the robot manipulator.

In an operational OOS scenario the **servicer will however face satellites that are significantly larger** than current experimental OOS vehicles. Figure 1-5 shows the launch mass development of major GEO satellite fleet (defined as larger than twenty satellites) owners/operators for the 1994-2010 time span. A **trend towards larger satellite launch masses** is evident for each fleet, with the majority of GEO satellites launched since 2000 having a launch mass of over 4000 kg, with the biggest approaching 6200 kg. Figure 1-6 plots satellite launch mass versus the semimajor axis of the orbit in the LEO realm. While the large majority of LEO satellites are below 2000 kg, there are a number of spacecraft in the 4000+ kg area. These satellites represent the high-value space assets

most suitable for future servicing operations and also important targets for any debris removal system. The biggest officially known objects in LEO are the ESA *Envisat* with a mass of about 8000 kg, the *Hubble Space Telescope* with about 11000 kg, as well as the U.S. signals and imaging reconnaissance satellites of the *Lacrosse* (14500 kg) and *Keyhole* (18000 kg) systems. The very **size of these systems rules out the use of the servicing schemes tested on the demonstrator missions**. *ETS-VII* and *Orbital Express* both captured the target object using a 2-3 m long robotic arm, then attached it to a docking port on the servicer bus and reused the manipulator for servicing operations.

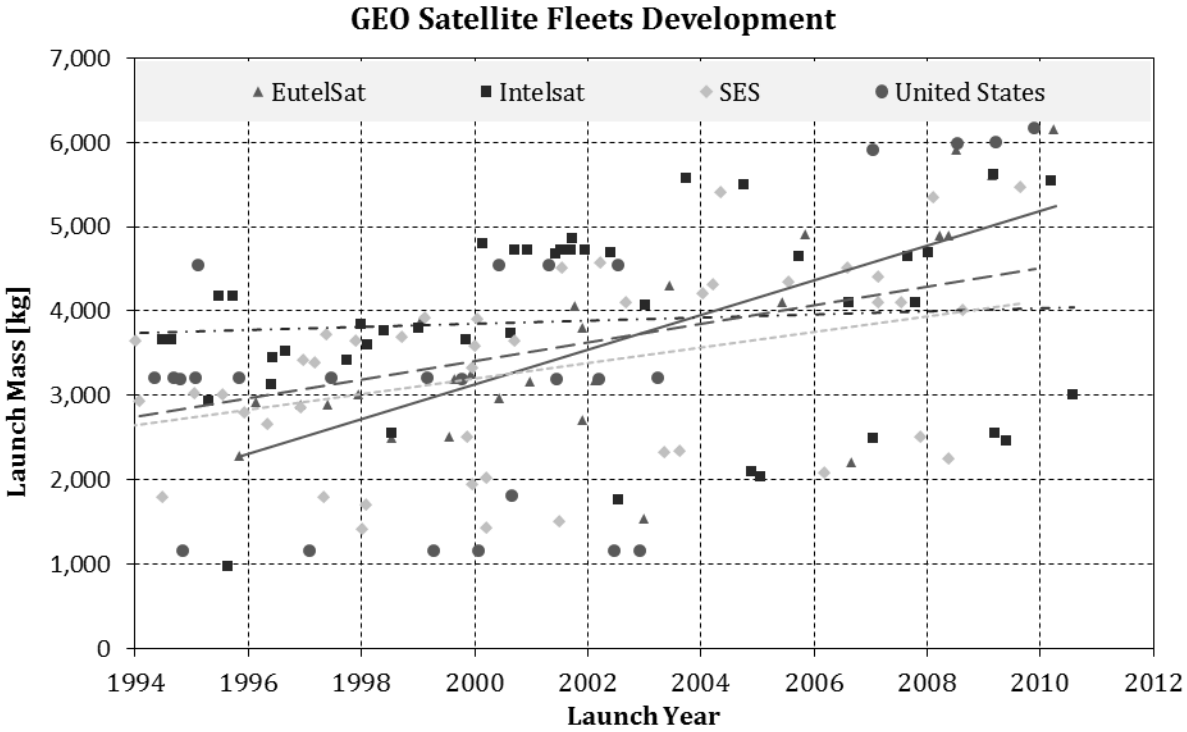

Figure 1-5: Active GEO communications satellites launch mass development for the satellite fleets of major operators. An upward trend in launch mass is visible, accompanying the trend towards larger, more capable satellites (based on data from [88])

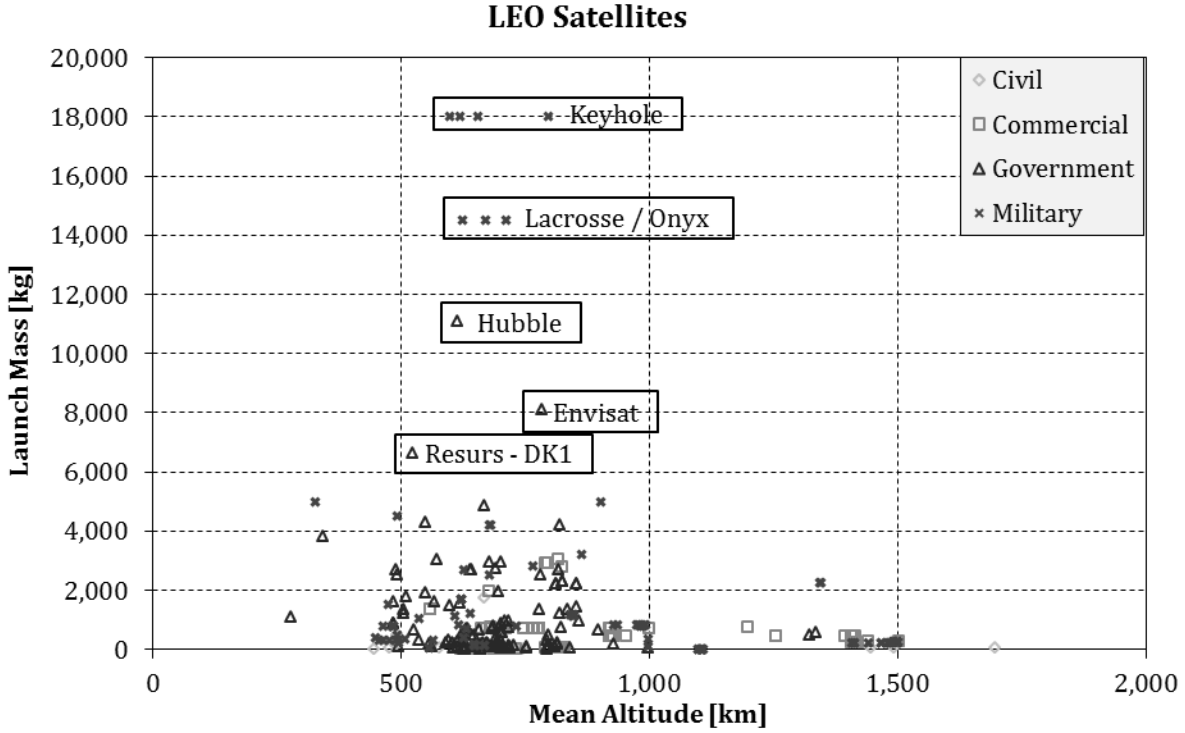

Figure 1-6: Active LEO satellites launch mass versus mean orbital altitude. The commercial, government and military high-value satellites suitable for OOS show launch masses of 5,000 – 18,000 kg (based on data from [88])

A GEO telecom satellite in the 6000 kg area has body dimensions of about 7 m x 4 m x 3 m and a solar array span of 48 m [89]. *Hubble* is almost 16 m long, has a diameter of 4.2 m, and a solar panel span of 12 m [42]. It is unrealistic to assume that such large spacecraft can be serviced using the same scheme. The servicer must be equipped with multiple robot arms or a robotic manipulator as big as the *Shuttle* RMS (with a reach of 15.2 m and a mass of 410 kg [68]) or the **servicing operations must be performed by a free-flying platform**, performing **multiple capture and release operations** at different points of the target object in the course of a servicing mission. Even if a degree of autonomy comparable to *Orbital Express* should be available on an operational OOS system, the difficulty of the associated guidance, navigation and control (GNC) task and the unpredictability of many servicing tasks will make **involvement of human operators on the ground mandatory**. Any OOS system will therefore be a **telerobotic system**.

1.5 Summary

Section 1 provided an overview over the motivations behind on-orbit servicing, as well as the applications and potential customers of an operational OOS system. It furthermore briefly described the - as of 2012 - only OOS system to have been used operationally, the *Space Shuttle*, as well as three robotic OOS demonstrator missions that are deemed the most sophisticated and influential OOS experiments so far.

Space Shuttle experience established that **OOS can be a valuable risk-reduction and capability-enhancing measure for high-value space assets**, as well as that the cost and risks of human OOS are too high for any future system. The experimental robotic systems proved that **telerobotic systems are capable of basic OOS tasks**. However, the experiments all assumed servicing targets which had smaller size and mass than the chaser and were furthermore of a cooperative nature. The scenarios were therefore not representative of any OOS missions to current high-value orbital assets and left a number of questions unanswered, especially in the fields of relative GNC and teleoperated proximity operations.

The experience of *Orbital Express* shows that the **involvement of human operators in off-nominal situations and during system malfunctions is mandatory** for the successful conclusion of robotic OOS operations. An involvement of the human operator in nominal situations might serve as a risk reduction measure.

Human operators must therefore be **enabled to gain situation awareness during rendezvous, proximity operations and docking**, and must be provided with **effective and efficient operator interfaces** to rapidly issue control commands to the chaser spacecraft.

2 Human Issues of Teleoperation

The tasks and many system characteristics of an OOS system are similar to other fields of mobile telerobotics. This chapter provides the basic definitions for the most important terms of telerobotics. It then proceeds to explore similarities between terrestrial telerobotics and OOS, as well as the major considerations of human-robot interface design which are relevant to this doctoral thesis.

2.1 Definitions

Robot

A robot is by definition a system functioning according to the **sense – think – act paradigm** [90] (see Figure 2-1). In order to sense its surroundings, a robot must be equipped with a **sensor system** appropriate for its environment. The sensor data must be processed and future actions must be decided upon by a **processing unit**, in order to achieve task goals. To enable the robot to achieve its goals, it must furthermore possess the ability to **manipulate its environment**. Depending on the task, this manipulation capability can be realized by complex manipulators and tools, or by simple locomotion systems like wheels, tracks or thrusters.

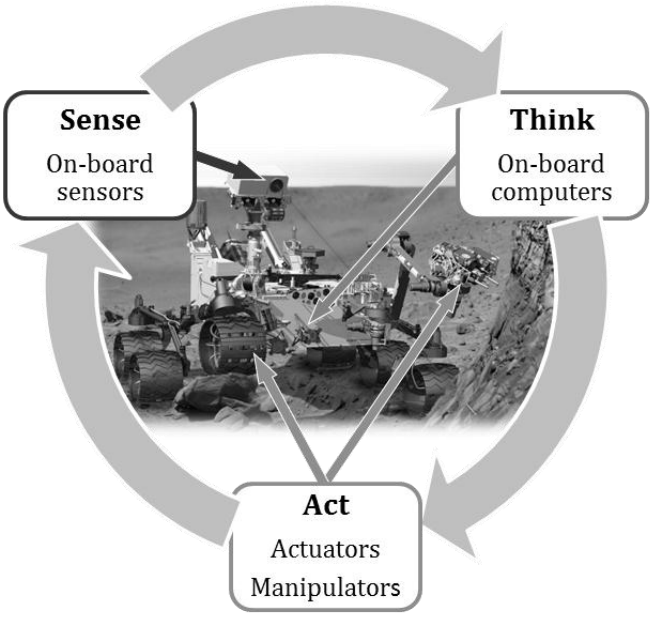

Figure 2-1: Defining capabilities of a robot, exemplarily shown for the NASA Mars Science Laboratory (MSL) (MSL image from [91]).

System Autonomy

The autonomy and thus on-board intelligence of a robotic system can be rated within Sheridan's **ten levels of automation** [86, 92] (see Table 2-1).

Table 2-1: The ten levels of automation as defined by Sheridan [86, 92]

Level	Human/computer task distribution
1	Human makes all decisions and performs all actions
2	Computer offers a complete set of alternatives
3	Computer narrows selection to a few alternatives
4	Computer suggests one alternative
5	Computer executes suggestion after human approval
6	Computer executes automatically if human does not veto within restricted time
7	Computer executes automatically, then mandatorily informs human
8	Computer executes automatically, then informs human only if asked to
9	Computer executes automatically and only informs human if it decides to
10	Computer makes all decisions and performs all actions, ignoring human

A truly autonomous system is therefore void of any human involvement. The automated systems of reality however usually provide the option of **human oversight** [86]. These systems are per definition controlled in **teleoperation**.

Teleoperation Systems

A **teleoperation system** combines the human capabilities of perception and problem-solving with the capabilities of a machine [93]. Such a machine extending a person's sensing and/or manipulation capability across "a barrier of distance, time or inconvenience" [92] is generally referred to as a teleoperator or a **telerobot** [92].

A teleoperation system thus consists of a **human operator** (or just operator for short), a **human-machine interface** (HMI), a **communication link** to bridge the barrier between operator and teleoperator, and the **teleoperator** [94, 95] (see Figure 2-2). The human operator contributes his inherent capabilities of sensory integration, pattern recognition, reasoning, adaptability, problem solving, learning, innovation, improvisation and decision-making [23, 87, 95, 96]. The teleoperator compensates for the human's weaknesses in sensory spectrum, strength, endurance, environmental tolerance, patience, speed, consistency and precision [87].

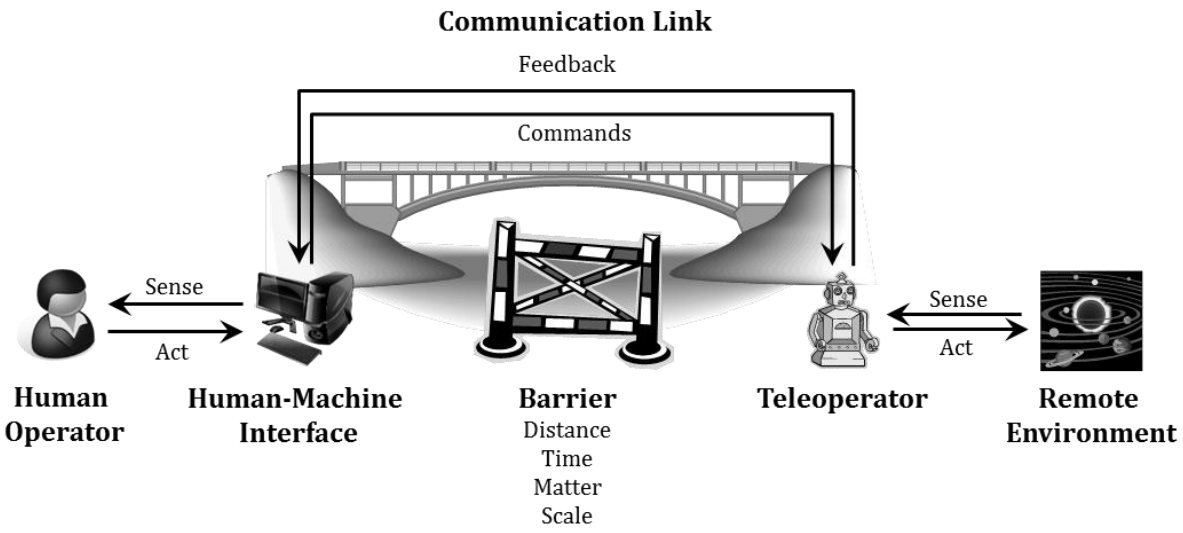

Figure 2-2: Schematic overview of the components of a teleoperation system. The human operator acts in response to sensor information provided by means of the human-machine interfaces (HMI). The HMI transforms his inputs into commands, which are transmitted via the communication link, in order to bridge the distance, time, matter or scale barrier between human operator and teleoperator. Based on the commands, the teleoperator interacts with the remote environment and retransmits sensor feedback to the operator.

A well-balanced teleoperation system utilizes both human operator and teleoperator in their optimum capacities. The human then fuses and interprets multiple sensor data streams, defines strategic goals and plans high-level task sequences to accomplish these goals, while the on-board computer performs closed-loop control like maneuvering, articulation of appendages, or collision avoidance [97]. Experience in military systems has shown that humans have always added the critical margin of performance when being part of the robotic system [96].

The teleoperation mode in which the human operator issues directives for the teleoperator to accomplish in closed loop and then receives a summarized results report is called ***supervisory control*** or ***supervised autonomy*** [92] . Supervised autonomy broadly covers all Sheridan levels between 2 and 8. Four levels of supervised autonomy were for example used on *Orbital Express*, from requiring ground approval before execution to fully automatic execution with ground analysis only in case of failure [55].

One way to improve the performance of a teleoperation system is to increase the teleoperator level of autonomy. This leads to greater system complexity since more sensors are required to gather information about the remote environment, and more processing power is needed to handle the increased amount of information [98]. Another option is to improve the human-machine interaction to show the human operator a more accurate teleoperation environment and so enable him[2] to better bring his capabilities to bear [98]. The ultimate goal of teleoperation interface design is

[2] For reasons of readability, the male singular is used for the operator or pilot throughout this dissertation.
[3] The rival theory for the causes of motion sickness is the postural instability theory. This theory states that situations

therefore to provide the human operator with the capability to act and perform as if he was present at the remote location [99, 100]. This concept, commonly referred to as *telepresence*, would greatly benefit system flexibility [100].

Telepresence

Presence is defined as the ability to move through an environment and manipulate it at will [101]. The term *telepresence* therefore broadly describes being present at a remote location. The exact definition of the term however varies in the technical and psychological disciplines. For robotic systems, telepresence is usually defined as high-fidelity remote control which allows the projection of natural human capabilities to the remote work site [101]. The capability mostly utilized is the human sensory apparatus [97, 102]. Since vision is the dominant sense for perception of the environment, the human operator requires high-quality visual information in order to feel present and to effectively and efficiently complete the remote task [95, 103]. The cameras in telepresence systems are then often configured as anthropomorphic stereo pairs [10]. With such a system ***visual telepresence*** can be achieved [104]. Other modalities such as auditory, tactile or kinesthetic feedback can also be included in order to improve the operator's perception of the remote environment [95]. When the operator receives sufficient sensory cues to be able to successfully conduct remote operations, this is also called ***functional presence*** [105]. Functional presence does not require the operator to have the feeling of actually being situated at the remote location.

The alternative definition of telepresence is a sense of actually being physically present at the remote location [92, 95, 104, 106]. This mental state is also called ***experiential telepresence*** [100].

The definition of telepresence used in this doctoral thesis is clearly that of functional presence. Achieving experiential telepresence in an environment as foreign and hostile as space would be very demanding of the human-machine interface, as well as counterproductive to operator performance, since the very nature of the environment limits astronaut performance. It is therefore preferable to have the operator situated in a familiar, comfortable working environment with a human-machine interface that provides sensory cues in sufficient quantity and quality to enable the operator to accomplish the complex task of rendezvous & docking.

2.2 Applications

Teleoperation systems are commonly used if humans are not able to occupy the physical space of the work environment, if humans would adversely affect the environment, of if human life and health could be compromised by the environment [95]. The classical application areas for teleoperated systems have therefore been space and deep undersea applications, work in nuclear power plant radioactive "hot cells", toxic waste clean-up, telesurgery, long-endurance or high-risk aerial surveillance, disaster site search & rescue, as well as mine-clearing and bomb disposal [95, 104, 106, 107].

All **deep-space probes** and all planetary probes and rovers like the *Lunokhods*, the *Vikings*, the *Mars Exploration Rovers*, *Mars Phoenix Lander*, as well as the *Mars Science Laboratory*, have essentially been telerobots [94, 108, 109].

Civilian ground telerobots perform **search & rescue** duties after disasters like landslides, earth quakes, Tsunamis or terrorist attacks like on September 11, 2001, or conduct damage assessments in toxic or radioactive environments like Chernobyl or Fukushima [110].

Military **unmanned ground vehicles** (UGVs) are used for mine clearing, explosives disposal, and increasingly also in combat operations [90, 110].

Unmanned aerial vehicles (UAVs) in sizes from birds to passenger planes are used to survey wild fires on one end of the spectrum, to military reconnaissance, target acquisition and actual combat on the other end [90, 110].

Unmanned underwater vehicles (UUVs) exist in sizes from micro UUVs lighter than 3 kg to heavy work class UUVS equipped with two and more heavy manipulators and capable of operating at depths of up to 3500 m [111]. They are extensively used in autonomous or remotely operated vehicle (ROV) configurations for deep ocean science, environmental monitoring and inspection, military applications, but above all in the natural gas and oil industry [110, 112]. Drill-heads, pipelines and oil platforms are constructed, inspected and maintained often solely by ROVs, and in contingencies such as the *Deepwater Horizon* oil spill in 2010, ROVs are the primary tool of damage control and mitigation [94, 113]. These tasks require high dexterity of the teleoperator and considerable skills and training of the human operators, who usually teleoperate the “free-flying” UUV via a fiber-optic tether. Figure 2-3 shows typical representatives of UUVs, UAVs and UGVs.

Figure 2-3: Typical representatives of the major mobile telerobotic classes. From left to right: Oceaneering Millenium Plus ROV at work at an undersea oil well [114], General Atomics Reaper UAV [115], iRobot Warrior UGV [116] disarming an IED.

Analogies to OOS Robots

The requirements placed on telerobot **dexterity** and teleoperation system **transparency** of OOS activities are certainly far beyond the capabilities of heritage space telerobotic systems. The fields of ground, air and underwater robotics however provide many examples for highly complex teleoperation tasks under similar environmental conditions as encountered by an operational OOS system. The solutions developed for these fields are therefore often applicable to the problems of OOS.

The **operation environment** of UUVs is in many respects comparable to the orbital worksite [117, 118]. A free-floating UUV must constantly be navigated and control in all six degrees of freedom [117, 119]. When manipulators are used, the disturbance torque perturbs the platform vehicle from its intended attitude, impeding station-keeping and reducing end-effector precision and accuracy [120]. Coordinated control schemes using dynamic models of the underwater robotic system are therefore needed to account for the coupling effects [120]. Other than dynamic models of space systems, these must also include hydrodynamic parameter uncertainties, ocean currents, as well as the effect of hydrodynamics of each link of the manipulator on vehicle motion [112]. The operator's awareness of the telerobot's surroundings is furthermore impeded by the oftentimes poor quality of video images, due to color distortion by the water and highly unfamiliar illumination conditions [117, 120]. The worksite environment is also often unknown, due to the lack of detailed, accurate and current maps of the sea floor [117]. This situation is reminiscent of OOS operations on an uncooperative target object.

The similarity of the underwater realm and space has therefore not only been used for astronaut training, but also during the development of operating procedures for *Deep Submergence Rescue Vehicles* (DSRVs) for which the rendezvous & docking procedures of the *Gemini* project were used as a prototype [118, 119]. UUVs have also been used in experimental scenarios for space and planetary exploration. In 1993, NASA guided the *Telepresence Remotely Operated Vehicle* (TROV) during exploratory trips in the Ross ice sea, Antarctica, in functional telepresence via a data relay satellite (Intelsat 178W) from NASA Ames Spaceflight Center [102, 121]. While the tasks accomplished by TROV were not complex, the system nonetheless proved the feasibility of telepresent operation via a geostationary data relay satellite and thus under the impact of the associated time delay.

Another class of vehicles that operate under similar **operational constraints** as an operational OOS system, albeit not with comparable task complexities, is formed by modern UAVs. In the skies over current military theaters of operations, multitudes of UAVs are used for reconnaissance, target acquisition and actual combat. While take-off and landing is usually commanded locally, surveillance, acquisition and target engagement is controlled in case of the USAF from Nellis Air Force Base near Las Vegas, Nevada [122]. The commands are then routed via fiber-optic cables to communication hubs in Europe and then via data relay satellites to the skies over Afghanistan, Iraq or other theatres [90, 110]. For this purpose these UAVs are equipped with steerable satellite antennas to close the communication chain.

2.3 Limitations

In order to achieve the high degree of control required for telepresence systems, the human-machine interface must be ***transparent***. Factors contributing to interface transparency are display quality, consistency of the presentation of the environment, the ability of the operator to interact with the environment and receive feedback, as well as clarity of causal relationships between user actions and the reactions in the remote environment [100]. Due to the demand for high transparen-

cy, telepresence systems are substantially afflicted by the general limitations of teleoperation systems: limited sensory information, degraded depth perception, time delay, sensor data fusion and integration, confidence in sensor data, knowledge of teleoperator activity, and failure detection [96, 123, 124].

The problem of limited sensory information is created by the limited availability of sensors on the telerobot, the restricted fields of regard of most sensor types, the lack of proprioceptive information about the teleoperator and its environment, as well as the limited bandwidth of the communication channel usually resulting in low definition and degraded quality of the sensor data presented to the human operator [105, 125]. This problem has been referred to as the ***keyhole effect*** [123] or as driving while "looking through a straw" [126].

Visual Information

Humans derive over 90% of sensory information from **visual stimuli** [111]. This is referred to as *visual dominance* [127]. The human visual system is capable of full, precise mapping in three dimensions and typically overrides auditory and somatosensory spatial information [127]. Most orientation cues are thereby derived from ambient vision, while focal vision provides object recognition and identification [127].

Low quality visual information and the increased scene distortion associated with video compression not only impede object detection and identification, they can also lead to increased cognitive workload and motion sickness symptoms [123]. In addition, a **narrow field of view** (FOV) can also lead to the loss of important distance cues, thereby degrading depth perception. Bandwidth limitations often force teleoperation systems to rely on **monocular vision**. In this case the operator must rely on depth cues like interposition, relative object size, relative object or texture density, light and shadow, angular elevation or motion perspective [106, 127–129]. In an unfamiliar environment depth perception can thus be challenging because of a lack of size cues. **Stereo vision** therefore facilitates navigation in unfamiliar environments by enhancing operator performance in depth perception and obstacle detection and identification [123]. The price for this performance increase is increased **bandwidth requirements** for real binocular stereo vision and increased operator stress ratings and motion sickness symptoms for artificially induced stereo vision [123].

A further impediment to depth and egomotion perception is a reduced **frame rate** of the visual channel [123]. Studies have shown that for operating UAVs, the frame rate of the video feed is more important for object identification and tracking tasks than image resolution [130]. A similar result was found for manipulation tasks [130]. Below a frame rate of 5 frames per second (fps), a loss of presence occurs. The operator dissociates from the low update rate and views the video as a series of screenshots [130]. An update rate of 10 fps is generally considered the minimum for effective and efficient teleoperation [92, 123, 130].

Signal Delays

Beyond the restrictions on sensory information, the **time delay** inherent in long-distance communication channels also severely impacts operator performance. Humans are capable of detecting latencies as low as 10-20 ms [123]. The total system latencies in complex teleoperation systems can reach up to multiple seconds, which substantially degrades performance. The higher the communication system latency, the higher is the level of automation required of the system in order to enable it to accomplish its task. The issue of communication time delays, which are of premier significance for space telerobotic systems, will be discussed in more detail in Section 3.1.

Situation Awareness

The limitations of teleoperation systems described above combine to limit the level of **situation awareness** (SA) the operator can achieve [117, 131], as well as to increase the **mental workload** placed on the operator [124, 132]. This workload is highest in direct control modes (Sheridan level 1), since the operator is required to divide his cognitive resources between sending commands to the teleoperator and interpreting returning information [133]. Indirect control, i.e. a higher level of teleoperator autonomy, reduces the operator workload but can also lead to reduced SA because active human involvement in teleoperator action is removed [133].

Situation awareness is defined as "[…] the perception of elements in the environment within a volume of time and space, the comprehension of their meaning, and the projection of their status in the near future" [134]. In other words, SA means being aware of what is happening around oneself and understanding what the occurring events mean with respect to current and future goals [127]. SA is therefore the result of a chain of cognitive processes dealing with the perception of the world surrounding a person and the interpretation of those perceptions [100].

For general robotics systems, SA therefore consists of **location awareness** (allows user to locate robot within the scenario) and **surroundings awareness** (recognition of immediate environment of the robot, which is essential for obstacle avoidance)[135]. In terms of navigation, which is of primary interest for this thesis, SA means determination of the actual **chaser position**, determination of the **target position**, and path and resource usage **planning** [136]. This subset of SA is in literature also referred to as ***spatial awareness*** or ***hazard awareness*** [137].

The main challenge of gaining and maintaining SA in teleoperation is that humans are used to a wide FOV (provided by the human eyes), coupled to a fast and flexible scanning system (the human neck). This allows them to quickly generate an accurate model of their surroundings within which to operate the vehicle [10]. This restriction leads to the fact that 30% of teleoperation time is commonly spent on gaining and maintaining SA [138, 139], thus severely limiting task performance. The use of advanced user interfaces and displays such as discussed in Section 2.4 can therefore increase operator SA and performance [138].

In order to overcome the general limitations of teleoperation, the human-machine interface must be designed to compensate for the weaknesses in teleoperator equipment and communication link

bandwidth. The overall goal is to increase operator SA while at the same time reduce his cognitive as well as physical workload. If a high level of SA in the remote environment is achieved, accompanied by a loss of SA in the local environment, telepresence as defined above is achieved [100].

2.4 Human-Machine Interfaces

The **human-machine interface** provides the human user of any technical system with the means to **interact** with its mechanical and electronic components. The HMI transforms the data received from the mechanical and electronic system components into output comprehensible for the human visual, auditory and tactile senses. At the same time, it provides the user with input options to change the system state. An example for an HMI encountered in everyday life is the combination of monitor, keyboard and mouse of personal computers (PCs). The monitor translates the digital electronics signals of the computer into graphical or textual visual output. The keyboard and mouse allow the user to react to the displayed data and to change the processes running on the computer.

A human-machine teleoperation interface thus consists of **data displays** and **control interfaces**, allowing the human operator to monitor and interpret sensor data from the teleoperator, and to transmit commands to the teleoperator.

2.4.1 Basic HMI Design

The display must be designed in order to support the operator in making **decisions**. The information content must be presented in a way that allows easy and quick **acquisition**, as well as efficient **analysis** [140]. The goal is for the display to present the operator with appropriate imagery and sufficient data to enable SA, realtime control and payload operations [96, 141]. In many situations, operators are not provided the data essential for gaining and/or maintaining SA, while at the same time they must mentally integrate a large amount of dispensable information about the mission state displayed over several monitors [133]. The displayed realtime data must be appropriate to enable the operator to transition seamlessly between supervisory and teleoperation control modes without significant loss of SA [96]. The format of the data must avoid any cognition conflict or monopolization of **mental resources** [96].

Control Functionality

The control and data input devices provided to the operator must be appropriate for **remote control** as well as subsystem and payload operation tasks [96]. Manual **control devices** should ideally only have a single function and must be easily located, grasped and manipulated [96]. Information and control devices needed for a particular set of activities should be situated within close proximity of each other and ideally be available with less than two key presses [96]. The HMI should furthermore support both high-level and low-level commands, to allow the operator maximum **flexibility** in sending efficient command sequences [10]. Rapid **feedback** to control inputs is needed to let the operator know whether his commands have been acknowledged, whether the actions are

performed properly or whether problems are occurring [96, 133]. An ideal display will furthermore attempt to **predict** the future results of an operator's commands by displaying possible constraint violations or predict the probability of a certain outcome [140]. This would enhance the probability of mission success.

The importance of HMI design does not diminish with increasing levels of teleoperator autonomy. Independently of a robot's autonomous operation capability, the human operator must still know where the teleoperator is, what it is doing, and how it is doing this [110]. However, as robots become more autonomous, the focus of the interfaces shifts from actual control to **monitoring** and **diagnosis** [110]. Nonetheless the quality of the HMI determines the quality of the system performance. A good interface can help the operator to gain and maintain SA, enhance goal setting under dynamic vehicle and mission conditions, as well as optimize human analytical processes and decision-making [96]. An HMI also has the potential of negatively influencing operator performance and thus degrading mission effectiveness [99].

Human Error

The HMI therefore has influence on the occurrence and magnitude of **human error**. In a badly designed HMI, the complex recognition of information during high-stress conditions increases the operator's mental and physical workload and thus also increases the likelihood of misrecognition and misoperation [142].This statement is supported by the statistics of **UAV mishaps**. UAVs suffer 100 times more mishaps per 1000 flight hours than manned aircraft [127]. More than half of these mishaps are attributed to problems with **human-systems integration** [138].

Typical Designs

A typical control station design presents the operator with a **sensor view** and/or **telemetry data** transmitted from the teleoperator, the **health status** of the teleoperator, a **map display** to maintain SA and facilitate navigation, as well as a history of the commands issued to the teleoperator [123]. HMIs have therefore been **largely unchanged** since the invention of underwater robotics in the 1970s [143]. Figure 2-4 shows examples of common control station layouts.

Current HMI designs present the operator with **difficult-to-interpret** camera imagery, as well as numeric robot telemetry data. The data is not provided in any **integrated** or intuitively **accessible** form [127]. The operator is thus overburdened with detailed, low-level data and must continuously scan the interface and cognitively integrate the data into a **mental model** of the vehicle's state and the situation [127]. A display providing direct presentations of high-level vehicle state projections could therefore greatly benefit operator SA [127].

Figure 2-4: Exemplary views of unmanned vehicle control stations. Left image shows Predator UAV control station in 2007 [144]. Right image shows science UUV control station in 2009 [145].

2.4.2 Visual Displays

Due to the human's **visual dominance**, the majority of information is conveyed visually, including digital values, status displays, 2D computer simulations, and camera images [142]. These displays are mostly not designed for operator immersion. The human generally has a horizontal FOV of 180°, and a vertical FOV of 120°. For operator immersion in the remote environment, a minimum horizontal FOV of 80° is adequate [146], while the sensation of reality usually saturates at around 100° horizontal FOV [147]. The spatial resolution of an immersive display is desired to be 60 pixels per degree [147]. These FOVs and resolutions cannot be realized using common on-board cameras and displays.

Field-of-View Compensation

The **limited FOV** of a camera can be overcome by using a **pan-tilt camera head**. Such a camera head is most useful in situations in which significant visual information exists to the side of the teleoperator, but if it is inefficient or difficult to rotate the robot to see it [126]. Using a camera that is controlled independently of the vehicle motion increases the operator's immersion and thus sense of telepresence [124]. At the same time the adjustable camera orientation can lead to **confusion** about the state of the robot and the orientation of the camera, thus increasing operator mental workload in navigation and delay compensation and thus resulting in poor SA [124, 126]. The difference between camera view point and expected motion can furthermore induce **simulator sickness** [124].

Pan-tilt cameras are most effective when combined with a **head tracker** in the HMI. Experiments have shown head-aimed vision to increase teleoperation mission performance by between 200% and 400% [131]. Head tracking thus increases operator performance more than stereovision or an increased camera FOV [130]. The cost of this performance increase is additional time delays between the motion of the head and the motion of the video, which can result in **loss of visual stability** and simulator sickness symptoms [96, 130]. This delay results from the need to track the head

motion and translate it into sensor motion, the update rate of the tracker, and the refresh rate of the display [148].

Head-Mounted Displays

Head tracking is usually combined with **head-mounted displays** (HMDs). An HMD is basically a pair of small LCD monitors that are suspended like goggles in front of the operator's eyes. HMDs thus offer an egocentric augmented reality display throughout the full FOV and therefore potentially offer **increased spatial awareness** and SA [148]. HMDs have the potential of providing operators with meaningful cues for SA, good workspace visibility and vehicle behavior feedback for effective performance [96]. In control studies of unmanned air, ground and underwater systems, HMDs were shown to have a positive impact on some control tasks. Experiments for control of helicopter UAVs using omni-directional cameras demonstrated that HMDs promote operator immersion, thus resulting in an enhanced feeling of telepresence and in quicker and more accurate task completion [96]. In precision target identification, designation and prosecution tasks, however, fixed display monitors with joystick-controlled cameras resulted in higher accuracy, shorter search times, lower workload and higher SA ratings [96]. In addition, all operators using HMDs complained of **discomfort** and simulator sickness symptoms like nausea, disorientation and eyestrain when using the HMD for extended periods of time [96]. An HMD can therefore actually increase operator **visual workload**, induce simulator sickness and **disorientation**, and decrease SA [148].

Stereo Vision

An advantage of HMDs is their natural capability to be used for **stereoscopic vision**, also referred to as stereo vision. Compared to monoscopic vision, stereovision facilitates remote manipulation tasks that involve ballistic movement, recognition of unfamiliar scenes, analysis of three-dimensionally complex visual scenes and the accurate placement of manipulators or tools within these scenes [123]. Stereovision is furthermore useful when image quality, task structure and predictability, user experience, and manipulator dexterity are suboptimal [123]. Higher levels of stereopsis have proved to be helpful to determine depth in teleoperation scenarios [130]. Stereovision is therefore ideally suited for the complex tasks of telerobotic OOS, including rendezvous & docking.

Human operators generally prefer stereoscopic displays over monocular vision [123]. In general, the advantage of stereoscopic displays in depth perception becomes greater with larger stereopsis, i.e. larger inter-camera distance [130]. Since the amount of stereopsis a human is able to fuse is limited, the best performance in depth-matching is achieved when the **inter-camera distance** is still less than the **inter-ocular distance** [123]. An ideal stereovision system uses a camera that recreates the functionality of the human vision system. Such a camera pair is able to adjust camera **convergence** and **focus**, in order for the convergence point and focal distance to remain on the same plane [113]. To maintain camera convergence, **range measurements** to the target object are necessary, requiring appropriate on-board sensors [113]. Experiments with UUVs have shown such camera systems to be effective in improving the visual perception [113].

The improved depth perception of stereovision systems must be traded off with their inherent disadvantages: increased **communication bandwidth** demand, system complexity, as well as a high incidence of **user discomfort** [146]. Artificially induced binocular stereo vision has the tendency to cause increased **operator stress** ratings, as well as simulator sickness symptoms [123]. In corresponding experiments, the majority of test subjects complained of increased **eyestrain**, ghosting images and a loss of resolution, making the displayed environment appear fuzzy and less real [146]. Eyestrain and the occurrence of simulator sickness are less when using stereoscopic displays with **shutter glasses**, instead of HMDs [130]. However, using a setup with a fixed monitor and shutter glasses limits the possible range of head tracking, therefore only minor head rotations and translations are allowed [130].

2.4.3 Data Fusion

The **fusion** of sensor information into a comprehensible data product is critical for HMI design. Sensor fusion is defined as the process of **collecting** data, **combining** it through a variety of methods and with a variety of sensing technologies, and **presenting** it as an integrated product, either to a human operator or to a machine [149]. The general idea behind this process is that combining the individual strands of data results in a richer, more intelligible output that is functionally greater than the sum of its parts [149]. Sensor fusion has long been used to improve automatic mapping processes, but can also be used to create capable and compelling user HMIs, enabling better understanding of the remote environment [150]. In military aviation, sensor fusion is used to combine live information from sensors and stored information from databases in order to improve cockpit efficiency during target acquisition and tracking, tasks which require high levels of SA and cognitive decision-making [150]. Figure 2-5 depicts an augmented reality sensor fusion display used for controlling military UAVs.

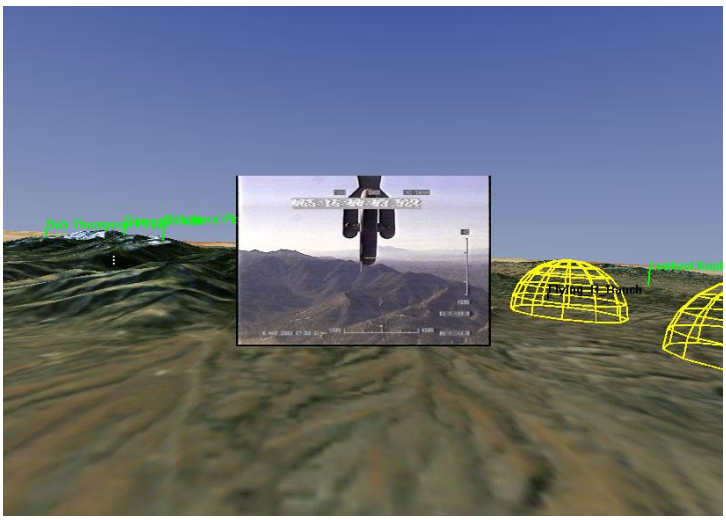

Figure 2-5: Augmented Reality display used for UAV operations [125, p.224]. The real camera view is surrounded by synthetic terrain imagery. Important information such as mountain peaks or danger zones are marked within the synthetic environment. Reproduced with permission of Gloria Calhoun (Air Force Research Laboratory) and the International Society for Optics and Photonics.

Sensor fusion can also be used in civil aviation to create enhanced or **synthetic vision** systems [150]. These would enhance the pilots' ability to detect runway features and incursions during landing, as well as obstacles and traffic in taxis, and would enable air traffic controllers to better operate in conditions of restricted visibility, e.g. through clouds or fog [150].

Augmented and Virtual Reality

Such systems providing artificially created visual information alongside realtime video data are called synthetic vision systems, **augmented reality** (AR) systems, or with growing artificial content, **virtual reality** (VR) systems. These systems can potentially overcome some of the perceptional limitations of teleoperation systems by ameliorating video characteristics and enhancing operator image interpretation [127] . In a 3D VR display, the operational space can be visualized synthetically, merging visualization data from multiple sources [133]. Within this display, the operator perspective can be changed between internal and external vantage points, thus providing a spatial perspective beyond the immediate vehicle camera view [121]. Vehicle state information like attitude, flight path or velocity vectors as well as environmental information like danger zones or flight paths of surrounding objects can be directly integrated into the main display [133]. In order for the VR system to be beneficial to the operator, an extremely accurate **world model** as well as highly accurate **CAD models** of the surrounding objects are required [141]. Otherwise, VR displays can be useless or actually damaging, by causing time-consuming and confusing **conflicts** between virtual imagery and realtime video [141]. In addition to this problem, too much visual information can also overload the operator with unimportant information [124], thus actually decreasing his SA. If no accurate model of the work environment is available, VR displays are of limited use [113] and can be detrimental. This is exactly the kind of operating environment of most OOS missions to uncooperative client satellites, and of all space debris removal missions.

2.4.4 Time Delay Compensation

In addition to serve as a means to enhance the operator SA of the remote environment, AR and VR displays can also to some degree compensate for low bandwidth or long **time delay** in the communication channel [121]. Due to these delays, the human operator is always late in perceiving and controlling the teleoperator. He is therefore unable to generate an accurate mental representation of the remote situation [106]. This limitation can be countered by the use of **predictive displays** or **commanded displays** [2, 124].

Predictive Displays

A predictive display is a mathematical simulation of the system behavior, propagated forward in time to generate a prediction of system movement over the time delay [151]. A predictive display thus requires an **accurate model** of the teleoperated system as well as the environmental parameters acting upon it. Creating a predictive display of an unknown environment is therefore a **considerable challenge**. A commanded display, on the other hand, merely shows the position of the teleoperator as commanded, without any mathematical modeling of the system behavior [151].

Predictive displays have been shown to reduce **task completion times** by 50% to 150%, compared to operator performance using live video alone [123]. Studies conducted during the *Ranger* program have furthermore shown that predictive displays provide 15% to 25% improvement in **task performance** when working with 1.5 s, 3 s and 5 s time delays [151].

Commanded Displays

Extensive studies concerning the utility of commanded displays have been conducted and published as part of the *Ranger* research and development effort. The results show that commanded displays are effective in reducing the increased task completion time due to communication time delays by 91% at 1.5 s delay, by 88% at 3 s delay and by 84% at 6 s delay [130] . The commanded display furthermore also reduced the task completion time by 22% without the presence of time delay. The reason for this is that the commanded display is used by the operators as a **planning tool** for more efficient manipulation [130] . In addition to reducing completion times, the use of a commanded display also reduced the **number of collisions** in a peg-in-hole task by 95% [130] . These studies showed that commanded displays are overall **twice as effective** as predictive displays in alleviating the effects of time delays on teleoperation performance [130] .

2.4.5 HMIs for Space Teleoperation

The teleoperation HMIs in use are a tradeoff between the various capabilities and limitations of representations and display elements stated above. The telepresent underwater vehicle TROV used the Virtual Environment Vehicle Interface (VEVI) for teleoperation via relay satellite, with a stereo monitor or a HMD displaying live stereo video or the off-line generated 3D model of the ROV and its environment [102]. The *Ranger* operator interface provided the operator with a mix of live video, VR simulations and control station panels. The stereo video was streamed from external and onboard cameras to stereo monitors using LCD shutter glasses [76]. The VR simulations allowed the operator to visualize the telerobot in its environment, displaying things that could never be observed from live video. The display offers multiple windows to allow simultaneous viewing of **different views**, while each view can be freely configured to allow the operator to move his vantage point freely about the virtual environment and to adjust the field of view [152]. Primary views are attached to each manipulator arm, the vehicle body and the worksite to improve SA by providing several frames of reference [152]. Telemetry data is continuously used to update the VR model and highlight changed system states to direct the operator's attention to important information [152]. Virtual graphics filters can be used to observe power consumption, temperature values and the global status for each manipulator joint by providing gradient of colors to indicate various levels. Within the VR display, the operator can furthermore produce a virtual cockpit with gauges, controls and sensor packages being placed in various positions on the display [76]. In addition, the operator uses two **hand controllers** to directly control the robot [152]. Figure 2-6 provides an overview of the Ranger operator control station and the VR control display.

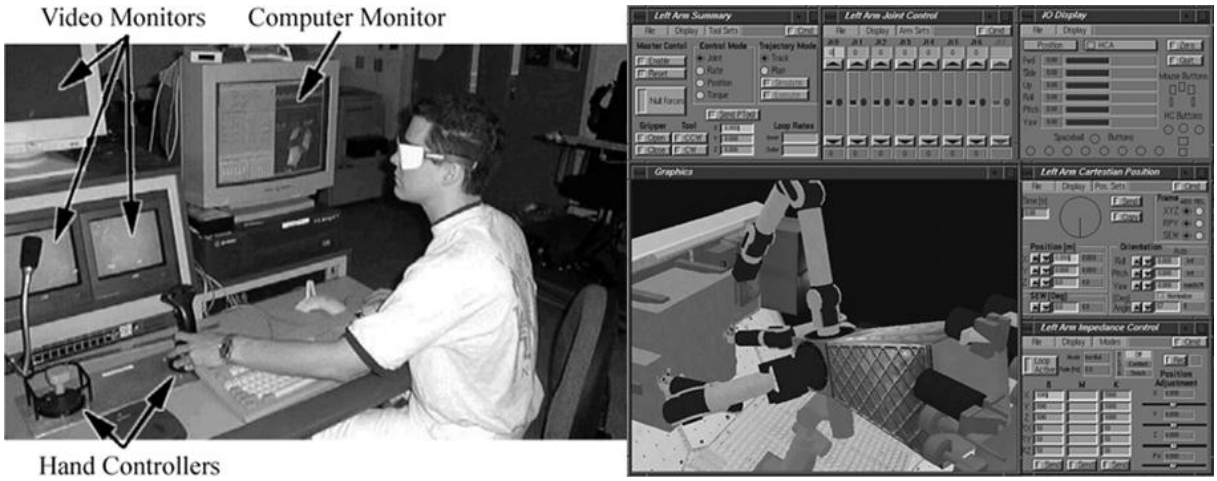

Figure 2-6: The Ranger operator station and the virtual control interface [152, p. 50, fig. 2 and3]. Reproduced with kind permission of Springer Science and Business Media.

Similar AR and VR user interfaces were also used for *ETS-VII* [153], as well as for the ROTEX robotic demonstration mission aboard the *Space Shuttle* [48].

While not a teleoperation HMI per se, a system sharing many characteristics was introduced aboard the *Space Shuttle* to facilitate rendezvous & docking operations. It is therefore highly relevant for this research. This Rendezvous and Proximity Operations Program (RPOP) is run on a laptop computer aboard the *Shuttle* to display relative position and attitude information [154, 155]. The *Shuttle's* **approach trajectory** in relation to the docking port is provided in a **graphical representation** (see Figure 2-7).

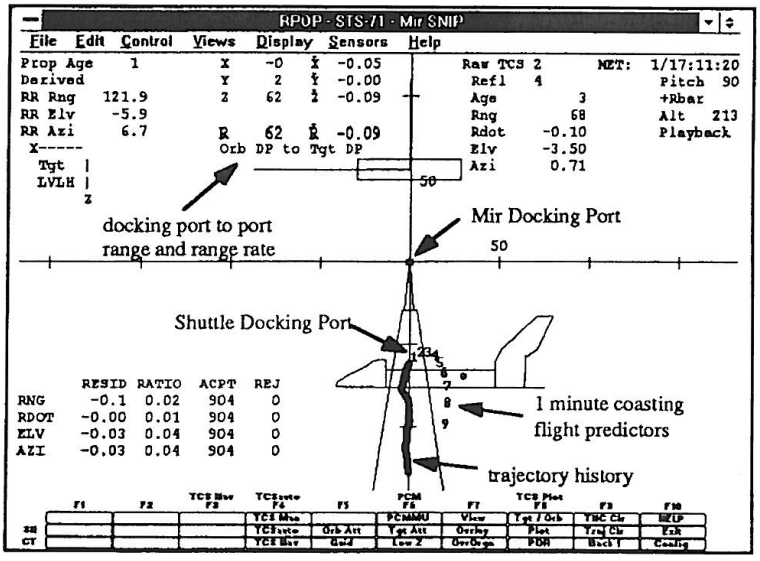

Figure 2-7: The Rendezvous and Proximity Operation Program (RPOP) run on a laptop in the Shuttle cockpit to facilitate the control of the final approach during rendezvous & docking. Range and range rate measurements, as well as attitude information is provided in numerical form, while the approach trajectory in relation to a docking port is represented graphically [155, p. 447]. Reproduced with permission of the American Astronautical Society Publications Office.

2.5 Spatial Disorientation and Simulator Sickness

A problem shared by all teleoperation HMIs is that of **visual-vestibular mismatch** and **spatial disorientation**, often leading to symptoms of **simulator sickness**. UAV operators mostly suffer from visual-vestibular mismatch, because their focal vision receives cues from the displays conveying motion, while ambient vision, vestibular and non-vestibular proprioceptive cues convey that the operator is at rest [127] . This can lead to spatial disorientation, reduced SA and simulator sickness symptoms. In rare cases, the effects of spatial disorientation can incapacitate the operator [127].

Spatial Disorientation

Spatial disorientation (SD) is the failure to correctly sense the vehicle's attitude, motion and/or position within a reference frame [127] . Frequent disorientation thus hinders the development of SA regarding the location of the robotic system [127] . Literature defines two types of SD: SD unrecognized or recognized by the operator. In unrecognized SD, the operator is unaware of changes in ownship motion or attitude. This is mostly caused by sub-threshold motion or inattention and accounts for about 90% of all SD-related accidents [127]. Recognized SD manifests itself in a noticeable difference between actual ownship motion or attitude and any one of the visual, auditory, tactile or vestibular senses [127].

Simulator Sickness

This sensory conflict or cue conflict is theorized to be the primary cause for **motion sickness** and **simulator sickness** [156, 157]. According to the cue conflict theory, motion sickness ensues when the sensory information about body motion provided by the eyes, the vestibular apparatus and other senses conflicts with the inputs that the central nervous system expects to receive [156][3]. This causes head ache, drowsiness, mental disorientation, pallor, cold sweating, nausea and eventually vomiting [156]. Simulator sickness is a form of motion sickness that does not require true motion of the body to create cue conflicts, but rather a visually induced sense of self-motion, called ***vection*** [156] . Vection is caused by the eyes detecting a change of position or a velocity in the periphery of the visual field. When the entire field moves (i.e. in the presence of high *visual flow*), subjects soon begin to feel they are moving themselves instead of the scenery around them. This is vection. If vection and the other senses conflict, motion sickness signs and symptoms can be the result, plus another major effect of simulator exposure: eye strain [157]. The incidence of simulator sickness is therefore dependent on the level, detail and density present in the simulator system [156] . Visual flow is mainly perceived by **peripheral vision**. A minimum FOV of 60° is therefore necessary to experience a sensation of motion exclusively from visual information. A **wide-angle display** therefore means both higher operator immersion and higher probability of incidence of

[3] The rival theory for the causes of motion sickness is the postural instability theory. This theory states that situations that produce motion sickness are unfamiliar to the subject. This leads to an inability to maintain postural control, which in turn causes motion sickness until the subject adapts to the new motion [156] .

simulator sickness symptoms, both brought along by vection. Another factor contributing to high visual flow is the maneuver intensity and velocity in the simulation. **Rapid maneuvering** causes high velocities of the objects in the environment. Since this is accompanied by no tactile or vestibular cues, cue conflict can ensue. Other factors are stereoscopy, display flicker, time delays and position tracking errors. Kolasinski [157] provides a detailed discussion of the signs and symptoms of simulator sickness, as well as their causes.

Simulator sickness must therefore be a **prime consideration** when designing a simulation or AR/VR system. In the experimental setup to be described in this doctoral thesis, neither HMDs nor a stereovision system are used. The video streams and graphical overlays are projected onto a planar 1.92 m x 1.05 m screen with 1280 x 720 pixels resolution, viewed from a distance of approx. 1.5 m. This generates a FOV of about 64°, which is barely sufficient for vection to occur. The visual scene displayed however contains little visual flow, since the object density of the final approach and docking scenario is low, as are the associated rotation rates and translation velocities. Therefore no occurrence of simulator sickness was expected, nor was any incident noticed during the evaluation experiments.

2.6 Summary

The use of telerobotic systems is common in the air, ground and underwater domains. The tasks accomplished by ground and underwater systems are in their complexity comparable to OOS operations. The communication links used for UAV control are in their capabilities and limitations similar to the links used for space teleoperation. There exists therefore no reason to expect the teleoperation of OOS tasks, especially rendezvous & docking and proximity operations, not to be feasible.

The HMIs used in these fields of telerobotics furthermore contain important lessons for the design of OOS operator interfaces. This concerns primarily the suitability of different display methods and modalities for high immersion and SA and low susceptibility to spatial disorientation and simulator sickness, as well as the use of AR and VR elements to deal with the effects of time delays in the system.

The **use of HMDs is not practical** for space teleoperation systems, because the long delay between head motion and motion of the camera will result in operator discomfort and possibly in simulator sickness symptoms.

Stereoscopic cameras are of limited value during the final approach and docking phase of an OOS mission. While they would greatly improve depth perception by the operator, they would also need to be designed to operate from far range to very close range. This can only be accomplished by using multiple stereoscopic cameras with different camera baseline, or by a system that mimics the human eyes' capability of convergence and focus. Such a camera system would be very complex and require precise pointing mechanisms, which are hard to qualify for the harsh conditions of the orbital environment.

VR and AR systems can be used to increase the amount of information available to the operator and to increase his SA. However, in the case of rendezvous & docking to an uncooperative target, the amount of information available about the target object might **not be sufficient to create an accurate virtual model**. And as it was discussed above, an inaccurate VR representation can be worse than no VR at all.

3 Space Environment

The major challenge for space telerobotics as compared to terrestrial applications is the **orbital operating environment**. It differs in many critical characteristics from Earth's air, land and sea environments. The main differences from a teleoperation perspective are the long distances to be bridged by the communications link, and thus the resulting signal travel delays, and the fact that Earth's environments are familiar to the operator from firsthand experience, whereas space is foreign in a number of aspects.

These peculiarities of the orbital environment are addressed in the following sections.

The **time delays** inherent in any teleoperation scenario were shown in Section 2.3 to be one of the major inhibitions to task performance of the teleoperation system. While the effects of the delay can be alleviated to some extent by HMI design, the delays must nonetheless be reduced to a minimum in order to achieve acceptable task effectiveness, efficiency, as well as safety. The main source of delay in space teleoperation is the **communication link**, introducing long signal travel delays due to the large distances between the system components.

While these delays affect the act of teleoperation per se, and thus in any environment, operator performance is further degraded by the characteristics of the **space environment**. On Earth, the operator knows about moving and working on ground, in the air and in water from everyday experience. He therefore instinctively understands the effects his commands will have on the motion of the vehicle and he will be able to monitor the effects relying on natural references in the environment. At the same time, the environment serves to stabilize the system behavior. This is not the case in space, as will be discussed in this chapter.

This chapter will provide a general overview over the effects of time delay on the operator as well as on system performance. It will then proceed to explore the different options existing for a space teleoperation communication chain to create a bridge between terrestrial and space applications. The final four sections will then focus on the characteristics of the orbital environment that have direct and special impact on teleoperated OOS system: **relative motion** in the involved coordinate systems, **spacecraft dynamics**, available **references** in the environment, as well as **lighting conditions** during OOS operations.

This discussion about the orbital environment ignores the environmental parameters that challenge every space system, like gravitational disturbances, electromagnetic and particle radiation, drag due to residual atmosphere, and thermal issues. An overview of the general space environment can be found in [158–160].

3.1 Roundtrip Time Delay

The time delays encountered in teleoperation can be classified into four distinct areas [161] (see Table 3-1).

Table 3-1: Classification of the behavior of teleoperation systems according to the roundtrip time delay [161].

Time Delay [s]	Teleoperation System Behavior
< 0.1 s	true realtime
< 1.0 s	near realtime
< 10 s	virtual realtime
> 10 s	autonomy

In the ***true realtime*** and ***near realtime*** domains, the operator feels a direct context between control inputs and the system response. He therefore performs the teleoperation tasks continuously. At time delays around 1 s, operators switch their control strategy from continuous commanding and compensating for delay effects towards a ***move and wait*** **strategy** in order to not suffer a loss of control [152, 162, 163]. If the time delay is in the range of several seconds, therefore within the ***virtual realtime*** domain, operators transmit a whole series of commands before awaiting the results and issuing the next command series [163]. While this approach allows to trade time for accuracy in the performance of tasks under delay [162], it significantly increases the time demand for teleoperation tasks [163], is very inefficient in terms of teleoperator usage, and can cause operator fatigue [10].

Impact of Time Delay

This tendency towards *move and wait* is evident in all teleoperation applications. The impact of time delay upon operator performance however differs in its details between different applications.

In teleoperation systems using **bilateral control**, i.e. a control loop with haptic feedback from the teleoperator to the human operator, time delay in the communication channel can cause the system to become **unstable** [164, 165]. Stoll found in his doctoral research [161] that roundtrip delays in the haptic and visual channels substantially **decrease task performance** and the **feeling of telepresence**. This effect is aggravated if the delays are variable. Operators also systematically tend to overestimate the delay, which furthermore impacts their performance. Stoll had test participants grab a servicing target object and perform a bayonet closure opening task under time delays of 0 s and 0.622 s. The long delay was generated by transmitting the haptic feedback data over the DRS *Artemis*. In order to represent the delay in the communication chain from a ground station via a DRS to an OOS vehicle and back, the feedback signal was transmitted via *Artemis* to its control station in Redu, Belgium, and then mirrored back via *Artemis* to the ground station in Munich. Using this experiment setup, Stoll determined that the mean completion time for the grabbing task tripled

between 0 s and 0.622 s delay, while the bayonet closure opening task time increased to 360%. Despite these performance reductions, participants were able to complete their assigned tasks and thus Stoll proved that telepresent OOS operations are feasible via a DRS communication chain and the associated roundtrip time delay of over 0.6 s.

Similar experiments were conducted during the *Ranger* program, albeit without haptic feedback. When positioning a 2-DOF manipulator, **completion times increased** with time delay. Compared to zero delay, the increase was 260% at 1.5 s of delay, and 580% at 6 s delay [151]. It was also determined that a short, variable delay can be more detrimental to operator performance than a longer but fixed delay [130].

Experiments on human-in-the-loop UGV control showed no noticeable effect of time delays on user performance between 0 s and 0.5 s, followed by a sharp decline in performance between 0.5 s and 1.0 s [96]. These studies also produced the interesting result that the impact on performance not only depends on the time delay, but also on the **control modalities**. So it was found that update delays following head movement in a head-tracking setup had a more profound effect on performance than delays in a hand-controlled setup [96]. This is another reason why no HMD is used in the teleoperation system described in this thesis.

Experiments concerning the **remote guidance** of free-flying space vehicles were conducted for *Ranger*. With operators guiding the SCAMP vehicle through an underwater obstacle course, no statistically significant difference in performance was found at 0 s, 0.1 s, 0.3 s, 0.7 s and 1 s time delay [163]. At 1.5 s delay, there was a marked increase in completion times, with the transition to *move and wait* becoming evident. While there was no significant difference between 1.5 s and 2 s, another increase in completion time occurred at 3 s delay [163]. During these experiments, the free-flyer was also successfully controlled over the internet at a roundtrip delay of 0.8 s. The communication time delay does therefore not speak against teleoperation of spacecraft proximity operations.

Further results were that **operator training** can alleviate the effects of time delay [163], and that operators generally prefer longer fixed delays over any variable delays [8]. Variable delays are common when sending commands over the internet [163], with internet delay measurements ranging between 0.8 s and 1.8 s [94]. This must be considered in planning space teleoperation communication chains using remote ground stations or access nodes to ground station or satellite networks.

Humans possess internal information processing capabilities which act intrinsically to compensate for system delays, as well as for the combined human perceptual delays of about 0.2 s [2]. The human operator can furthermore be supported in coping with the delay by the HMI, as was discussed in Section 2.4. However, in order to maximize system performance, the roundtrip time delays should be minimized at their sources.

Sources of Time Delays

The sources of signal time delays lie in data synchronization and limited data transmission capacities, data sampling and processing, the distance to be travelled, data routing via one or multiple DRS, and the ground station not being collocated with the operations center [2]. The demand for reduced roundtrip time delays therefore has substantial impact on the **planning** and **organization** of the **communication chain** for an OOS mission.

3.2 Space Communications

There exist two alternatives for communicating with a spacecraft in Earth orbit. Either **direct contact** between a ground station and the spacecraft, or **contact via a DRS**. Direct contact can only exist when the spacecraft is within the FOV of a ground station. The timing of these overflights can be inappropriate for effective and efficient mission operations [2], and the duration of direct passes is very brief, for LEO satellites in the range of eight to ten minutes. If this duration is to be extended, there exists either the option of involving a **ground station network** spanning large parts of the globe, or to use one or multiple DRS [2, 161]. Either option introduces communication time delays into the teleoperation system.

Mission Examples

A notable teleoperation experiment using a single ground station setup and thus benefiting from minimum time delays is DLR's ROKVISS (Robotikkomponentenverifikation auf der ISS – robotic component verification on the ISS). ROKVISS' main component was a small robotic arm with two torque-controlled joints mounted on the outside of the Russian module *Zvezda* [48] from 2005 to 2011. The arm was equipped with a stereo camera and a lighting system and was used for experiments with a mechanical contour device to verify the robotic system's function and performance [48]. The experiment received commands and transmitted haptic feedback data and the stereo video stream during direct downlink passes with a duration of eight minutes [48]. It used its own S band antenna, thus achieving data downlink rates of 4 Mbit/s and uplink rates of 256 kbit/s [166], which is sufficient for the setup using a stereo video stream plus a haptic channel operating at a sample rate of 500 Hz [48]. Due to the short direct link, the roundtrip time delay was below 0.02 s [166].

Orbital Express serves as an example for a telerobotic mission utilizing a ground station network. Since its systems were highly automated, the ground operators were mostly relegated to monitoring duties, instead of active realtime teleoperation, as was discussed in Section 1.3.4. In order to achieve complete communications coverage of the mission, the spacecraft were placed in a circular 492 km orbit, at 46° inclination [47]. This orbit created favorable coverage windows with the AFSCN [167].

Extended or even continuous coverage of an orbital mission can also be achieved by using one or multiple DRS in GEO. Using one DRS, uninterrupted contact times of minimum 42 minutes can be

achieved, although multiple hours are theoretically possible, if the LEO orbit is selected accordingly [161][4]. If beyond this period continuous coverage is required, multiple satellites must be used, such as the GEO constellation of the NASA TDRSS [168]. The use of TDRSS however increases the signal travel delays by the distance to be travelled between the individual satellites, as well as by routing the signals via the internet through NASA TDRSS station in White Sands, New Mexico for upload to the satellites. Delays between 3 s and more than 11 s can therefore be encountered [71].

ETS-VII used a communication architecture involving TDRSS relay links in S band [169]. The resulting downlink data rate was 1.5 Mbit/s, with roundtrip time delays accumulating to up to 7 s, necessitating the use of predictive VR displays for effective teleoperation [77, 170]. Another space robotics experiment working with a TDRSS link was ROTEX, the first remotely controlled space manipulator system. It was flown in 1993 aboard *Space Shuttle Columbia* as part of the Spacelab-D2 mission [48]. The system's most notable achievement was the capture of a free-flying object within its enclosed work cell. This feat was accomplished despite time delays of 5 s to 7 s via TDRSS by providing the operators with predictive VR displays.

OOS Communication Chain Tradeoffs

The single DRS solution can therefore be advantageous for OOS missions if the contact time of about 45 minutes is sufficient, which is the case for properly planned and executed final approach and docking maneuvers. Using the experimental setup with the *Artemis* link, Stoll [161] measured a mean roundtrip delay of 0.622 s, with a standard deviation of 0.066 s. Other quality of service criteria influencing operator immersion, such as delay jitter, bit error ratio and packet loss, were also found to be within acceptable ranges. As was discussed above, the relayed communications setup enabled stable bilateral control of a manipulator during typical OOS tasks.

A thorough study of communication architecture options was conducted during *Ranger* mission operations preparations [71]. It shows that more than the time delay and communication link characteristics must be considered when selecting the communication architecture for an OOS mission. Other factors such as ground station location, data security requirements, facility availability, mission priority, manpower demand, and organizational effort can have a higher impact on mission planning for telerobotic missions than link quality of service. While this serves as an example for similar studies to be conducted for future operational OOS systems, it is beyond the scope of this thesis and therefore not described in more detail.

3.3 Orbital Coordinate Systems

The trajectories of spacecraft in Earth orbits are commonly defined within the *Earth Centered Inertial* (ECI) coordinate frame, often also called the *ijk* system after its axes. Axis *i* points from the

[4] Such a deliberate orbit selection is of course not possible in OOS scenarios, since the chaser's orbit is dictated by its target object.

center of Earth towards the first point of Aries, which is the direction in which the Sun is seen on March 21. Axis *i* is therefore parallel to the line of intersection between Earth's equatorial plane and the ecliptic plane of the solar system. Axis *k* points towards geographic North, while *j* completes the right-handed coordinate system. Within ECI, a spacecraft's state vector can be defined in Cartesian coordinates. However, more intuitive and thus more commonly used are the **Keplerian elements**, which define the position and motion of a spacecraft by establishing first the orientation of the orbit in space in relation to the ECI axes, and by then specifying the position of the spacecraft within the orbit in reference to notable points on the orbit (see Figure 3-1).

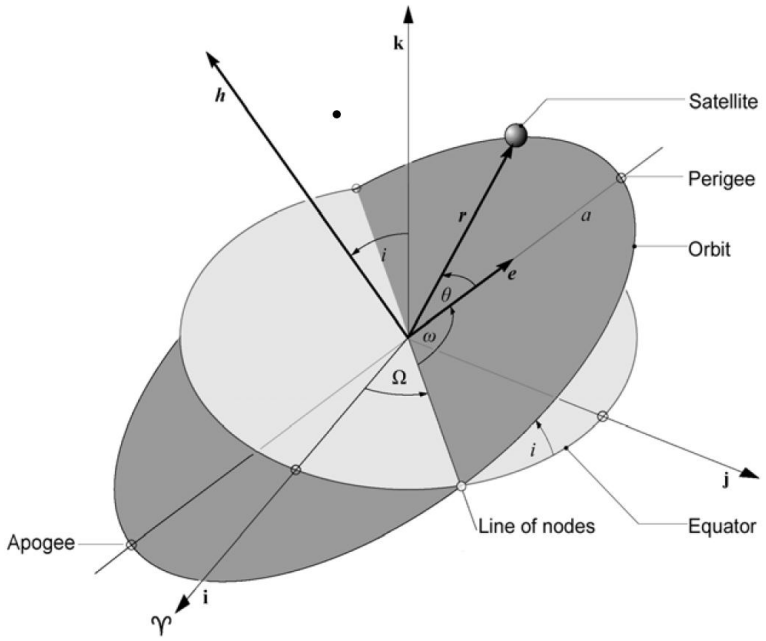

Figure 3-1: Earth Center Inertial coordinate system and the Keplerian elements [171, p. 149]. Axis i *points towards the vernal equinox, i.e. the position of the Sun as seen from Earth during spring equinox (March 21). Axis* k *points toward geographic North, while* j *completes the right-handed coordinate system. Four Keplerian elements serve to define size and orientation of the orbit in space. The* semimajor axis a *is half the distance between the point closest to (*periapsis*) and the point farthest from (*apoapsis*) the central body. The* right ascension of the ascending node Ω *is the angle between axis i and the* line of nodes *connecting the points in which the orbit ascends and descends through the equatorial plane. The* argument of periapsis ω *is the angle between the line of nodes and the apsidal line connecting periapsis and apoapsis. The* inclination i *is the angle between the orbital plane and the equatorial plane. The position of the spacecraft in the orbit is defined by the* radius r *giving the distance between the spacecraft and the central body, and the true anomaly θ, i.e. the angle between* r *and the line of apsides. Reproduced with permission of Wiley-VCH.*

While the ECI system and Keplerian elements are suitable for the major part of satellite operations, they are impractical to use during rendezvous & docking. During this mission phase the chaser spacecraft motion is commonly described in the ***Local-Vertical Local-Horizontal*** (LVLH) coordinate system of the target object [160, 172] (refer to Figure 3-2).

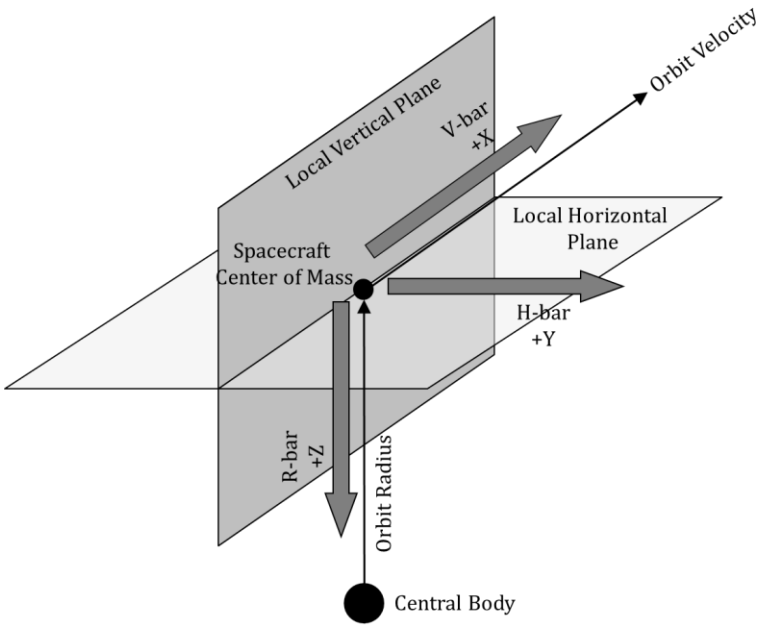

Figure 3-2: The Local-Vertical Local-Horizontal (LVLH) coordinate system for (near-)circular orbits. Axis x *points along the orbit velocity vector and is therefore also called* V-bar*. Axis* z *points toward the center of the central body and is also referred to as* R-bar*. Axis* y *completes the right-handed coordinate system and is called* H-bar; x *and* y *define the* local horizontal *plane,* x *and* z *the* local vertical*, also referred to as* orbital plane*.*

LVLH is convenient in that it only describes the **relative motion** between the spacecraft involved, and therefore only the motion components relevant for rendezvous & docking. The drawback of LVLH is that it is no longer an inertial system and any maneuvers within it are therefore subject to external disturbances (centrifugal force and Coriolis force) due to the coordinate frame's accelerated motion around the central body.

Clohessy-Wiltshire Equations

Within LVLH, the relative motion of two spacecraft in a circular orbit can be derived from Newton's equations [173]. The *x* and *z* components describe the motion within the orbital plane of the target spacecraft, while the *y* component is the out-of-plane motion.

$$\ddot{x} - 2\omega\dot{z} = a_x \qquad \textit{Eq. 3-1}$$

$$\ddot{y} + \omega^2 y = a_y \qquad \textit{Eq. 3-2}$$

$$\ddot{z} + 2\omega\dot{x} - 3\omega^2 z = a_z \qquad \textit{Eq. 3-3}$$

The parameter ω is the mean motion of the target spacecraft on its orbit, calculated from the semi-major axis a and Earth's gravity parameter $\mu_\oplus$.

$$\omega = \sqrt{\frac{\mu_{\oplus}}{a^3}} \qquad \textit{Eq. 3-4}$$

In addition to the coordinates x, y, z and their derivatives, these equations further contain the angular rate ω of the target vehicle orbit, as well as the components a_x, a_y, a_z of the acceleration acting on the chaser spacecraft. After their developers, these equations are commonly called ***Clohessy-Wiltshire* (CW) equations** [174, 175]. In the case of impulsive maneuvers, i.e. instant velocity change as opposed to long thrust arcs, and the absence of external accelerations the CW equations can be solved [171, 176] and thus result in a set of CW targeting equations for **maneuver planning**:

$$x(t) = x_0 - z_0(sin\ \omega t - \omega t) + \dot{x}_0\left(4\frac{sin\ \omega t}{\omega} - 3t\right) - \dot{z}_0\frac{2}{\omega}(cos\ \omega t - 1) \qquad \textit{Eq. 3-5}$$

$$y(t) = y_0\ cos\ \omega t + \frac{\dot{y}_0}{\omega} sin\ \omega t \qquad \textit{Eq. 3-6}$$

$$z(t) = z_0(4 - 3\ cos\ \omega t) - \dot{x}_0\frac{2}{\omega}(1 - cos\ \omega t) + \dot{z}_0\frac{sin\ \omega t}{\omega} \qquad \textit{Eq. 3-7}$$

$$\dot{x}(t) = -z_0 6\omega(cos\ \omega t - 1) + \dot{x}_0(4\ cos\ \omega t - 3) + \dot{z}_0 2\ sin\ \omega t \qquad \textit{Eq. 3-8}$$

$$\dot{y}(t) = -y_0\omega\ sin\ \omega t + \dot{y}_0\ cos\ \omega t \qquad \textit{Eq. 3-9}$$

$$\dot{z}(t) = z_0 3\omega\ sin\ \omega t - \dot{x}_0 2\ sin\ \omega t + \dot{z}_0\ cos\ \omega t \qquad \textit{Eq. 3-10}$$

The vector of initial maneuver velocities $(\dot{x}_0, \dot{y}_0, \dot{z}_0)^T$ is the impulsive velocity change $\boldsymbol{\Delta v}$ generated by the spacecraft's thrusters added to the initial relative velocity between the spacecraft $\boldsymbol{v}_i$. The vector $(x_0, y_0, z_0)^T$ is the initial position of the chaser relative to the target, while $\big(x(t), y(t), z(t)\big)^T$ is the relative position at time t.

Relative Trajectories

The targeting equations show that the out-of-plane motion component (y) is decoupled from the component (x, z) within the orbital plane. The resulting out-of-plane motion is therefore a harmonic oscillation around the initial position of the chaser, while any maneuver in x and z direction results in complex geometric trajectories. Figure 3-3 shows the **relative trajectories** resulting from a 0.1 m/s impulse in V-bar direction and an impulse of equal magnitude in R-bar direction at x = -200 m behind the target. If during docking approach an impulse is commanded straight towards the target, the resulting trajectory will actually lead the chaser "above" and away from the target. An impulse directed away from the target will result in the chaser passing underneath the target. In contrast, a "downward" impulse will actually take the chaser into an elliptical trajectory, initially downwards and then towards the target. An upward impulse from a position behind the target will

take the chaser up and away from the target. This ellipse can be used for fly-around maneuvers or for safe-return trajectories during docking approaches. Refer to [176] for a detailed discussion of the relative motion resulting from different initial conditions. A study concerning the **optimization of CW transfers** regarding propellant consumption, maneuver time, and line-of-sight to the target object was conducted in a Bachelor's thesis contributing to this doctoral research [177].

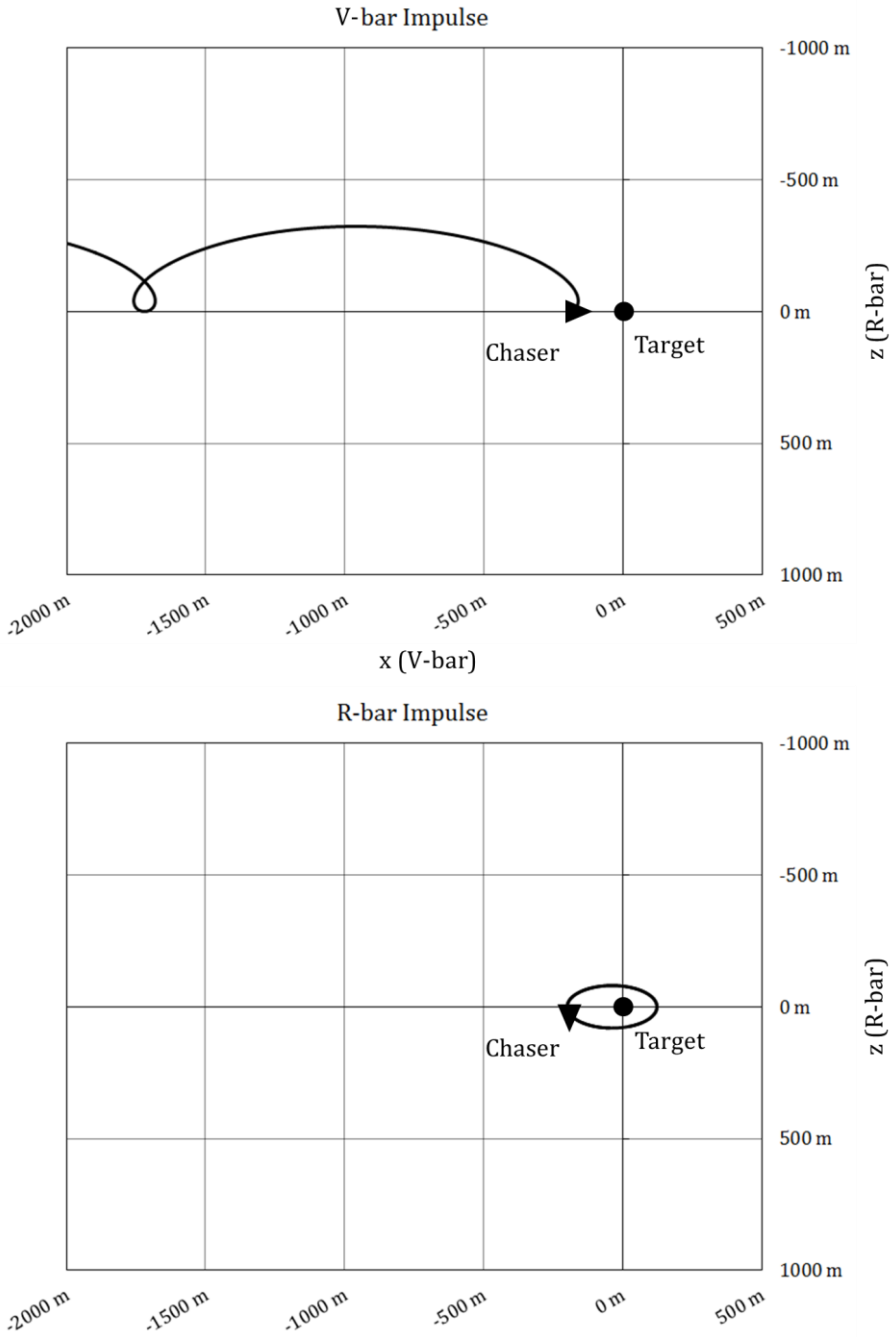

Figure 3-3: Chaser trajectory in relation to target. The upper trajectory results from a 0.1 m/s impulse along the V-bar (in direction of flight) at a position of 200 m behind the target. The lower trajectory is the result of a 0.1 m/s "downward" impulse along the R-bar.

The CW equations are derived for circular orbits but can be used as a first guess for elliptical orbits up to an eccentricity e = 0.4 [178]. Further analytical derivations of the relative motion exist for higher eccentricities [179]. These derivatives of the CW equations for **eccentric orbits** are often referred to as **Tschauner-Hempel equations** [180].

Finite-Thrust Relative Maneuvers

The other major limitation of the CW equation is their assumption of **perfectly impulsive maneuvers**. While these assumed impulsive maneuvers are beneficial to human control [174], rendezvous maneuvers during the terminal phase can nonetheless almost never be considered to be ideally impulsive [181]. Usually, numerical approaches need to be resorted to in order to solve the spacecraft trajectories resulting from finite thrust maneuvers [181], but there also exist some analytical approaches useful for maneuver planning. Van der Ha [181], for example, developed a set of CW state transition and force matrices for time-variant control forces. Using these equations, the finite-thrust levels required for rendezvous within a prescribed interval can be calculated. Additionally, an analytical solution to the fuel-optimal rendezvous problem under finite, circumferential thrust conditions has been formulated, i.e. for finite-thrust maneuvers with the propulsion acting along the orbit tangent [181].

Williams and Tanygin [175] describe CW targeting equations for **low-thrust maneuvers**. Their approach introduces acceleration $\boldsymbol{a} = (a_x, a_z)^T$ into the in-plane CW equations:

$$x(t) = \frac{1}{\omega}\left\{-2\left(\dot{z}_0 + \frac{2a_x}{\omega}\right)cos\,\omega t + \left[4\left(\dot{x}_0 - \frac{a_z}{2\omega}\right) - 6\omega z_0\right]sin\,\omega t\, a_x\omega t^2 + \left[6\omega z_0 - 3\left(\dot{x}_0 - \frac{a_z}{2\omega}\right) + \frac{a_z}{2\omega}\right]\omega t + \left[\omega x_0 + 2\left(\dot{z}_0 + \frac{2a_x}{\omega}\right)\right]\right\} \quad \textit{Eq. 3-11}$$

$$z(t) = \frac{1}{\omega}\left\{\left[2\left(\dot{x}_0 - \frac{a_z}{2\omega}\right) - 3\omega z_0\right]cos\,\omega t + \left[\dot{z}_0 + \frac{2a_x}{\omega}\right]sin\,\omega t - 2a_x t + \left[4\omega z_0 - 2\left(\dot{x}_0 - \frac{a_z}{2\omega}\right)\right]\right\} \quad \textit{Eq. 3-12}$$

For **use in the simulations** run over the course of this research, these equations were differentiated in order to derive the in-plane velocity components of a spacecraft during a thrust maneuver.

$$\dot{x}(t) = -3\dot{x}_0 + 6\omega z_0 + \left(4\dot{x}_0 - 6\omega z_0 - 2\frac{a_z}{\omega}\right)cos\,\omega t + \left(2\dot{z}_0 + 4\frac{a_x}{\omega}\right)sin\,\omega t + 2\frac{a_z}{\omega} - 3a_x t \quad \textit{Eq. 3-13}$$

$$\dot{z}(t) = \left(\dot{z}_0 + 2\frac{a_x}{\omega}\right)cos\,\omega t - \left(2\dot{x}_0 - \frac{a_z}{\omega}\right)sin\,\omega t - 2\frac{a_x}{\text{ù}} \quad \textit{Eq. 3-14}$$

Using these equations, the trajectory resulting from finite-thrust arcs during relative maneuvers can be computed. This can be used for predicting a spacecraft's trajectory resulting from the ma-

neuver command. If $a_x = a_z = 0$, these expressions are reduced to the standard CW equations and describe the natural drift of the chaser due to the existing relative velocity.

3.4 Spacecraft Dynamics

The motion of objects on Earth is substantially influenced by their environment. Gravity pulls all objects down and thus creates a natural direction of motion in absence of other external forces. All objects are furthermore surrounded by gaseous, liquid or solid media. Motion within these media generates **resistive forces** acting upon the moving object in the form of friction or pressure. While these forces counteract every form of propulsion, they also serve to **stabilize** an object's motion.

In the example of an underwater vehicle, which is in its degrees of freedom similar to a spacecraft [118, 119], the resistance of the surrounding water dampens any angular motion due to disturbance torques created by manipulator motion. The equilibrium of gravity and buoyancy furthermore creates a stable attitude into which the vehicle returns after commanded or disturbed motion.

A spacecraft, on the other hand, cannot rely on external stabilizing forces. Its **attitude control system** must therefore at all times compensate for the **disturbance torques** of appendages like robotic manipulators, pointing antennas, or moving solar arrays [79, 182–184]. If these disturbance torques overwhelm the attitude control system, the result can be a **loss of signal** due to the antenna losing contact with the ground station or DRS [79], or the uncontrolled spacecraft motion can lead to **collisions** and thus **mission failure** or loss of spacecraft. The **continuous control** of the spacecraft attitude is therefore a major requirement for teleoperated space systems.

3.5 Orientation in Orbit

The terrestrial environment is abundant with **visual references** for relative position determination and orientation during teleoperation. The major **attitude reference** is the local horizon, which can either be the actual Earth horizon or other objects with known or assumed orientation, e.g. buildings, trees, etc. With these references, both the target attitude as well as the chaser attitude, for control purposes also referred to as ownship attitude, can be visually estimated. Other natural or artificial objects in the environment serve as references for relative position and velocity estimation. The **distance** of familiar objects can be judged by comparing their **apparent size** to their real size. This real size is known or can be assumed with confidence for objects like trees, buildings, roads, etc. These then serve as the references against which a target object's size and distance can be judged by cast shadows, size comparison, as well as **occlusion** [129]. Teleoperation becomes challenging in the absence of such references, for example in adverse visual conditions (e.g. darkness, fog) or in the case of **unstructured environments** such as encountered underwater.

The only natural references generally available in Earth orbit are the limb of the Earth, the Sun, the moon and stars. The Sun and stars are commonly used for **spacecraft attitude determination**

with sensors measuring the angle between the spacecraft body coordinate system and the vector towards the reference object [185]. The human operator, however, cannot use the celestial objects in the background of a scene to estimate a target object's attitude with confidence. If the Earth's limb is within the FOV of the camera used, it is as valuable a reference as the horizon in a terrestrial setting. It can therefore be used to judge target attitude and rotation rates.

These references do not convey any information about **target motion** in relation to ownship [186]. If target dimensions are known, this can serve as a first indicator of target distance. As the next section will discuss, **lighting conditions** in orbit can cause part of the target object to be in shadow and thus invisible to visible light sensors. Any distance estimate based on apparent target size is therefore likely to be afflicted by a considerable error [186]. **Radial approach rates** can be estimated by the apparent change in target size. Whether the operator perceives this change depends on the target distance, the rate of change of that distance, as well as on the viewing duration [187]. **Angular line-of-sight motion**, on the other hand, can be detected by the unaided human eye with high accuracy, allowing target tracking during rendezvous operations [188, 189].

The visual scene furthermore contains no information regarding the target's position in relation to ownship orbit, which is critical for maneuver planning.

Figure 3-4 shows a direct comparison between terrestrial and orbital environments and thus demonstrates the limited availability of references in orbit.

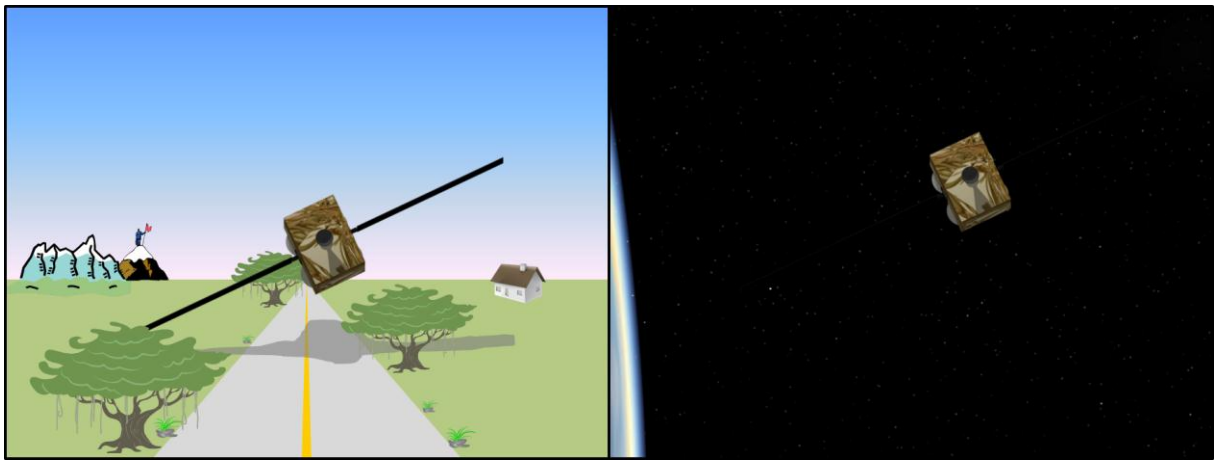

Figure 3-4: A typical terrestrial setting compared to an orbital setting. In the terrestrial environment, numerous natural and artificial references are available to estimate target orientation, size, distance and velocity. In the orbital environment, the target is not completely visible. Furthermore, there are no ambient references which can be used to estimate its distance, hence velocity, and its position within the orbit.

3.6 Lighting Conditions

Most terrestrial environments are naturally illuminated by soft, diffuse light[5]. Sunlight is scattered by the atmosphere and reflected by objects in the environment. The natural illumination is therefore multi-directional, which leads to reduced contrast and soft shadows.

This difference between lit and shaded areas is substantially more extreme in the orbital environment. The dominating light sources in orbit are the Sun and Earth albedo, i.e. sunlight reflected from the Earth's surface.

Contrast

Direct sunlight is an intense **point-source** light creating glaring illuminated surfaces and hard shadows [190, 191]. This combination creates **contrasts** which are often beyond the dynamic ranges of camera sensors, thus resulting in the **loss of scene data** [190] (see Figure 3-5). **Earth albedo** lighting is similar to terrestrial illumination in being an extended, diffuse and thus almost shadow-less light source [190].

The illumination conditions in orbit change rapidly over the course of an orbit [191]. Varied illumination conditions have been shown to adversely influence distance estimation performance by the unaided human eye [186].

Figure 3-5: Two views of Soyuz spacecraft on final approach to ISS [192]. These views are exemplary for the lighting characteristics encountered during proximity operations, particularly the contrast between lit and shaded sides of spacecraft. These contrasts can be beyond the dynamic range of camera sensors and can furthermore impede the determination of object dimensions, as well as the visual tracking of structural features.

[5] The great exception to this is the underwater environment, in which the absorbing, color-distorting and back-scattering medium water causes non-uniform and multi-directional illumination and hence poor visibility [117, 120]

Spacecraft Surfaces

The illumination conditions during proximity operations are furthermore influenced by the **surface properties** of the target object. The insulation material covering spacecraft bodies commonly consists either of highly reflective **metallic foils** or featureless **white blankets** that loosely cover the spacecraft structure [193]. Such surfaces cause **glare** as well as **specular reflections** and a lack of distinct and visually stable features such as lines or corners [190]. Figure 3-6 provides an example for the optical properties of Multi-Layer Insulation (MLI) surfaces.

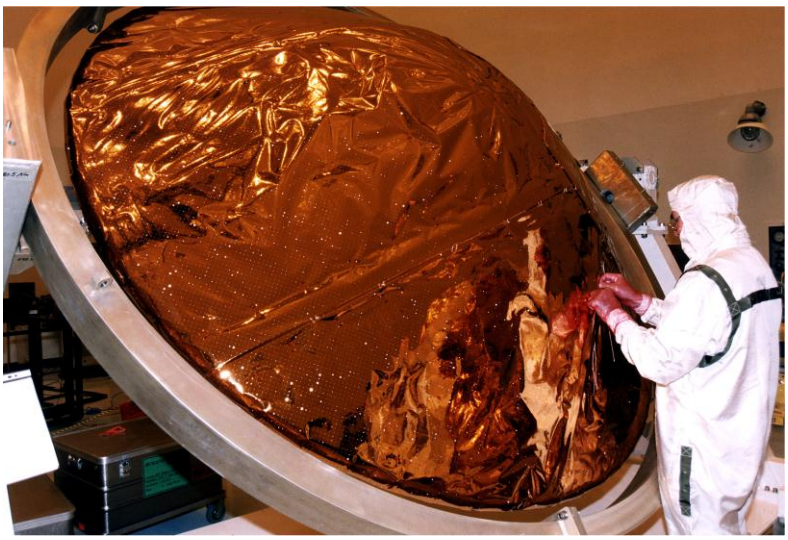

Figure 3-6: Multi-Layer Insulation covering the Huygens *lander [194]. Highly reflective surfaces such as these are common on spacecraft and can cause intensive light reflections and glare, as well as hide spacecraft structural features important for relative navigation.*

Sun Angle

The poorest viewing conditions are encountered when the sun is directly behind the target, which means that the observer (or sensor) must look directly at or near the sun in order to view the target [189], which can hurt eyes and damage cameras. On one of the *Hubble* servicing missions, the Shuttle crew had to use welding goggles in order to be able to discern the space telescope against the sun [70]. Similar adverse viewing conditions result from the target being within line-of-sight of the Moon or near Earth's horizon on the lit side of the Earth [189]. Another extreme occurs if the Sun is directly behind the approaching chaser spacecraft, which can result in blinding reflections on the target surfaces, or in shadows cast by the chaser body, making the use of artificial lighting necessary. The preferred position of the sun is therefore behind and above/below or to the sides of the chaser vehicle. This ensures illumination of the docking target while preventing shading by the chaser, as well as glare by specular reflection of the sunlight.

3.7 Summary

Time delays have been shown to have a substantial **detrimental effect** on teleoperation system performance. While the usual impact is the **increase of task completion time**, delays can also lead to **instabilities** in control loops if haptic feedback is used.

The main source of delay in a space teleoperation scenario is the **communication link** between the human operator and the spacecraft. When selecting the communication architecture for an OOS mission, there therefore exists a **tradeoff** between communication window duration, roundtrip time delay, as well as other considerations like cost, availability, reliability and system complexity. Preceding research demonstrated that the use of a single DRS results in continuous contact times of approx. 45 minutes per orbit of the OOS spacecraft, while resulting in **mean roundtrip delays of 0.622 s**. While this certainly represents an optimum number resulting from optimum system settings and no data security and verification requirements whatsoever, it shows that relayed communications links can be optimized to **meet the requirements of realtime teleoperation**.

It is therefore expected that the roundtrip delay in a DRS setup will **not be a challenge** for teleoperated rendezvous & docking.

The characteristics of the **space environment**, especially the **relative trajectories** resulting from the motion in accelerated coordinate frames, the **complex dynamics** resulting from the absence of external dampening and stabilization forces, the near-absence of **external references**, as well as the **lighting conditions** create a challenging environment for robotic systems. Combined with the general limitations of telerobotic systems and the additional challenge of the delayed communications link, the environment has **severe impact on the relative navigation and positioning task** which must be mastered for teleoperated rendezvous & docking.

4 Rendezvous & Docking

Rendezvous & docking of spacecraft, as well as associated proximity operations, represent some of the most complex maneuvers to be accomplished in spaceflight. In order to accomplish successful rendezvous and mating of two spacecraft, absolute and relative navigation on orbit, sensing of a target object in space, precise attitude determination and control, maneuver planning and the use of highly complex mechanisms must be mastered. This chapter describes the purpose of rendezvous & docking, the mission steps to be taken to achieve that purpose, the sensors employed and the different strategies pursued in operational and experimental systems. Finally, limitations of the currently (2012) existing systems and requirements for any future developments are provided.

4.1 Purpose

The purpose of any rendezvous & docking mission is to establish **physical contact** between two or more spacecraft. After a mechanical connection has been established, electrical and fluid couplings can follow. Therefore rendezvous & docking is a prerequisite for any OOS mission to satellites in Earth orbit.

As the term *rendezvous & docking* implies, the involved operations are divided into two distinct phases, each with their individual goals. During the ***rendezvous*** part of the mission, the involved spacecraft are guided to meet in the same volume of space, at the same time. In most applications, the target object is inert, and the chaser performs all maneuvers, in order to arrive at the right spot in the right time. However, there exists an exception to this rule, called a *control box rendezvous*. In this variant, the target spacecraft executes a number of maneuvers after the chaser is launched in order to enter the targeted volume of space at a designated time. This reduces chaser vehicle propellant consumption, naturally at a cost to the target. It therefore can only be performed with targets having orbit maneuvering capabilities, which usually rules out space stations and a large number of satellites. Nonetheless, this type of rendezvous was performed on some *Space Shuttle* missions (STS-49 to service Intelsat VI, as well as STS-72 and also planned for the contingency mission to *Atlantis*' rescue during *Hubble* Servicing Mission 4, STS-400) [70].

The goal of the ***docking*** phase of the mission is to establish physical contact between the involved spacecraft. Although commonly the term *docking* is used for this phase, there actually exist two distinct cases: *docking*, or *capture and berthing*. During *docking*, the chaser approaches the target with non-zero relative velocity, brings its docking tool into alignment with the target's counterpart, and establishes a firm structural connection by using its own momentum. Docking therefore only relies on the maneuvering capabilities of the two spacecraft and on functioning docking tools. This approach was used during *Gemini* and *Apollo*, and still is in use with the *Soyuz*/*Progress*, the *Space Shuttle* and *ATV* missions to *ISS*. In *capture and* ***berthing***, the interceptor is maneuvered into close proximity of the target and an initial mechanical connection between both is established by a robotic manipulator. This manipulator can either be situated on the chaser (as is the case with the *Shuttle*

RMS used for capturing the *Hubble Space Telescope*), or on the target vehicle, which is the approach taken with the SSRMS on *ISS* capturing the *HTV* [195] and the *Dragon* capsule. The choice of the manipulator's location is on the one hand dependent on the involved sizes and masses of the spacecraft, with the attitude of a heavier spacecraft being less influenced by the disturbance torques caused by the movement of the manipulator. On the other hand, a space manipulator is a very complex, and hence expensive, mechanism. It will therefore be mounted on the spacecraft with the longer lifetime and/or reentry capability, and thus not on disposable spacecraft like *HTV*. The captured spacecraft is moved by the manipulator to a berthing position, which is a feature similar to a docking port. There, the final structural, electrical and fluid connections are established and the chaser performs its servicing mission or forms an additional propulsion stage for orbit maneuvering.

4.2 Mission Phases

In the general case, rendezvous & docking missions involve the **chaser** spacecraft, which begins the mission on the launchpad, and the **target** spacecraft, which is usually already in orbit by the time of the chaser launch. Exceptions include the OOS demonstration missions, in which both chaser and target were launched on the same rocket, then separated in orbit, and performed rendezvous & docking maneuvers from various distances [47, 77]. This approach was primarily chosen to reduce system complexity and launch cost, and also to ensure minimum mission success even if components of the rendezvous & docking system failed.

The main phases of such rendezvous missions are: launch, phasing, far-range rendezvous, close-range rendezvous, and docking [196]. Since this doctoral thesis is concerned with the performance of teleoperated rendezvous & docking systems during **final approach**, this section focuses on the mission steps far-range and close-range rendezvous, as well as docking. A summary of launch window selection as well as phasing issues can be found in [176].

4.2.1 Far-Range Rendezvous

The objective of the far-range rendezvous phase is to transfer the chaser from the phasing orbit to a **first aiming point** in the vicinity of the target, where close-range rendezvous begins. In order to accomplish the transfer, the target must be acquired by the relative navigation sensors of the chaser [196]. The range at which the target is acquired depends on the target size and supportive equipment, and the chaser's sensor suite. For the *Space Shuttle*, mission control hands over rendezvous guidance to the orbiter's crew at 74 km from the target [197], at which point a target like *ISS* can be tracked using star trackers or radar. The far-range approach ends at a range of the order of hundreds of meters. At this point, the *close-range rendezvous* and *proximity operations* begin.

During far-range rendezvous the relative approach velocity must be reduced to a safe level. Additionally, the dispersions in position, orientation and angular rate must be reduced to meet the conditions required for proximity operations [196].

There exist two general approaches to far-range rendezvous maneuvers: *coelliptic rendezvous* and *stable orbit rendezvous*.

Coelliptic Rendezvous

Coelliptic orbits are **coplanar elliptical orbits** with a common occupied focus. The arguments of perigee ω are equal, meaning that the lines of apsides of the orbits are congruent. In addition to this, the differences in perigee and apogee radii are equal [198]. In the LVLH frame, coelliptic orbits appear as two parallel lines (see Figure 4-1). This allows for easy, intuitive, and robust maneuver planning by means of so-called ***trigger angle targeting***. This technique was developed during the *Gemini* program and allows astronaut pilots to reliably achieve rendezvous by pointing the chaser spacecraft at the target at a certain trigger angle τ relative to the direction of flight, using a cueing device similar to a sextant, and engaging the orbital maneuvering thrusters [199].

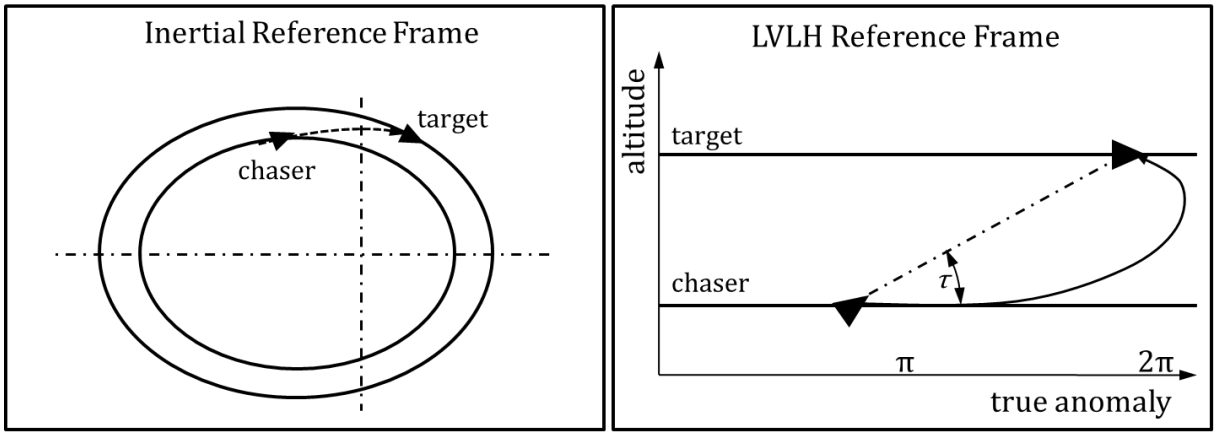

Figure 4-1: Coelliptic orbits in inertial and spacecraft reference frames (based on [199, p. 496]).

The coelliptic rendezvous approach facilitates manned rendezvous missions and enabled the successful rendezvous & docking missions during the *Gemini*, *Apollo*, *Skylab* and early *Shuttle* programs [155, 200, 201]. For these manned rendezvous missions trigger angle targeting was particularly attractive, because it allowed the use of the astronauts' eyes and simple elevation cueing for maneuver triggering in case of the failure of the rendezvous radar system. After applying the initial velocity change Δv along the line-of-sight at terminal phase initiation (TPI), the pilot performed one or two mid-course correction maneuvers, before finally approaching the target for docking. During final approach, the pilot benefitted from a low inertial line-of-sight approach rate during final braking and approach, as well as from good visibility of the target against the star background [43].

Due to its **simplicity** and **robustness** trigger angle targeting can also be beneficial for robotic missions like OOS. Since the TPI maneuver is applied along line-of-sight, in which direction the robotic spacecraft is most likely already pointed in order to aim its sensors at the target, the atti-

tude control system must only send a trigger signal once the right angle to the line of flight is reached. This can also easily be accomplished in teleoperation by a human operator, since all that is needed for successful rendezvous is a **camera image** and an **attitude reference**. This makes it a simple system, which is also robust concerning the failure of individual sensors. For current space station operations, this approach was however replaced by the so-called *stable orbit rendezvous*.

Stable Orbit Rendezvous

Stable orbit rendezvous profiles have the interceptor spacecraft achieve a naturally stable **station-keeping point** ahead or behind the target object in the same orbit (see Figure 4-2). In the LVLH coordinate frame centered on the target this stable position lies along the positive or negative V-bar. From this point, the final intercept maneuver is initiated.

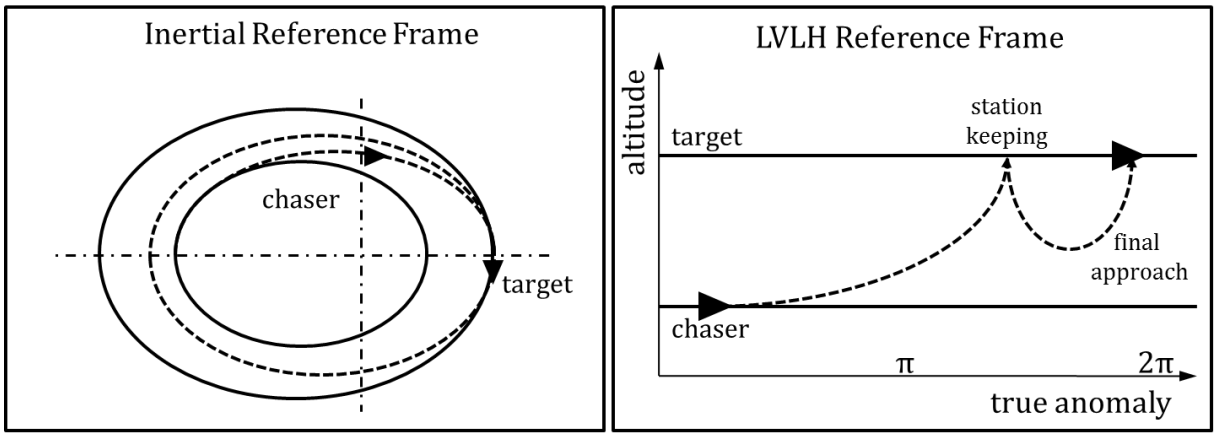

Figure 4-2: Stable orbit rendezvous with station-keeping behind target on V-bar.

Such a stable orbit rendezvous supports inertial approaches with lower relative velocity than the inertial approaches of the coelliptic profile [70]. In addition, a stable orbit profile desensitizes the mission timeline from trajectory considerations, as the chaser could theoretically remain at the holding point for indefinite periods of time. Stable orbit station-keeping at multiple kilometers of distance to the target (15 km for *Space Shuttle ISS* approaches [202]) was also preferable to the close-range (at distances of tens of meters) station-keeping associated with coelliptic approaches, due to the need for continuous crew monitoring and the resulting propellant expenditure at such close distances. This is especially important in the case of spacecraft teleoperation, in which no continuous control or monitoring communication link might be available during the mission. Therefore crew and mission control procedures were expected to be less complex. However, simulations and operational experience proved that the complexity in operations remained unaltered [43].

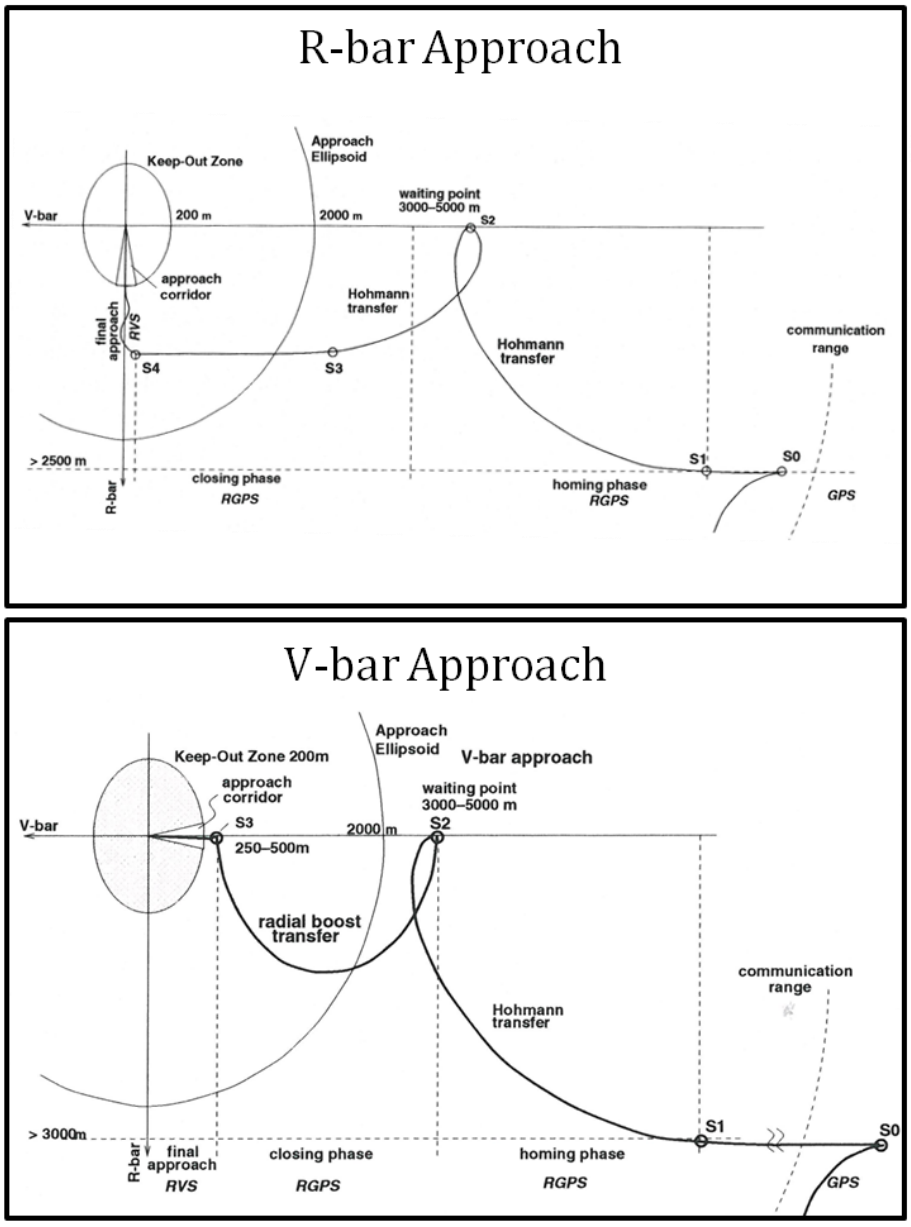

Figure 4-3: ISS *stable orbit approaches (figure adapted from [196, pp. 145 and 156]). The R-bar approach can be used by the* Space Shuttle*, while the* ATV *rendezvous is along the V-bar.* ISS *safe-approach procedures introduce waiting points, a keep-out zone around* ISS *and an approach corridor which approaching spacecraft must use. Reproduced with permission of Cambridge University Press.*

Stable orbit rendezvous thus allows the chaser spacecraft to hold the approach at a **safe distance** to the target in order to assess the situation and plan the final approach maneuver. From this station-keeping point, docking is initiated by additional tangential or radial thrust maneuvers, depending on the direction of final approach and safety considerations (see Figure 4-3 for *ISS* stable orbit approaches).

The advantages of stable orbit profiles over coelliptic approaches are **lower propellant consumption** and **stable station-keeping points** on V-bar, leading to less demand on crew (or robot) position monitoring and correction [43]. Hence, the stable orbit rendezvous has become the **standard** for *ISS* operations for *Space Shuttle*, *Soyuz* and *ATV*, as well as for other rendezvous operations, such as with the *Hubble Space Telescope* [70].

At the stable holding point, the final approach maneuver is initiated. This forms the transition into *close-range rendezvous*, also referred to as *proximity operations*.

4.2.2 Close-Range Rendezvous

The close range rendezvous phase of the mission, also called **proximity operations**, comprises the chaser closing in on the target, and the **final approach** until immediately before docking or capture [196]. This phase begins within hundreds of meters from the target (600 m for the *Space Shuttle* [43]) and ends at a distance of a few meters, either when docking is imminent or when the target is within capture distance of the manipulator. Proximity operations can be considered the most critical part of the rendezvous mission. During this phase even minor control errors can cause accidents. During *ISS* approaches, the *Shuttle* crew takes **manual control** over the orbiter once its passes underneath the station on its inertial V-bar approach. From this point forward, the pilot "flies" the *Shuttle* on final approach [202]. For *Progress* and *ATV*, the crew aboard *ISS* closely monitors the arriving spacecraft's behavior during closing, with the ability of either commanding an autonomous abort and evasion maneuver for *ATV*, or of manually flying the *Progress* to the docking port.

Final Approach

Final approach is usually conducted either along the target's V-bar, R-bar, or in rare cases along the orbit normal, referred to as H-bar (see Figure 4-4). In order to facilitate human monitoring and control, final approach trajectories are planned to be as close to straight lines as possible. This is realized by so-called *hopping* or *forced translation* trajectories.

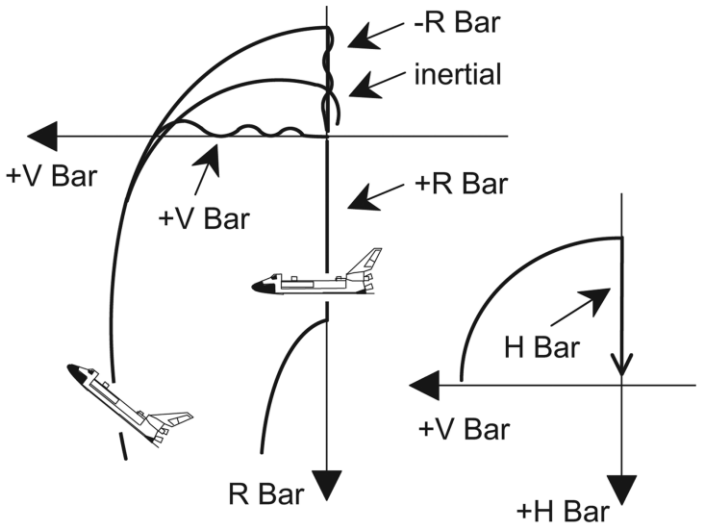

Figure 4-4: Space Shuttle *proximity operations approaches [43, p. 948]. The* Space Shuttle *was designed to mainly utilize V- and R-bar approaches. However, H-bar approaches have also been simulated.*

A *hopping* approach along the V-bar is realized by employing short radial thrusting maneuvers. The spacecraft's natural motion as expressed in the CW equations will cause the vehicle to make a short hop before returning to the centerline where an opposite maneuver must be used in order to stop the motion. Without this maneuver, the spacecraft would complete an ellipse and return to its starting point. In order to optimize this approach for astronaut pilots, who exclusively have an aviation background, the multipulse **glideslope transfer** was developed [174, 203]. In this approach, the individual pulses are commanded in order for the end points of the semi-ellipses to follow a glideslope towards the target, comparable to the glideslope leading to a runway (see Figure 4-5).

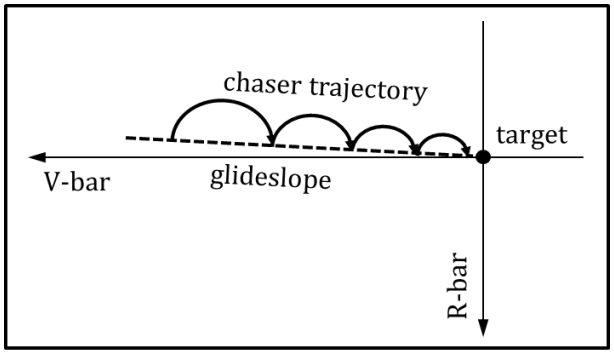

Figure 4-5: Multipulse glideslope approach. The final approach to the target is split into a number of individual hops. The individual pulses are commanded in order for the chaser motion to follow a glideslope towards the target. This facilitates human control.

For a ***forced translation*** along the V-bar, the spacecraft's thrusters in the tangential direction are fired to produce forward motion. As was shown with the CW equations, this also causes the spacecraft to move upwards from the intended line of approach. This is countered by almost continuous-

ly engaging the thrusters in the radial direction, which forces the vehicle back onto the line. Thus any distance can be traversed in a quasi-straight line, while at high propellant consumption [174]. Forced translation can also be achieved along the R-bar, with tangential thrust to compensate for the coupled motion. This approach was originally designed for docking with *Mir* and can be used for docking with *ISS* [43]. It was also used on *Hubble* servicing mission STS-82 [70]. This closing "from below" not only allows precise approach of a docking port, it also provides natural braking due to orbital mechanics since the spacecraft moves against the local gravity vector. This reduces reaction control system (RCS) thruster activity, and thus propellant consumption as well as the risk of ***plume impingement*** on the target spacecraft [70]. For more details on plume impingement and its impact on approach and mission planning, refer to Appendix A.1.

Out-of-Plane Maneuvers

In this section only approaches within the orbital plane have been described. This is not to imply that only these approaches exist (an out-of-plane approach is shown in Figure 4-4) but that these are unusual, due to the high propellant cost of out-of-plane maneuvers and the high probability of collisions in case of control systems' failure. However, there exist examples for out-of-plane proximity operations. During the *Shuttle's* first mission to *Mir*, the station's crew separated the *Soyuz* and flew it to a safe distance out of the orbital plane in order to be able to film the *Shuttle's* separation and departure [155]. Such out-of-plane maneuvers can also be required when the rendezvous target is in a spinning or tumbling motion.

Tumbling Targets

The rendezvous approaches described to this point all assumed either a target with stable attitude, either through gravity gradient stabilization or active attitude control like the *ISS* or *Hubble*, or slowly spinning or tumbling targets like Earth observation or communications satellites that were captured by a significantly larger interceptor, namely the *Space Shuttle* [43]. A different situation presents itself when a rapidly spinning or tumbling object, such as a three-axis stabilized satellite with a malfunctioning AOCS, or freely tumbling space debris objects, must be captured by a chaser spacecraft of comparable mass and size. This can be the case on robotic OOS missions. In this case, no fixed approach profiles can be defined in advance, but the approach maneuvers must be planned in situ, either by an autonomous robotic system or by the human operators.

To do this, the robotic chaser would take up a stable holding position at 30 m – 100 m from the target to observe the target's motion and estimate its dynamic states such as the quaternion and the angular velocity vector, using active or passive sensors and image pattern recognition techniques. Using these estimated parameters, the robot or ground operators create a capture plan and approach trajectory considering target motion, lighting conditions, collision avoidance, error compensation ability, etc. [84]. In the case of realtime teleoperation investigated in this research, the human operator can also be used to estimate target motion and thus plan the final approach.

One option is to position the chaser on an extension of the target's angular momentum vector and spin-up the chaser until it matches the target's rotation rate [204]. The manipulator of the interceptor would then grapple the target, and after a rigid mechanical connection is achieved, the interceptor's AOCS would gradually reduce the rotation rate of the coupled spacecraft [204].

Another option is for the chaser to approach the chaser on a fly-by trajectory in a plane perpendicular to the target's axis of angular momentum using CW guidance laws. This trajectory would be scaled such that at the point of closest approach, the chaser velocity would match the velocity of the targeted grasping point on the target object [84]. This allows for easy capture by the manipulator and subsequent detumbling of the spacecraft. Alternatively, if capturing cannot be achieved, the chaser's trajectory would allow it to escape from the target without any additional collision avoidance maneuver [84].

Since the target's angular momentum vector will be oriented arbitrarily in space, the resulting terminal trajectories will require out-of-plane maneuvers, involving the disadvantages stated earlier. Additionally, the chaser's AOCS must be designed to be able to dampen the tumbling motions of potential target satellites which can be large Earth observation satellites like *Envisat* with a mass of 8000 kg [205], or GEO telecommunications satellites with masses of up to 6000 kg and solar array spans of up to 46 m [89]. During the de-tumbling phase, such large solar arrays or large unfolded antennas are drivers regarding the maximum deceleration since at too high stresses these could break off and thus prematurely end the repair mission and enter the ranks of uncontrollable space debris objects. Additionally, the manipulators used to capture and stabilize such behemoths must be able to withstand the resulting shocks and forces, which appear to be specifically challenging on the fly-by approach. Some concepts thus envision capture mechanisms like harpoons or nets, but such systems either seem unlikely to ever reach operational maturity or have already been discarded in detailed design studies [206].

Another approach to the problem of tumbling targets is to de-tumble them before commencing capture operations. One method studied used mechanical impulses and in both numerical simulations and actual experiments proved to be effective to reduce the target object's angular momentum [207].

4.2.3 Docking

The docking phase is the conclusion of the rendezvous & docking process. It encompasses **capture** of the target by the chaser (or vice versa), establishment of a rigid **structural connection** [196], and the subsequent connection of fluid, gas, electrical, propellant and communication lines, as well as the establishment of a pressurized passageway, if crew transfer is part of the mission goals. As stated in Section 4.1, this can be achieved either by **docking** or **berthing**, where docking means that the active spacecraft positions itself and establishes the physical connection using its own momentum; in berthing either the target or chaser is captured, positioned and connected by a robotic manipulator to a berthing mechanism. Berthing thus allows contact to be made at a near-zero closure rate, which means a higher level of control for the operator and avoids the process of

one vehicle basically flying into the other [208]. It is therefore the generally preferable approach [209] but comes at the cost of requiring a complex, heavy and expensive manipulator system [208]. In addition, for capture and berthing with a manipulator on small chaser satellites, the disturbance torques caused by the manipulator might either overwhelm the chaser AOCS capability to compensate, or AOCS maneuvers might hinder precise capture by the manipulator. In these cases, the chaser may deactivate its AOCS in order to become a free-floating platform [210]. This requires precise models of the chaser spacecraft's dynamics in order to be able to capture the target and avoid collisions, as well as either considerable on-board processing power or a mission timeline that permits computing the dynamic model on the ground and uploading resulting manipulator commands. The choice between docking and capture/berthing therefore brings significant trade-offs in mission and spacecraft design.

Whichever choice of mating approach is made, the complex task requires the use of specifically designed docking or berthing mechanisms. These have to absorb the impact of two colliding vehicles, dampen any relative motion, achieve a stable structural connection, make an exchange of consumables, electrical power and/or crew possible, and after completion of the mission unlatch and separate the two vehicles reliably [211].

Docking System Capture Envelopes

The choice of docking/capture mechanism drives the precision required during final approach, also called the **docking envelope**, and thus the capabilities of the rendezvous & docking control system. Table 4-1 provides typical capture envelopes of the currently used docking systems for docking maneuver planning [211–214]. A detailed overview of the docking systems listed in the table is provided in Appendix A.2.

Table 4-1: Docking system capture envelopes (based on [211–214])

Docking System	Radial Offset [m]	Roll [°]	Pitch/Yaw [°]	Translation Rate [m/s]	Roll Rate [°/s]	Pitch/Yaw Rate [°/s]	Contact Rate [m/s]
Androgynous Peripheral Attachment System (Space Shuttle/ISS)	± 0.24	± 4	± 4	0.06	0.4	0.4	0.40
Apollo Docking System	± 0.31	± 10	± 10	0.15	1.0	1.0	0.31
ATV Docking System	± 0.10	± 5	± 5	0.02	0.4	0.15	0.05 – 0.10
Common Berthing System (ISS/HTV/Dragon)	± 0.025	n/a	n/a	0.0	n/a	n/a	0.0
Orbital Express Capture System	± 0.05	± 5	± 5	n/a	n/a	n/a	< 0.03
Russian Docking System (Soyuz/Progress)	± 0.30	± 7	± 7	0.10	0.7	0.6	0.30

For the experimental studies conducted for this thesis, the docking envelope of the ***Orbital Express Capture System*** (OECS) will be assumed. Where no data on OECS is available, the ATV Docking System values are adopted.

Natural Capture Interfaces

The lack of suitable capture interfaces is one of the main technical obstacles for OOS. The only feature that can be seen as some kind of interface standard is the launch interface on every satellite, as well as the nozzle of the apogee kick motor on geostationary satellites. Therefore, these interfaces feature most prominently in OOS concepts. The U.S. Naval Research Laboratory's *SUMO* design is equipped with interfaces for most fielded launcher adapter rings [63], while Kayser-Threde's *Smart-OLEV* is designed to be equipped with a DLR docking mechanism designed to capture motor nozzles [48].

The preceding sections depicted the physical and methodical baselines of rendezvous and docking, plus the tolerances such maneuvers must be designed to meet. The following section proceeds to explore the sensor systems necessary to acquire the target object amid the celestial background and determine the relative position and velocity with sufficient accuracy to allow proximity operations of two spacecraft.

4.3 Sensors

Rendezvous & docking sensors must enable the chaser to acquire the target at distances of tens of kilometers and then reliably track it down to ranges of centimeters. This large distance spread cannot be covered by any single sensor, so the chaser carries an array of different sensors, referred to as a sensor suite.

In general, sensors can be classed into two categories: active and passive. Active sensors detect and track a target by actively transmitting and receiving signals. Passive sensors rely on the target's emissions to discern position and motion. Combinations of sensors using both principles are usually employed on rendezvous spacecraft. An overview of these systems is provided in the following sections. For more details, refer to Appendix A.3.

4.3.1 Active Sensors

Active sensors emit signals and then process the echo received from the target to determine the range and range rate as well as angular position and motion. The laser ranging systems commonly used are scanning laser range finders or lidar (light detection and ranging). Radio-based systems either use radar or radio frequency (RF) guidance principles, as with the Russian *Igla*/*Kurs* guidance system.

Lidar

Laser rangefinders transmit laser in visible or invisible wavelengths and use the light bounced back from a target's surface or dedicated reflectors to determine the distance to the target. Scanning laser rangefinders, called **lidars**, use an articulated sensor head in order to scan a target with multiple laser pulses. They are thus able to either generate an image of the target or track surface features or reflectors. A number of different lidar systems are in use aboard spacecraft, most notably on the *Space Shuttle*, *ATV*, *HTV* and some of the recent robotic rendezvous & docking demonstrators [43, 155, 215].

The limitation of most lidars is the dependency on **retro-reflectors** on the target, as well as small FOVs [215].

Radar

The principle behind radar is the emission of a series of **radio waves** against a target, with the time-of-flight between transmission and the detection of the reflected waves being measured to determine distances. The range rate is determined by measuring the **Doppler shift** between outgoing and incoming waves. The range and accuracy of radar can be increased by having a **transponder** aboard the target actively transmit a response pulse whenever it receives a radar wave. Radar is the original active sensor used in rendezvous & docking, seeing use during *Gemini* and *Apollo* [197], as well as by the Space Shuttle [43, 197].

Radio navigation: Igla/Kurs

Apart from radar, radio waves can also be used for another sensing approach, called RF direction finding. The basic explanation of this approach is that a **radio transmitter** on the target continuously broadcasts a homing beacon, and the chaser uses one or a number of antennas to determine the direction of the signal's maximum intensity and follows it to its source. This approach is common in aviation where it is used to guide aircraft between waypoints and towards airports.

The only space RF homing system in operational use is the Russian ***Kurs*** (course) system, with its predecessor *Igla* (needle) [202, 216]. While the *Kurs* system has successfully served *Mir* and *ISS*, there are some limitations restricting its usability for OOS systems. Using automated mode only, i.e. without intervention by crew aboard chaser or target, *Kurs* has a rendezvous **success rate** of only 85% [4]. Apart from **reliability issues**, the major limitation to the use of *Kurs* in OOS systems is its high impact on both the chaser and target **mass** and **power** budgets. The total mass of the *Kurs* equipment on *Soyuz*/*Progress* is about 85 kg, while consuming 270 W of power. On the target side, total mass ranges at about 80 kg, with a power consumption of 250 W. This is far beyond the capabilities of OOS spacecraft which must be small and cheap in order to be commercially viable.

Although active sensor systems make acquiring and tracking targets independent of ambient lighting conditions, provide high measurement accuracies over a wide range envelope and enable relatively simple automatic approach procedures, they share some **significant limitations** for their use in OOS systems. As discussed, these systems combine **high power consumption** with often **significant mass**. In addition, they also are **expensive** and have a rather **small field of view** [217], which means that the chaser spacecraft can be forced to perform sweeping motions in order to support the sensor's scanning of the sky.

These limitations render active sensors less attractive for OOS missions than passive systems.

4.3.2 Passive Sensors

Passive sensor systems use freely available emissions of the target in order to sense the target's position, attitude or even geometry. Since spacecraft usually (in the absence of the *Kurs*/*Igla* rendezvous system) do not emit omnidirectionally at radio frequencies, only optical sensors in the visual or infrared (IR) spectra are used to directly acquire and track target objects. These optical systems comprise star tracker cameras and video systems. While often spotlights or laser diodes are used to illuminate the scene in order for these systems to work in the dark, they are nonetheless classified as passive systems in this context.

The chaser can furthermore utilize a global navigation satellite system like GPS in order to determine its own position, and by means of a data link to a similarly equipped target satellite also acquire and track the target with sufficient precision to perform rendezvous maneuvers.

Optical Sensors

Optical systems, also referred to as space vision systems, in general provide three-dimensional information about the observed object's position and orientation in space [190]. These systems utilize ambient light reflected by the target's surfaces, or the IR emissions due to the target's surface temperature, to sense a bright object against the dark background of space. Therefore, space vision systems are sensitive concerning the environmental optical conditions in space, which place stringent requirements on space vision systems. Nonetheless optical systems have numerous advantages making them sensors of choice for current and future rendezvous & docking systems, especially in the context of robotic OOS.

At **long ranges**, optical sensors can detect and track objects before these can be acquired by radar. Star trackers, which are otherwise used for aligning inertial measurement units, were used for that purpose aboard the *Space Shuttles* [43].

During the rendezvous missions of *Gemini*, *Apollo*, the *Space Shuttle* and also *Soyuz*, the **pilot's eyes** have been one of the primary sensors during close-range proximity operations. For final approach and docking, the crews relied heavily on visual observations of the **docking targets** [197]. These docking targets are special geometrical features within or adjacent to the target spacecraft's docking ports, enabling the approaching pilot to judge his relative **distance**, radial **displacement**, as

well as yaw, pitch and roll **angles**. A visual docking target basically consists of a base plate marked with linear or angular scales, and a cross mounted on a standoff above the base plate. The size of the cross as seen by the pilot is an indicator of range to target, the displacement of the cross in relation to the base plate delivers cues regarding the chaser's lateral and angular relative position. Figure 4-6 illustrates the visual docking targets' concept, as well as the view of the target installed on *Mir* as seen from a *Space Shuttle*.

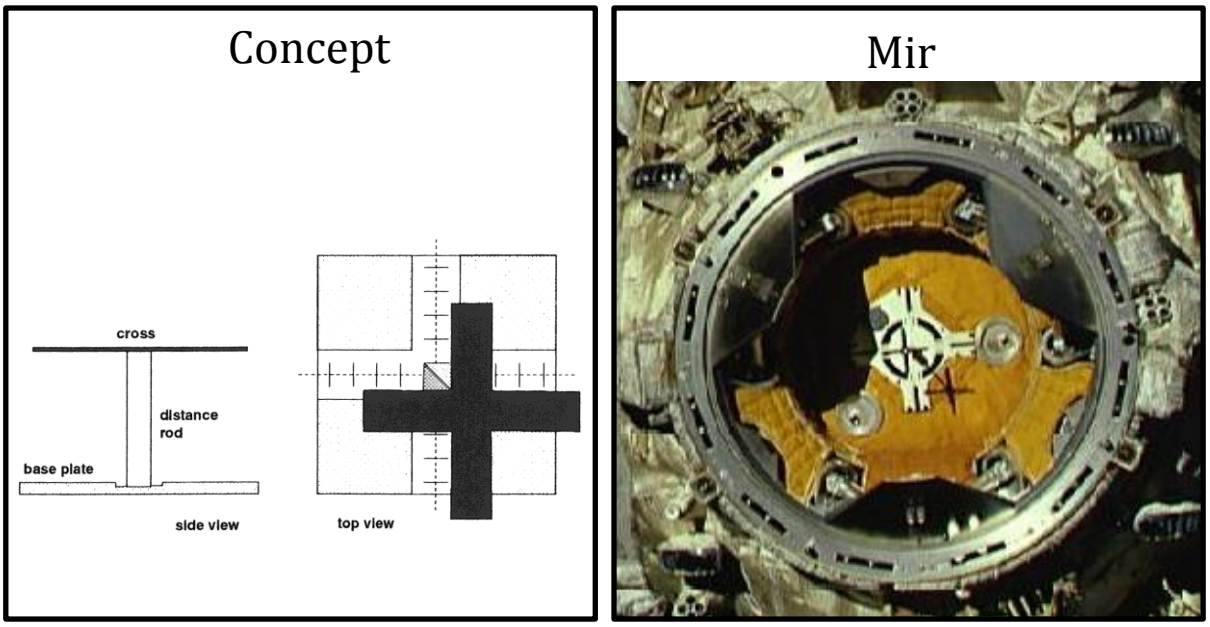

Figure 4-6: Visual docking target concept and as installed within APAS ring on Mir (adapted from [196, p. 216] and [192]). Left picture reproduced with permission of Cambridge University Press.

In order to support the pilot to judge his position and orientation relative to the target, NASA introduced the ***Crew Optical Alignment Sight*** (COAS) [43]. COAS essentially is a reticle projected onto a glass plate within the pilot's field of view, similar to a HUD (see Figure 4-7). Using the angular cues provided by the reticle, the pilot can orient the vessel and fly the docking maneuver.

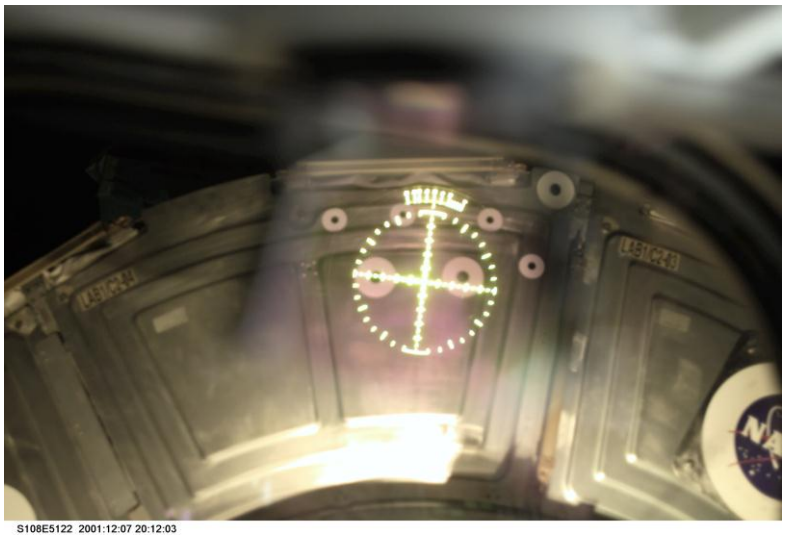

Figure 4-7: COAS during an approach of ISS [192]

In addition to COAS, the Shuttle crew is supported by a **Closed-Circuit Television** (CCTV) system. The centerline camera is positioned at the center of the orbiter's docking mechanism and pointed straight "up" [197]. Another camera is pointed at the docking system from the side. Using visual rulers on the flight deck screens, the crew can accurately determine the distance to the docking targets, with the COAS used for deriving the guidance angles [43].

Machine Vision Systems

Apart from using camera systems simply as a means to supplement the human eyesight, they also form the center of any ***machine vision system***. These systems, since long crucial to terrestrial robotics, are becoming central to unmanned space rendezvous missions, with *HTV* operationally using a system based on the *ETS-VII* experiences [218]. Machine vision systems use monoscopic or stereoscopic, visual or IR cameras to determine a target's position and pose in space.

At long ranges (approx. 100 m – 20 m) the vision system must determine **bearing** and **distance** of the target, as well as its approximate orientation and motion. These parameters are to be further refined and determined accurately and with high confidence at medium ranges of 20 – 2 m. Within short range below 2 m, artificial lighting is available to illuminate the scene and well-defined features on or around the capture interfaces can be used to obtain a **position** and **motion** solution with sufficient accuracy to permit a final docking or capture maneuver [190].

Machine vision systems use the acquired video data in image processing algorithms in order to determine target distance, pose and motion. These algorithms can be broadly categorized into three approaches: *target-based*, *model-based*, and *non-model-based*.

Most current space vision systems are ***target-based***, i.e. they rely on the installation of easy-to-detect and high-contrast visual targets on satellites and payloads [219]. Such targets are shaped similarly to the **visual docking targets** for manually guided rendezvous. Figure 4-8 provides an exemplary illustration of such a target pattern for automated rendezvous & docking.

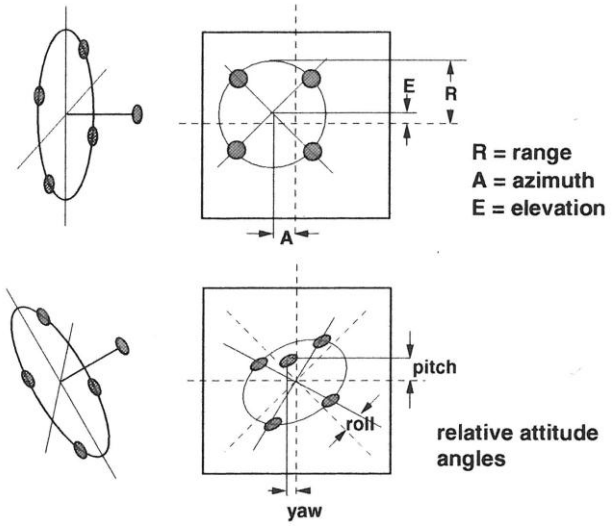

Figure 4-8: Target pattern for automated docking [196, p. 274]. The relative position between the reflector on the stand-off and the reflectors in the plane, as well as the geometry of the reflectors as observed by the sensor system, conveys information about the relative position and orientation of sensor and target. Reproduced with permission of Cambridge University Press.

Since visual targets are limited in their utility by distance and viewing angles, they can only be used in specific tasks. This requires the definition of all operations of interest concerning a satellite during the design phase and precludes any unexpected tasks [219]. Nonetheless, target-based vision systems have been fielded on operational and experimental spacecraft. Examples are the *Video Guidance System* (VGS) tested aboard the *Space Shuttle* [197, 215], the *Advanced Video Guidance Sensor* (AVGS) used on NASA's *Demonstration of Autonomous Rendezvous Technology* (DART) mission and *Orbital Express* [220], and the *AutoTRAC Computer Vision System* [220].

***Model-based** techniques* do not require the a priori installation of any artificial targets, since they rely on existing **geometry** and **structure** to obtain position and orientation data. Instead, these techniques require **a priori** knowledge of the target's geometry, so a CAD description containing the known structure, shape, textures, transmittance and reflectance is required [217]. While obtaining this data for any kind of *future* commercial OOS missions is assumed to be without major problems, it can be challenging for debris removal missions and close to impossible for military rendezvous missions. In addition to a **geometric model** of the target, the chaser spacecraft needs the capability to reliably detect natural object features for matching the model to the sensor data. This **feature detection** can be difficult at certain distances, viewing angles and illumination conditions encountered on orbit. In general, model-based vision systems using natural object features are most suitable for **close range operations**, when these features can reliably be tracked, and when an **initial pose** is approximately known [217, 219].

A vision system using that approach is Boeing's *Vis-STAR* (Vision based Software for Track, Attitude and Ranging), flown on *Orbital Express* [80]. A special target plate mounted over the capture interface is used in addition to an edge tracker algorithm, as an aid to precisely align both vehicles. Another model-based state estimation system using video images is *Natural Feature Image Recog-*

nition (NFIR) [220]. This system also shows performance problems when the target is moving too fast or is mostly outside the field of view, and under harsh illumination conditions.

Machine vision algorithms that require no a priori knowledge of the target's shape, textures or other visual attributes are referred to as **non-model-based** *techniques*. These techniques use **arbitrary surface features** of the target object and do not require establishing and maintaining direct correspondence between small numbers of high level target and model features [219]. Basically, such a technique works like the human brain. It detects and tracks prominent features on the target, establishes a pattern of the feature's motion and maps this motion onto a template in memory or a mathematical function. The challenge in these systems lies in the frequent failure of target tracking for feature points which change shape due to perspective projection, appear and disappear due to occlusion, or move against a changing background [217].

As of June 2012, it can be stated that no non-model-based vision system matches the pattern recognition and tracking capabilities of the human eye/brain combination, making **human involvement** a **requirement** for rendezvous & docking to unknown or unfamiliar target objects.

A **limitation** shared by machine vision systems is that they have difficulties when trying to **identify spacecraft** on orbit. While it is assumed that for many future OOS missions the target's design documents and CAD models will be available [219], a number of solar arrays and antennas will nonetheless be rotating about one or multiple axes relative to the central body of a satellite to be serviced, which can significantly **alter the spacecraft's appearance** from one moment to the next [209]. In addition to this, spacecraft **surface characteristics** and the **illumination conditions** discussed in Section 3.6 pose challenging problems for imaging cameras and the algorithms of vision systems [221].

Global Navigation Satellite Systems (GNSS)

Global Navigation Satellite Systems like the American GPS, Russian GLONASS, European Galileo and Chinese COMPASS-Beidou consist of large fleets of satellites in multiple orbital planes at mainly medium Earth orbit (MEO) altitudes (around 20 000 km of altitude). Using GNSS, a spacecraft can determine its position and thus its orbit to within 0.1 m [222]. If both target and chaser spacecraft are equipped with GNSS receivers and furthermore an intersatellite data link, they can share their position data and the interceptor can thus compute its rendezvous maneuvers. Such systems based on GPS were tested on *ETS-VII* [77, 202] and were a factor in the failure of *DART* [202]. GPS is now being operationally used for *HTV* [195], as well as *ATV* [223]. The use of GNSS for **operational** OOS missions is **not feasible**, since the current generation of target satellites is commonly neither equipped with GNSS nor the required intersatellite link systems.

Each **single sensor system** has its own advantages and disadvantages, as well as an optimum **operational envelope**. Currently no single sensor is able to provide relative position and posture data with the required precision over the complete approach from far range rendezvous down to contact. Rendezvous spacecraft therefore use a **combination of different sensors**, also referred to as ***sensor suites***. The complex sensor suites used by the *Space Shuttle* [43, 155], *ETS-VII* [77], *Orbital Express* [80], *ATV* [224] and *HTV* [195] are good examples.

Passive rendezvous & capture sensor systems have many advantages in the areas of s**ystem mass** and **power consumption** over active sensors. Coupled with the **human brain**'s powerful capabilities of object and pattern recognition, they have formed the **backbone of human-guided rendezvous & capture**. With the growing capabilities of computer hard- and software, space vision systems, combined with GPS and some active sensor systems, will be the center of future rendezvous sensor suites. However, the current sensor and computer vision technology still requires **dedicated sensor targets** on target objects or extensive **a priori information** about target geometry. Neither of these might be available on operational OOS mission, particularly for space debris removal scenarios. In these cases monitoring and analysis of sensor data, above all video data, by **human operators** will still be an **essential part of teleoperation**.

4.4 Target Behavior

Target behavior, both expected and actually encountered, plays a **fundamental role** in the design of rendezvous & capture systems. This behavior can be characterized as the product of three factors: the target's **equipment**, its **character** and its **attitude profile**. This product determines whether the target is to be considered *cooperative* or *uncooperative* for rendezvous & capture and also subsequent OOS.

In order to be **cooperative**, an object must be *equipped* with some kind of beacon or **sensor target** and a **docking fixture** [225]. This allows the interceptor to acquire, track, approach and capture the target. If no such active or passive equipment is available, the target is considered uncooperative [225].

The *character* of a target is *cooperative*, when it wants to be approached and will do anything in its power to assist the chaser. It would be unfavorable for mission success if the target performed any active attitude control maneuvers while the chaser is in close proximity. Another interesting event would be when the target fired a thruster after the chaser attached itself to its nozzle. The clearest example for a cooperative character is *ISS*. *Hubble* also arrested its solar arrays, folded its high gain antenna and closed its instrument cover when the *Shuttle* approached, triggered by ground commands [70]. Future satellites designed to be serviced might be commanded by the chaser to shut down their AOCS and move their antennas and solar arrays into resting positions to allow the chaser a safe approach.

An *uncooperative* target does not offer these options. It will continue to perform as before regardless of the chaser's approach. Furthermore, it is not equipped with sensor targets, reflector or beacons which would facilitate relative attitude estimation [85]. Malfunctioning satellites of the current generation can fit into this category, as well as space debris objects.

The target's *attitude profile* is also a decisive factor in judging cooperativeness. When the target is in a **stable attitude**, i.e. either inertially stable in all three axes or stable in the LVLH frame, it can easily be approached and captured. If it is however rolling or **tumbling** due to residual spin or uncontrolled atmospheric torquing, magnetic torquing from satellite eddy currents, solar radiation, etc. [226], the capture and docking process becomes significantly more complicated or even impossible. For most target objects to be approached during OOS missions, the body rates of the target will **not be available** a priori [85].

The product of target equipment, character and attitude profile determines whether rendezvous & capture and OOS is at all feasible and what kind of approach, docking interface and sensor array is required to perform the mission.

4.5 Summary

Rendezvous & docking is the **critical capability** for any operational OOS and space debris removal system. It involves precise relative guidance, navigation and control from far ranges down to final approach and docking. The maneuvers flown during far-range and close-range rendezvous are dictated by the **relative motion** of the spacecraft as described in Section 3.3. The **precision** of the final approach maneuvers is mainly dictated by the **operational envelope** of the docking and capture system.

Spacecraft use a number of **active and passive sensors** for relative navigation and maneuver planning. For robotic OOS missions, the performance of most active sensor systems is limited by the **power and mass restrictions** of small spacecraft. Passive, camera-based machine vision systems are limited by either requiring the a priori installation of **sensor targets**, the a priori knowledge of **target geometry**, or substantial sensing and **computing capabilities** for feature detection and identification on uncooperative targets. The capabilities of machine vision systems are therefore currently inferior to human pattern recognition and spatial modeling capabilities.

As of early 2012, the only operational spacecraft able to rendezvous with and capture uncooperative targets is the U.S. *Space Shuttle* (see Section 1.3.1 for an overview of *Shuttle* OOS operations). The considerations going into the *Shuttle's* design (refer to [23, 43]) thus need to be regarded when an operational servicing infrastructure is being designed. Servicer spacecraft must be **adaptable** to a wide range of different target geometries, masses, and behavior, flexible enough to be able to change approach procedures in the face of changing circumstances, and robust enough to recover from initial failures and thus be able to try again. In all past and current space systems, only **manned systems** possess this kind of flexibility. So if future OOS systems are to be unmanned, they either require **enormous leaps** in robotic sensing and decision-making technology in order to work, or they will require the **active involvement** of human operators; as situational aware observers when possible, but as telepresent controllers when necessary.

CHAPTER B:
AUGMENTATION METHODS AND EVALUATION

If we knew what we were doing, it wouldn't be called research, would it?

Albert Einstein

5 Evaluation Environment

The technologies and methods developed in the course of this doctoral thesis must be evaluated in representative environments and scenarios in order to confirm or refute the research hypothesis. The verification tests will be user studies in which test participants will be tasked to complete rendezvous & docking scenarios which are designed to evaluate individual system components and finally the integrated, complete *ThirdEye* system. These tests thus require a simulation environment which is able to recreate the **relative motion** between a realtime teleoperated chaser spacecraft and its target. In order to achieve a **high visual fidelity** of the simulation and in order to be able to utilize **hardware components** developed in the course of the research program, it was necessary to create a hardware simulator instead of spaceflight simulation software.

For this purpose, an integrated **hardware-in-the-loop** (HIL) proximity operations simulation testbed called RACOON (Realtime Attitude Control and On-Orbit Navigation) laboratory was created in cooperation with other research projects. The development, implementation and integration of the simulation environment were a major part of the technical work for this doctoral thesis.

The evaluation environment consists of three components. First, an **operator interface** representing a teleoperation ground control station; second, a **simulated space segment** in which the relative motion between the involved spacecraft as well as lighting conditions can be simulated; third, a **communication setup** simulating the properties of a ground-to-space communication chain via single DRS. These individual segments were implemented by students under my supervision, as well in cooperation with a number of my colleagues. The implementation details are described in the following sections.

5.1 Teleoperation Ground Control Station

A satellite **mission control center** (MCC) was available at the start of this research project. Its original purpose was to serve as ground control segment for small-satellite Earth observation missions, as well as for CubeSat missions. This original setup was thus optimized for **small-satellite operations** and team interaction and had an elliptical layout (see Figure 5-1).

Figure 5-1: Original mission control center layout. The MCC was optimized for small-satellite operations and team interaction and thus had an elliptical layout.

For the realtime teleoperation simulations run for this doctoral thesis, the setup was changed to a more traditional, **forward-oriented** layout, in order to maximize the operators' awareness of the remote situation. During the redesign, the existing furniture and much of the existing computer hardware was reused, while additional computers, an additional projector and new network wiring were introduced. The adapted setup is illustrated in Figure 5-2.

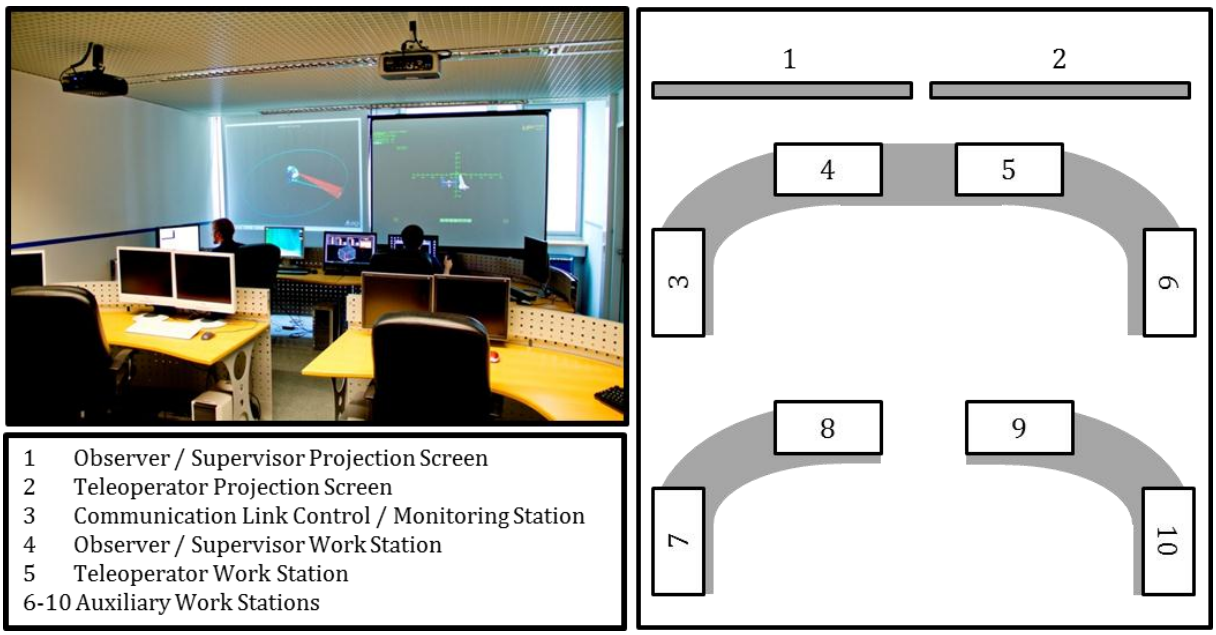

Figure 5-2: Overview of the RACOON lab mission control center. Only the front row of work stations is used for the ThirdEye experiments. Projection screen 1 displays mission and status information for the mission observer/ experiment supervisor working at work station 4. The operator on work station 5 uses projection screen 2 as main display. The status of the communication link can be monitored and controlled on work station 3.

Operator Station

In the new setup, the operator and the experiment supervisor sit **side-by-side** in front of two projection screens and a number of monitors. The operator is seated in front of the right-hand projection screen which shows the **operator display**. While only monoscopic video was used during the *ThirdEye* evaluation experiments, the operator's projector is a **stereoscopic projector** designed to be used with liquid crystal shutter glasses. The operator workstation is accordingly equipped with a high-performance nVidia graphics card capable of stereo vision. The interface devices used by the operator to control the chaser spacecraft are a keyboard and multiple HMI devices such as **joysticks** and a 6DOF **space mouse**. A custom computer program called *ControllerAdapter* is used to interface to the input devices joystick, space mouse, keyboard and WiiMote. It was specifically developed for this doctoral research program and serves to read the button and axis activity of the devices and to convert these actions into network data streams.

Figure 5-3: Operator sitting at his workstation. The main output is displayed by a video projector. The small monitor is used for auxiliary data. The main input devices are keyboard, joystick and space mouse, which are interfaced by a custom-built computer program.

Supervisor Station

The experiment **supervisor** controls the mission simulations from his workstation, which is positioned to the left of the operator workstation. The heart of the supervisor station is the s**imulation control computer**. This computer is equipped with a 24 in. touchscreen for intuitive and efficient data input. For the *ThirdEye* mission simulations and evaluation experiments, a **simulator control GUI** was developed. It allows quick and easy setting of the simulation parameters orbit altitude, simulation scale factor, roundtrip time delay, maximum linear and angular accelerations, maximum velocities and rates, initial relative position and velocity, as well as initial chaser and target attitude angles and rates. These parameters can be set individually, or as a group by selecting pre-defined test scenarios. The position, velocity, attitude and rate values computed by the relative motion simulation software, as well as the feedback values returned from the space segment realtime

motion controller, are displayed as numbers as well as a position plot to the right of the input fields. Furthermore, the GUI can be set to write all relevant maneuver data to log files. These files constitute the main source for the objective performance data analyzed in the course of *ThirdEye* evaluation. Figure 5-4 shows a screenshot of the GUI during a simulation run.

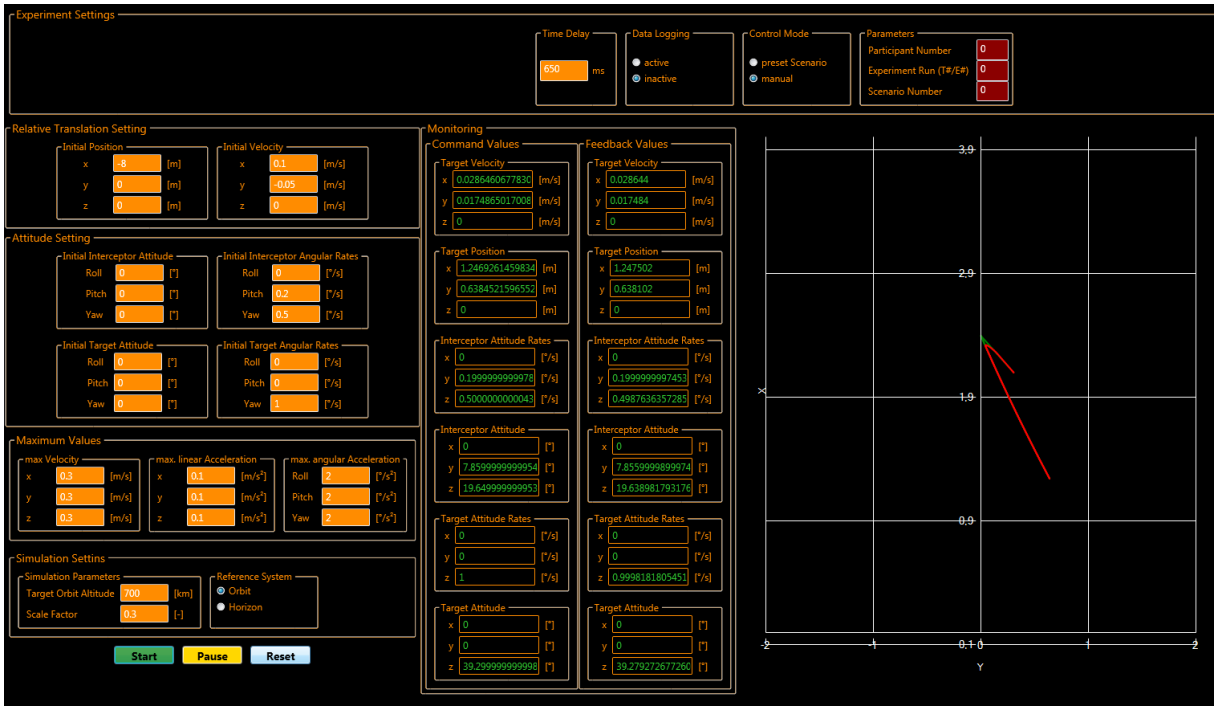

Figure 5-4: Simulator control GUI developed for the ThirdEye experiments. The top input area allows setting the simulated roundtrip time delay, activating data logging, selecting manual or preprogrammed scenario definition, and defining scenario number, test participant number, as well as test run number. The orange fields on the left side serve for manual setting of the simulation parameters orbit altitude, scale factor, as well as initial relative position and velocity, and chaser and target attitude and rates. The telemetry data display occupies the center of the GUI. The left column displays the commanded position, velocity, attitudes and rates as computed by the relative motion simulator software, whereas the right column shows the real values as returned by the realtime motion controller. Nominal values are shown in green, while off-nominal and potentially dangerous values are printed red. The right side of the GUI shows a plot of the relative position, which facilitates situation monitoring during simulation runs.

Data Exchange

The operator and supervisor workstation exchange data with each other as well as the simulated space segment mainly by means of the Real-Time Innovations (RTI) *Data Distribution Service* (DDS) [227]. Control station architectures based on DDS have earlier been used in *Ranger* [228] and NASA's *Robonaut 1* [229], and thus have a heritage in space systems simulation and control. The DDS middleware handles all network connections and also manages data exchange between programs running on the same computer. This capability greatly enhances the flexibility of the control station and simulator setup, while at the same time making programming more efficient. Any of the HMI software and control programs developed for this doctoral thesis can be run on any computer

within the simulation setup without loss of functionality. This flexibility enables its use for other current and future research programs.

5.2 Simulated Space Segment

The **space segment simulation** must provide a reasonably realistic representation of the **relative motion** of two spacecraft during proximity operations, final approach, and docking. The simulation must furthermore be able to receive user maneuver commands via input devices like keyboard, joystick or space mouse, and to convert these inputs into translation and rotation maneuvers in real time. In order to increase the credibility of the verification experiments as well as to allow the inclusion of **real sensor hardware** into the simulation, the development of an **HIL simulation environment** was started at the beginning of this research project. However, as this HIL setup would not be available from the start, it was decided to utilize spaceflight **simulation software** for prototyping and testing of the HUD elements of the *ThirdEye* system, as well as to investigate alternative means of HIL simulation in case the RACOON simulator would not become operational in time.

5.2.1 Orbiter Spacecraft Simulator

Orbiter is a realtime **spaceflight simulation** and visualization software. It was developed by Martin Schweiger at the University College in London, UK for spaceflight demonstration and education [230]. It is available for free download [231]. *Orbiter* combines a Newtonian physics engine and a 3D visualization with an application programming interface (API), allowing users to create vessels, scenarios and user-interface modules for the simulation. This makes it an ideal choice for quickly setting up space mission scenarios for user studies. Figure 5-5 provides an example scene from *Orbiter* showing the available simulation and visualization capability.

Orbiter natively supports command input by keyboard and joystick. Software add-ons for free configuration of joysticks and for usage of six degrees-of-freedom devices like a space mouse are available on the Internet and have been used in this research project.

Orbiter was used for **prototyping** and testing the proximity operations HUD described in Section 6. For the purpose of maneuver data logging and exchange, a software plug-in was developed that allowed broadcasting spacecraft state data from *Orbiter* via DDS to other applications, primarily Matlab/Simulink.

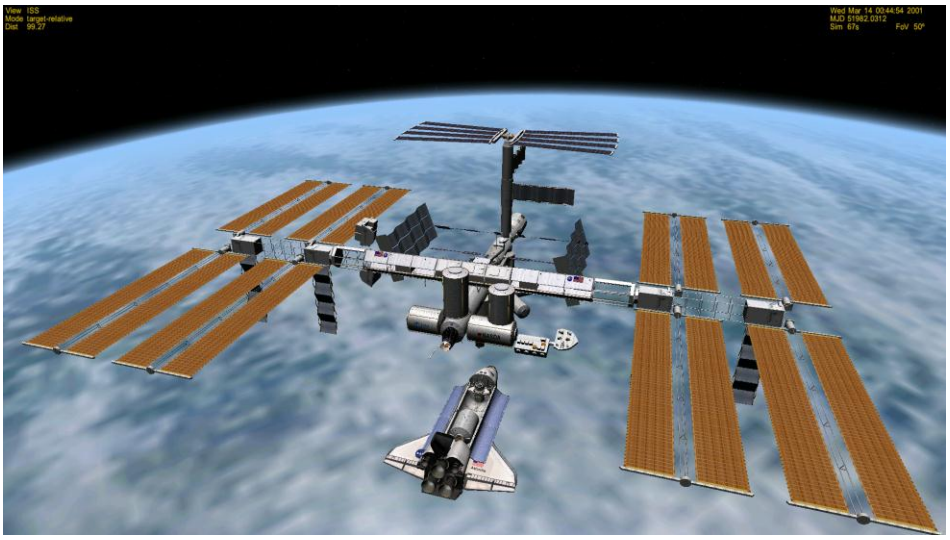

Figure 5-5: Example scene from Orbiter*, showing* Space Shuttle Atlantis *in proximity operations with* ISS*.*

5.2.2 RACOON Proximity Operations Simulator

The development of a **proximity operations simulator** for *ThirdEye* evaluation was initiated at the onset of my doctoral research in 2008. The desired goal was to have a simulator represent relative motion in all three axes of translation as well as about three axes of rotation for both the chaser and target vehicles. Two student research theses were conducted under my supervision to design the mechanical layout of such a simulator [232], as well as to implement the required control electronics and software [233]. Due to budget and manpower reasons, this simulator project was put on hold after two years of research and development. In early 2011 it was restarted in cooperation with my colleague Andreas Fleischner and named *Realtime Attitude Control and On-Orbit Navigation* (RACOON) laboratory. With the support of a number of staff and students, it became operational after six months of final development and construction, by August 2011. RACOON is designed for joint use over multiple research projects and will be developed in a number of capability increments.

Mechanical Design

For the initial configuration, designed to be used for the *ThirdEye* evaluation experiments, it was decided to only simulate relative motion between two spacecraft within the **orbital plane**. This is usually considered sufficient for most proximity operations simulation purposes [234]. The core of this simulator configuration core is a 5 m x 4 m **motion platform** which allows translation along the horizontal x and y axes, and rotation about the vertical z axis. This is supplemented by an additional two degrees-of-freedom (azimuth and elevation) **slewing mechanism** (refer to Figure 5-6)[6].

[6] Later versions of the simulator will feature an additional rotary three degrees-of-freedom mechanism, designed to allow the simulation of tumbling target objects.

This configuration was completed by August 2011, after which it was used for the *ThirdEye* evaluation experiments.

For the *ThirdEye* experiments, all active mechanical and electronic components of the experimental system were concentrated in the **chaser satellite model** carrying the *ThirdEye* hardware. The **target satellite** was a lightweight structure mainly constructed of wood and had no electronic components and no mechanisms and thus did not need power and data connections. The target satellite was therefore placed on the platform while the chaser satellite model with the *ThirdEye* hardware (see Section 7.3.1) was mounted on the slewing mechanism. This setup requires the inverse simulation of the target's motion relative to the chaser in order to generate realistic video data for the operator, thus increasing the computation and programming demands, while reducing the necessary amount of wiring and the mass to be supported by the motion platform.

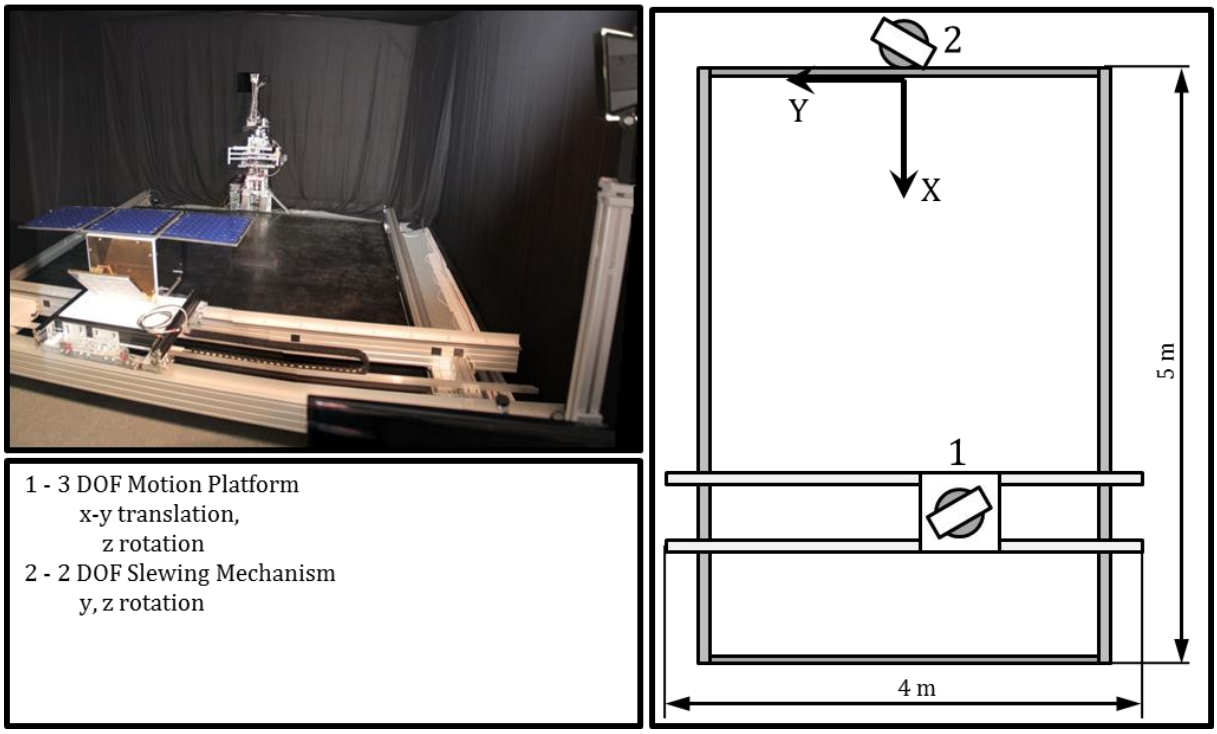

Figure 5-6: RACOON hardware-in-the-loop proximity operations simulation setup. The setup combines a 3 DOF motion platform (2 DOF translation, 1 DOF rotation) with a 2 DOF slewing mechanism. It therefore allows the simulation of docking approaches within the orbital plane. The motion envelope for the platform is 5 m in x direction and 4 m in y direction, with unlimited rotation about the z axis. The mechanical limits of the slewing mechanism envelope are ±90° in elevation (about y axis) and ±180° in azimuth (about z axis). However, this envelope is further restricted by the shape and dimensions of the object mounted on the mechanism. For the ThirdEye experiments, the azimuth angle was limited to ±90°, the elevation to ±20°.

The relative motion simulation setup is enclosed by a cage supporting black curtains in order to eliminate the optical references in the environment and thus create almost realistic optical conditions. Lighting is provided by a single 50 W **halogen lamp** which can be placed arbitrarily within

the cage[7]. While this lamp is certainly not sufficient to represent the approx. 1400 W/m^2 intensity of direct sunlight, it nonetheless suffices to create stark contrasts between lit areas and shadow on the target, and also causes surface glare in the camera images (see Figure 5-7). For the *ThirdEye* experiments, the lamp was positioned to the right and behind the chaser satellite mockup on the slewing mechanism, and was directed at a point approx. 1 m in front of the chaser's yaw axis.

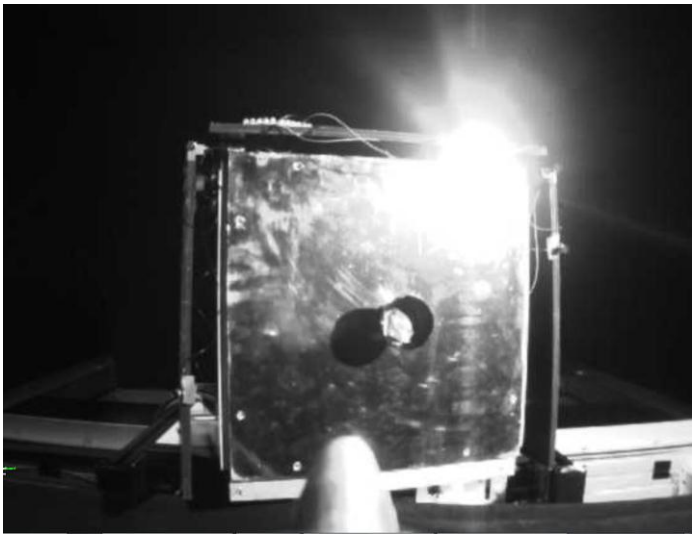

Figure 5-7: Glare on the target object, generated by the combination of highly reflective surfaces and intense lighting. Such glare is typical for optical conditions during final approach and docking and represents one of the major challenges for machine vision systems.

Software

The five axes of the simulation setup are actuated by stepper motors controlled in open loop by a **realtime controller** running on a National Instruments CompactRIO (compact realtime input/output) system. This realtime controller accepts position and velocity input via UDP/IP connection from any control software. This controller is the backbone of the RACOON simulation setup and was designed and implemented by Andreas Fleischner.

The **control software** for simulation of in-plane relative motion between two spacecraft was custom-implemented by me for the *ThirdEye* experiments. The software uses the initial conditions set in the simulator control GUI (described in Section 5.1) and the user commands gained with *ControllerAdapter* to derive the relative position and velocity via the CW equations for constant-thrust maneuvers (equations 3-11 - 3-14). Current attitude angles and rates are computed in real time by a set of attitude rotation operations. As this control software is identical to the prediction software used for the attitude and trajectory prediction HUD, it will be described in detail in Section 6.5.

[7] Later versions of the simulator setup are to include a realistic lighting simulation. One side of the setup will be equipped with a Sun simulator providing a high-intensity, parallel-beam light source, while the other side will feature an Earth albedo simulator with soft lighting.

Satellite Models

The **target object** used in the experiments is a cubical satellite mockup (see Figure 5-8). Its top and two of the sides are covered by blue panels representing **solar arrays**. These panels were initially intended to be used in an extended position during *ThirdEye* experiments, but were after initial simulation runs folded down in order to prevent damage to the simulator hardware. The other sides of the satellite model are covered by highly reflective gold and silver foils representing **MLI surfaces**. On the front, the satellite carries a **slanted antenna**. This creates a collision hazard during approaches of the rotating target and thus requires **collision avoidance**. On the back, a conical nozzle serves as the **docking interface**. In order to prevent damaging the simulator during failed docking attempts, the nozzle was fabricated from flexible plastic. Near the throat of the nozzle rests a target plate with a diameter of 30 mm. When the experiments are run at the scale factor of 0.3, the size of the target plate thus recreates the ±50 mm positioning tolerance of the *Orbital Express Capture System* (refer to Table 4-1 and Appendix A.2.5).

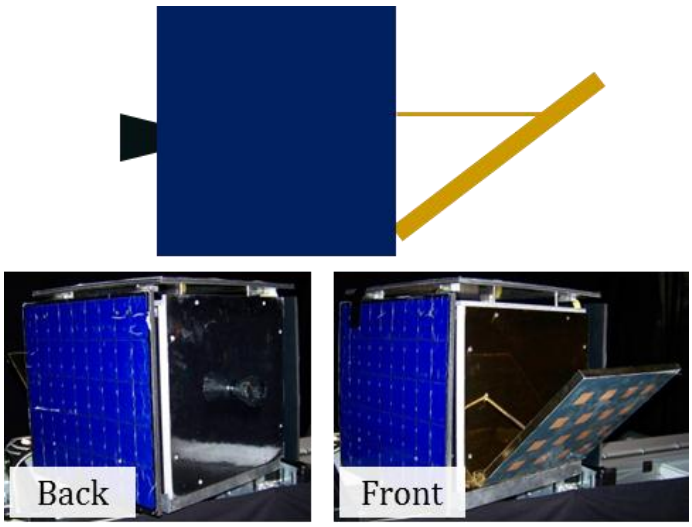

Figure 5-8: Target satellite used in the ThirdEye evaluation experiments. The cubical satellite mockup is covered by blue panels representing solar arrays on the top and two sides. All other sides are covered by silver and gold foil representing MLI. On the back, the satellite features a conical nozzle serving as a docking interface. On the front, a slanted antenna creates a collision hazard during approaches of the rotating target.

The **chaser satellite** mockup is built around a support structure mounted onto the 2DOF slewing mechanism. This structure is composed of standard aluminum profiles which carry the *ThirdEye*, a camera and a **docking probe**. This docking probe corresponds to the nozzle on the target object (see Figure 5-9). It is positioned directly in front of the pitch and yaw axes of the 2DOF slewing mechanism. This position corresponds to being directly in front of the **center of mass** on a real spacecraft. The docking probe has a length of 120 mm and a base diameter of 20 mm. Its conical tip carries a small switch which engages once the docking probe hits the target surface. On this cue, the realtime controller of the setup halts all motion, which concludes an experiment run. For safety reasons, the system must be reset manually before the next run can begin.

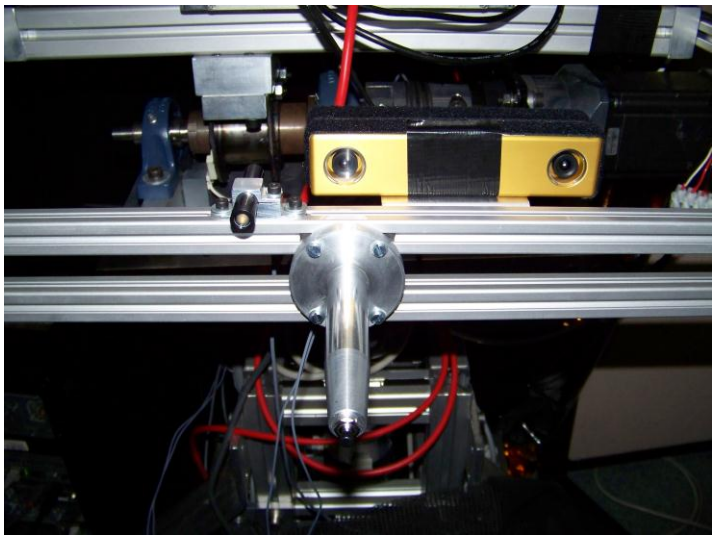

Figure 5-9: Front of the chaser satellite mockup. The docking probe is positioned directly in front of both yaw and pitch axes. It carries a small switch which engages at contact to target and halts the simulator motion. A Bumblebee2 camera is mounted above it so that its right lens is directly over the docking probe. This camera serves as the main sensor during the docking experiments. The black cylinder on the left of the camera is a laser pattern generator. It was not used in the ThirdEye evaluation experiments.

A Point Grey Research Bumblebee2 stereo camera [235] served as the main sensor during the *ThirdEye* experiments. The right lens of the camera is positioned directly over the base of the docking probe. The probe is therefore in the middle of the video images the operator sees. The cameras streamed 8 bit grayscale video at a resolution of 640 x 480 pixels at a frame rate of 15 fps, which is within the acceptable boundaries for teleoperation [151]. The video compression method used was a Joint Photographic Experts Group (JPEG) standard with 50% loss.

The design of the target satellite and its construction from standard aluminum profiles allows for rapid integration of additional or alternative sensor hardware. This makes it flexible enough to serve in other current or future research projects.

Figure 5-10 provides an overview of the RACOON configuration for the *ThirdEye* experiments.

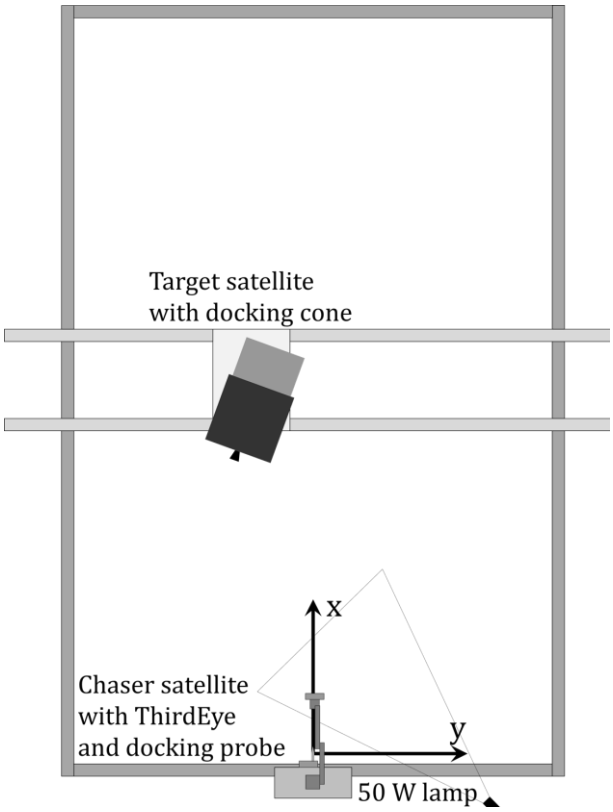

Figure 5-10: ThirdEye evaluation experiment setup. The target satellite with its antenna and the docking cone is mounted on the 3DOF motion platform. The chaser satellite setup with the primary camera, the ThirdEye and the docking probe is mounted on the 2DOF slewing mechanism. The scene is illuminated by a 50 W lamp positioned to the right and behind the chaser satellite, with the light pointed right in front of the chaser.

5.2.3 Alternative Fallback Options

The availability of the RACOON simulation setup for the *ThirdEye* experiments was not certain at the beginning of this research project. In order to ensure the availability of an adequate evaluation environment, a number of alternative solutions were investigated. These were required to provide the degrees of freedom of the RACOON setup, but with lower accuracy and precision, and also lower mass bearing capability.

Slewing Mechanism

An **alternative 2DOF** slewing mechanism was designed and implemented in student research projects. In one student project [236] under my supervision, a 2DOF pointing mechanism [237, 238] originally developed in the course of the *Lightweight Intersatellite Antenna* (LISA) development project [239] was adapted to carry the Bumblebee2 stereo camera, a laser rangefinder, and a laser pointer equipped with a diffractive pattern generator [240]. The control software, developed in the course of a Master's thesis [241], is able to teleoperate the mechanism via UDP/IP connection and to interface to a joystick. It furthermore has provisions to transmit the azimuth and elevation angles and rates to the 3dSVK version of the attitude HUD (refer to Section 6.3.3).

This pointing mechanism, as shown in Figure 5-11, allows a motion envelope of ±30° in elevation and ±90° in azimuth. The elevation limit is due to the maximum torque sustainable by the coupling in the elevation drive. The azimuth angle is limited by the power supply and control wires leading to the elevation motor. While this pointing mechanism does not allow the mounting of the *ThirdEye* robotic camera arm, it would still provide a motion envelope sufficient for limited docking experiments.

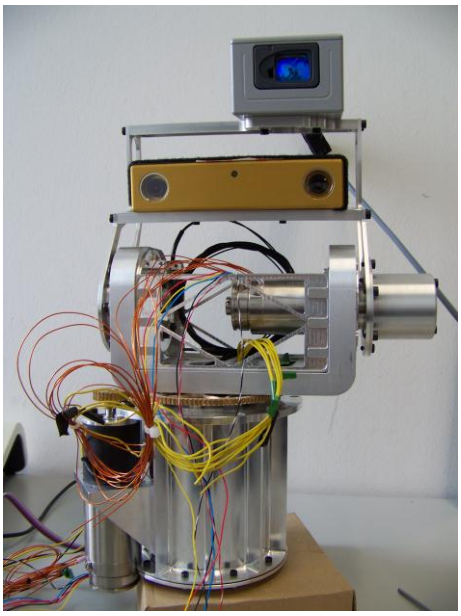

Figure 5-11: The LISA 2DOF antenna pointing mechanism as adapted to the needs of ThirdEye evaluation. A laser range finder is mounted above the Bumblebee 2 stereo camera. Note the absence of the laser pattern generator, which was not yet included in the initial design stage depicted here. It can be attached to the mechanism underneath the range finder, directly atop the right-hand lens of the camera.

Since the RACOON simulator became available in August 2011, the alternative 2DOF mechanism was never used for rendezvous & docking experiments. It was also planned to be used in an experiment series investigating the projection of laser patterns onto the target surface during final approach, and its impact on alignment precision between chaser and target. These experiments were however also conducted in the RACOON setup, once it became available [240].

The alternative 2DOF was used for a student thesis investigating the performance and functionality of a laser rangefinder on highly-reflective MLI surfaces under different surface conditions and incidence angles [236].

Omnidirectional Platform

Another alternative solution was investigated to provide the three degrees of freedom (translation in the horizontal plane, rotation about the vertical axis) required for the **target object**. The prime requirement was to provide linear motion independent of the rotation rate and angle about the vertical axis, which is characteristic for motion in space. The solution was to use a small **robotic**

platform moving on **omnidirectional wheels**. The mechanical design and control software implementation was completed in the course of a student thesis [242]. The resulting target platform is able to perform linear movements in the horizontal plane while rotating independently about the vertical axis (see Figure 5-12). The three wheels are actuated by direct current (DC) motor units equipped with an encoder and a closed-loop controller that receives wheel rate commands by I^2C bus.

These motor units, above all the encoders with a resolution of 1°, did neither provide sufficient **precision** to allow the operator using a joystick to reliably command trajectories and velocities, nor did **dead-reckoning** using the combined encoder signals of the three wheels represent the true motion of the platform.

In order to create a system fully usable for rendezvous & docking experiments, the omni-platform must be operated on a perfectly level surface providing sufficient grip for the smooth plastic wheels to prevent wheel slip, and additional external or internal orientation or position sensors are required. These could be absolute sensors mounted above the simulator, tracking target points on the platform. An alternative would be to increase the accuracy and precision of the dead-reckoning approach by mounting additional sensors on the platform. A possible design is to use the optical sensors of computer mice. Such a system is discussed in [243].

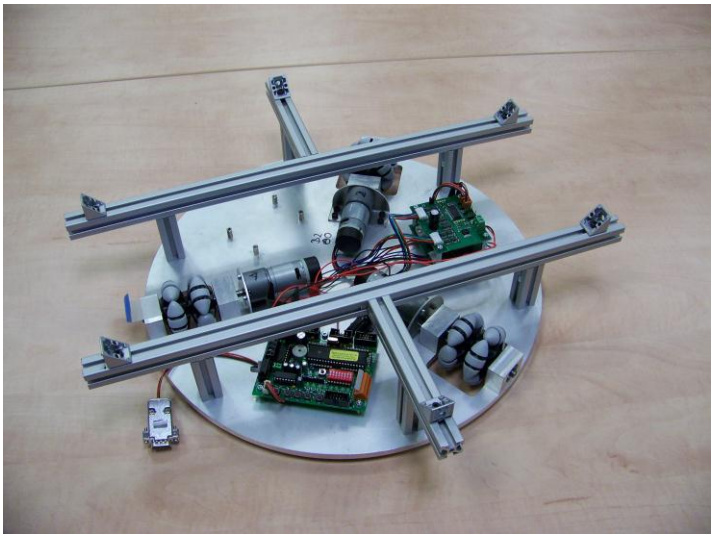

Figure 5-12: Omnidirectional target platform designed for simulation of satellite in-plane motion. The three omnidirectional wheels allow translation motion within the horizontal plane independent of the rotation state about the vertical axis. The platform is controlled by serial communication via RS232 cable or radio interface.

While the RACOON setup was equipped with a rubber floor in order to accommodate the omni-platform, it was decided to use the RACOON simulator instead of the omni-platform for target object simulation due to its higher accuracy and precision, as well as due to its ability to carry heavier objects.

5.3 Communication Setup

The communication setup of the simulation environment has two different tasks. First, the components of the ground control segment and the simulated space segment must be able to communicate with each other within the respective segments. This task is accomplished by the use of RTI DDS as mentioned above, plus a small number of peer-to-peer UDP and TCP/IP connections.

Second, the communication setup must also provide means to simulate the teleoperation communication chain from ground operator to chaser spacecraft via DRS. The RACOON simulation environment provides two approaches for this task.

The first approach, which was used in the *ThirdEye* evaluation experiments, is to **simulate** the signal **roundtrip delays** encountered in the teleoperation chain by buffering the command and telemetry data streams. Following the reasoning of Stoll [161, 244], who showed that the exact location of the roundtrip delay in the communication chain is not relevant to operator perception, the video and telemetry signals were both buffered by the full roundtrip delay directly before displaying them to the operator.

Due to the high data volume of the **video streams**, a special program was written (in cooperation with my colleague Jan Harder) to buffer them for the delay time. The **telemetry** is buffered in the *ThirdEye Proximity Operations GUI* program before generating the HUD displays.

For the *ThirdEye* experiments, the simulated delay was set to be 650 ms, which again follows Stoll's measurements (refer to Section 3.1). Including the additional time delays in the local network, this results in total roundtrip time delay of about 700 ms.

The second approach is to actually send the command and telemetry data streams over a DRS for the simulations. For this purpose, the DDS data streams are bundled and translated into standard UDP/IP streams which are then transmitted via a High Data Rate Modem (HDRM) and the Ka band communication infrastructure available at the institute [245]. DRS available for such experiments are ESA *Artemis* and Eutelsat *Hotbird 6*. While this setup is more realistic than the simulated roundtrip time delay, it nonetheless restricts **experiment times** to the availability of the relay satellites and introduces the satellite link as critical component.

Since the exact nature of the communication link and signal delays are not the focus of this research project, it was decided to use the **simulated delay approach**, which causes no limitation of the significance of the research results.

5.4 Summary

An end-to-end **simulation and evaluation environment** was **established for the experiments** described in this doctoral thesis. It consists of a teleoperation ground control center, a proximity operations testbed, and a communication link simulation.

While some parts of the **ground control center** were available at the start of the research project, the layout was optimized for realtime teleoperation and all **HMI interface software** including input device interface and simulator control software was **created for this thesis** by me and a number of students working under my supervision.

The HIL **proximity operations simulator** was created in the course of my doctoral research **in cooperation** with other research projects and colleagues, foremost Andreas Fleischner. The resulting RACOON simulator configuration is tailored towards the requirements of the *ThirdEye* experiments. The **simulation software** computing the relative position and velocity, as well as chaser and target attitude angles and rates was designed and implemented **specifically for the *ThirdEye* experiments**, although it can easily be configured to serve other research projects. A number of alternatives to RACOON were studied in the course of student research projects. Two of these, an **alternative 2DOF slewing mechanism** and an **omnidirectional positioning platform** were built and tested. Since RACOON became available in time and had substantially better performance, they were never used in actual rendezvous & docking experiments.

Preceding research had measured the **roundtrip time delays** to be expected in a teleoperation **communication chain via a single DRS**, and had also shown that the exact location of the delay in the communication chain has no impact on operator performance. It was therefore decided to utilize a **simulated roundtrip time delay of approx. 0.7 s** in the *ThirdEye* evaluation experiments. A dedicated program was written in cooperation with my colleague Jan Harder to buffer the video streams, while the telemetry was buffered in subroutines of the *ThirdEye Proximity Operations GUI* program.

The exchange of video, commands and telemetry data via network per DDS, UDP and TCP also makes it possible to integrate a real DRS into the communication chain. Due to **availability issues**, this **real satellite link** setup was **never used** in the *ThirdEye* experiments, but could be used in future research projects.

6 Proximity Operations HUD

Knowledge of ownship position, attitude and motion, as well as the prediction of this state into the future for maneuver planning and time-delay compensation are the first two elements necessary to achieve operator SA during teleoperated rendezvous & docking. A Head-Up Display was designed to provide the necessary information in an accessible way, in order to facilitate intuitive understanding of critical state data. Based on different designs for attitude representation, different display coordinate reference systems and different versions of a trajectory prediction display, a HUD configuration was identified in a series of experimental user studies which offered best user performance in attitude maneuver command, relative position estimation and translation maneuver command tasks. The results of the design process and the evaluation studies were published over a span of four years [246–248].

This section provides an overview of the motivation behind the choice of an HUD to augment operator SA. It then proceeds to discuss general requirements of HUD design. Subsequently, the specific design of the *ThirdEye Proximity Operations HUD* is discussed. The Chapter then proceeds to describe the evaluation experiments and analyze their results. The final Section describes the changes made to the HUD in its final implementation for the integrated *ThirdEye Proximity Operations GUI*.

6.1 Motivation

During final approach and docking in the course of an OOS mission, the operator needs a maximum of knowledge about **ownship orientation and motion** within the LVLH reference frame, as well as about target motion. As was discussed in Section 3.5, the orbital environment does not provide sufficient natural references for the operator to be able to deduct this information from video images alone. Such references must therefore be provided in a **synthetic display** alongside critical ownship information such as roll, pitch, yaw angles and velocity. The proper integration and presentation of such vital information provides an enhanced understanding of the ownship state within its operational environment and thus enhances operator SA [99]. In order to be of maximum use to the operator, this information must be presented in an accurate, accessible and easily interpretable manner [99]. An integrated display then reduces operator scanning time as well as the need to integrate spatial information from multiple sources and therefore facilitates attention focus and management [125]. A well-organized display can convey self-motion cues without occluding the primary sensor image [125].

Head-Up Display Functionality

Head-up displays display orientation, position and velocity data as a graphical overlay over live video or a real outside view. They constitute therefore a simple form of an AR display that does not require a detailed graphical model of the environment and its elements, which is difficult to attain during rendezvous & docking operations. HUDs provide a clear advantage in the detection of events

in the HUD symbology as well as in the environment [249], as compared to the display of information on separate screens or the classical "head-down" aviation displays. This capability to display critical information within the primary sensor display without a need for modeling the chaser spacecraft's environment as required for more elaborate AR or VR displays, makes a HUD especially useful for the purpose of conveying the ownship state information critical during final approach and docking, as well as to provide a trajectory prediction display.

HUD Development

The basic idea leading to HUDs is to reduce a pilot's workload by integrating important state information directly into his field-of view. In this manner, the pilot does not need to shift his gaze and focus from the outside world to the instrument board and back. This results in **reduced workload** and **increased situation awareness** during mission phases with high attentive requirements, especially during takeoff and landing, and in combat situations. The idea was first formulated in the late 1940s, and since the 1960s, HUDs have become a standard feature of combat airplanes [250]. Over time, the displays have evolved both in representation and content. In the beginning, mostly basic flight data (artificial horizon, altitude and velocity) and a projected gunsight were displayed. Later HUD versions are much more complex, showing trajectory predictions, threat information or even three-dimensional (3D) representations of the environment [251]. Figure 6-1 provides an exemplary view of a common aviation HUD.

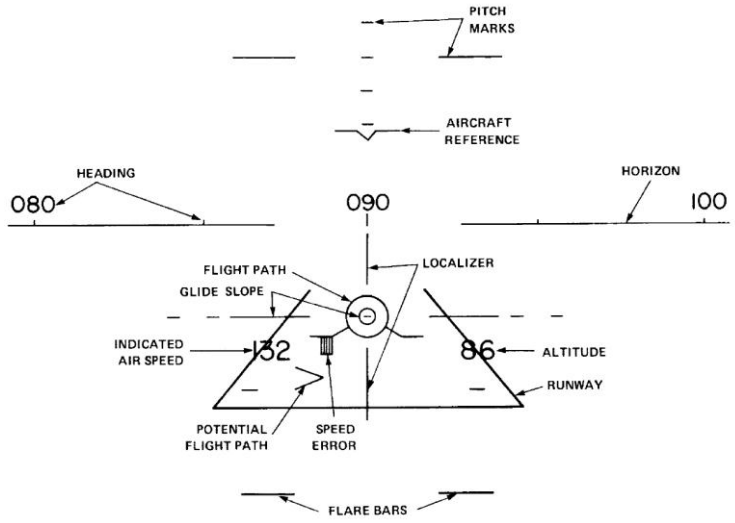

Figure 6-1: Head-Up Display as commonly used in aviation [252, p. 3]. The HUD displays information critical to the piloting task, such as the horizon line, heading, altitude, air speed, pitch angle and flight path. Similar symbology is to be used in the ThirdEye Proximity Operations HUD*.*

The benefits of the HUD have not gone unnoticed by the commercial aviation, telerobotics and automotive communities. Therefore, they have been introduced into the cockpits of commercial airliners, business jets, cars and also robotic vehicles, most prominently UUVs.

Space Teleoperation HUDs

Besides the benefits of the information displayed in the HUD, the HUD symbols furthermore provide **stable alignment features** against which the movement of objects in the FOV can be measured. This prevents the illusion of stationary objects in the environment having a radial motion [187], which increases operator SA during proximity operations of spacecraft

However, no publication could be found treating the usability of different HUD designs and display methods for space teleoperation. The aim of the research summarized in this chapter was therefore to develop a **proximity operations HUD** displaying ownship **attitude data** as well as a realtime **trajectory prediction** overlaying a life video stream. In order to identify the combination of the HUD elements attitude representation, coordinate reference system, and trajectory prediction display method most usable for in-orbit teleoperation, the experimental version of the proximity operations HUD was designed and implemented to include multiple attitude representations, coordinate systems and trajectory prediction displays in order to evaluate the individual elements in user studies. These studies both serve to fill the research gap identified in literature research, as well as to identify the HUD to be used in the *Third Eye Situation Awareness Enhancement System*.

6.2 Design Considerations

Head-up displays serve to integrate essential state information with a view of the environment. Compared to "head-down displays" common in automobiles and civil/commercial aircraft, as well as to the display of information across multiple screens, as still widespread in the fields of mobile telerobotics and space operations, HUDs can minimize scanning and the effort required to access and monitor all information elements.

Display Clutter

The integrated display of information can however also lead to ***display clutter***, if too much information is drawn to the screen. Information clutter may inhibit the processing of fine detail in the sensor imagery because of overlay clutter and can thus cause loss of occlusion cues, which in 2D displays are important for perceiving depth [125]. Display clutter can also lead to important elements of the environment being obscured by synthetic display elements [249], thus leading to reduced SA and operator effectiveness. This can be prevented by different means of "decluttering" displays. The most effective **decluttering** method is to limit the amount of information to be displayed in the graphical overlay. Alternatively, gauges and state information can be designed to change color or pop up if important thresholds are crossed in order to gain operator attention [141]. Pop-up gauges are successfully employed in collision warning and steering guidance systems in the automotive sector [141]. Such alarm displays should always be grouped together and must be labeled appropriately; there also should be a central system error and health summary [141].

Symbol Colors

The individual display elements of a synthetic vision system can furthermore be optimized in shape, color, brightness, size, transparency and style; font size, color and background; as well as in the degree of information content [125]. Symbol color and size and thus the usability of a display are obviously dependent on the background color of the sensor view, as well as scene clutter and the light level [125].

Since, when not directly looking at Earth, the space environment is devoid of most colors, the choice of **symbol contrast** is most important for symbol discernibility and readability in the *ThirdEye Proximity Operations HUD*. This is especially the case if the video stream from the chaser vehicle is in grayscales. During close-range proximity operations, the hues in the sensor imagery range from black over shades of grey (MLI surfaces) to bright white. The HUD symbols were therefore implemented in **bright green**, since this color makes symbols discernible both in front of black and white backgrounds. Bright green is furthermore the color used in the majority of aviation HUDs and is thus in its appearance familiar to many potential operators. To account for operator preferences and the use of color video, the user interface is to incorporate the function of manually switching the HUD to other colors, most importantly white and yellow (for dark backgrounds) and dark blue (for bright backgrounds). The color red is to be reserved for emergency messages and time delay displays.

Attitude Representation

In addition to selecting the appearance of the individual symbols, it is important to determine in what geometry these symbols are displayed. This decision is dependent by the operator's **frame of reference**. The underlying question is, whether the operator perceives the display as representing the vehicle within the external world (outside-in, exocentric or world-referenced view) or rather the external world moving around the vehicle (inside-out, egocentric or vehicle-referenced view) [99]. The answers to this question lead to the ***outside-in*** and ***inside-out*** HUD representations. Figure 6-2 shows an example of both HUD representations for an attitude display.

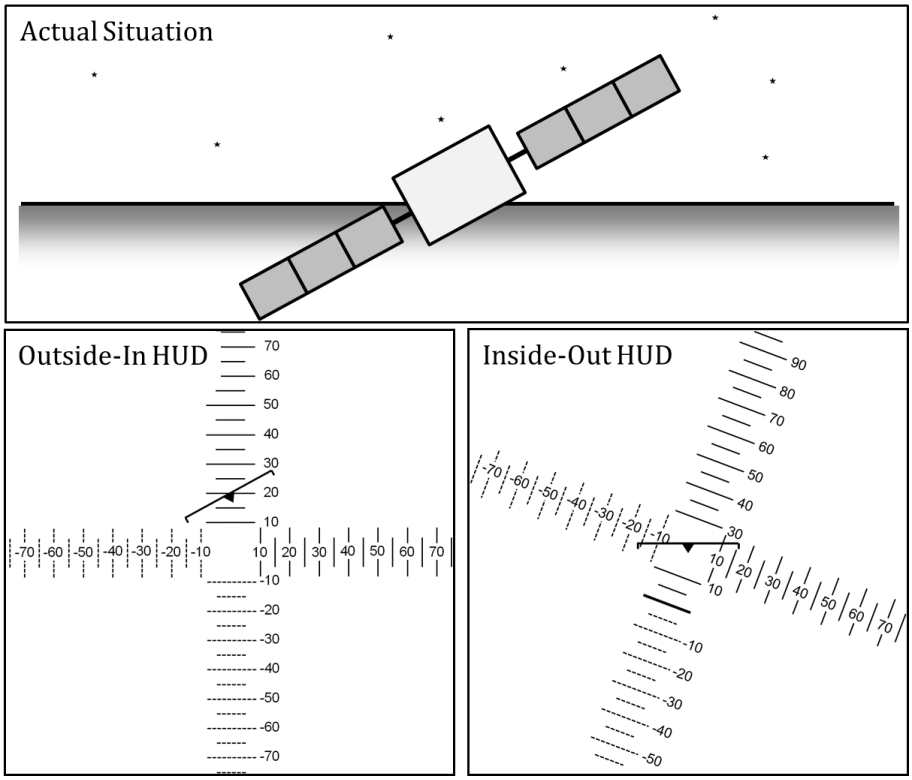

Figure 6-2: Outside-in and inside-out attitude representations. The top image shows the spacecraft attitude with respect to Earth horizon. On lower left, this situation is represented in an outside-in HUD. The attitude reference remains fixed in place, while the ownship symbol is displaced and rotated according to the spacecraft attitude. This represents the view an external observer would have of the spacecraft within its environment. In the inside-out HUD (lower right) the ownship symbol remains fixed, while the attitude references are displaced and rotated around it; thus representing the view a pilot in the spacecraft would have of the situation.

The cost and benefits of both outside-in and inside-out displays have been researched in the field of aviation [253] as well as underwater robots [99]. In aviation [253], the inside-out display showed advantages, if the HUD was used as the primary flight reference. Its disadvantages, on the other hand, were found to be that pilots need more training to master the moving-horizon display; pilots encounter difficulty in maintaining spatial orientation during instrument flight, especially in terms of aircraft roll angles; pilots experienced "roll-reversal" errors during recoveries from unusual attitudes. These weaknesses of the inside-out display were shown to be actual strengths of the outside-in display. Outside-in displays reduced roll-reversal errors with novice pilots and pilots with minimal training when recovering from unusual attitudes; experienced pilots also preferred the use of outside-in displays and showed better performance using them. There are also indications that many pilots actually use an outside-in **mental model**, even when using inside-out displays [253].

The results of the display comparison for UUV operators [99] show that outside-in displays are generally suited for teleoperation of vehicles, while replicating findings of the aviation study. The inside-out display performed worst in control reversal occurrences, and operators expressed a

clear preference for the outside-in display. It was however also stated that not all principles of display design employed in aviation are readily applicable to the underwater environment. The outside-in display was found reasonable to employ in the UUV application, since the operators are actually physically and psychologically outside the vehicle, a situation that applies to all kinds of teleoperation and thus also to teleoperated proximity operations.

Some explanations were offered to why outside-in displays performed better. The higher incidence of control-reversal errors with the inside-out display was attributed to the fact that the inside-out depiction of pitch and roll supports the principle of pictorial realism (displaying what a pilot would see) but violates the **principle of the moving part** [99]. A movement of a control input device causes movement of the display elements in the opposite direction, which is counter-intuitive to the operator's mental model and thus increases the likelihood of control reversals. Another explanation for outside-in superiority was offered by Previc [253]. He states that a moving horizon symbol is less likely than the actual Earth to be the ground against which the vehicle moves, since to meet operator/pilot experience ground figures should ideally be relatively formless, lie behind the figure and yet appear uninterrupted by it.

Cognitive Tunneling

When using HUDs with either presentation method, operators tend to use the HUD for primary control and the outside view only for monitoring purposes [252]. The reason given for this is that the symbology is more compelling than the outside scene, with more immediately perceivable change going on, thus calling for greater attention [252]. This can lead to a condition called *cognitive tunneling*, when the operator is so focused upon the synthetic displays or single elements of it that important events in the outside scene or other important objects in the synthetic scene are no longer attended [125]. HUDs particularly induce a **narrowing of attention** to processing the routine information in the symbology under high workload conditions [249]. These factors must be considered when using HUDs to increase operator SA.

6.3 Implementation

The proximity operations HUD was implemented in three different environments in order to allow a wide range of experiments.

The initial implementation was as a plug-in for the *Orbiter 2006* spaceflight simulator, which was used for the HUD evaluation experiments.

This implementation was then migrated to stereo-video display software produced by Point Grey Research, Inc. called *3d Stereo Video Kit* (3dSVK), where it was used for the display of the azimuth and elevation angles of the teleoperated 2DOF mechanism carrying a stereo camera described in Section 5.2.3. The HUDs for both *Orbiter 2006* and 3dSVK was implemented in a student research project under my supervision [254].

After the evaluation experiments, the final version of the HUD was incorporated into the *ThirdEye Proximity Operations GUI* and used during the *ThirdEye* evaluation experiments (see Section 8).

These versions of the proximity operations HUD differ in their implementation code and in details of the display, owing to the evolutionary nature of their development. The general elements of the HUD, attitude display, coordinate reference systems and trajectory predictions are however equivalent for all versions and will be explained in this Section.

6.3.1 Attitude and Trajectory Prediction Displays

The attitude of a vehicle is usually expressed by the **roll, pitch and yaw angles** of the vehicle relative to a reference frame. The pitch angle (also referred to as elevation) is the angle between the vehicle's longitudinal *x* axis (usually pointing in the viewing direction of the pilot or the main sensor) and a reference plane. The roll angle (also referred to as bank) is measured between the vessel's transversal *y* axis (for the purpose of the *ThirdEye Proximity Operations HUD* defined as pointing from the center of mass of the spacecraft along the solar arrays of a generic satellite) and the reference plane. The yaw angle (also azimuth) is measured within the reference plane and relative to a reference direction, for example the direction of flight.

Attitude Sphere

For use of a HUD, the vessel is surrounded by a fixed virtual attitude sphere, within which yaw, pitch and roll angles are displayed using a ladder representation (see Figure 6-3). Angles can either be defined in the interval $[0°, 360°]$ or $[-180°, 180°]$. The latter interval is used in the *ThirdEye Proximity Operations HUD*, with the yaw angle being measured about the reference *z* axis (pointing down), the pitch angle about the spacecraft body *y* axis (pointing right) and the roll angle about the spacecraft body *x* axis (pointing forward). Yaw angles are therefore positive for clockwise rotations within the reference plane, roll angles for clockwise rotation within the spacecraft *y*-*z* plane, and pitch angles are measured positive for upward-tilting motion of the spacecraft.

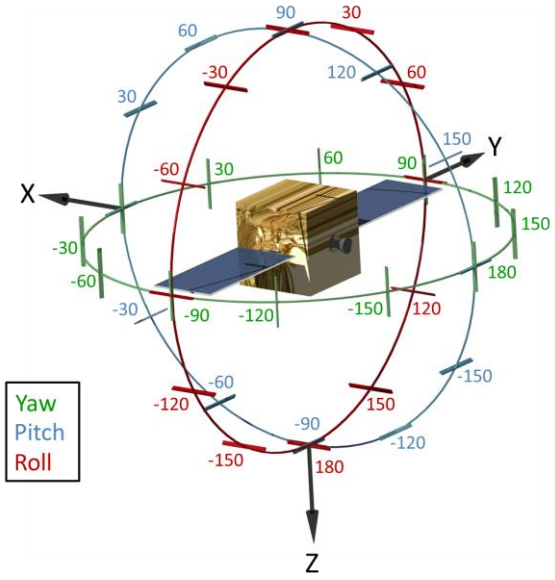

Figure 6-3: Satellite attitude sphere used for the attitude HUD. The sphere is fixed in space. The satellite's attitude as measured within this sphere is displayed by the HUD.

Reference Frames

For terrestrial applications, the obvious choice of reference plane for an attitude display is the local horizontal plane. Against this, the pitch and roll angles of aircraft are commonly measured. The azimuth is measured relative to the North vector of the geographic coordinate system[8]. This reflects the operator's intuitive natural reference.

This reference frame is not practical for space vehicles. Since a spacecraft does in general not significantly change its global direction of flight, which is determined by the orbital movement, this direction along the velocity vector, V-bar in the LVLH system (refer to Section 3.3), is a practical reference direction for azimuth determination.

Three **reference planes** were identified as suitable for space operations: the orbital plane (local vertical plane in LVLH), the local horizontal plane, and a plane defined by the *x* and *y* axes of the target satellite's body-fixed coordinate system (also referred to as Vessel system). These planes have different characteristics and advantages.

The **orbital plane** is spanned by the velocity vector ***v*** and the chaser spacecraft's radius vector ***r***. Since plane-changing maneuvers are very expensive in terms of fuel expenditure, most orbital maneuvers occur within this plane. It is therefore almost a static reference and comes closest in meaning to the operators' **natural reference frame**. However, there exist no natural cues for this reference plane and when the Earth's horizon is within the spacecraft's field of view, this can lead to

[8] Yaw angles are in aviation commonly defined in aerodynamic terms as the angle between the airflow vector and the aircraft's longitudinal *x* axis. Azimuth is the angle between direction of flight and geographic north.

a sensory conflict and thus to confusion and degradation of operator SA. Simulator sickness is not expected to arise from this mismatch, as the visual flow encountered is low (refer to Section 2.5).

The local **horizontal plane**, spanned by the velocity vector ***v*** and the orbit normal ***n***, is therefore the more "intuitive" reference, but has little significance for orbital maneuvering. It is nonetheless implemented as part of this investigation, in order to compare it to the orbital plane in terms of operator performance.

Once the chaser spacecraft has approached the target vehicle and final approach and docking maneuvers are imminent, navigation is no longer performed relative to Earth but to the target vehicle. It may therefore be beneficial for the operator to have attitude information presented in a reference frame with the principal reference direction being the vector from the chaser's center of mass to the target's center of mass. This reference system is called the ***docking reference system***. Since chaser and target need not necessarily be within the same local orbital or local horizontal plane, these planes are unsuitable choices for reference plane of this docking system. Instead, the chaser's body *y* axis is suggested to be used in addition to the chaser-target vector to define the reference plane. Within the docking reference system, no roll angles can therefore be measured. In the case of coaxial docking, which will be assumed within this thesis, the roll angle is mostly relevant for interface positioning at actual contact and not during intermediate-range approach and proximity operations. The limitation of the docking reference system to a pitch and yaw display is therefore acceptable for the purpose of the *ThirdEye Proximity Operations HUD*.

Limitations of the Docking Reference System

The docking reference system is easy to establish when using a software simulation like *Orbiter*, in which full state vectors are available for all objects in the environment. For real-world applications, the relative vector between chaser and target center of mass must be determined with high accuracy in order for the docking reference system to be useful. This requires a powerful suite of on-board sensors in combination with ground-based target observations. Since the purpose of this research is to reduce the demands on on-board sensors by introducing the human operator into the rendezvous & docking system, the docking reference system will be relegated to basic research purposes only.

Trajectory Prediction

As discussed in Section 3.3, the relative maneuvers between two spacecraft occur in a rotating reference frame and result in **counterintuitive trajectories** described by the CW equations (equations 3-5 to 3-10). Since these trajectories are difficult for the operator to propagate into the future, and since teleoperation in space involves communication roundtrip time delays, the *ThirdEye Proximity Operations HUD* is to include a **trajectory prediction** based on the actual control inputs. This trajectory prediction display is to provide the operator with a simple, accessible and clear graphical representation of the trajectory the chaser spacecraft will follow in the near future. Since the basic

assumption of this research is sparse available information about the environment, this prediction display must be able to work with chaser state information and periodic range measurements only.

6.3.2 Implementation in Orbiter

The *Orbiter* simulation core cannot be manipulated by module developers. However, it can be accessed by functions provided in object classes. For the HUD development in the 2006 version of *Orbiter*, the concerning class is called *VESSEL2*. This class is used to define spacecraft to be included in the simulation. It provides functions to define, among others, propulsion systems, mass properties, orbital elements, multi-function displays (MFDs) and HUDs. The HUD method, called *clbkDrawHUD* is manipulated to create the OOS HUDs. The drawing functions for the predictive display and for the attitude display are called by this method. The basic functional structure of this system is depicted in Figure 6-4.

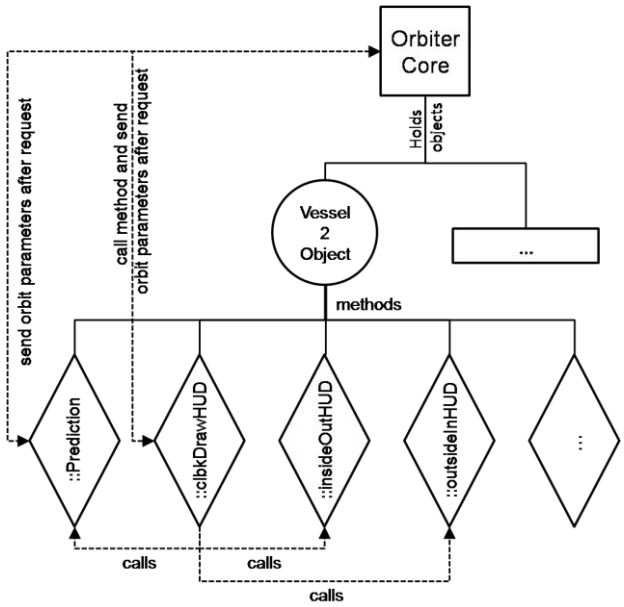

Figure 6-4: Functional structure of the Orbiter *Proximity Operations HUD. The* Vessel2 *object held by the* Orbiter *core calls the* clbkDrawHUD *method for display of a HUD. This method then calls the* Prediction*,* insideOutHUD *and* outsideInHUD *methods according to user selection. These methods receive the orbit parameters from the* Orbiter *core upon request.*

Since *Orbiter* processes a spacecraft's position, velocity, angular rate, and angular position as a twelve-element state vector within the *Geocentric Ecliptic Inertial* (GEI) reference frame, the first step in the HUD generation is to create the transformation matrix between GEI and the Orbit, Horizon or Docking coordinate systems.

This task is facilitated by the fact that this investigation is focused on **circular orbits**. The velocity vector $\boldsymbol{v}_\mathbf{i}$ is therefore the normalized $(\dot{x}, \dot{y}, \dot{z})^T$ vector in the GEI frame. The radius vector $\boldsymbol{r}_\mathbf{i}$ is given by $(x, y, z)^T$. It is important to note that for unknown reasons *Orbiter* uses *left-handed coordinate systems*. The base vectors $\boldsymbol{e}_{\mathbf{0,x}}$, $\boldsymbol{e}_{\mathbf{0,y}}$ and $\boldsymbol{e}_{\mathbf{0,z}}$ of the Orbit system are therefore derived from following equations [254].

$$\boldsymbol{e}_{0,x} = \frac{\boldsymbol{v}_i}{|\boldsymbol{v}_i|} \qquad \textit{Eq. 6-1}$$

$$\boldsymbol{e}_{0,y} = \frac{\boldsymbol{r}_i}{|\boldsymbol{r}_i|} \qquad \textit{Eq. 6-2}$$

$$\boldsymbol{e}_{0,z} = \boldsymbol{e}_{0,x} \times \boldsymbol{e}_{0,y} \qquad \textit{Eq. 6-3}$$

These base vectors define the transformation matrix $\boldsymbol{A}_{\boldsymbol{0}}^{\boldsymbol{i}}$ from GEI to the Orbit system [254].

$$\boldsymbol{A}_{\boldsymbol{O}}^{\boldsymbol{i}} = [\boldsymbol{e}_{0,x} \quad \boldsymbol{e}_{0,y} \quad \boldsymbol{e}_{0,z}] \qquad \textit{Eq. 6-4}$$

Using these three vectors, both the **orbital plane** and the **local horizontal plane** are defined (see Figure 6-5).

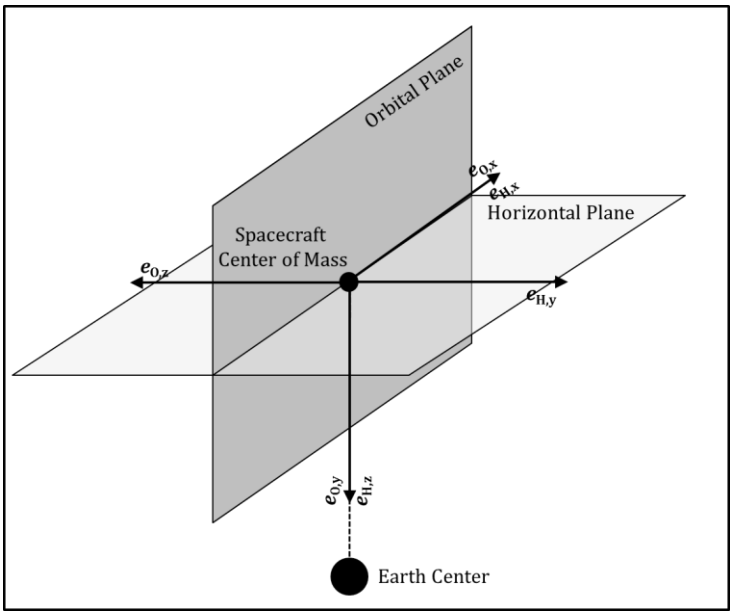

Figure 6-5: Orbital and horizontal plane as defined by the local inertial radius and velocity vectors

Orbit system

In order to derive the roll angle φ within the Orbit system, the z axis of the Orbit system must be transformed from the GEI system to the spacecraft's Vessel coordinate system. The *Orbiter* API offers the dedicated function *GetRotationMatrix* for this purpose, computing the transformation matrix $\boldsymbol{A}_{\boldsymbol{vessel}}^{\boldsymbol{i}}$. The transformed base vector for the z component is therefore calculated by [254]:

$$\boldsymbol{e}_{0,z,\mathrm{vessel}} = \boldsymbol{A}_{\boldsymbol{vessel}}^{\boldsymbol{i}} \cdot \boldsymbol{e}_{0,z} \qquad \textit{Eq. 6-5}$$

The cross product of the vessel's z axis and $\boldsymbol{e}_{\mathbf{O,z,vessel}}$ yields the auxiliary vector $\boldsymbol{c} = (c_x, c_y, c_z)^T$ [254].

$$\mathbf{c} = \begin{pmatrix} \mathbf{0} \\ \mathbf{0} \\ \mathbf{1} \end{pmatrix} \times \boldsymbol{e}_{\mathbf{O,z,vessel}} \qquad \textit{Eq. 6-6}$$

The spacecraft roll angle φ_0 is then the result of the arctangent of the y and x components of $\boldsymbol{c}$ [254].

$$\varphi_O = -\arctan\left(\frac{c_y}{c_x}\right) \qquad \textit{Eq. 6-7}$$

Since the attitude angles follow the rotation sequence yaw (ψ) – pitch (ϑ) – roll (φ), the spacecraft velocity vector within the vessel system must be rotated around the vessel x axis by $-\varphi_0$ in order to follow the reverse rotation sequence, before the pitch and yaw angles can be calculated.

The pitch angle is defined as the angle between the Vessel system's z axis and the Orbit system x-y plane. After the spacecraft velocity vector has been transformed from GEI into the Vessel coordinate system by the corresponding *Orbiter* function, ϑ_0 can be calculated from the velocity components [254].

$$\vartheta_O = -\arccos\left(\frac{v_{z,vessel}}{\sqrt{v_{z,vessel}^2 + v_{x,vessel}^2}}\right) \qquad \textit{Eq. 6-8}$$

The yaw angle is calculated in a similar fashion. For ψ_O it is important to include a case switch for positive and negative x component of the velocity vector [254].

$$\psi_O = \pm\arccos\left(\frac{v_{y,vessel}}{\sqrt{v_{y,vessel}^2 + v_{x,vessel}^2}}\right) \qquad \textit{Eq. 6-9}$$

Horizon system

The calculations for the Horizon system can largely be copied from the Orbit system. As Figure 6-5 shows, the Horizon system's coordinate axes are derived from the Orbit system's axes in rotating by -90° around the shared x axis. The pitch angle in the Horizon system is therefore the negative yaw angle in the Orbit system; the Horizon yaw angle is equal to the Orbit pitch angle.

$$\varphi_H = \varphi_O - 90° \qquad \textit{Eq. 6-10}$$

$$\vartheta_H = -\psi_O \qquad \textit{Eq. 6-11}$$

$$\psi_H = \vartheta_O \qquad \textit{Eq. 6-12}$$

Docking system

The Docking system is based on the **relative position vector** between the target and the chaser. Since no natural reference plane is available for this coordinate system, the chaser Vessel *x-y* plane was chosen to assume this role. The roll angle within the Docking system is therefore by definition zero. The pitch and yaw angles are derived by rotating the relative position vector, which is provided by *Orbiter* in GEI coordinates, into the chaser Vessel system. The angles can then be calculated by Eq. 6-8 and Eq. 6-9 by using the components of the relative position instead of the velocity.

An additional feature of the Docking system HUDs is that they position a rectangle around the target object to facilitate target acquisition and tracking by the operator. The position of this rectangle within the operator FOV is calculated by the relative position in Vessel coordinates and a correction factor for the projection of the scene onto the screen (see page 118 for more details on this factor).

The availability of the relative position vector is only given if **high-precision position data** is available for the target object. This is the case in any simulation environment and for approaches of active satellites in OOS scenarios, but is not expected to be the case for uncooperative targets in debris removal scenarios. The Docking system can therefore be used for **fundamental research** purposes only, but not for actual realistic mission simulations.

Velocity indicator

Since the HUD is to be used in proximity operations and capture/docking scenarios, a valuable piece of information for the operator is the chaser spacecraft's momentary deviation v_Δ from the circular orbit velocity v_c. This is derived by Eq. 6-13 and Eq. 6-14 [254].

$$v_\Delta = |\boldsymbol{v}| - v_c \qquad \textit{Eq. 6-13}$$

$$v_c = \sqrt{\frac{\mu_\oplus}{r}} \qquad \textit{Eq. 6-14}$$

A value of $3.98690 \cdot 10^{14}\ \frac{m^3}{s^2}$ was used for Earth gravitation parameter $\mu_\oplus$, and r is the absolute of the spacecraft orbit's radius vector.

For the Docking system HUDs, v_Δ is defined as the relative velocity between chaser and target. This is derived from the inertial relative velocities plus a corrective vector $\boldsymbol{v}_{\mathbf{cor}}$ accounting for the rotation rate ω of the Docking coordinate system. The elements of $\boldsymbol{v}_{\mathbf{cor}}$ are dependent of the relative x and z positions of chaser and target in the Orbit system, as explained by the CW equations (equations 3-5 to 3-10) [254].

$$\boldsymbol{v}_{cor} = \begin{pmatrix} -\omega\, r_{rel,z,O} \\ 0 \\ \omega\, r_{rel,x,O} \end{pmatrix} \qquad \textit{Eq. 6-15}$$

The velocity deviation v_Δ is depicted in the HUD by a set of concentric circles (see Figure 6-6).

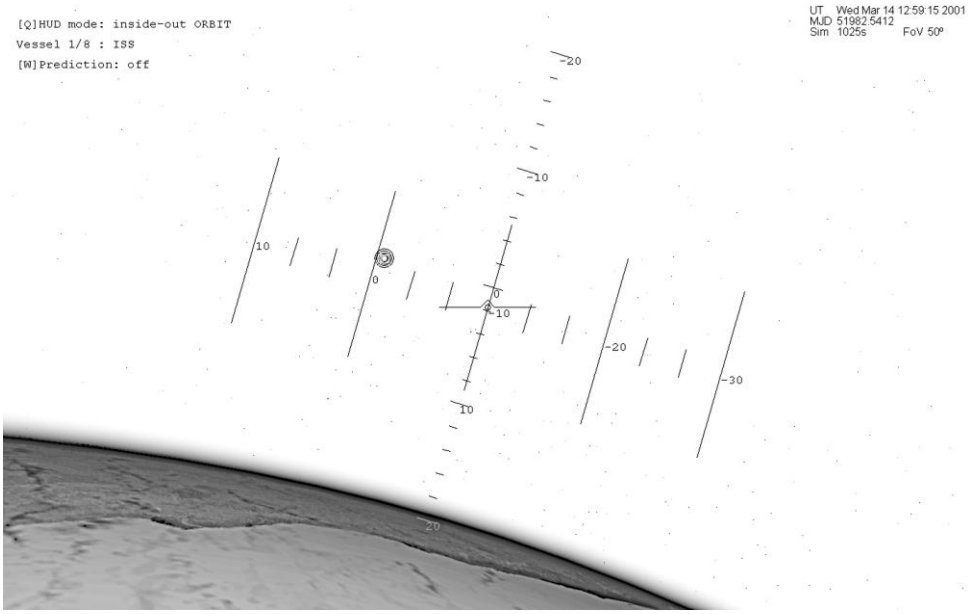

Figure 6-6: Exemplary view of an inside-out HUD with the velocity deviation indicator. The indicator displays the deviation of actual velocity to the circular velocity at the current spacecraft altitude. This display can be used for maneuver planning purposes during orbit transfers and proximity operations.

The number of circles contains information about the value of the deviation, in order to convey intuitive knowledge about the spacecraft's motion to the operator. Since the Orbit/Horizon and Docking coordinate systems are expected to be used in different mission phases and thus also to contain different information in v_Δ, the HUD also uses different scaling for the velocity circles between these displays (see Table 6-1).

Table 6-1: Scaling of velocity deviation display. The number of concentric circles indicates the deviation from circular velocity in the Orbit and Horizon HUDs and the relative velocity between chaser and target in the Docking HUD [254].

Number of circles	v_Δ in Orbit/Horizon HUD [m/s]	v_Δ in Docking HUD [m/s]
2	5	0.2
3	10	0.5
4	20	1
5	50	5
6	100	20

Trajectory prediction

The **trajectory prediction display** visualizes the relative motion between the spacecraft based on the **CW equations** (equations 3-5 to 3-10). The base values for the computations are the relative position and velocity vectors provided by the *Orbiter* core. These are first transformed into the LVLH system for circular orbits by the appropriate coordinate transformation (equations 6-1 to 6-3). Since the LVLH system is rotating around Earth with the target, the velocity correction $\boldsymbol{v}_{\mathbf{cor}}$ (Eq. 6-15) must be used. As the *Orbiter* core continuously updates the spacecraft state vectors by taking into account all acting forces, including the commanded maneuver thrust, the **continuous propagation** of the CW equations yields the prediction of the relative trajectory based on current maneuver command inputs. The prediction time can be implemented arbitrarily. In order for the predictive system to be usable as an orbital maneuvering aid during final approach, the timescale is set to 1000 s.

The resulting trajectory curve can then be displayed in either a 2D or 3D representation (see Figure 6-7). The 2D display shows two views of the CW trajectory in the Horizon system: once as seen "edge-on" along the negative *y* axis (representing the coupled motion within the orbital plane), and once as seen from "above" along the *z* axis (representing the motion within the horizontal plane). For the 3D display, two coordinate systems are available: the Orbit system and the Vessel system. In the 3D Orbit system, the trajectory is shown independent of the chaser spacecraft's attitude in space and thus also of maneuver thrust directions. In the 3D Vessel system, the trajectory is provided in relation to the spacecraft's orientation and thus the viewing direction of the operator. The Vessel display requires the transformation of the CW path coordinates from Orbit to Vessel system, which is achieved by an *Orbiter* function (refer to Eq. 6-5).

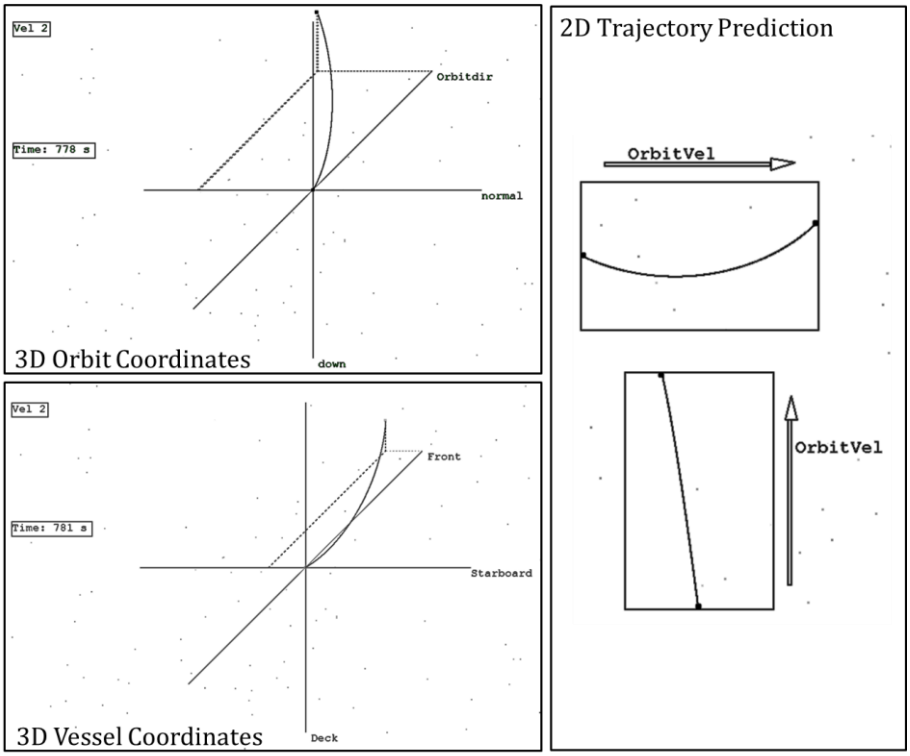

Figure 6-7: The three trajectory prediction displays used in the Orbiter *Proximity Operations HUD. The 2D display shows the trajectory in the Horizon system as seen "edge-on" along the negative y axis and "from above" along the z axis. This results in two separate displays providing the motion within the orbital plane and the motion within the local horizontal plane. The upper 3D display shows the trajectory in the Orbit system without providing an indication of the chaser spacecraft attitude and thus the operator-centric maneuver direction. The lower 3D display shows the trajectory after transformation into the Vessel system. The trajectory is thus shown in the chaser spacecraft body coordinate system, which gives the gives the operator a clear indication of the flight path in relation to maneuver directions.*

Since the trajectory prediction is based on the original CW equations, it is limited in its use to (near-)circular orbits and cannot take into account external disturbance forces. The prediction does therefore not account for the effects of the inhomogeneity of Earth's gravity field and the drag due to the remaining atmosphere. It is furthermore not usable for low-thrust maneuvers, since the CW equations assume impulsive velocity change.

Drawing Functions

After the relative attitude angles and the velocity deviation have been calculated by the method *clbkDrawHUD*, these parameters are then passed to the selected display method *InsideOutHUD* or *OutsideInHUD* to actually draw the HUD to screen. These methods utilize standard *Windows Graphical Device Interface* (WinGDI) functions, namely lines, ellipses, polygons and rectangles. The pitch and yaw angles are represented by **ladder scales**, the roll angle is either depicted by banking the vessel symbol in the outside-in display or rotating the azimuth/elevation representation around the vessel in the inside-out display.

For the outside-in method *OutsideInHUD*, the first step in the implementation is to draw the coordinate system. The position and size in this operation is dependent on the screen's resolution, since the display should always cover the same area, independent of the individual screen's settings. The horizontal (yaw) axis is labeled from -180° to 180°, the vertical (pitch) axis from -90° to 90°, both in 20° increments. The second step is to draw the actual attitude indicator symbol (in the following also referred to as **ownship symbol**). This symbol is defined by a point array, which is generated around a specific center point. The scale of this symbol in relation to screen resolution is identical to that of the coordinate axes, in order to achieve a visually consistent display. The spacecraft's roll angle is indicated by the ownship symbol's rotation around this center point, while the yaw and pitch angles are expressed by the symbol's displacement along the horizontal and vertical axes. The velocity circles are positioned at the intersection of the azimuth and elevation axes. Figure 6-8 shows the resulting outside-in attitude HUD as implemented in *Orbiter*.

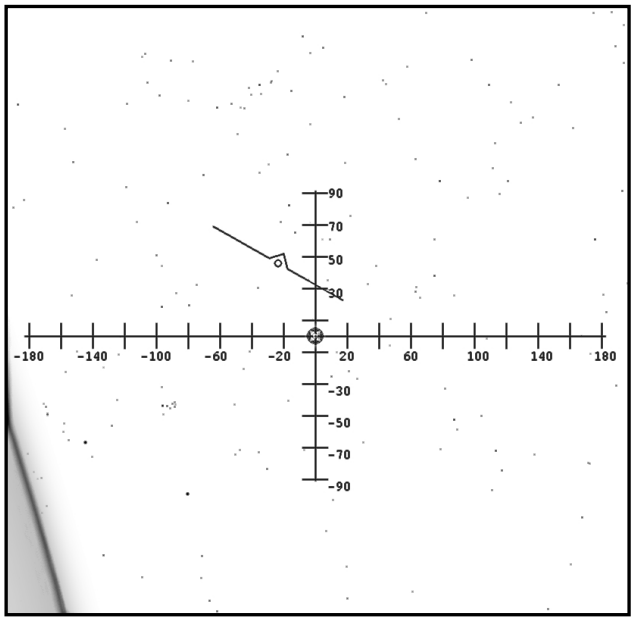

Figure 6-8: Outside-in attitude HUD as implemented in Orbiter. *The roll angle is indicated by the ownship symbol's rotation within the display. Pitch and yaw angles are expressed in ownship symbol displacement along the vertical and horizontal axes. The velocity deviation indicator circles are drawn at the crossing point of the horizontal and vertical axes, since this is by definition the direction of orbital velocity in both Orbit and Horizon system.*

The inside-out drawing method *InsideOutHUD* is more complex and thus requires more processing. The only object drawn statically within the representation is the ownship symbol in the screen's center. This is the same symbol as in the outside-in HUD, but without any rotational or translational manipulation. The pitch and yaw coordinate axes however are not fixed on the screen but translate and rotate in order to display the spacecraft attitude. The first step to draw these scales is to translate the lines to the correct position by a value linearly dependent on the pitch and yaw angles. At the intersection of the axes is the spacecraft's current attitude. From this center point, the axes are drawn to a distance of 4/9 of the vertical FOV. The angular scales are defined by an array of lines, orthogonal to the axes' direction, labeled in 10° intervals. For the pitch axis two unlabeled lines, and

for the yaw axis four unlabeled lines are interposed between these for orientation purposes. Since the basic idea of a HUD is for the vessel to be surrounded by an attitude sphere (see Figure 6-3), the coordinate axes form loops, which means that theoretically their ends are connected to the beginnings. This is practically achieved by extending both ends by half the maximum FOV, which is in the range of 45°. If this computational step is missing, the display will not work correctly near the limits of the axes.

In order for the inside-out display to be of maximum use for the operator, the displayed angle scales must correspond to the real visual angles of the scene. This means that an object which is seen at a visual angle of 30° from the center of the image must coincide with the 30° pitch or yaw angle line. The HUD drawing function must therefore account for **projection deformation**. Since a camera picture is always a projection from the three-dimensional world to a planar surface, in this case the monitor, there will inevitably occur distance errors on the screen. In the description of the implementation so far, the axes are positioned on the screen with linear scaling, which means that one degree of rotation corresponds to a certain number of pixels by which the axis scale is moved. Due to the projection errors, this is only valid near the center of the screen. In order to exactly position the angular scales in relation to objects in the environment, a correction must be performed, which is dependent on the **projection method** used. This correction allows the operator to reliably estimate the angular position of an object, even when it is situated at a high viewing angle, where optical deformation is at its maximum. In *Orbiter*, the used projection model is that of a "**pinhole camera**".

The correction is performed for each line by means of a **correction factor** S_{corr}, calculated with the line displacement angle α_{line} and the spacecraft pointing angle α_{vessel}, which is a combination of the roll, pitch and yaw angles [254].

$$\alpha_{offset,x/y} = \alpha_{line,x/y} - \alpha_{vessel,x/y} \qquad \textit{Eq. 6-16}$$

The *Orbiter* core uses a pure pinhole camera model in the horizontal *x* direction of the monitor. The correction factor is therefore the quotient of the actual position in the projection and the linear approximation of this position [254].

$$S_{corr,x} = \frac{\tan \alpha_{offset,x}}{\alpha_{offset,x}} \qquad \textit{Eq. 6-17}$$

In the vertical *y* direction of the screen, an additional cosine factor must be introduced in the denominator to account for vertical and horizontal deformation [254].

$$S_{corr,y} = \frac{\tan \alpha_{offset,y}}{\alpha_{offset,y} \cdot \cos \alpha_{offset,x}} \qquad \textit{Eq. 6-18}$$

The corrected point coordinates of the scale lines are then given by [254]

$$\boldsymbol{P}_{\boldsymbol{line,corr}} = \begin{pmatrix} S_{corr,x} \\ S_{corr,y} \end{pmatrix} \boldsymbol{P}_{\boldsymbol{line}} \qquad \textit{Eq. 6-19}$$

After this correction is performed, the lines can be rotated around the screen's center to display the roll angle. The points which define the line are transferred from Cartesian to polar coordinates. The polar angle is incremented with the roll angle and the coordinates are transformed back to Cartesian coordinates for drawing. Figure 6-9 shows the resulting attitude HUD.

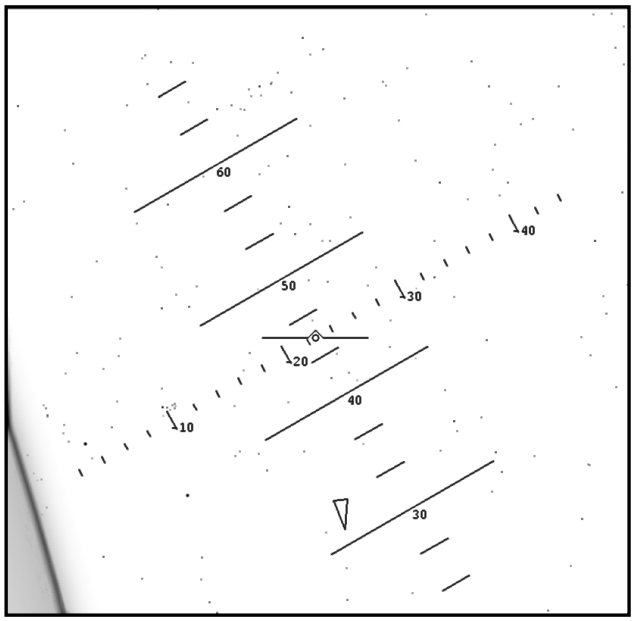

Figure 6-9: Inside-out attitude HUD as implemented in Orbiter. The roll angle is indicated by the rotation of the pitch and yaw angle scales around the fixed ownship symbol. Pitch and yaw angles are indicated by a translation of the angular scales. In order to account for HUD projection deformation, a correction factor is used in drawing the symbols. The velocity deviation indicator and thus the direction of flight is outside the FOV. Its direction is indicated by the triangle in the lower portion of the figure.

The method *Prediction* for drawing the trajectory prediction displays is straightforward. The trajectory spline is approximated by a high number of lines drawn between the CW data points. A red square symbol always represents the chaser, with a blue square serving as target symbol.

The 2D display elements are positioned at the right side of the screen, next to the attitude HUD, and are framed by rectangles. If the chaser approaches the target from "behind", its symbol is drawn in the vertical center of the left border of the upper display, and in the horizontal center of the lower border of the lower display. If the approach is from "in front" of the target, the chaser symbol is drawn on the right border and the upper border, correspondingly. The blue target symbol is positioned along the borders of the rectangles, depending on its actual relative position to the chaser. The **scale** of the display is continuously varied in order to always keep the target symbol within the confines of the rectangles.

The 3D displays require more space than the 2D display in order to be usable. They are therefore drawn to the screen *in place of* the attitude HUD. The coordinate axes as well as the trajectory are drawn in an **oblique projection**. Dashed auxiliary lines are drawn from each of the axes to both the center point and the end point of the trajectory in order to increase the usability of the projection (see Figure 6-7).

The display is always scaled such that the target symbol is drawn at the maximum of one of the axes. Furthermore, parts of the trajectory spline exceeding the drawing area defined by the axes are cut off. While this **dynamic scaling** maximizes the use of the available space, it also removes any information regarding the distance between chaser and target. It is assumed that the operator will have the target within sight and that therefore either visual distance cues or other distance measurements are available. However, relative velocity and the time required to reach the end point of the trajectory are provided in two rectangles at the left side of the display (see Figure 6-7).

Display Configuration

The attitude and trajectory prediction HUDs can be configured prior to use by means of a **configuration file** and during use by **keyboard commands**.

The configuration file is named *hudconfig.txt* and must be placed within the folder of the executable. Table 6-2 provides a summary of the configuration file parameters[9].

Table 6-2: Overview of the Proximity Operations HUD configuration file for Orbiter*. The configuration file settings determine the total prediction time and prediction time step of the trajectory prediction display, the onset of the mid-point auxiliary line, as well as the scaling of the HUD display [254].*

Parameter	Meaning	Range
PredictionTime	Maximum propagation time [s] for the trajectory prediction	[1 5000]
PredictionStep	Propagation increment [s] for the trajectory prediction	[1 100]
AuxiliaryLine	Minimum prediction time until an auxiliary line is drawn to the mid-point of the trajectory. If set to -1, no auxiliary line if displayed	[-1 5000]
HUDScale	Size of the entire HUD display in relation to screen width	[0.5 1.5]

During use, the operator can switch between attitude HUD modes, coordinate systems and docking targets, and can switch the trajectory prediction display on or off and switch through the prediction display modes by a number of control keys. Table 6-3 provides a list of the control keys and the associated functions.

[9] There further exists the parameter GroundMode which, when active, makes two more HUD modes available which can be used for flight operations near the planetary surface. These are not discussed here since they are not related to proximity operations. Details can be found in [254]

Table 6-3: Overview of the keyboard commands for proximity operations HUD configuration in Orbiter. *Using these command keys, the operator can select docking targets, switch between attitude HUD modes, active the trajectory prediction and switch between prediction display modes during operations.*

Key	Action
1	select next docking target
2	select previous docking target
Q	switch attitude HUD modes
W	toggle trajectory prediction
E	switch trajectory prediction modes

The basic idea behind the configurability of the *Proximity Operations HUD* by keystroke was that it allows the operator to change the HUD configuration reflecting the requirements of the mission phase or situation and also his preferences. The side effect is that it facilitates the evaluation experiments.

6.3.3 Implementation for 3dSVK

In addition to *Orbiter*, the proximity operations HUD needed also to be implemented for a "real-world" proximity operations simulation setup in order to run hardware-in-the-loop *ThirdEye* evaluation experiments. The HUD must therefore be implemented as an overlay for live video streams and be able to receive attitude and position data from external sources via network connection.

The camera used in the ThirdEye experiments is a Point Grey Research Bumblebee2 stereoscopic camera. Its stereo video stream can be displayed by stereoscopic projectors or monitors, using nVidia or CrystalEyes liquid crystal shutter glasses. The software used for stereoscopic display is the Point Grey 3d Stereo Visualization Kit (3dSVK). It forms a direct interface between the camera and an nVidia graphics card and creates a stream compatible to DirectX, which can then be displayed in the stereo video setup.

The 3dSVK HUD was designed to be used with the alternative 2DOF slewing mechanism described in Section 5.2.3. The 3dSVK attitude HUD functions purely as a **visualization device**, which means that the correct attitude data must be provided to the display in the coordinate system of choice. The trajectory prediction method, on the other hand, contains the CW propagation algorithm as well as the coordinate transformation functions necessary to draw the 2D, 3D Orbit and 3D Vessel displays. The nominal data interface to the 3dSVK HUD is via UDP (User Datagram Protocol). The definition of the UDP packet format is provided in [254].

The implementation of the HUD in 3dSVK is almost identical to the *Orbiter* HUD. The major difference is that the 3dSVK HUD incorporates **attitude prediction** functionality, since it is designed to be used in realistic realtime teleoperation scenarios which include roundtrip time delays. The

3dSVK HUD therefore does not display the actual pitch and yaw angles as received via UDP, but rather predicted attitude angles propagated from the actual angles by using the actual attitude rates and the time delay set in a configuration file.

The angles are then converted into the HUD representation by means of DirectX drawing functions, which are compatible to the 3dSVK/nVidia interface. When using the **shutter glasses**, the resulting HUD is then seen as **2D image overlay** hovering in front of the 3D scene. This requires the operator to constantly switch his focus when working with the HUD, which can lead to increased eye strain, headache, etc. The goal for future versions of this HUD should therefore be to integrate the symbols into the 3D scene, making the HUD an element of the environment at the distance of other major display elements, like the target object during proximity operations.

6.3.4 Implementation for the ThirdEye Proximity Operations GUI

The proximity operations HUD as developed and tested in *Orbiter* was then implemented for the *ThirdEye Proximity Operations GUI* (more in Sections 6.5 and 7.3.4). While this GUI does not offer stereoscopic projection of the camera video streams, it integrates *ThirdEye* status displays with live video, the attitude HUD, as well as the trajectory prediction. The calculation and drawing functions developed for *Orbiter* were converted into a stand-alone application. This application directly receives attitude angles and relative position data in LVLH coordinates from the proximity operations simulator. Major coordinate transformations are therefore not necessary. The data interface is provided by using DDS, as explained in Section 0.

The WinGDI drawing functions used within *Orbiter* were replaced by open graphics library (OpenGL) functions. This facilitates the integration of live video and AR elements into one display. OpenGL is furthermore available on the majority of computers, supporting the migration of the display to different operating environments. In the initial HUD implementation for *ThirdEye Proximity Operations GUI*, the appearance of neither the attitude HUD nor the trajectory prediction was changed from the *Orbiter* implementation. The HUD was however adapted subsequently after the HUD evaluation experiments as well as the *ThirdEye* pilot evaluation experiment series.

6.4 Evaluation

The final goal of the *ThirdEye Proximity Operations HUD* development project was to design and implement a HUD with high usability for the *ThirdEye Situation Awareness Enhancement System*.

Usability in this context is defined as the positive impact the HUD has on **operator performance** during proximity operations. This performance is measured in terms of task success rate, task completion times, maneuver velocity change (Δv) demand, as well as maneuver precision.

The basic display features influencing operator performance were the attitude representation method (inside-out vs. outside-in), the reference coordinate system used (Orbit vs. Horizon vs. Docking), as well as the trajectory prediction display mode (2D vs. 3D Orbit vs. 3D Vessel). Since no

literature could be found concerning the evaluation of different HUD designs for teleoperation of spacecraft proximity operations, the *Orbiter* proximity operations HUD as detailed above was used for such a study.

6.4.1 Experiment Setup

For the HUD evaluation experiments, the *Orbiter* spaceflight simulation environment as described in Section 5.2.1 was used.

Orbiter and the HUD module were run on a Windows 7 office **desktop computer**. The video was projected onto a 192 cm x 105 cm screen with 1280 x 720 pixels resolution. The test participants were seated with their eyes approx. 1.5 m in front of the screen. The computer was equipped with a Saitek *Cyborg Evo Force* joystick and a 3DConnexion *SpaceExplorer* for input devices.

Figure 6-10: Input devices used during the HUD evaluation experiments. The Saitek Cyborg Evo Force joystick is shown to the left, with the 3DConnexion SpaceExplorer 6DOF input device to the right.

Attitude and position data was extracted from *Orbiter* by another custom module which uses DDS to publish the maneuver data to a Simulink data-logging model. While this setup was originally designed for the transmission of the data via Ethernet and therefore data-logging on a remote computer, the data-logger was run in background on the simulation computer for these experiments. Figure 6-11 provides a schematic overview of the experiment setup.

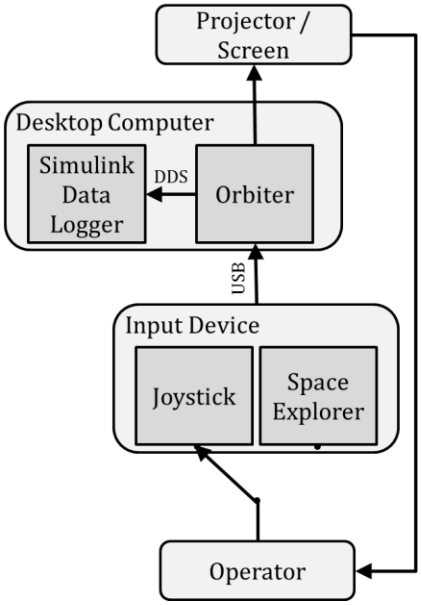

Figure 6-11: HUD evaluation experiment setup. The operator had the option of joystick and SpaceExplorer to control the spacecraft. The control inputs were propagated by Orbiter and the resulting scene is projected onto a screen. Selected maneuver data was transmitted via DDS to a Simulink data logger.

Experiment Structure

The evaluation experiments were divided into three separate experiment series. **Series I** tested the **general utility** of an attitude HUD for space operations, as well as the differences in user performance in attitude maneuvering and estimation of relative positions generated by the inside-out and outside-in attitude representations. **Series II** tested the impact of the orbit and horizon **reference systems** on estimation of relative positions for approach maneuvers. The subject of **series III** was the usability of the **trajectory prediction** modes.

Participants

The participants for each series were recruited from the students and researchers at TU Munich's Institute of Astronautics (LRT). The reasoning behind this selection is that this group represents the pool from which operators of future telerobotic space systems will most likely be recruited: aged 20-60, with technical education and above-average experience using computers and simulation systems.

The participants were all male, aged between 25 and 57. Their average spaceflight simulation experience, subjectively rated between 1 (low) and 5 (high), was between 1.73 and 2.00 for the three series. Average flight simulation experience ranged between 2.10 and 2.91. The input device experience was only asked for in series I. Its average value was 3.00 for the joystick and 1.55 for the *SpaceExplorer*.

The following sections provide the analysis of the data obtained during the three experiment series.

6.4.2 Attitude HUD Evaluation

Experiment **series I** had 11 participants. Each of these had to complete three tasks: an attitude correction task, a series of attitude maneuvers and a series of relative position estimations.

For each of these tasks, the **independent variable** was the type of attitude HUD used.

The objective **dependent variables** were task success/failure, the time to complete the task, as well as the cumulative magnitude of the control input. This magnitude is a representation of the intensity of the commanded thrust maneuvers, and thus of propellant consumption. By multiplying the completion time and the control input magnitude, a number indicating total expended impulse is computed.

In addition to these objective measures, the participants also answered a number of **questions**. These concerned the participants' confidence about their orientation in space and the direction in which they had to steer, their ability to control the spacecraft rotation rates, as well as the required concentration for the control task. At completion of the experiment series, the participants were further asked which HUD they preferred in the attitude correction and maneuvering tasks, as well as the relative position estimation task.

Prior to the actual experiment run, the participants individually completed approx. 20 minutes of **training**, during which they were introduced to the different HUD modes as well as the input devices and had to complete a number of maneuvers representative of the experiment tasks. At the end of the training, each participant had to select the input device he would use for the experiment. 73% opted for the joystick, 27% chose the *SpaceExplorer*. This distribution was expected, given the low familiarity the participants professed with the six-axis input device.

Attitude correction

In the attitude correction task, the spacecraft was initially in an **arbitrary attitude** with the Earth outside the field-of-view. The participants had to return the spacecraft to a 0° roll, 0° pitch, 0° yaw attitude in the Horizon reference system. This means that it was to point in the direction of flight, with the *x*-*y* body plane parallel to the local horizontal plane. The tolerance bands were ±5° in pitch and yaw and ±2.5° in roll, which was based on the capture envelopes of existing docking mechanism, in particular the OECS (refer to Table 4-1). The participants had to accomplish this task once without HUD assistance, then with each of the inside-out and outside-in HUDs.

Figure 6-12 shows the average **success rates** for the three situations. Without the HUD, only 27% of correction maneuvers were successful, whereas the use of the inside-out HUD or the outside-in HUD improved operator performance to 82% and 72%.

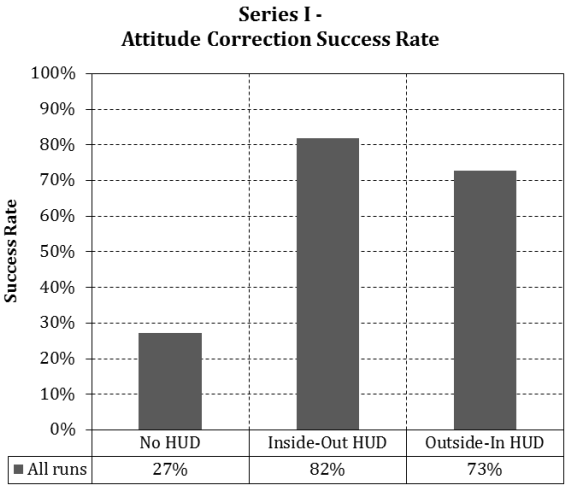

Figure 6-12: Attitude correction success rate in experiment series I. The use of any HUD substantially increases the maneuver success rate.

This jump in performance due to the use of a HUD is also evident for the **average time** to complete a successful maneuver, as well as the **total impulse** spent during a successful maneuver (see Figure 6-13).

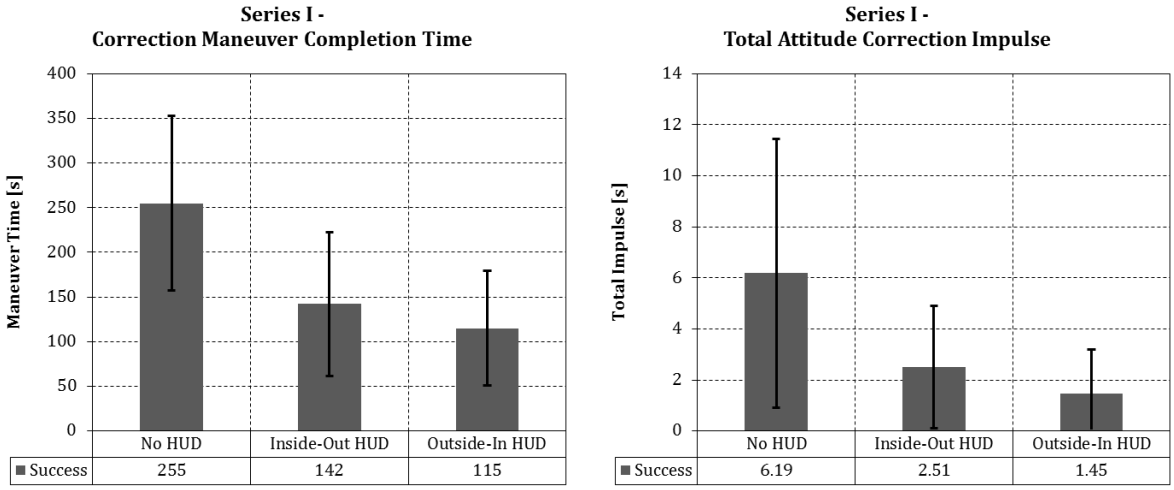

Figure 6-13: Maneuver times and total impulse demand for the attitude correction task. The mean maneuver times are reduced by about 50% with the use of an attitude HUD. The total impulse is reduced by 60% using the inside-out HUD and by 75% with the outside-in HUD.

The total impulse is here defined as the product of cumulative control input magnitude and time to complete, and is therefore given in seconds. The low number of data points available for successful task completion in the case without HUD results in insignificant differences between the HUD activity modes in analysis of variance (ANOVA) and Tukey honestly significant difference (HSD) tests (refer to [255] for more information on ANOVA, and to [256] for Tukey's HSD test). The plots nonetheless show that both the time and the impulse required for a successful attitude correction is substantially lower with an HUD than without it.

This trend is also visible in the participant ratings of the correction **maneuver difficulty** and the **concentration** required during the task (Figure 6-14). The plots show that test participants rate the task difficulty lower using any of the attitude HUDs, while simultaneously stating that the required concentration during the task is higher without HUD.

This clearly shows the utility of an attitude HUD for teleoperated attitude maneuvering.

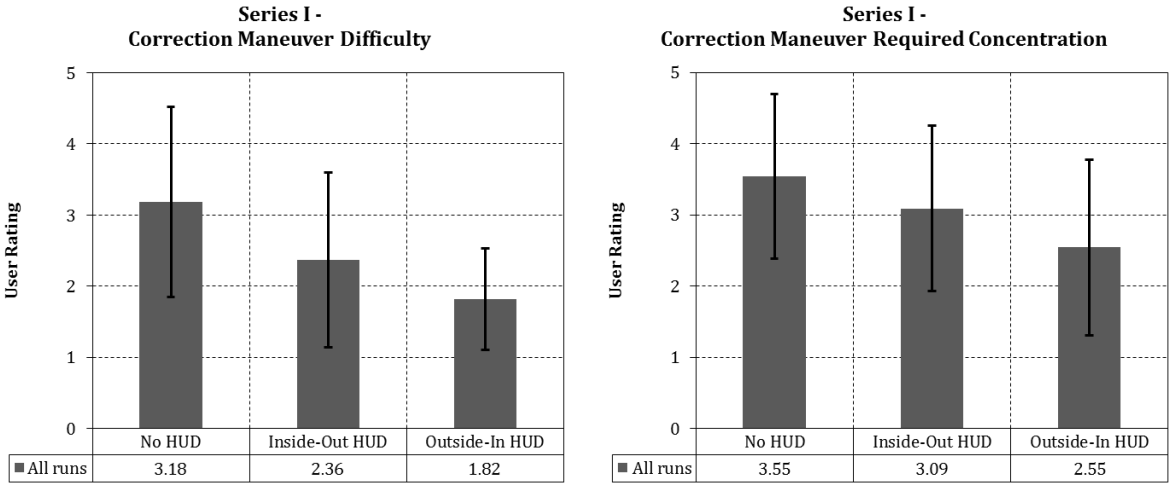

Figure 6-14: Attitude correction task difficulty and required concentration. The mean participant rating of task difficulty is lower for active attitude HUDs than without HUD. At the same time, the concentration required during the task is rated higher without HUD than with any of the attitude HUDs.

The data also indicates better operator performance with the outside-in HUD as compared to the inside-out HUD. This trend is weak and must therefore be confirmed in the second test of the series.

Attitude maneuvering

In the attitude maneuvering task, the participants had to achieve six different attitudes in series. A maneuver was considered successful if the operator managed to keep the spacecraft within ±5° of pitch/yaw and ±2.5° in roll angle of the commanded attitude for the duration of 5 s.

Of the data obtained by testing the 11 participants, one participant's data set had to be discarded for the outside-in test, since it was discovered after the experiment series that the Simulink data logger had experienced memory issues.

The mean **success rate** in the attitude maneuver series is given in Figure 6-15. Its average over all participants is 21% for the inside-out HUD and 65% for the outside-in HUD.

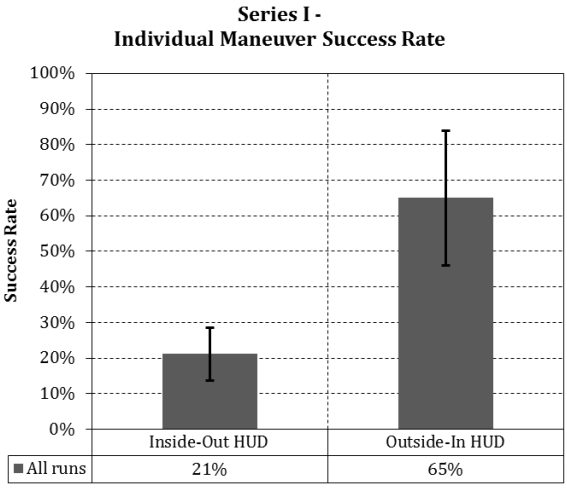

Figure 6-15: Mean success rates for individual maneuvers in the attitude maneuvering task. The mean success rate using the outside-in HUD is 65%, compared for 21% using the inside-out HUD.

This indication of higher utility of the outside-in representation is reinforced by the statistics for **maneuver time** and **total impulse** per successful maneuver (Figure 6-16). These are determined by dividing the time and impulse spent by each participant for the complete maneuver series by the number of successful maneuvers. The mean time spent for each successful maneuver using the outside-in HUD is about 1/3 that for the inside-out HUD. Using the outside-in HUD the participants furthermore used on average 31% of the impulse required with the inside-out HUD. It can therefore be stated that an outside-in attitude presentation enables the operator to show superior performance in attitude maneuvering compared to using an inside-out HUD.

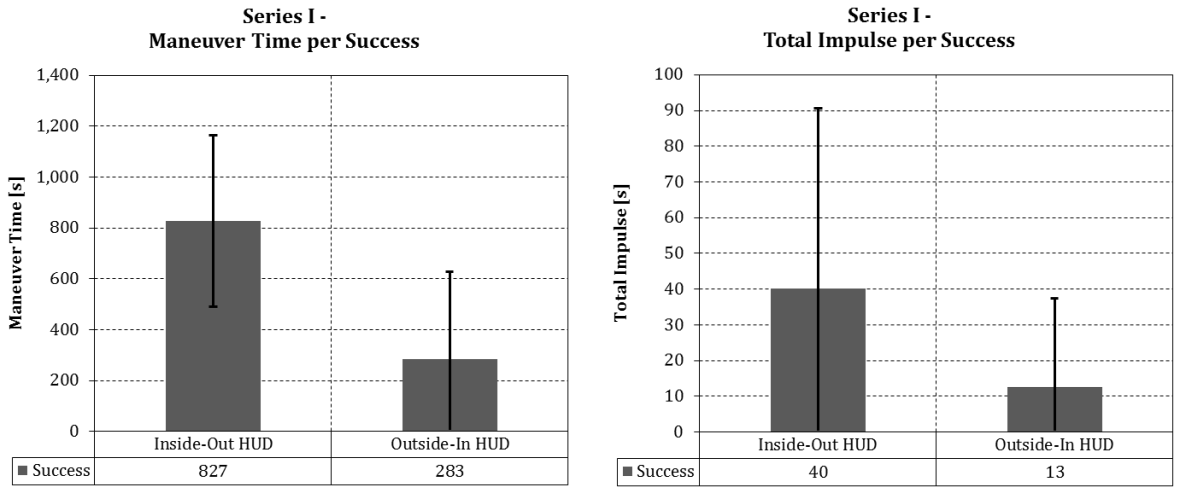

Figure 6-16: Maneuver times and total impulse expenditure per successful attitude maneuver. Both measures indicate higher operator performance using the outside-in HUD compared to the inside-out HUD.

The participant ratings of **confidence** in attitude knowledge, required **concentration** during the attitude maneuver task, control direction confidence, and **controllability** of attitude rates, provided in Figure 6-17 are an interesting comparison to the objective performance data.

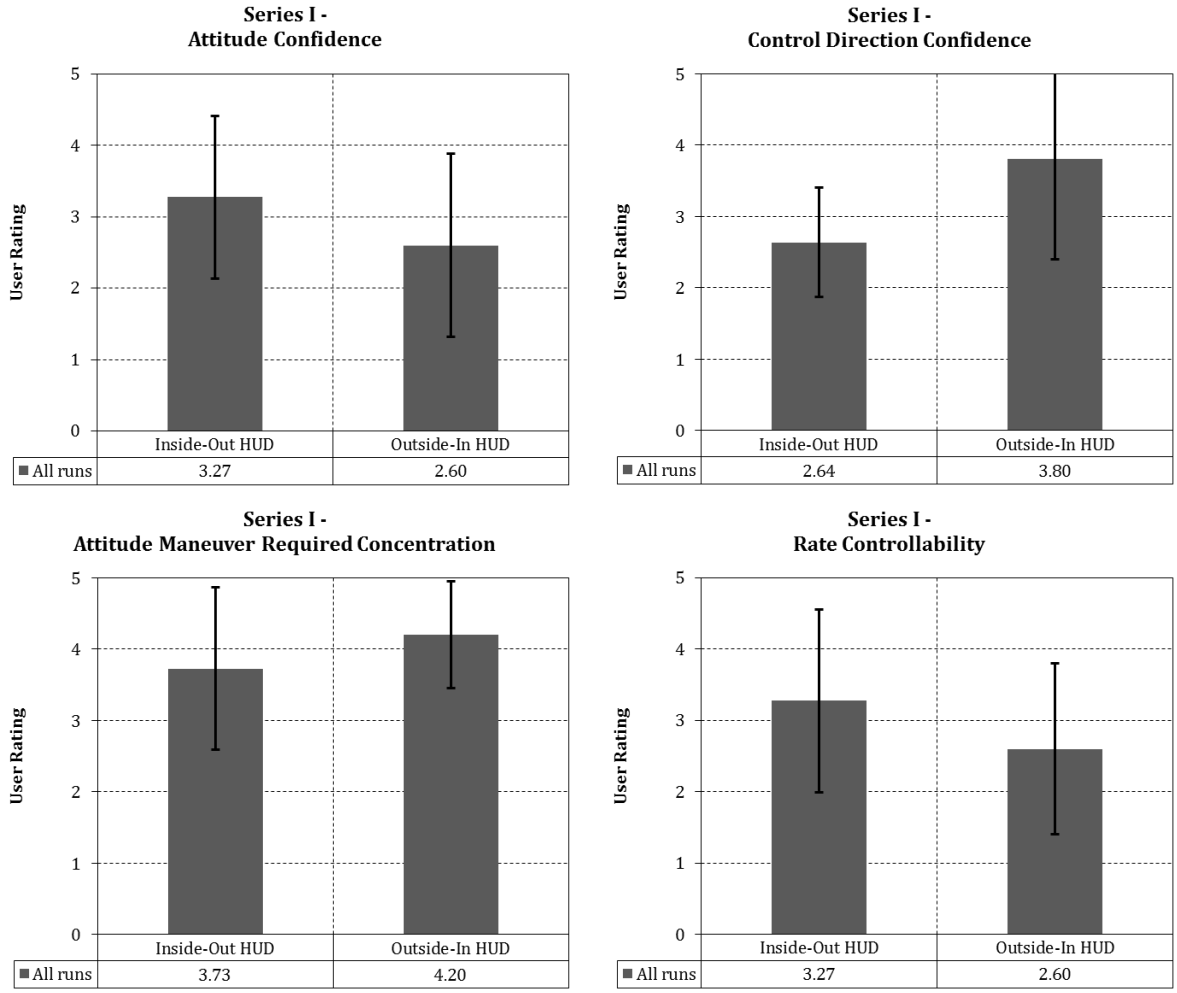

Figure 6-17: Participant feedback data for attitude confidence, control direction confidence, required concentration, and rate controllability during the attitude maneuvers. The participant ratings show that test participants had less confidence of attitude knowledge using the outside-in HUD, but at the same time more confidence in which direction they had to guide the spacecraft to reach the commanded attitude. The required concentration was rated higher with outside-in HUD, and the controllability of the rotation rate lower.

Based on this user feedback it can be stated that while the outside-in HUD generated higher operator performance, it was also perceived as less practical and intuitive. One reason for this might be that the inside-out HUD was more familiar to many participants, since it is widely used in flight simulations. The outside-in HUD uses an unfamiliar display method, which probably requires a longer familiarization period than provided during training prior to experiments.

Relative position estimation

The third experiment in series I addressed the question whether a difference exists between inside-out and outside-in displays for the task of judging a **target's position** in relation to the chaser's body coordinate system as well as to the local orbital system. For this purpose, the participants were confronted by four scenarios in which a target object was within close range of the chaser spacecraft. The four cases were defined by whether or not the Earth was within the FOV, and by using the inside-out or outside-in HUD. Using visual information only, the participants had to judge the target's relative position within the body-fixed and orbital coordinate frames and mark it **qualitatively** in the questionnaire.

With Earth in view, the inside-out HUD allowed the participants to correctly judge the target's position in the body-fixed coordinate system in 73% of the cases, compared to 45% using the outside-in system (compare Figure 6-18). The opposite performance is evident for the position in the local orbital coordinate system. The outside-in HUD intuitively depicts the chaser's attitude within the orbital coordinate system. The participants thus find it easier to estimate the targets' relative positions within this system.

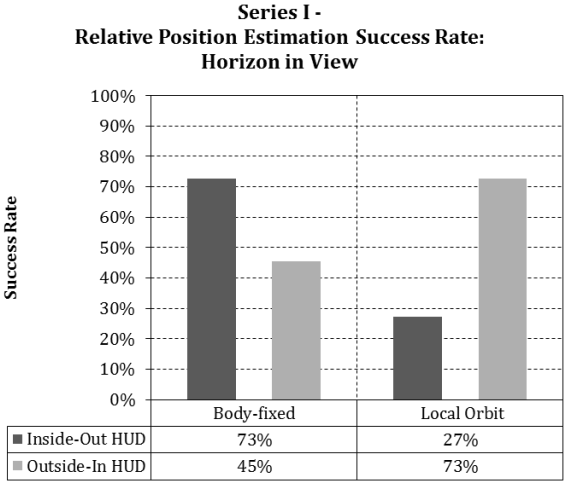

Figure 6-18: Success rates in the relative position estimation task with horizon in view. The inside-out HUD was most helpful in the body-fixed coordinate system, while in the local orbital coordinate system the participants benefitted most from the outside-in HUD.

The overall low performance with the body-fixed coordinate system, as well as the difference between the HUDs however forms a surprise. The relative position in the body-fixed system can be discerned by looking at the simulator image and marking in what quadrant of the picture the target is situated. Apparently the HUD confused the participants so that 27% for the inside-out and 55% for the outside-in display were overwhelmed by this task. This could be due to the *cognitive tunneling* effect described in Section 6.2.

Another cause for confusion within the body-fixed system seems to be the presence of Earth within the FOV. When Earth is not within view, the participants judge the target position correctly in 91% using the inside-out display, and 82% using the outside-in display (see Figure 6-19). Compared to

the results with horizon in view, this indicates better operator performance if the HUD is the only attitude reference available. However, without Earth as a natural reference, none of the participants was able to position the target within the orbital coordinate system using the inside-out HUD, while 36% were successful with the outside-in HUD.

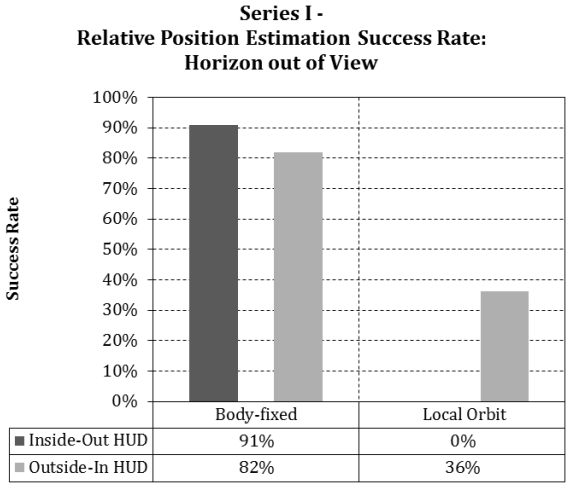

Figure 6-19: Success rates in the relative position estimation tasks without horizon in view. For the body-fixed coordinate system the inside-out HUD shows slightly better performance than the outside-in HUD. In local orbital coordinates, only the outside-in HUD enabled participants to estimate the target's relative position.

Experiment series I therefore showed that an **attitude HUD significantly increases operator performance** during attitude maneuvers. Furthermore, an **outside-in representation is superior in performance** compared to an inside-out attitude display, in that it enables the operator to perform attitude maneuvers more successfully and efficiently. For estimating relative spacecraft positions, the outside-in display is of higher utility when the orbital coordinate system is used as a reference. Since this coordinate system is used for maneuver planning during proximity operations, this therefore shows that the outside-in HUD is the superior attitude representation for a proximity operations HUD. These results backed by the objective data are furthermore supported by the experiment questionnaire. At the end of the experiment series, the participants were asked which HUD they preferred in attitude correction/maneuvering and position estimation tasks, and which HUD was easier to use in each of these tasks (see Figure 6-20). For *attitude maneuvering*, the outside-in HUD was strongly preferred and considered to be easier to use. For the *position estimation* tasks the inside-out display was preferred and considered easier to use. This reflects the data logged during the experiment. It must be noted that the ratio of indifferent responses is higher for the questions concerning the positioning tasks than for the attitude maneuvering tasks.

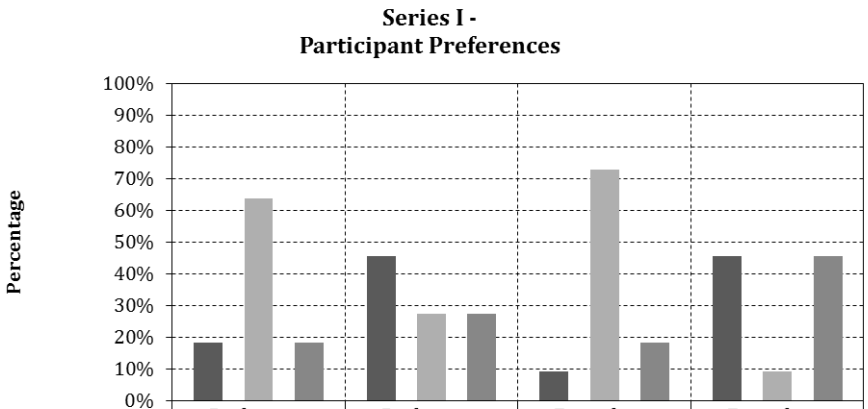

	Preference: attitude	Preference: position	Ease of use: attitude	Ease of use: position
Inside-Out HUD	18%	45%	9%	45%
Outside-In HUD	64%	27%	73%	9%
Indifferent	18%	27%	18%	45%

Figure 6-20: Participant HUD preferences after experiment series I. The outside-in HUD ranks foremost in preference and ease-of-use for the attitude maneuvering task. In the position estimation task, the inside-out HUD is ranked in participant preference and ease-of-use.

6.4.3 Reference System Evaluation

Experiment **series II** tested for the different effects the orbit and horizon **reference systems** have on the relative **position estimation** task.

The **independent variable** in this experiment series was the coordinate reference system.

The **dependent variables** were user preference, determined by questionnaire, and in-plane, out-of-plane and total position estimation success rates.

The 11 participants received about 15 minutes of training to familiarize themselves with the outside-in attitude HUD and the coordinate systems of the HUD. After training the participants answered the question which coordinate system they preferred (Figure 6-21).

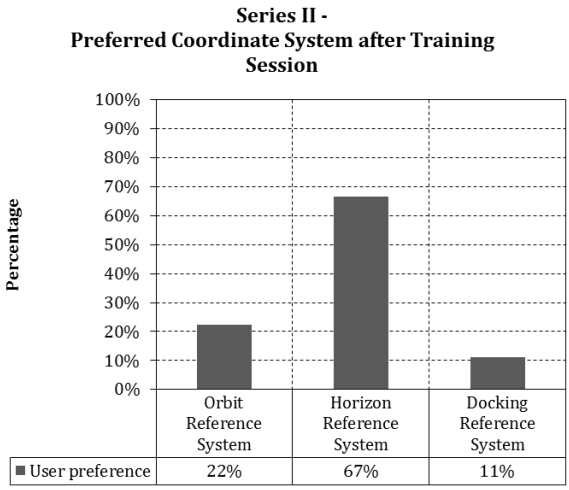

Figure 6-21: Preferred coordinate system after training session. Right after training, 67% of participants preferred the Horizon coordinate system over Orbit and Docking.

The responses show a strong preference for the Horizon reference system, which was expected, since with Earth in view, this reference system is the most intuitive of the three. The Docking reference system was only used during the training session and was not part of the ensuing experiment run, since by its nature is not capable of assisting the operator in estimating positions relative to the orbital plane.

The participants were then shown a PowerPoint slideshow with 20 scenarios similar to the ones used in the third experiment of series I. In order to reduce experiment complexity, the attitude HUD used was exclusively the **outside-in representation**, reflecting the results of experiment series I. In ten scenarios, the Orbit reference system was used, in the further ten the Horizon reference system. The participants had to qualitatively estimate the target's position in relation to the chaser within the orbital plane (forward/aft, left/right), as well as in relation to the interceptor's local orbital plane (above/below or within the plane), and mark the positions on the questionnaire. Figures 6-22 and 6-23 show the mean results of these estimations separately for in-plane position component, out-of-plane position component, as well as the total position estimation. In order for the total position estimate to be correct, both the in-plane and out-of-plane components must be estimated correctly.

For **in-plane position**, a maximum estimation success rate of 100% was achievable using the Horizon reference system, whereas merely 60% were the maximum using the Orbit reference system. The mean success rates are 42% for the Orbit reference system, compared to 54% for the Horizon reference system.

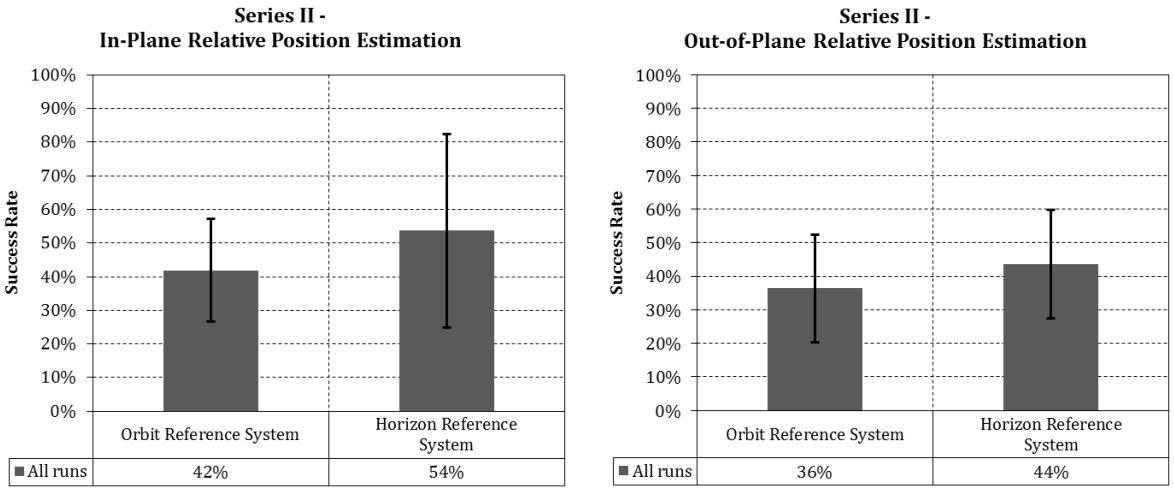

Figure 6-22: In-plane and out-of-plane relative position estimation results. Both plots indicate higher mean participant performance with the Horizon reference system, as compared to the Orbit system.

For the more difficult **out-of-plane position** estimation task, the maximum success rate in both reference systems was 70%. However, the mean success rate shows a slight superiority of the Horizon reference system, with 44% as compared to 36% for the Orbit reference system. This is surprising, since it was expected that estimating the out-of-plane component would be facilitated by the system using the actual orbital plane as the main reference. The fact that the Horizon reference system corresponds with the natural attitude references available in the scenario seems to increase the participants' ability to orient themselves in space and thus also enhance their situation awareness.

This trend is also visible in the statistics for **total estimation** success (Figure 6-23). Using the Horizon reference system, participants were more often able to correctly identify the relative position of the target, with a maximum of 60% and a mean of 25%. These low numbers also show the difficulty of the task and the need for other assistance systems beyond the attitude HUD for proximity operations maneuver planning.

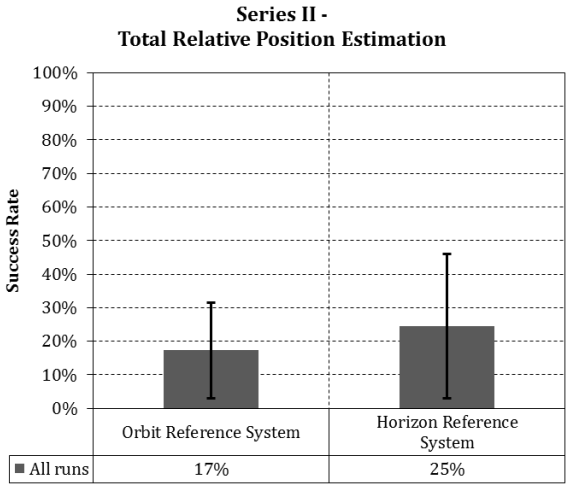

Figure 6-23: Total relative position estimation results. In the Horizon reference system, 25% of participants were successful in estimating relative position, compared to 17% in the Orbit system.

6.4.4 Trajectory Prediction HUD Evaluation

The third experiment series comprised the most complex task for the participants. The chaser spacecraft was placed at distances of 200 m and 500 m from a target (represented by a model of the *Hubble Space Telescope*). The participants had to **approach** the target, being supported by the 2D, 3D Orbit and 3D Vessel trajectory prediction displays. Each participant had to complete five approaches with each of the prediction displays. An approach was considered successful if the chaser was stopped within a sphere with radius 20 m surrounding the center of mass of the target, with the rotation rates being reduced to zero. The relative velocity tolerance was ±0.05 m/s, the rotation rate tolerance ±0.0285°/s.

The **independent variable** was thus the type of trajectory prediction display used.

Dependent variables were user preference, approach success rate, approach completion time, accumulated translation and rotation maneuver impulses, as well as the approach velocity when entering the 20 m sphere.

The test was run with 12 participants (the maneuver data of two of them was lost due to a malfunction of the Simulink logger and could not be recovered). The participants first individually trained using a single scenario, in order to get familiarized with the translation controls of the joystick, the trajectory prediction displays, as well as the maneuvering task.

User Preference

At the end of the training session, the participants were asked their prediction display preferences (see Figure 6-24). 64% of the participants preferred the 3D Vessel display over the others. This preference was expected since the 3D Vessel display was considered to be the most intuitively accessible display. After the experiment runs, the participants were again asked to state their pref-

erences. The 3D Vessel display was still preferred over the 3D Orbit display, but came in second after the 2D system. This difference in user rating is not reproducible from the maneuver data.

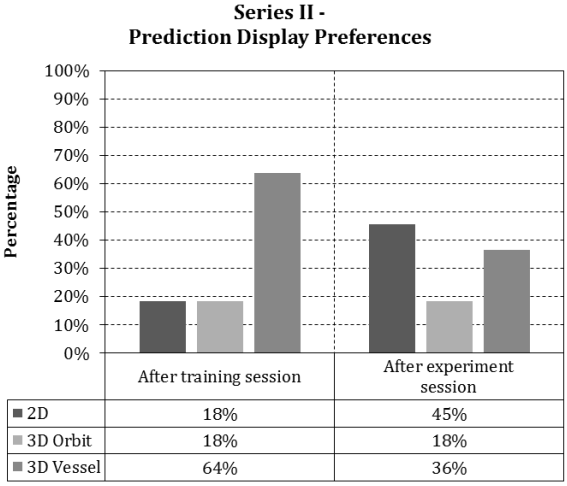

Figure 6-24: Prediction display preferences after training session and experiment session. Participants initially showed a strong preference for the 3D Vessel display, in which the trajectory prediction is drawn in a 3D representation rotating with the spacecraft attitude. After the experiment, operators prefer the 2D display over the 3D Vessel display and the 3D Orbit display. This subjective ranking is not supported by the maneuver data.

Maneuver Data

During the actual experiment runs, the Simulink logging model again developed problems which were not noted until after the completion of the experiment series. This resulted in varying data sampling rates. In order to obtain comparable results, it was decided to discard all approaches during which the maximum time between samples was larger than 0.2 s, resulting in a minimum sampling rate of 5 Hz. For the 2D display, 11 out of 50 runs were thus discarded, for 3D Orbit 14 of 50, for 3D Vessel 11 of 50. The remaining maneuver data was furthermore separated according to the initial distance to target. The 200 m and 500 m runs were randomly distributed for each prediction display, resulting in a distribution of 200 m: 500 m cases of 27:12 for 2D, 23:13 for 3D Orbit, and 19:20 for 3D Vessel.

The first surprising result of the experiment series was that on the 200 m approach, every participant was able to successfully complete every approach maneuver. On the 500 m approach, there was one failure both using the 2D and 3D Vessel prediction displays. Figure 6-25 shows the times required to complete the 200 m and 500 m approaches. The **mean times** are almost equal between the three display options, both for the short and the long initial distances.

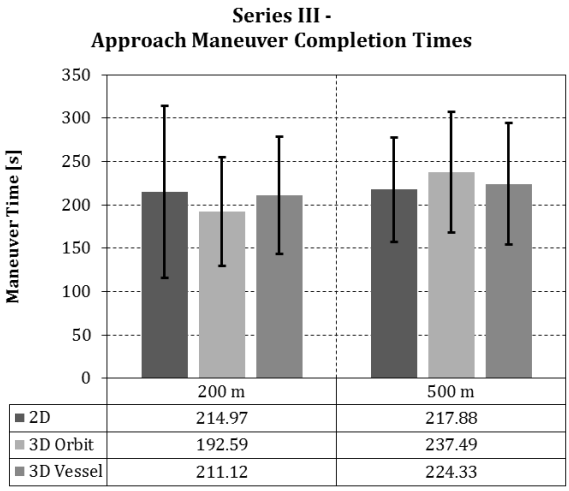

Figure 6-25: Mean maneuver completion times for the 200 m and 500 m approaches. The plots show that the difference between the three display modes is negligible. Total maneuver completion times furthermore do not differ between 200 m and 500 m approaches.

It is also interesting to note that it took the participants almost exactly as long to complete the 500 m approach as it did the 200 m. This is explained by the fact that the participants accelerated longer in the long-range scenarios, resulting in average and maximum relative velocities of almost twice the value for the 500 m approaches.

The data for the total **translation impulse** expended during the approaches (Figure 6-26) show a slightly worse performance for the 2D display at 200 m. Such an effect is not evident at 500 m initial distance, at which the total translation impulse for all three display versions is almost equal.

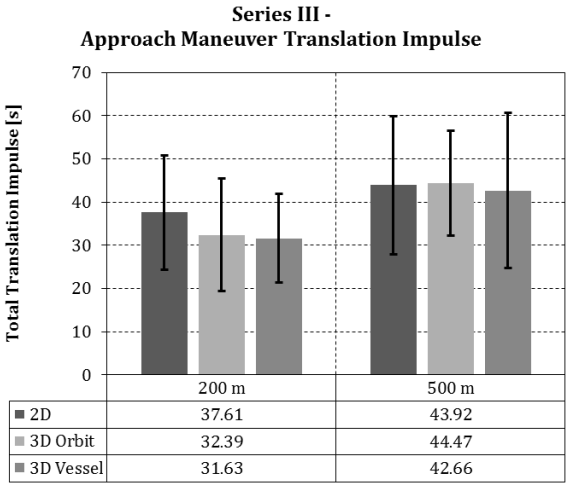

Figure 6-26: Mean total translation maneuver impulse expenditure for the 200 m and 500 m approaches. While at 200m the 2D display appears to cause higher mean total impulse, the general trend shows there to be no difference between the display modes.

The measured data for total impulse for **rotation maneuvers** (Figure 6-27), as well as **relative velocity** at the 20 m mark (Figure 6-28), which is an indicator for the required braking thrust and thus the severity of plume impingement, is just as inconclusive.

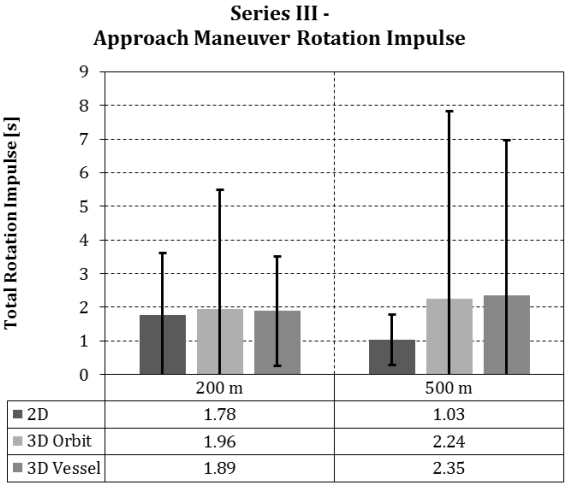

Figure 6-27: Total rotation maneuver impulse expenditure for the 200 m and 500 m approaches. The differences in mean values do not allow any ranking of the display variants.

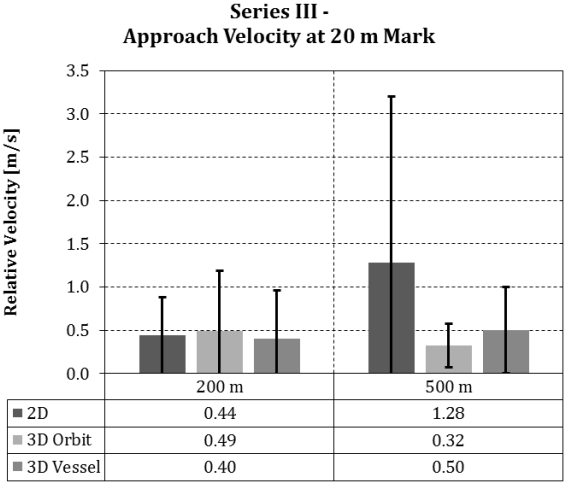

Figure 6-28: Approach velocities at 20 m distance mark for the 200 m and 500 m approaches. The differences in mean values do not allow any ranking of the display variants.

It is therefore concluded that there exists **no difference** in operator performance due to the trajectory prediction display version.

Participant Comments

Participants stated that the advantages of the 2D display were its clear presentation and the fact that the attitude HUD was in view alongside it. The 3D displays had the general disadvantage of being more difficult to understand due to the 3D content being projected onto the 2D plane and due to the low resolution of the *Orbiter* drawing functions. With the 3D Orbit display, it was not possible

to discern the spacecraft attitude rates. These were however visible in the 3D Vessel display. A problem the 2D and 3D displays shared was missing scale indicators with which to measure distances.

Based on these comments, the maneuver data, and the user rankings, it was decided that the **3D Vessel** display had the biggest growth potential in order to overcome the shortcomings of the 3D displays implemented in *Orbiter*, and to introduce the advantages of the 2D displays. The 3D Vessel display was therefore to be refined based on participant comments and own observations, before integrating it into the *ThirdEye* user interface.

6.4.5 Conclusions

The user studies show that the availability of an attitude HUD greatly facilitates teleoperated attitude maneuvering in an orbital environment. An outside-in attitude representation is furthermore superior to an inside-out display in supporting operator attitude maneuvering performance.

This result is in agreement with findings for the comparison of inside-out and outside-in display for unmanned underwater vehicles [99]. The results presented have also shown the outside-in display to be the superior HUD for estimating target relative positions within the orbital plane, which is important for long-range approach maneuvers. At short ranges, when the target position in the chaser body coordinate system is more relevant, the inside-out display is the better option. For such position estimation tasks a coordinate reference system based on the local horizontal plane is indicated to be preferred over an orbital plane reference system. This could be due to the agreement between artificial and natural attitude cues for the Horizon reference system. However, the differences in operator performance measured during these experiments are too small for a definitive statement. More research in this field is therefore needed.

The trajectory prediction display variants designed for supporting approach maneuvers generated no differences in operator performance when compared against each other. However, operator perception accredited the 2D and 3D Vessel displays with higher usability than the 3D Orbit display. The 3D vessel display was therefore to be further detailed and refined for integration into the *ThirdEye* system.

6.5 Integration into the ThirdEye Proximity Operations GUI

The HUD elements developed and evaluated were intended to be included in the integrated *ThirdEye Situation Awareness Enhancement System*. Following the results of the evaluation study described above, this final version of the HUD will have the following characteristics. First, the *ThirdEye Proximity Operations HUD* system will use an **outside-in HUD** referenced to the **local orbital plane**. Although the Horizon reference system proved superior in the experiments, the Orbit system was selected for the reason that the current RACOON simulation environment only supports in-plane movement (see Section 5.2.2). Second, due to participant comments during the experiment

runs, **pitch and yaw rate indicator** strips and numerical displays were added, as well as a **roll angle and rate** indicator, and a numerical display for the approach velocity and distance relative to the target. Third, the **trajectory prediction display** is provided in a separate window to the left of the camera views. The **3D Vessel system** is implemented with some changes compared to the experimental version in *Orbiter*. The 3D axes are no longer projected onto the 2D plane but actually drawn in 3D using *OpenGL* drawing functions. The display scale is changed with target distance in order to fully use the available drawing space. The horizontal and vertical planes are visible in light gray, with the scale indicated on the borders. The target symbol size is changed with the distance to target.

The following sections provide the details of the implementation of the attitude and trajectory prediction displays.

6.5.1 Attitude Display

The HUD experiments run in *Orbiter* did not account for the effects of the **roundtrip time delay**. The compensation of the time delay is however a requirement for the *ThirdEye* system. The *ThirdEye* attitude HUD therefore incorporates two attitude representations. One, drawn in red, depicts the spacecraft attitude angles as received in **spacecraft telemetry**. This telemetry is delayed by half the roundtrip time delay once it reaches the operator. Maneuver decisions and commands based on this output do therefore not reflect the delayed reality and can thus entail future corrective actions, which leads to increased energy consumption and potentially also a loss of control.

The HUD therefore provides a **prediction** of the spacecraft attitude based on the current command input. This **commanded attitude display** (refer to Section 2.4) is drawn in green. Using this display, the operator is immediately made aware of the effect of his command inputs, without having to wait for the telemetry feedback. For this prediction, the operator inputs made by joystick or space mouse are interpreted as angular accelerations, which is the case if user commands directly articulate thrusters or control-moment gyros. These accelerations are derived from the deflection of the control device and the maximum angular acceleration of the system, which in the case of *ThirdEye* simulations is set in the simulation control software. Throughout the *ThirdEye* experiments, a maximum angular acceleration $\alpha_{max} = 2\ °/s^2$ was used.

Prediction Algorithm

At each time step of the prediction algorithm, which was set to 10 ms for the experimental *ThirdEye* system, the recent **attitude vector** with respect to the Orbit system $\boldsymbol{\theta_{i,0}}$ is computed from the attitude and rate vectors $\boldsymbol{\theta_{i-1,1}}$ and $\boldsymbol{\omega_{i-1,1}}$ at the end of the preceding time step.

$$\boldsymbol{\theta_{i,0}} = \begin{pmatrix} \varphi_{i,0} \\ \vartheta_{i,0} \\ \psi_{i,0} \end{pmatrix} = \boldsymbol{\theta_{i-1,1}} + \boldsymbol{\omega_{i-1,1}} \Delta t \qquad \textit{Eq. 6-20}$$

This attitude vector $\boldsymbol{\theta_{i,0}}$ present at the beginning of time step *i* is used to derive a **direction cosine matrix** (DCM) $\boldsymbol{A_{i,0}}$.

$$\mathbf{A_{i,0}} = \begin{bmatrix} 1 & 0 & 0 \\ 0 & \cos\varphi_{i,0} & \sin\varphi_{i,0} \\ 0 & -\sin\varphi_{i,0} & \cos\varphi_{i,0} \end{bmatrix} \begin{bmatrix} \cos\vartheta_{i,0} & 0 & -\sin\vartheta_{i,0} \\ 0 & 1 & 0 \\ \sin\vartheta_{i,0} & 0 & \cos\vartheta_{i,0} \end{bmatrix} \begin{bmatrix} \cos\psi_{i,0} & \sin\psi_{i,0} & 0 \\ -\sin\psi_{i,0} & \cos\psi_{i,0} & 0 \\ 0 & 0 & 1 \end{bmatrix} \qquad \textit{Eq. 6-21}$$

The commanded **angular accelerations** $\boldsymbol{\alpha_i}$ are integrated twice to derive the change angles $\boldsymbol{\Delta\theta_i}$ and hence the DCM $\boldsymbol{A_{i,\Delta}}$.

$$\boldsymbol{\Delta\theta_i} = \frac{1}{2}\boldsymbol{\alpha_i}\Delta t^2 \qquad \textit{Eq. 6-22}$$

The DCMs $\boldsymbol{A_{i,0}}$ and $\boldsymbol{A_{i,\Delta}}$ are then multiplied to derive the total DCM $\boldsymbol{A_{i,1}}$ for time step *i*.

$$\mathbf{A_{i,1}} = \mathbf{A_{i,\Delta}} \cdot \mathbf{A_{i,0}} \qquad \textit{Eq. 6-23}$$

This combination of rotation matrices for constant rotation rates and angular accelerations accounts for any guidance commands issued while the spacecraft is in a rotary motion. In this case, the base coordinate frame in which the acceleration commands are issued must be pre-rotated by the existing rotation, prior to including the accelerations.

The final DCM $\boldsymbol{A_{i,1}}$ yields the **updated attitude angles** $(\varphi_{i,1}, \vartheta_{i,1}, \psi_{i,1})^{\mathrm{T}}$ and the associated **angular rate vector** $\boldsymbol{\omega_{i,1}}$ (see equations 6-24 - 6-27) after time step *i*. These values serve as input for the next time step.

$$\varphi_{i,1} = -\arctan\left(\frac{A_{i,1(2,3)}}{A_{i,1(3,3)}}\right) \qquad \textit{Eq. 6-24}$$

$$\vartheta_{i,1} = -\arcsin\left(-A_{i,1(1,3)}\right) \qquad \textit{Eq. 6-25}$$

$$\psi_{i,1} = -\arctan\left(\frac{A_{i,1(1,2)}}{A_{i,1(1,1)}}\right) \qquad \textit{Eq. 6-26}$$

$$\boldsymbol{\omega_{i,1}} = \frac{\left(\boldsymbol{\theta_{i,1}} - \boldsymbol{\theta_{i,0}}\right)}{\Delta t} \qquad \textit{Eq. 6-27}$$

Prediction Accuracy

The **accuracy** of the predictive display obviously depends on the quality of the spacecraft model used for the propagation of spacecraft states. While this is no problem for the *ThirdEye* prototype

and its evaluation, since both prediction and simulation are based on the same model, it will require frequent synchronization and recalibration during a real space mission. **Synchronization** can only occur when the spacecraft attitude is stationary, since then the commanded and predicted attitudes and rates should be equal. Any operations plan for a teleoperated rendezvous & docking mission must therefore incorporate such synchronization stops in order to minimize the drift between commanded display and reality.

Visualization

The pitch and yaw angles are visualized on the screen just as in the outside-in HUD evaluated in *Orbiter* (compare figures 6-8 and 6-9). Following user remarks during the HUD evaluation experiments, a dedicated **roll angle indicator** was added. This indicator is a circular angle scale surrounding the ownship symbol.

Further additions to the HUD induced by user comments are roll, pitch and yaw **rate indicators**. These are realized as combinations of strip indicators and digital displays and thus provide both a quick-to-understand graphical display and a precise read-out. It is important to note that the digital value displayed is the value derived from the attitude predictor. It was decided to display the commanded rate rather than the real attitude rate since the commanded display is supposed to be used in commanding the spacecraft, while the telemetry feedback display is to be used for monitoring purposes. The maximum length of the **indicator strips** was set to 10% of the vertical screen size, in order to not overly clutter the display. This maximum length represents a rotation rate of 2 °/s, which in the ThirdEye experiments was the rate attained after 1 s of maximal angular acceleration.

The roll rate indicator is integrated into the roll angle indicator. When a positive roll rate is commanded, a green ring segment appears which extends in clockwise direction[10]. As the existing rate of the spacecraft is received from telemetry, another concentric ring segment is drawn in red, outside the commanded rate ring.

The pitch and yaw rate indicators function analogously. The pitch rate indicator is situated at the right-hand end of the yaw angle scale. The commanded pitch rate is drawn in green, the actual rate in red, positive in the upward direction. The yaw rate indicator is drawn at the top end of the pitch scale. The strip indicators for positive yaw rates extend to the right.

The participants of the HUD evaluation experiments furthermore remarked the utility of an **approach rate display** when flying approach and docking maneuvers. A graphical display for the approach rate was considered, but in order to reduce display clutter, a digital display was selected. This was initially positioned in the upper left corner of the HUD, so as not to interfere with the pitch and yaw rate indicators. The approach rate is provided in meters per second. This unit should be evaluated in future studies, because it causes deceptively low display values during a typical final approach. A display in centimeters per second might therefore be more valuable to the operator.

[10] Negative roll rates are visualized in counterclockwise direction.

Figure 6-29 shows the attitude HUD as implemented for the *ThirdEye* system.

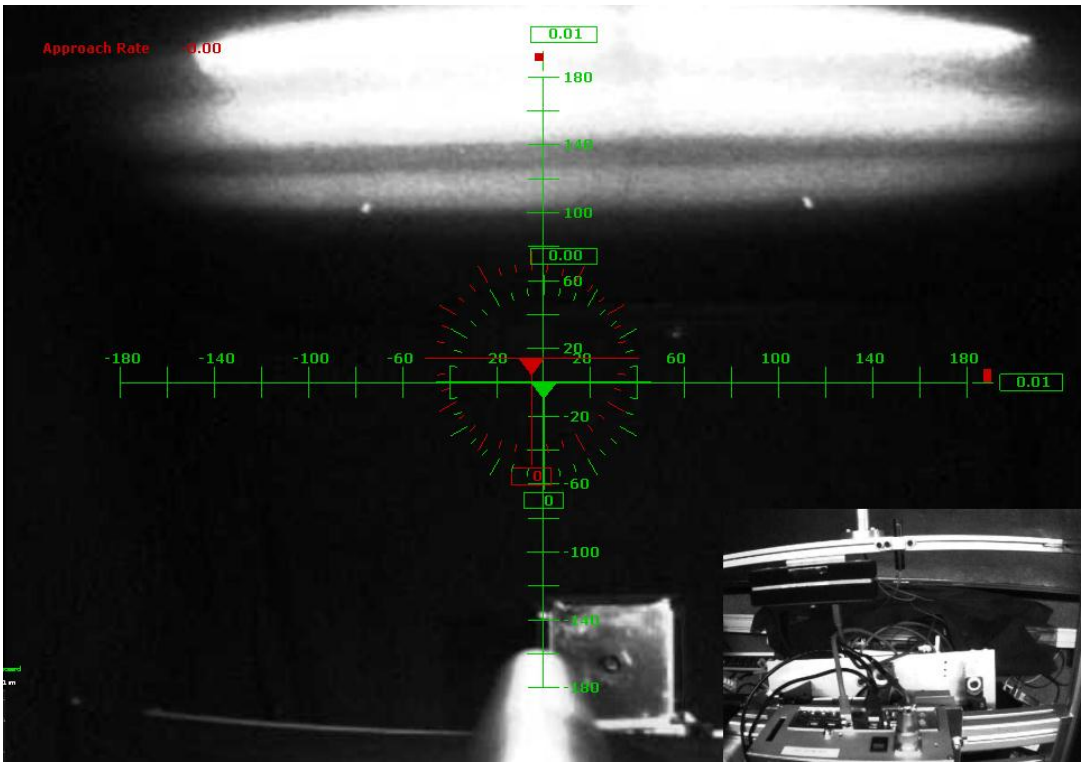

Figure 6-29: Attitude HUD implemented for the ThirdEye system. Note the roll angle indicator, the pitch and yaw rate indicators, as well as the approach rate display, which show both commanded attitude values provided by a predictive algorithm, as well as actual attitude information gained from telemetry. These features differentiate the ThirdEye HUD from the HUD implementation evaluated in Orbiter. In the lower right corner of the figure the additional video image provided by the ThirdEye robotic camera arm is shown.

6.5.2 Trajectory Prediction Display

In the *Orbiter* implementation, the trajectory prediction system could use the spacecraft **velocity vector** computed by the *Orbiter* core as input for propagation with the CW equations. This simulation core is not available in the *ThirdEye* system. The propagation of the relative trajectory is therefore based on the modification of the **CW equations** for continuous thrust motion discussed in Section 3.3 (equations 3-11 to 3-14). Since the RACOON simulation environment does at this stage only support **in-plane motion**, the out-of-plane *z* components of the position, velocity and acceleration vectors are ignored. This restriction of the simulation environment is also the reason why the Orbit reference system is used in the *ThirdEye* implementation, instead of the Horizon reference system as indicated by the results of the HUD evaluation experiments.

Prediction Algorithm

The coordinate transformation between the LVLH coordinate frame used in equations 3-11 to 3-14 and the Orbit coordinate frame used in the *ThirdEye* trajectory prediction is given by

$$\begin{pmatrix} x \\ y \\ z \end{pmatrix}_{O} = \boldsymbol{A}^{\boldsymbol{O}}_{\boldsymbol{LVLH}} \cdot \begin{pmatrix} x \\ y \\ z \end{pmatrix}_{LVLH} \qquad \textit{Eq. 6-28}$$

With the transformation matrix $\boldsymbol{A}^{\boldsymbol{O}}_{\boldsymbol{LVLH}}$

$$\boldsymbol{A}^{\boldsymbol{O}}_{\boldsymbol{LVLH}} = \begin{bmatrix} 1 & 0 & 0 \\ 0 & 0 & -1 \\ 0 & 1 & 0 \end{bmatrix} \qquad \textit{Eq. 6-29}$$

The **initial position** $(x_0, y_0)^T_O$ of the chaser spacecraft in relation to the target is set in the simulation control GUI, along with the **initial relative velocity** $(\dot{x}_0, \dot{y}_0)^T_O$.

Accelerations acting upon the chaser are computed by multiplying the controller input, which in the case of translation control can be -1 and 1, with the maximum acceleration set in the simulation control GUI. Throughout *ThirdEye* experiments, the maximum linear acceleration in all axes was 0.1 m/s, with a maximum relative velocity of 0.3 m/s. The accelerations $\left(a_x, a_y, a_z\right)^T_B$ commanded by the operator[11] must be transformed from the spacecraft body-fixed coordinate system into the Orbit system. This is accomplished by the DCM $\boldsymbol{A}^{\boldsymbol{O}}_{\boldsymbol{B}}$, which rotates the body-fixed coordinate system by the roll angle φ, the pitch angle ϑ and the yaw angle ψ.

$$\begin{pmatrix} a_x \\ a_y \\ a_z \end{pmatrix}_{O} = \boldsymbol{A}^{\boldsymbol{O}}_{\boldsymbol{B}} \cdot \begin{pmatrix} a_x \\ a_y \\ a_z \end{pmatrix}_{B} \qquad \textit{Eq. 6-30}$$

$$\boldsymbol{A}^{\boldsymbol{O}}_{\boldsymbol{B}} = \begin{bmatrix} \cos\psi & \sin\psi & 0 \\ -\sin\psi & \cos\psi & 0 \\ 0 & 0 & 1 \end{bmatrix} \begin{bmatrix} \cos\vartheta & 0 & \sin\vartheta \\ 0 & 1 & 0 \\ -\sin\vartheta & 0 & \cos\vartheta \end{bmatrix} \begin{bmatrix} 1 & 0 & 0 \\ 0 & \cos\varphi & -\sin\varphi \\ 0 & \sin\varphi & \cos\varphi \end{bmatrix} \qquad \textit{Eq. 6-31}$$

The position and velocity at each time step resulting from the initial position and velocity and the accelerations commanded by the operator are then propagated forward in time for drawing by means of the standard CW equations (Eq. 3-5 - Eq. 3-7), analogously to the *Orbiter* implementation. The **propagation time** can be set by the operator to the following values: 1 min, 10 min, 30 min, 60 min, as well as the orbital period of the target object. For the *ThirdEye* evaluation experiments described in the next chapter, the default trajectory propagation time was 10 min.

[11] A direct acceleration control mode was adopted for the HUD and ThirdEye experiments instead of velocity control. This represents a realistic case in which operator commands directly cause thruster firings. A pioneer study in teleoperation of docking maneuvers [7] found that the acceleration control mode was acceptable to the operators and caused low propellant consumption. The same study also found that rate command, attitude hold control of the spacecraft attitude is preferable over direct rate command or acceleration command modes. However, a direct acceleration command mode is used for attitude maneuvering in this doctoral research, because then operator performance cannot be confused with controller performance.

Visualization

The drawing function of the 3D Vessel prediction display was modified to reflect user comments regarding display accessibility. Figure 6-30 shows the resulting display. The majority of changes aimed at improving the perception of target distance in the display. The **scaling** of the display is dynamic in order to fully utilize the available drawing space at all times. The scale is set so that half the width, height, and depth of the drawing space represent the major component of the relative position vector. The horizontal and vertical planes of the display are then filled with a **distance grid**. The scaling of this grid is detailed in Table 6-4.

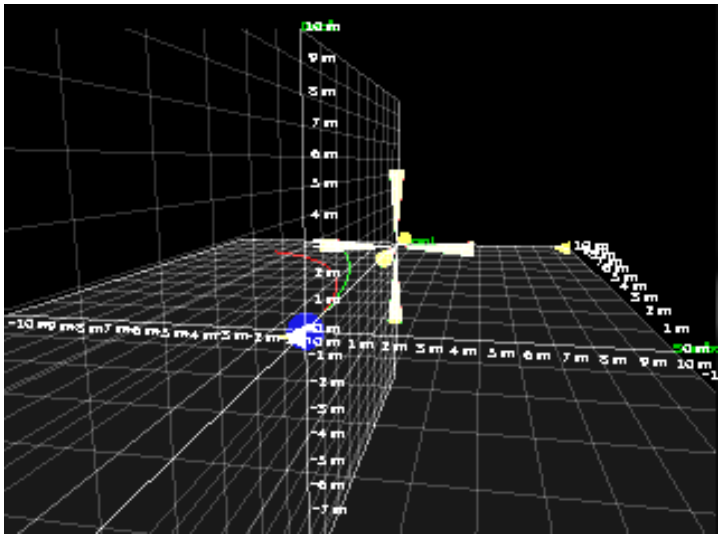

Figure 6-30: ThirdEye trajectory prediction display. The display follows the principle of the 3D Vessel display evaluated in Orbiter. The display is scaled dynamically to fully utilize the available drawing space. Ownship is symbolized by a blue ball in the center of the display. The position of the target is indicated by red and green crosshairs as well as three triangular position indicators running along the x, y and z axes. The crosshairs are sized dynamically with target distance. Operator perception of the distance is furthermore supported by distance grids in the horizontal and vertical planes. These grids are also scaled dynamically in order to maximize utilization of drawing space as well as readability. The commanded trajectory is drawn in green, the predicted trajectory based on telemetry feedback in red.

Table 6-4: Scaling of ThirdEye trajectory prediction display distance grid. The scaling of the distance grid is adjusted dynamically, depending on the distance to the target. This provides a display fully utilizing the available drawing space and readable distance information.

Target Distance	Distance Grid Scale
> 1000 m	1000 m
> 100 m	100 m
> 10 m	10 m
> 1 m	1 m
> 0.001 m	0.1 m

The distance of the target is furthermore indicated by **triangular position indicators** running along the edges of the horizontal and vertical planes, and by the size of the **target symbol**. On the one hand, the OpenGL drawing functions used for the HUD automatically change object sizes with their depth. Due to the dynamic scaling described above, this effect had to be augmented in order to arrive at a steady change of target size with distance. The size s of the target symbol is therefore derived by the following equation, with x being the x component of the target relative position vector.

$$s = s_0 \frac{1}{1+x} \qquad \textit{Eq. 6-32}$$

In order to make the operator aware of the effects of **time delay** on his control inputs, the predicted trajectory is drawn twice. The green trajectory represents the **commanded flight path** immediately propagated based on command inputs. The red trajectory is the flight path propagated from **spacecraft telemetry** values.

The trajectory prediction display is displayed to the left of the camera view and the attitude HUD, as shown in Figure 6-31. This is again supposed to reduce display clutter and to maximize the visibility of the live camera video, which is the main sensor information available to the operator during the docking approaches. Note the *ThirdEye Robotic Camera Arm* status display in the upper left corner, as well as the secondary camera view provided by the arm-mounted camera in the lower right corner (refer to Section 7.3 for more details).

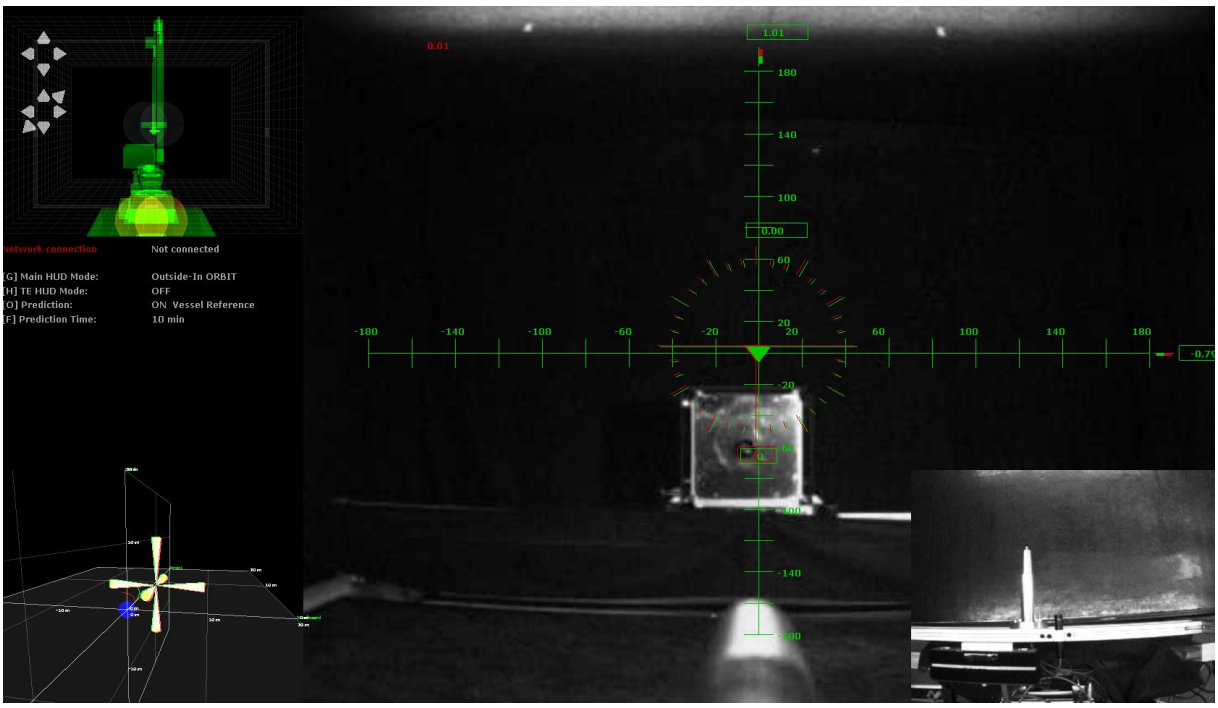

Figure 6-31: Attitude HUD and trajectory prediction display integrated into the ThirdEye proximity operations GUI.

6.6 Summary

A **proximity operations HUD** integrating ownship attitude information and a trajectory prediction into the camera video stream was hypothesized to **enhance operator performance** during final approach maneuvers.

In order to test this hypothesis and to identify the HUD configuration most beneficial to the operator, an **experimental proximity operations HUD** was implemented to be experimentally evaluated in the ***Orbiter* spaceflight simulator**. The experiments to be conducted were an evaluation of the **general effect of an attitude HUD** on operator performance, the **comparison of inside-out and outside-in attitude representations** in attitude maneuvering and relative position estimation tasks, the **comparison of two different coordinate reference frames** in a relative position estimation task, as well as the **comparison of three different trajectory prediction display modes** in their effects on operator performance in a close-range approach task.

The results of this experimental study show that (1) an **attitude HUD has significant impact** on operator performance in spacecraft attitude maneuvers, (2) an **outside-in HUD is superior** to an inside-out HUD, (3) a reference system based on the **local horizontal plane** is to be preferred if possible, and (4) there exist **no measurable differences between the tested trajectory display modes**.

Based on these evaluation results, the ***ThirdEye Proximity Operations HUD*** was implemented. It used the evaluated **outside-in attitude HUD** based on the **local orbital coordinate system**, with the addition of a **roll angle indicator** and an **angular rate indicator** display. It was furthermore enhanced by an **attitude prediction algorithm** to account for the signal travel delays encountered in space teleoperation. The **trajectory prediction algorithm** was changed to reflect the fact that less information about the spacecraft state is available in real applications than in spaceflight simulation software. The display visualization was furthermore changed to reflect the participant comments during the evaluation experiments. The prediction display is drawn next to the video stream and attitude HUD in order to declutter the display. Additional distance cues are provided by means of a dynamically scaling **distance grid**, **position indicator symbols**, plus dynamically scaling **target symbols**. In addition to the flight path and target marker based on received spacecraft telemetry, a **flight path projection based on current maneuver inputs** is shown.

7 The Third Eye

The proximity operations HUD enables the operator to understand and predict the ownship motion in space. It does not provide any information regarding the target object. The operator can therefore not gain information about the relative state of chaser and target by the HUD alone. Another source of information is hence necessary to achieve the SA required for efficient and safe final approach and docking.

As discussed in Section 2.4, a common approach in the field of robotics is to create a virtual model of the chaser, the target, and their relative motion in order to gain full SA. This approach requires detailed knowledge of the geometry and motion of the target object. In OOS scenarios, especially the space debris removal use case, such information may not be readily available, thereby limiting the utility of such a VR or AR display.

It is therefore proposed to provide the operator with additional camera vantage points. These enable him to look at the situation from different directions and thus generate a complete mental model of the relative position, orientation and motion between chaser and target spacecraft. The option selected to provide these additional, independent vantage points is to use a robotic camera arm, referred to as the *ThirdEye*.

The following sections provide the background behind the development of the *ThirdEye*, as well as the essential details of its design and construction[12]. It then proceeds to describe the experiments conducted to select the control input device, and the experiment series evaluating the utility of the *ThirdEye* system during final approach and docking of a generic, uncooperative target object.

7.1 Motivation

Teleoperated docking of spacecraft was investigated as early as during *Project Gemini*. Studies looking into the feasibility of docking with a camera mounted in the nose of a *Gemini* spacecraft showed that this approach is feasible, but very difficult due to insufficient visual information of the relative position [7]. Visual targeting aids installed on the target object were therefore found to be necessary in order to reduce pilot error during teleoperated docking [7]. Since such beacons or markings are not available on the majority of OOS targets, especially in space debris removal scenarios, other means of supporting the operator in the relative navigation task during the final meters of approach are necessary.

Existing Systems

One of the technically easiest and most flexible approaches is to provide the operator with multiple camera views showing the target object from different vantage points. The differential views con-

[12] An overview of the *ThirdEye* design has also been published [257]

vey the critical information about relative position and orientation. A limited realization of this approach was employed on the *Space Shuttle*. The *Shuttles* used CCTV cameras mounted in the payload bay and looking at the docking mechanism from the side [1]. The *Shuttle* crew could use these additional camera views to judge relative distances by means of laying acetate distance scales onto the camera screens [1]. Such a fixed secondary camera was sufficient for the *Space Shuttle* since it could be mounted at the proper distance from the APAS docking system in the extensive payload bay, and, since both *Shuttle* and the docking targets *Mir*/*ISS* featured stable attitude in LVLH, it served only to determine relative position, not orientation. For smaller vehicles, especially ROVs or servicer satellites that approach target objects in varying attitudes and non-zero rotation rates, a camera mounted on an extendable manipulator arm can serve to provide a third-person viewpoint from any direction of interest. This can be beneficial for perception of size, distance and direction, and thus support cognitive map formation and navigation [127] .

In telemanipulation tasks, observer cameras have frequently been used to provide such external viewpoints. A so-called *Roving Eye*, which is a mobile robot equipped with a pair of cameras, has for example been developed to support the crane operator during construction work [258]. *ETS-VII* used the combination of a hand eye camera and a shoulder camera for controlling the telemanipulation tasks [170].

Ranger was equipped with a camera arm carrying a stereo camera pair. This arm mimicked the degrees of freedom of a human torso and head [72]. *Ranger* furthermore used the *SCAMP* free-flying camera platforms to provide external views of the worksite for Ranger control [72]. It is not known whether *SCAMP* was solely used during servicing operations or also during final approach and docking.

Limitations

The main limitation of such multiple vantage point systems is that in general, the growing amount of available information can lead to degraded operator performance as the cognitive effort of controlling the additional entity providing the information can deflect the operator from the main task of controlling the primary vehicle [127] . The extra information itself, e.g. when displayed across multiple monitors, can lead to diffusion of attention disrupting operator performance [127, 187] . This effect can furthermore be aggravated if movable cameras are used, as this leads to the additional confusion about the orientation of the camera in relation to the vehicle [126].

The ThirdEye

To my knowledge, none of the existing systems have been dedicated to the purpose of enhancing operator SA during teleoperated final approach and docking. Furthermore, no mention of experimental verification of such a system could be found in literature research. This research gap is to be closed by the *ThirdEye* system and evaluation experiments. This system consists of a **robotic camera arm** providing the flexible vantage point, and an **operator interface** allowing efficient and

intuitive control of the camera arm, plus providing the additional camera views and information about the arm's posture and viewing direction.

7.2 Requirements

The *ThirdEye* is to be used primarily during **final approach and docking**. After successful docking, the system is to serve inspection purposes and support manipulation tasks of the spacecraft main manipulators. Based on the manipulator characteristics of *ETS-VII* and *Orbital Express*, and driven by any spacecraft component's requirement of minimizing mass and power budgets, the *ThirdEye* shall have a **range** of about 3 m. Since the evaluation experiments in the RACOON lab will be run at a scale factor of 0.3, in order to represent a the final 10 m of approach, the laboratory mock-up version of the *ThirdEye* shall have a range of 1 m.

In order to be able to fully utilize the *ThirdEye*, the operator needs to have full control of the camera arm system, without being distracted from his main task [146]. He must therefore be able to position the *ThirdEye* camera and to align its FOV, while simultaneously controlling the approaching spacecraft. The *ThirdEye* **operator interface** shall therefore provide an intuitive **one-hand input device** allowing the operator to precisely control the arm using the left or right hand, while operating the spacecraft using another one-hand input device. Since the cognitive workload of integrating the secondary camera images into the mental model of the operator is to be minimized, a three-dimensional **virtual representation** of the arm is to be provided to the operator. This ***ThirdEye* situation display** shall depict both the commanded display of the arm as well as the actual position as reported in telemetry, in order to compensate for roundtrip time delays. The spacecraft attitude HUD shall furthermore overlay the secondary camera image, so that the operator is enabled to keep awareness of the spacecraft attitude motion at all times.

In order to prove the utility of the *ThirdEye* in the teleoperated final approach and docking scenario, a demonstrator system based on these requirements must be implemented within the RACOON simulation environment and its utility be verified in a series of user studies.

7.3 Implementation

The highest operational flexibility for a flexible vantage point system would be provided by a free-flying subsatellite carrying a camera and other sensors, similar to *SCAMP* (refer to Section 1.3.2), *AERCam* (see Section 1.2.1), or the Jet Propulsion Laboratory's (JPL) *Micro-Inspector* [259].

Free-Flyer System Study

A design for such a free-flying sensor platform has been in studied in a Master's thesis contributing to this doctoral thesis [260]. In order to meet the requirements, the free-flyer must be equipped with an AOCS, a sophisticated automatic controller for station-keeping and collision avoidance, docking sensors and interfaces to connect to the chaser satellite, the sensor payload required for

the *ThirdEye*, sufficient on-board computing power to accomplish the navigation, maneuvering and data-compression tasks, a communication link to the chaser spacecraft, and an electrical power system (EPS) capable of supplying the subsatellite with sufficient power for any required duration. The chaser spacecraft must be equipped with the appropriate intersatellite communication system, a docking interface, as well as the power supply system required to recharge the subsatellite after use. Another requirement for extended missions is the capability of refueling the subsatellite when it is attached to the docking interface.

The requirements for a stand-alone EPS, intersatellite communications system, on-board computing power, docking interface and replenishment by the chaser spacecraft could be simplified by using a tethered subsatellite instead of a free-flyer, similarly to the ROV *Jason Jr.* being controlled from the submersible *Alvin* [261]. This would however introduce the dynamics of the tether, which could lead to the additional risk of collisions as well as to entanglement of the tether with both the chaser spacecraft and the target object.

Robotic Camera Arm Solution

The choice was therefore made to realize the *ThirdEye* as a **robotic camera arm**. This brings some disadvantages, such as a reduced motion envelope and limited range, as well as disturbance torques acting upon the chaser spacecraft. The overall system complexity is however reduced and operations do not have to account for three vehicles acting independently in six degrees of freedom. The robot arm's posture is known at all times, substantially reducing the effort for *ThirdEye* position and FOV control and monitoring, as well as for collision avoidance. *ThirdEye* system mass, cost and complexity is considered to be lower using the robot arm, compared to a free-flyer. System capability in the final approach and docking applications will not be reduced substantially by selecting the robotic arm concept.

As no commercial robotic arm meeting the required combination of payload mass, reach and financial budget could be found (as of 2008), it was decided to custom-build it at LRT. The *ThirdEye* laboratory version was implemented in a number of student projects [262, 263]. Furthermore, a prototype automatic target pointing algorithm was developed and tested in computer simulations [264]. The following sections provide an overview of the mechanical design as well as the control software implementation and the pointing algorithm. Details on the mechanical design are provided in [263]; the *ThirdEye Control* software is described in [262], along with the experiments evaluating the input devices. Meschede's thesis [264] provides the details on the automatic pointing algorithm, as well as on the corresponding software implementation and computer simulations

7.3.1 ThirdEye Camera Arm Mechanical Design

The *ThirdEye* robotic camera arm is a robotic arm with **five degrees of freedom** carrying a Bumblebee2 stereo camera (see Figure 7-1). Figure 7-2 illustrates the kinematic layout of the robotic camera arm, with a picture of the arm as integrated into the RACOON simulation environment provided in Figure 7-3.

Figure 7-1: CAD model of the ThirdEye robotic camera arm. Note the belt-driven elbow and camera head elevation joints. This design was chosen to reduce the mass of the limbs and thus the motor torque requirements. The CAD model does not show the secondary electronics box which is mounted to the right side of this view.

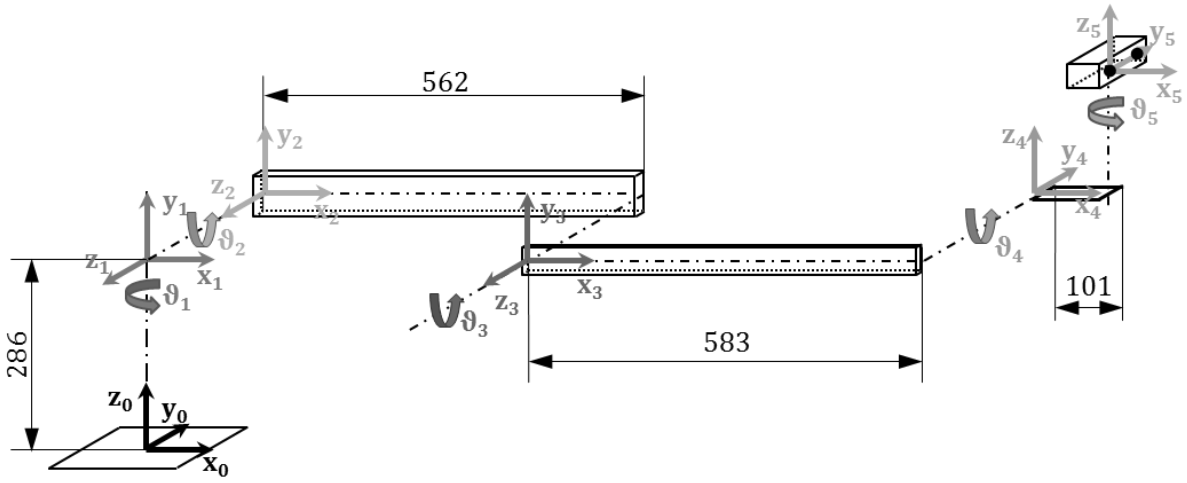

Figure 7-2: Kinematic alignment of the ThirdEye robotic camera arm. Shoulder azimuth (ϑ_1), shoulder elevation (ϑ_2), and elbow elevation (ϑ_3) angles serve to position the camera head within the envelope of interest during final approach and docking. The camera head elevation (ϑ_4) and azimuth (ϑ_5) angles orient the camera FOV.

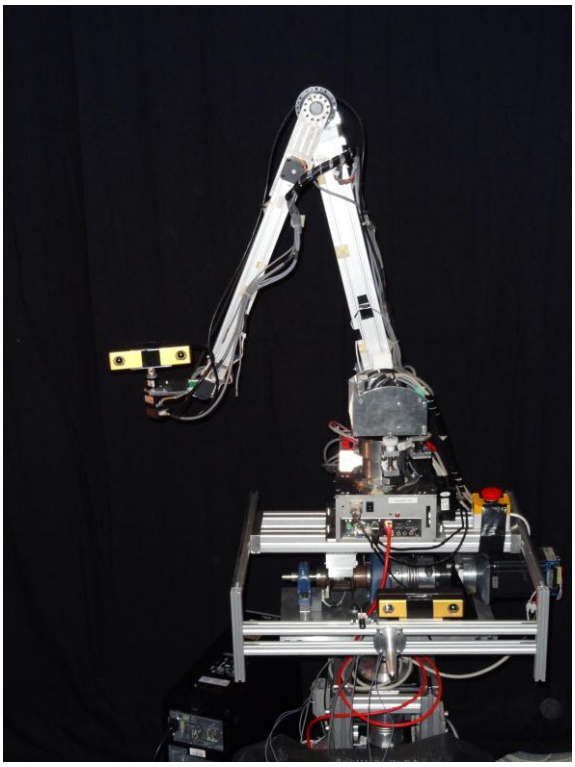

Figure 7-3: The ThirdEye camera arm as integrated into the RACOON simulation environment. The arm is fully retracted. This pose can be used for short-range operations. Note the housing of the shoulder and elbow elevation motors sitting atop the cylinder housing the shoulder azimuth axis. This housing is mounted atop the primary electronics box containing the embedded control computer. The secondary electronics box containing the motor controller cards is occluded by the arm.

Kinematic Layout

The shoulder azimuth and elevation angles (ϑ_1 and ϑ_2), as well as the elbow angle (ϑ_3), serve to position the camera head anywhere within the envelope of interest during final approach and docking (see Figure 7-4). This envelope is defined by the length l_1 = 0.562 m of the upper arm, and l_2 = 0.583 m of the lower arm. The camera head itself is pointed towards any target by the joint angles ϑ_4 and ϑ_5. This design therefore provides the required motion envelope, while its inverse kinematics, i.e. the calculation of the individual joint angles based on the desired final position and orientation of the camera head, can be solved analytically.

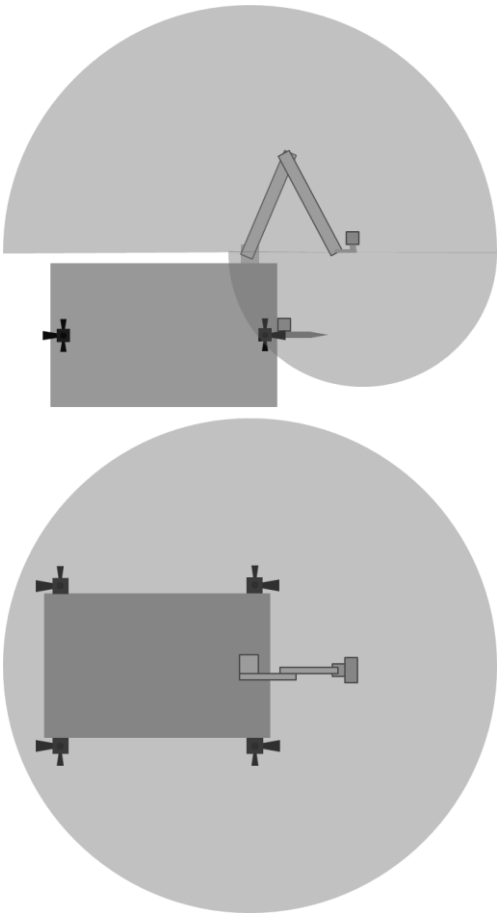

Figure 7-4: ThirdEye positioning envelope for final approach and docking. For clarity, some parts of the complete envelope have been omitted, only showing those sections most interesting for proximity operations. The camera head can be positioned so that the camera can be pointed at the docking interface from above, both sides, and at an angle from below. The exact size and shape of this envelope depends on the relative dimensions of camera arm and spacecraft, as well as on the position of the camera arm's base joint. This figure assumes approximately equal arm and spacecraft lengths.

Drive System

The elbow and the camera head elevation stage are belt driven with the motor mounted near the shoulder, respectively the elbow joints. This serves to reduce the mass of the limbs and thus the required motor torques, which then allows the use of smaller and lighter motors. All motors are **stepper motors**. The arm is therefore stable as long as power is supplied to the motors. Due to the use of stepper motors it was originally intended not to use joint encoders, but as it turned out during the initial testing phase of the arm, step-loss in the motors occurred, making precise control of the arm's posture impossible. Differential **optical encoders** were therefore retrofitted onto the driven shafts of the joints. In addition, the drive shafts of the shoulder azimuth and elevation joints were equipped with anti-backlash gears to increase their precision.

Electronics

The original arm design included custom-designed and custom-built control electronics located in the electronics box at the base of the arm. With the introduction of the encoders, two commercial *Trinamic Motion Control* encoder cards were added in order to be able to reliably read the encoder data in all five axes. After additional problems with the home-built electronics surfaced, it was decided to fully replace them with the Trinamic cards. This also led to a complete reprogramming of the arm's control software in order for it to properly interface with the controller cards. A major problem was to establish a stable and reliable connection between the *Linux* operating system and the controller cards via USB. In total, the development and implementation of the arm took 2.5 years, with multiple students contributing to the project under my supervision.

Computer

The finished arm is equipped with an **embedded control computer** contained within the electronics box underneath the housing for the shoulder azimuth axis. The computer uses a *Fedora Linux* operating system and was specifically designed to interface with the custom-built motor control electronics. The control software *RControl* running on this computer receives joint position commands via TCP/IP. These joint positions are then converted into numbers of motor steps and transmitted to the two motor controller cards mounted in a secondary electronics box attached to the back of the robot arm's base. Actual joint positions are measured by the controller cards via the differential optical encoders on the driven shafts. The encoder counts are converted into joint angles by the *RControl* software and then transmitted via TCP/IP. Since differential and not absolute encoders are used, the zero reference position for axis 5 must be set manually prior to startup. The encoders for axes 1 through 4 are initialized using magnetic switches right after control program start.

The embedded computer was configured to automatically start *RControl* on startup. No further user input is required. The *ThirdEye* camera arm is thus a **self-contained unit**, only requiring 220 V electrical power and an Ethernet connection. It is therefore very flexible and can easily be integrated into any HIL simulation setup such as RACOON.

Design Assessment

In retrospective, and with better understanding of the system and its complexity, it can be stated that the decision to custom-build the arm, including its electronics and software, should not be repeated.

The problems experienced with the electronics and the software set back the research project by over one year. While the mechanical design became sound with the introduction of the encoders and anti-backlash gears for the shoulder azimuth and elevation drives, there now exist simpler and more powerful systems on the market. The use of the Trinamic motor controller cards proved to be a simple and elegant solution. Since they interface to any computer via USB, no dedicated, embedded control computer is necessary. The communication and control function should therefore be

delegated to a more powerful desktop computer. This would in no way impede the camera arm's functionality, nor its integration into a simulation environment.

7.3.2 ThirdEye Control Software Design

The camera arm's hardware control software *RControl* receives its command inputs from the *ThirdEye Control* software running on the operator workstation. *ThirdEye Control* accepts user commands from a variety of input devices and converts these into joint angle commands using forward and inverse kinematics. Details about *ThirdEye Control* design and implementation are provided in [262].

In **forward kinematics**, the user inputs individually control shoulder azimuth and elevation, as well as camera head azimuth and elevation. The elbow angle is changed in concert with the shoulder elevation when the operator commands a stretching motion of the arm.

With **inverse kinematics**, the operator commands the position of the camera head. The individual joint angles needed for the arm to reach this position are computed by the control algorithm. For arms with a higher number of DOFs, including axis redundancies, this often yields a mathematically over-determined set of equations, which cannot be solved analytically. Since DOFs 4 and 5 do not influence the camera head's position in space but only its orientation, this leaves three joint angles for three translations of the camera head. This set of equations can be solved analytically and be computed in real time.

The generated **joint angles** are transmitted to the *RControl* software via TCP/IP. The data packets have a length of 50 bytes and consist of a 6 byte header, the joint angle and velocity commands for all five axes multiplied by 1000 and transmitted as integer values, and an integer timestamp in milliseconds. After executing the motion commands and reading the arm's actual position from the encoder feedback, *RControl* retransmits an identically formatted packet containing the real joint positions and velocities, along with a timestamp. The detailed definition of packet formats is provided in appendix A.

Status Display

This command and feedback data is used by *ThirdEye Control* to provide a **graphical representation** of the camera arm showing both commanded and actual pose, as well as the view cones of the spacecraft-mounted and arm-mounted cameras (see Figure 7-5). This display is drawn to screen using *OpenGL* drawing functions, which makes it easily adaptable for different system platforms and also easily modifiable for additional content or future purposes.

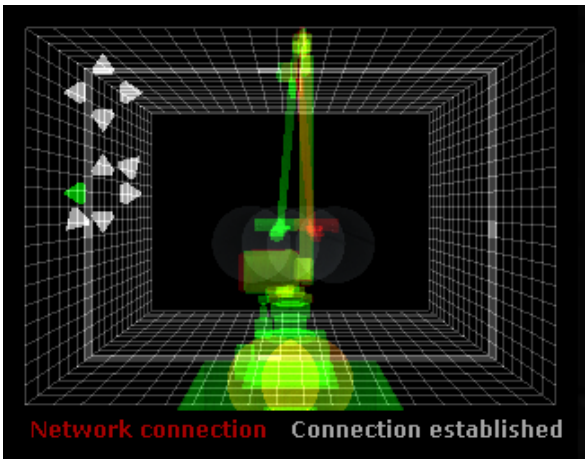

Figure 7-5: Graphical representation of ThirdEye posture provided by ThirdEye Control. The display shows the commanded posture in green, with the actual posture based on encoder feedback in red. The view cones of the primary, spacecraft-mounted camera, and the secondary, arm-mounted camera are indicated by white and orange shading. The view cone of the camera shown in the big primary display is shaded in orange, the camera shown in the small secondary display in white. For inverse kinematics control, the camera head's position in space is provided within a three-dimensional grid. The chevrons drawn into the upper left corner indicate the activity of the input device. The upper four chevrons show commands for the camera head. Green chevrons indicate active rotations, red chevrons signal that the axis limits have been reached. The lower six chevrons show the active motion commands for azimuth and elevation of the shoulder joints, as well as for extension of the arm. The text on the bottom notifies the operator whether the TCP/IP connection to the ThirdEye hardware control software has been established.

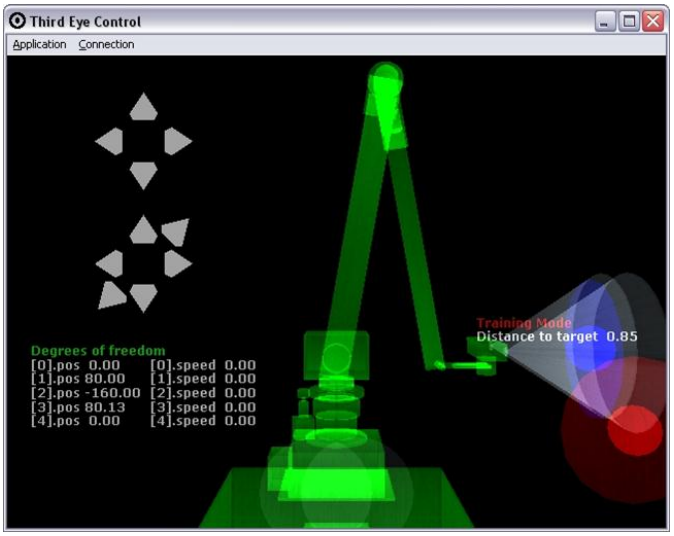

Figure 7-6: ThirdEye Control training mode. A series of three red balls is displayed consecutively. The operator must bring the blue ball within the FOV of the camera into contact with the red balls in order to accomplish the training task. The distance to target is provided in order to facilitate the operator's comprehension of the three dimensional task [262].

Training Mode

In addition to the features shown in Figure 7-5, the *ThirdEye Control* status display also has a training mode in which a series of three balls is consecutively positioned within the motion envelope of the arm (see Figure 7-6). The operator needs to overlay these balls with another ball within the *ThirdEye* camera's view cone in order to successfully accomplish the training task.

This training mode was used in a study aimed at determining which input device provided the best operator performance in positioning the *ThirdEye*.

Control Modes

Four **forward kinematics** control modes were initially implemented for the camera arm:

- Keyboard
- Joystick
- WiiMote and head-tracking
- SpaceNavigator and head-tracking

With keyboard and joystick, individual joint angles and arm extension are commanded by keys, joystick axes or joystick buttons. The *WiiMote* control mode uses the accelerometers of a Nintendo *Wii* remote controller (WiiMote) to command shoulder azimuth and elevation angles, while the movement of the *WiiMote* towards or away from the screen extends or retracts the arm. The *WiiMote's* position is determined by the controller's infrared camera tracking a set of stationary IR LEDs mounted underneath the projection screen in the mission control center. Since experiments conducted for *Ranger* showed that head-tracking can lead to increased operator performance in telerobotic applications [130], it was decided to implement and test a simple **head-tracking system** also based on the *WiiMote*. For this purpose, the operator wears a goggle frame supporting IR LEDs on both sides of the head. The vertical and horizontal motion of these LEDs is tracked by a *WiiMote* positioned underneath the screen. Tilting the head thus results in azimuth and elevation motion of the camera.

This head-tracking system was also combined with a 6 DOF *SpaceNavigator*. The operator uses rotation of the "puck" around the vertical axis for commanding shoulder azimuth, rotation about the lateral axis for shoulder elevation, and translation towards and away from the screen for arm extension.

To support the operator in the camera positioning task, two **viewpoint stabilization** modes were implemented. With active ***tilt stabilization***, the camera head's elevation angle will be automatically controlled to counteract the up and down motion resulting from arm extension/retraction and shoulder elevation motion. The camera head will therefore always retain the elevation angle commanded by the operator. Analogously, the ***pan stabilization*** mode holds the camera head's azimuth angle steady during arm shoulder azimuth motion. These stabilization options thus serve to decouple camera head position and orientation control.

Control Mode Evaluation

The usability of the four input modes and the utility of the camera stabilization modes were evaluated in an experiment series with 13 participants, whose results have been published in [265]. For these tests, the *ThirdEye Control* **training mode** was used. Each participant had to complete the series of three positioning and targeting tasks using each of the input modes and each of the stabilization modes.

The **independent variables** of this experiment series were thus the combinations of input modes and stabilization modes.

The **dependent variables** were task completion time and input mode user intuitiveness rating. The time to complete each experiment run was measured and serves as operator performance indicator. Each participant was furthermore issued a questionnaire in which he could provide criticisms and recommendations for system improvement, as well as rank the intuitiveness of the input modes from 4 (most intuitive) to 1 (least intuitive)[13].

Figure 7-7 shows the task **completion times** for the 16 different combinations of input mode and stabilization mode. The results of the participant ranking are provided in Figure 7-8. The comparison of task completion times between the input modes shows that the *WiiMote* and head tracking mode generates an overall mean 95% higher than for the other input modes. Not shown is that using this input mode, four participants were not able to reach even one of the three targets, while two more participants aborted the test runs after successfully hitting the first target. They perceived the *WiiMote* input mode as uncontrollable. The completion times for keyboard, joystick, and *SpaceNavigator* with head tracking are almost equal. The joystick shows the lowest mean completion times for unstabilized control, 23% lower than keyboard and 44% lower than SpaceNavigator.

The stabilization modes do not cause significant changes in task completion times. For keyboard and joystick, the modes without head tracking, both pan stabilization and pan & tilt stabilization caused an increase in completion times. Using tilt stabilization, completion times were decreased for keyboard but actually increased for joystick. For *WiiMote* with head tracking, all stabilization options increased completion times. The stabilization modes only caused consistent improvement in operator performance for the *SpaceNavigator* with head tracking input mode. The decrease in task completion time compared to unstabilized control was 18% for pan stabilization and about 25% for tilt and pan & tilt stabilization.

Overall it can be stated that tilt stabilization seems to have the most beneficial or least detrimental impact on operator performance. Due to the differences between unstabilized mode and tilt stabilization being not statistically significant, it was decided to use the unstabilized control mode in all further *ThirdEye* experiments.

[13] In the questionnaire issued to the participants during the experiments, the ranking was defined in opposite direction from 1 (most intuitive) to 4 (least intuitive). For reasons of clarity and accessibility, the ranks were converted into the ranking system used in this thesis (see Figure 7-8). This conversion did not change the relative rankings of the control modes.

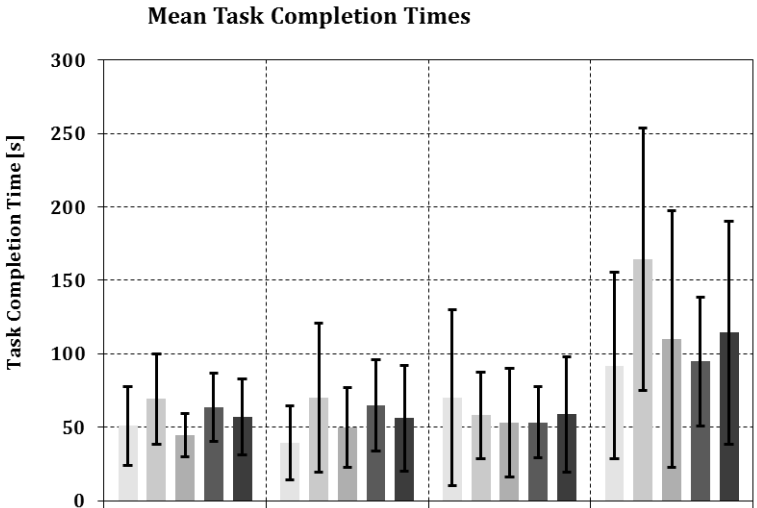

	Keyboard	Joystick	SpaceNavigator and Head Tracking	WiiMote and Head Tracking
Unstabilized	50.86	39.27	70.32	91.75
Pan Stabilized	69.11	70.12	57.96	164.32
Tilt Stabilized	44.37	49.98	53.08	109.83
Pan & Tilt Stabilization	63.62	64.87	53.21	94.78
All Stabilization Modes	56.99	56.06	58.64	114.26

Figure 7-7: Task completion times of the ThirdEye input mode evaluation experiments. The WiiMote control mode generates overall 95% longer task completion times than the other input modes. The completion times for keyboard, joystick, and SpaceNavigator are almost equal, with the joystick showing the lowest mean completion time for unstabilized control, 23% lower than keyboard and 44% lower than SpaceNavigator. The stabilization options do not cause significant changes in task completion times.

Further information for the selection of the most beneficial control mode can be derived from the mean user **intuitiveness ratings** shown in Figure 7-8. The ranking clearly shows the participants' preference of keyboard and joystick over *SpaceNavigator* and *WiiMote* with head tracking. According to statements by the participants, the intuitiveness ranking for keyboard was caused by its familiarity from daily use, as well as from the fact that it allowed the commanding of arm motion in discrete steps. The joystick's main advantage is that it enables an operator to command all degrees of freedom without changing the grip.

The main difficulty using the *SpaceNavigator* was to decouple rotation and translation commands. Most participants tended to tilt the *SpaceNavigator's* puck about the *y* axis when they intended to command translation along the *x* axis, and vice versa. This problem can be addressed by operator training, but adds another factor to a stressful and mentally intensive task.

Precisely controlling the virtual arm by *WiiMote* was considered by all participants as either difficult or impossible. According to participant statements, the use of the input device alone required the full attention of the operator. It is therefore unsuitable for the control of a device designed to support the operator in the challenging maneuvering and docking task.

Both *SpaceNavigator* and *WiiMote* also suffered from the head tracking mode. The main issue stated by participants was that the head tracking did not allow them to move their head without issuing a command. The option of manually switching the head tracking off was only used by a small number of participants.

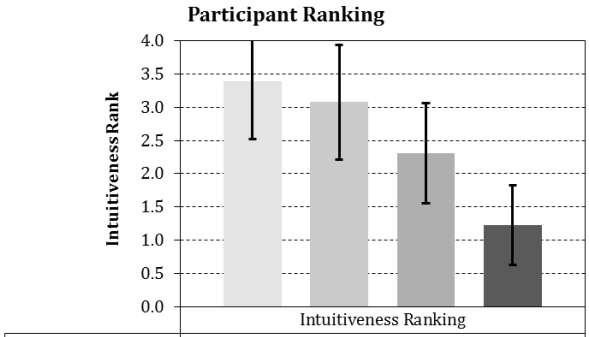

	Intuitiveness Ranking
Keyboard	3.38
Joystick	3.08
SpaceNavigator and Head Tracking	2.31
WiiMote and Head Tracking	1.23

Figure 7-8: User ranking of the intuitiveness of the input modes evaluated for ThirdEye control. Low ranking indicates high intuitiveness. Keyboard has 16% lower ranking than joystick, although the difference is not significant. SpaceNavigator is 40% higher than these two, and WiiMote again 40% higher than SpaceNavigator.

Inverse Kinematics Control

Following participant comments as well as observations made during the experiments, another *SpaceNavigator* control mode was implemented, utilizing the device's six degrees of freedom. In this inverse kinematics control mode, the operator positions the camera head using the three translations of the puck. The orientation of the camera head is controlled independently by the puck's rotation about its vertical and lateral axes. While this control mode is highly intuitive, it still requires considerable operator training in order to be able to control the translations and rotations independently. It was therefore not used in the *ThirdEye* evaluation experiments, in order to reduce the total amount of training.

Input Device Selection

Based on both the task completion times and the intuitiveness ranking it was decided to use the **joystick** as *ThirdEye* input device. It was selected over keyboard due to its superior performance in the unstabilized control mode and due to the fact that the rendezvous & docking task of the *ThirdEye* evaluation experiments required the operator to control the arm one-handed, while with the other hand operating the spacecraft. In the keyboard control mode, the operator needs two hands to control camera head position and orientation simultaneously.

7.3.3 The ThirdEye Automated Target Pointing System

After the *ThirdEye Control* input mode experiments showed the difficulty many operators had with precisely controlling the camera arm, and participant comments indicated the high mental workload associated with this task, it was decided to develop a prototype **automatic target pointing system**. This task was accomplished in a student's research thesis under my supervision [264].

The basic idea is to mount a laser rangefinder atop the camera carried by the *ThirdEye* and to use it to measure the distance between the camera head and the object in the center of its FOV. Since the position and orientation of the camera within the robot arm coordinate frame is known, the knowledge of this distance results in the position of the target object also being known. This position can be expressed in Denavit-Hartenberg (DH) coordinates[14] and then be used to control the arm during platform motion so that the camera remains pointed at the target at all times.

Since the motion of the target is not known in the *ThirdEye* proximity operations scenario, only the **chaser attitude motion** is therefore to be compensated, as well as the **relative translation** as described by the CW equations.

Figure 7-9 provides an overview of the pointing system and its major components.

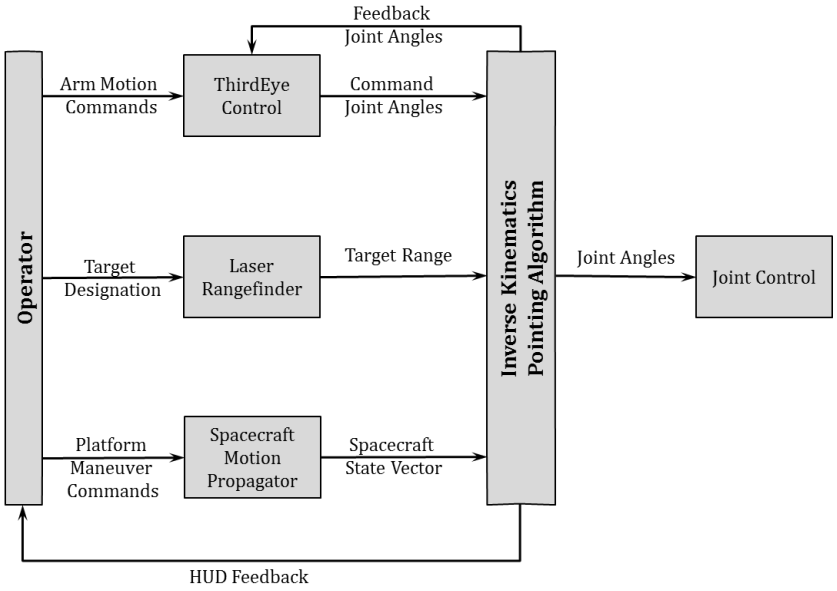

Figure 7-9: Schematic of the automatic pointing algorithm developed for the ThirdEye *robotic camera arm. The commanded joint angles and the target range measured by a laser rangefinder establish the coordinate of the target object in the robot arm's base coordinate frame. The spacecraft motion propagator computes the motion of the base coordinate frame based on operator maneuver commands. The inverse kinematics pointing algorithm then computes the joint angles required to keep the target object within the camera's field of view and sends these angles to the robotic joint controllers, as well as the HUD and* ThirdEye *Control for visualization.*

[14] There exist two different conventions for DH coordinates, regarding the assignment of coordinate frames and the transformation matrix sequence. One according to Spong [266], the other according to Craig [267]. Both are widely used in engineering. The DH notations used in this dissertation are based on Craig's method.

Pointing Algorithm

Denavit-Hartenberg coordinates describe the position and orientation of robotic arm joint *i* in reference to a Cartesian coordinate system P_{i-1} centered on joint *i-1*. Each joint coordinate system in the DH notation is defined as follows: Axis z_{i-1} points along the rotation (or translation) axis of joint *i-1*. Axis x_{i-1} points along the length of limb *i-1* and is therefore orthogonal to both z_{i-1} and z_i. Axis y_i completes the right-handed coordinate system. Figure 7-2 shows the joint coordinate systems for the *ThirdEye* camera arm.

The position and orientation of any joint coordinate system P_i can therefore be derived from P_{i-1} by a series of four coordinate transformations [267]. First, the coordinate system is rotated by α_i about the x_i axis to meet the joint axis z_i. Following this, it is translated by a_i along x_i to define the location of z_i. The coordinate frame is then rotated by ϑ_i about the z_i axis. Finally, the coordinate system is translated by d_i along axis z_i to complete the new joint coordinate system P_i.

The parameters ϑ_i, d_i, a_i, and α_i are called the DH parameters. While a_i and α_i are fixed parameters for any robotic manipulator, ϑ_i is variable for rotatory joints, and d_i for prismatic joints.

The four transformations can be described by the following homogenous transformation matrices [267].

$$\boldsymbol{R}_{x_i,\alpha_i} = \begin{bmatrix} 1 & 0 & 0 & 0 \\ 0 & \cos\alpha_i & -\sin\alpha_i & 0 \\ 0 & \sin\alpha_i & \cos\alpha_i & 0 \\ 0 & 0 & 0 & 1 \end{bmatrix} \qquad \textit{Eq. 7-1}$$

$$\boldsymbol{T}_{x_i,a_i} = \begin{bmatrix} 1 & 0 & 0 & a_i \\ 0 & 1 & 0 & 0 \\ 0 & 0 & 1 & 0 \\ 0 & 0 & 0 & 1 \end{bmatrix} \qquad \textit{Eq. 7-2}$$

$$\boldsymbol{R}_{z_{i-1},\vartheta_i} = \begin{bmatrix} \cos\vartheta_i & -\sin\vartheta_i & 0 & 0 \\ \sin\vartheta_i & \cos\vartheta_i & 0 & 0 \\ 0 & 0 & 1 & 0 \\ 0 & 0 & 0 & 1 \end{bmatrix} \qquad \textit{Eq. 7-3}$$

$$\boldsymbol{T}_{z_{i-1},d_i} = \begin{bmatrix} 1 & 0 & 0 & 0 \\ 0 & 1 & 0 & 0 \\ 0 & 0 & 1 & d_i \\ 0 & 0 & 0 & 1 \end{bmatrix} \qquad \textit{Eq. 7-4}$$

The total coordinate matrix $\boldsymbol{A}_{\boldsymbol{i}}^{\boldsymbol{i-1}}$ for any joint P_i in the coordinate frame P_{i-1} is therefore the result of the concatenation of the four individual transformation matrices.

$$\boldsymbol{A}_{\boldsymbol{i}}^{\boldsymbol{i-1}} = \boldsymbol{R}_{x_i,\alpha_i}\boldsymbol{T}_{x_i,a_i}\boldsymbol{R}_{z_{i-1},\vartheta_i}\boldsymbol{T}_{z_{i-1},d_i} \qquad \textit{Eq. 7-5}$$

The coordinate matrices for each joint are then multiplied in order to describe any joint's position and orientation in relation to the robotic manipulator's base coordinate frame P_0, by the transformation matrix $\boldsymbol{A_i^0}$. The inverse of this matrix can therefore be used to compute the individual joint angles required to achieve a given end-effector position.

For the target pointing application, the end-effector of the kinematic chain is the target position as measured by the laser rangefinder. This results in the DH parameters given in Table 7-1, with the distance a_6 between camera head and target [264].

Table 7-1: Denavit-Hartenberg parameters of the ThirdEye robotic camera arm and the designated target object. The target's position within the robot arm's base coordinate system is defined by the five joint angles and the distance from camera head to target measured by a laser rangefinder.

Joint	ϑ_i	d_i [mm]	a_i [mm]	α_i
0	0	286	0	0
1	ϑ_1	0	0	π/2
2	ϑ_2	0	562	0
3	ϑ_3	0	583	0
4	ϑ_4	0	101	-π/2
5	ϑ_5	0	0	0
6	0	0	a_6	0

The equations resulting from the multiplication of the six transformation matrices are underdetermined and cannot be solved analytically. This problem can be solved by using the decoupled motion between camera head pan/tilt and the position of the camera head. Within the motion envelope of the camera head, it can be used to point the camera at the target. In order for the camera to point directly at the target, the z component $z_{t,4}$ of the target position in the coordinate system P_4, and the y component $y_{t,5}$ in the coordinate system P_5 must be zero. These boundary conditions lead to the equations for the joint angles ϑ_4 and ϑ_5 (for details refer to [264]).

$$\vartheta_4 = \arctan\left(\frac{y_{t,4} - d_5\frac{\sqrt{x_{t,4}^2 + y_{t,4}^2}}{x_{t,4}}}{x_{t,4}}\right) \qquad \textit{Eq. 7-6}$$

$$\vartheta_5 = \arctan\frac{y_{t,5}}{x_{t,5}} \qquad \textit{Eq. 7-7}$$

Once the boundaries $\vartheta_{4,min/max}$ and $\vartheta_{5,min/max}$ of this envelope are reached, the position of joint 4 and thus the camera head is changed. For this purpose, the inverse kinematics of joint 4 are solved iteratively, until the target is back within the motion envelope of the camera head.

In order to prevent the occurrence of singularities in the required joint angles, keep-out zones are defined for the position of joint 4. If the algorithm generates a trajectory moving through one of these zones, the trajectory is instead directed along its borders. This prevents infinite angular velocities for ϑ_1, ϑ_2 and ϑ_3, which are calculated by the following [264].

$$\vartheta_1 = \arctan\left(\frac{y_{4,0}}{x_{4,0}}\right) \qquad \textit{Eq. 7-8}$$

$$\vartheta_2 = \pm\arccos\left(\frac{x_{4,2}^2 + y_{4,2}^2 + a_2^2 - a_3^2}{2a_2\sqrt{x_{4,2}^2 + y_{4,2}^2}}\right) + arctan\frac{y_{4,2}}{x_{4,2}} \qquad \textit{Eq. 7-9}$$

$$\vartheta_3 = \mp\arccos\left(\frac{x_{4,2}^2 + y_{4,2}^2 - a_2^2 - a_3^2}{2a_2a_3}\right) \qquad \textit{Eq. 7-10}$$

Relative Motion Propagation

This system is not designed to be tracking the target object, but to generate pointing angles after initial target designation. For this purpose, the chaser satellite attitude motion and trajectory relative to the initial target position are fed into a homogeneous coordinate transformation matrix which continuously changes the robot arm's base coordinate system P_0. The arm pointing algorithm therefore propagates the spacecraft relative motion under the assumption that the target craft is not conducting active orbital maneuvers. This assumption is valid in an OOS context.

The pointing algorithm cannot however track target object features if the target is in a rotation or tumbling motion. In this case, the camera will be pointed at a changing point on the target object body, not the point it was initially aimed on. The disturbance torques generated by the motion of the arm are also not included in this propagation algorithm, since it was designed to be used only in a laboratory environment.

ThirdEye Integration

The chaser spacecraft motion propagator and the target pointing algorithm were both implemented as an extension to the *RControl* software running on the *ThirdEye's* embedded computer. *ThirdEye Control* was furthermore modified to provide an input mechanism for target designation via keyboard, joystick, or space mouse, as well as to incorporate the trigger command into its TCP/IP data packets.

Due to mechanical interface issues between the laser rangefinder and the completed *ThirdEye* camera arm assembly, the target pointing system was not part of the *ThirdEye* evaluation experiments. Its algorithms were however tested in a computer simulation created with the 3D rendering software *Blender*. This test showed the functionality of the pointing system in keeping the simulat-

ed camera pointed at the designated target object under any chaser spacecraft attitude and orbit maneuvers. The system can therefore be included in any future version of the *ThirdEye* system.

7.3.4 The ThirdEye Proximity Operations GUI

The design goal of the *ThirdEye* system is to increase the situation awareness of the operator during proximity operations in order to increase teleoperation performance. To meet this goal, the information from the sources *Proximity Operations HUD*, primary and secondary camera, and *ThirdEye* status display must all be integrated into an accessible operator interface. This integrated display is called the *ThirdEye Proximity Operations GUI*.

The general **layout** of the *ThirdEye Proximity Operations GUI* is described in detail in Figure 7-10. The dominating information in the display is the main video view and its attitude HUD overlay. The **main video** by default shows the view of the chaser spacecraft primary camera. The **secondary view**, by default the *ThirdEye* camera, is shown as picture-in-picture in the lower right corner of the display (the position was later changed to the lower left corner as discussed in Section 7.4.3).

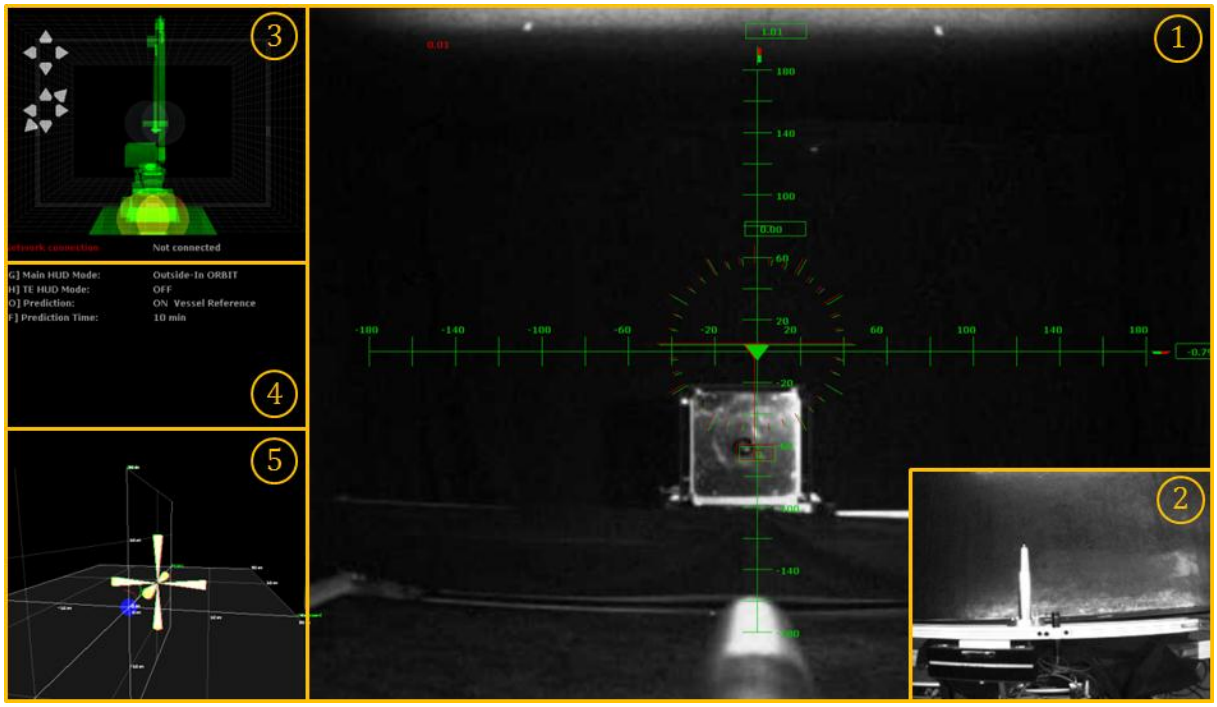

Figure 7-10: Layout of the ThirdEye Proximity Operations GUI. The display functional sections are highlighted. Section 1 contains the main video stream, in this case the chaser primary camera view, and its attitude HUD overlay. Section 2 shows the secondary camera, in this case the ThirdEye view. Section 3 provides the ThirdEye status display and posture prediction. Section 4 contains information about the state and activity of the individual display elements main view attitude HUD, secondary view attitude HUD, prediction display mode, and prediction display propagation time.

By pressing 'C' on the keyboard, the operator can switch the *ThirdEye* view to the main camera display. Key 'V' switches the display into **single-camera mode** and thus eliminates the *ThirdEye*

camera view and the *ThirdEye* **status display** in the upper left corner. The keys 'G' and 'H' serve to toggle the primary and secondary view attitude HUDs.

The **trajectory prediction** display in the lower left corner can be toggled by key *"O"*. The **propagation time** for the predicted trajectory can be set by pressing key 'F'. Five propagation time settings are available: 1 minute, 10 minutes, 30 minutes, 60 minutes, and one orbit revolution. The default setting is 10 minutes.

After the first pilot *ThirdEye* evaluation study (refer to Section 7.4.3), two **hotkeys** for *ThirdEye* camera arm postures were introduced. Key press '1' activates the close-range pose, with the camera aimed at a point approx. 2 m in front of the chaser satellite; key '3' sets the *ThirdEye* into neutral position, with the camera aimed straight ahead.

The status of the individual elements is displayed centered on the left side, right above the trajectory prediction display.

Table 7-2 provides an overview of the control keys available to the operator in the *ThirdEye Proximity Operations GUI*.

Table 7-2: Control keys for the ThirdEye Proximity Operations GUI. These keys allow the operator to adapt the GUI to different situations and mission phases. The default settings are underlined.

Key	Action	Settings
1	Set *ThirdEye* in Close-Range pose	[active, inactive]
3	Set *ThirdEye* in neutral pose	[active, inactive]
C	Switch main and secondary camera views	[primary camera in main view, *ThirdEye* in main view]
F	Set Trajectory Prediction propagation time	[1 min, 10 min, 30 min, 60 min, 1 orbit]
G	Toggle main view HUD	[active, inactive]
H	Toggle secondary view HUD	[active, inactive]
O	Toggle Trajectory Prediction display	[active, inactive]
T	Designate target	[active, inactive]
V	Toggle single-camera mode	[active, inactive]

7.4 Evaluation Test Campaign Planning

The hypothesis behind the investigation of the *ThirdEye* system is that the combination of an attitude HUD for knowledge of ownship attitude, a trajectory prediction for knowledge of future motion relative to a target, and of a flexible, secondary vantage point providing information about the relative position and orientation of target and chaser spacecraft serve to increase operator task performance during final approach and docking to an uncooperative target.

In order to test this hypothesis in mission simulations, a number of task metrics are required.

7.4.1 Metrics

The task of controlling the final approach and docking is a task of correctly perceiving the remote environment and navigating from the initial point to a target point in both space and time. These are two task-specific metrics that are frequently used in evaluation experiments of telerobotic systems [123].

Literature shows [136], that operator performance in the task metric navigation can be rated in the following criteria: effectiveness, efficiency, and effort.

Effectiveness

Effectiveness is the measure of how well the task is completed. This can be measured by the percentage of navigation tasks successfully completed [136]. Applied to *ThirdEye* evaluation, this can be translated into the percentage of **successfully completed** docking approaches. This serves as the primary criteria for *ThirdEye* performance.

Efficiency

Efficiency is defined by the time or resources required to complete the task. The time to complete the task is generally considered to be a good measure of task efficiency [136]. In space teleoperation, however, there exists a strict tradeoff between the time required to complete a task, and the resources, i.e. propellant and electrical power, expended to complete the task. The primary task efficiency evaluation criteria for the impact of the *ThirdEye* system are therefore the **accumulated velocity change** Δv and the **accumulated rotation rate change** $\Delta\omega$ during a docking approach. These measures are derived from the logged telemetry data by multiplying the commanded angular and linear acceleration for each simulation time step with the time elapsed during the time step and summing these numbers up over the course of each experiment run.

$$\Delta v_i = \Delta v_{i-1} + \sqrt{a_{x,i}^2 + a_{y,i}^2}(t_i - t_{i-1}) \qquad \textit{Eq. 7-11}$$

$$\Delta \omega_i = \Delta \omega_{i-1} + \sqrt{\alpha_{y,i}^2 + \alpha_{z,i}^2}(t_i - t_{i-1}) \qquad \textit{Eq. 7-12}$$

The **task completion time** T therefore serves as a secondary efficiency measure.

Operator Task Load

The third traditional metric for the navigation task is ***effort***, i.e. the workload of the operator during the task [136]. A measure of operator workload frequently used in spaceflight-related investigations is the NASA ***Task Load Index*** (NASA TLX) [136]. NASA TLX is designed to measure the workload as the cost incurred by the human operator in order to accomplish the mission requirements and is mainly used for interface design and evaluation [268]. The test subject is issued a questionnaire in which he is to provide weighted ratings in six categories. These subscales serve to evaluate

the individual workload associated with mental, physical and temporal demands of the task, the levels of effort and frustration encountered by the subject during the task, as well as the level of satisfaction with the performance during the task [269]. The weighting of these categories is accomplished by having the subject decide, which member of each paired combination of the six categories is more relevant to the personal definition of workload. The rating within the category is then done using a seven degree Likert scale. The rating of each category is multiplied by the weight of the category, and the results are summed up to derive the overall **TLX score**.

Docking Safety

Besides effectiveness, efficiency, and workload, three more metrics are of interest for *ThirdEye* evaluation. The first is task *safety*. For the purpose of *ThirdEye* evaluation, this is represented by the **relative axial and radial velocities** at time of docking contact, $v_{C,ax}$ and $v_{C,rad}$. The higher the axial docking velocity, the higher the shock force at contact, which could lead to substantial damage on both chaser and target spacecraft. A high radial or lateral contact velocity could lead to the destruction of the docking interface, both in the cases of dedicated and natural interfaces.

Approach Precision

The second additional metric is *approach precision*. The measure for precision is the **relative angle** between chaser and target at the time of docking contact. This angle δ_D is calculated from the docking pitch and yaw angles ϑ_D and ψ_D.

$$\delta_D = \sqrt{\vartheta_D^2 + \psi_D^2} \qquad \textit{Eq. 7-13}$$

Operator Situation Awareness

Another metric of importance for *ThirdEye* evaluation is *operator SA*. The *ThirdEye* system is designed to increase SA during final approach and docking. Its impact on operator SA is therefore a primary metric for the evaluation of its performance.

Operator SA cannot be derived from objective measurements, although it has been suggested to measure it implicitly, by assuming that better task results are generally caused by better SA [138]. Generally, however, operator SA is derived from subjective measures in which the test subjects self-assess their levels of SA [138]. It has been suggested to use TLX to test SA as a covariate to operator task load [268]. This approach is supported by the finding of a number of studies that SA is not an independent phenomenon, but a consequence of operator workload [268].

There however exist dedicated evaluation techniques for SA. An overview of these techniques is provided in [270] and [271]. Frequently used in the domains of telerobotics and aviation are the ***Situation Awareness Global Assessment Technique*** (SAGAT) and the ***Situation Awareness Rating Technique*** (SART). Both measures provide an index of how well operators are able to acquire and integrate information in a complex environment [272].

In **SAGAT**, the simulation is interrupted periodically and all operator displays are blanked [82]. The operator is then asked a series of questions to assess his knowledge about what was happening in his environment at the time of the simulation freeze [272]. Such questions in a teleoperated vehicle context can be about the current attitude angles, the current heading and speed, distances to way-points, and which accelerations currently act upon the vehicle [99]. The correctness of the operator replies can serve as an objective measure to operator SA.

SART has the operator answer a standardized questionnaire *after* a simulation run. The questionnaire consists of ten questions in the three categories supply of operator resources, the demand on these resources, as well as the understanding of the situation [271, 273]. The subjects answer these questions by means of seven-level Likert scales. The SART score is derived from the mean scores for each of the rating categories and is a direct measure of operator SA.

Endsley [272] discusses the different performance of SAGAT and SART in measuring operator SA. While SAGAT shows the better performance, it also has the higher impact on experiment design, as well as on the requirements of the test setup [270]. The requirement for periodic freezing of the HIL simulation can cause high accelerations and motor slip in the simulation environment. This could degrade the position and velocity measurements which serve as primary evaluation metrics for the *ThirdEye* system.

It was therefore decided to **use SART** for SA evaluation and to accept the degraded performance in tracing operator SA. SART has the additional benefit of using the standardized questionnaires, which precludes the need to create a custom set of questions. The amount of training needed for the test subjects to understand the SART questionnaire is also minimal. It is nonetheless recommended that future studies aimed at investigating the development of operator SA during approach and docking tasks use SAGAT and that the test setup is modified accordingly.

Metrics Hierarchy

The five metrics have different importance to rendezvous & docking system design. This is reflected in their evaluation hierarchy for the *ThirdEye* experiments:

1. Approach success
2. Operator situation awareness and task load
3. Docking safety
4. Docking precision
5. Docking efficiency

This order is used in all pilot experiments as well as in the actual evaluation experiments.

7.4.2 Experiment Design

The *ThirdEye* evaluation experiments have the human operator teleoperate final approach and docking maneuvers in the RACOON simulation environment from the ground control center via local network connections, with a simulated signal roundtrip delay of approx. 0.7 s.

The **control loop** for all *ThirdEye* evaluation experiments is shown in Figure 7-11. The experiment scenario was set by the experiment supervisor on his workstation next to the operator workstation. The operator issued maneuver commands by means of two joysticks. The right-hand joystick served for spacecraft control, the left-hand joystick for control of the *ThirdEye* camera arm. The spacecraft maneuver commands were transmitted to the simulated space segment using the RTI DDS. The *ThirdEye* was commanded directly via TCP/IP, as described in Section 7.3.2. The proximity operations simulator moved the target spacecraft model as commanded and returned position, velocity and attitude telemetry data via DDS to both the test supervisor station and the *ThirdEye* display. The *ThirdEye Proximity Operations GUI* display software used it to draw the HUDs and the video images.

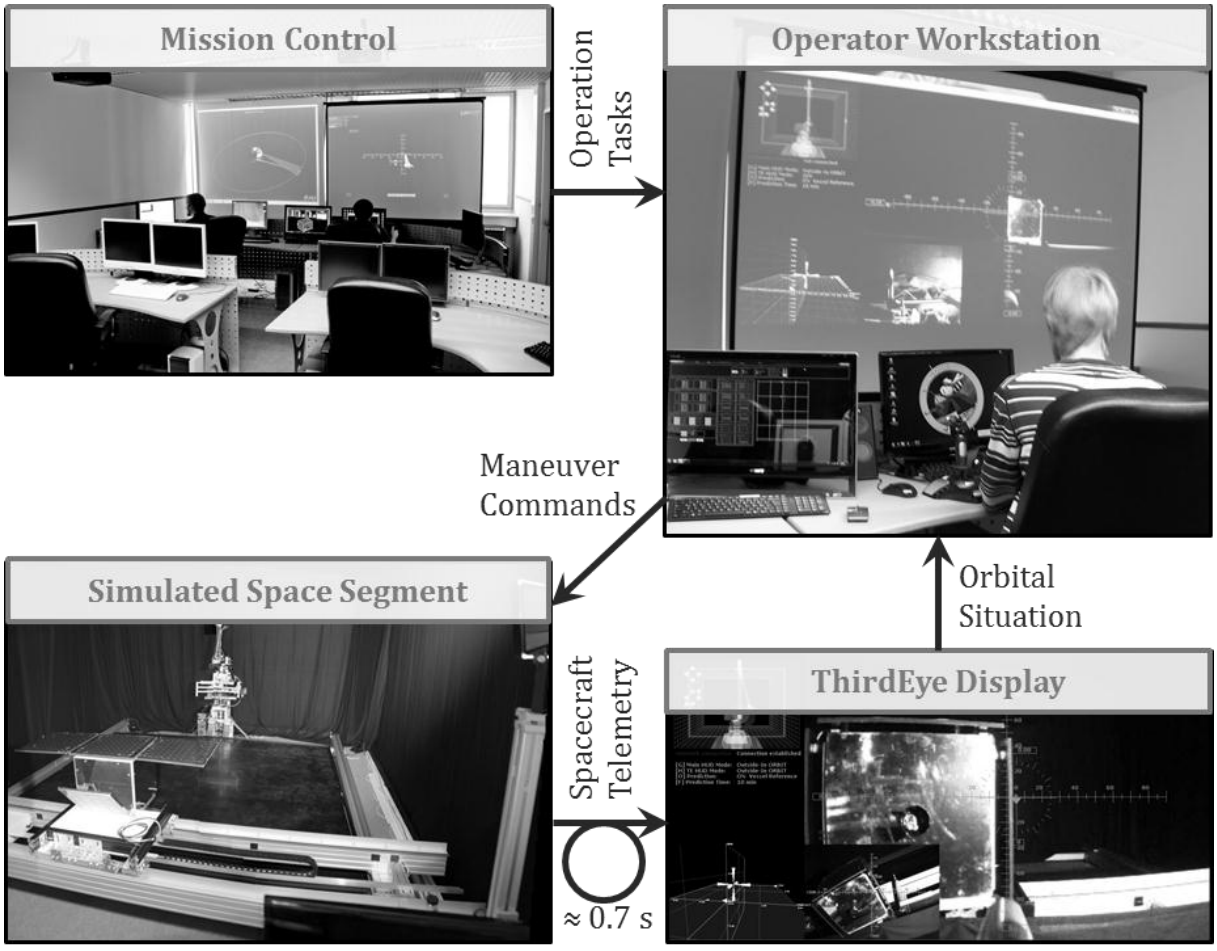

Figure 7-11: The realtime teleoperation control loop used in the ThirdEye evaluation experiments. The experiment supervisor sets the mission scenario and thus the operation tasks from his workstation in the mission control room. The operator situated at his workstation receives information about the orbital situation by means of the integrated ThirdEye display. He then issues maneuver commands which are realized by the simulated space segment. The telemetry, which is artificially delayed by about 0.7 s to represent the communication chain via a single DRS, is used by the ThirdEye display to create an intuitive representation of the orbital situation.

The simulation control software running on the supervisor station logs the telemetry data to a text file. From this it can easily be extracted for analysis purposes.

This control loop results in the **computer and network setup** shown in Figure 7-12.

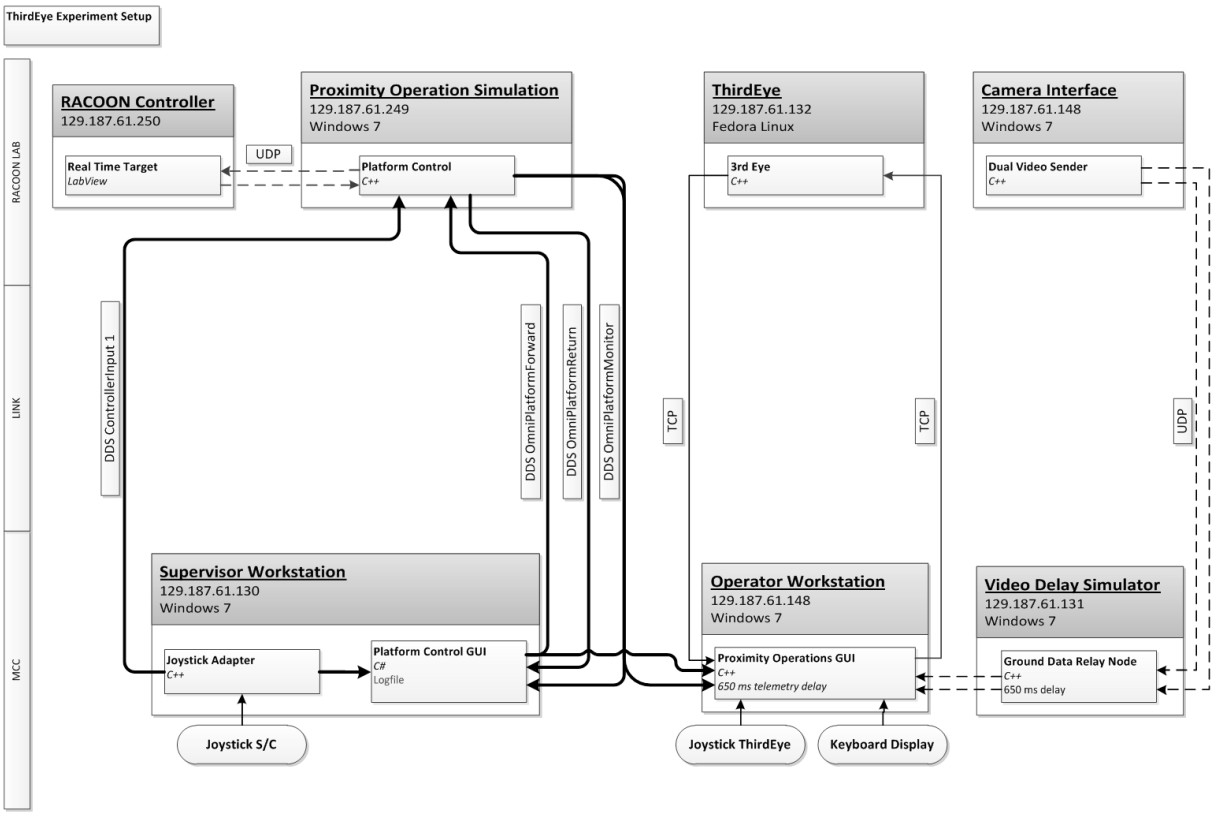

Figure 7-12: ThirdEye experiments computer setup. Three computers were located in the MCC: the supervisor workstation running the simulation control software, the operator workstation running the ThirdEye Proximity Operations GUI, and the video delay simulator introducing 650 ms signal delay to the video stream. Four computers were needed in the RACOON testbed. The RACOON controller ran the LabView realtime control program for the simulator hardware, the proximity operations simulator ran the simulation software for spacecraft relative motion, the ThirdEye computer controlled the ThirdEye camera arm, and the camera interface compressed and transmitted the video streams from the two cameras. The video streams are transmitted by UDP, ThirdEye control data by TCP, and all spacecraft commands and telemetry are sent using DDS.

Test Scenarios

The test series shall reproduce typical situations encountered during final approach and docking to small, uncooperative target objects. Since no literature exists for these situations, as the only uncooperative objects approached and captured up to date are satellites that were grappled by astronauts or the *Space Shuttle* RMS, a set of **test scenarios** had to be defined. These scenarios are influenced by those developed for a study of pilot aids for the *Crew Exploration Vehicle* (CEV) *Orion* [5]. In that study, the pilots assumed manual control at a distance of 3 m from the target, at a linear approach velocity of 3 cm/s. This generated a nominal experiment run time of 100 s. In order to test pilot perception, a radial offset error in initial position was introduced.

The test scenarios for the *ThirdEye* evaluation experiments are similar. A **nominal approach time** of 100 s was considered reasonable in order to give the operators time to understand target position and motion and to maneuver the camera arm into the right position. Since the mean **approach rate** was estimated to be around 10 cm/s, this resulted in an initial **target distance** of 10 m.

The test plan for the first **pilot tests** had each participant complete a series of **three approaches** with varying difficulty, each with use of the *ThirdEye* camera arm and without.

Difficulty setting 1 had the target right **in front** of the chaser satellite, with 0° yaw angle in the orbital coordinate system.

In **difficulty setting 2**, the target had a **lateral displacement** of 0.3 m, and a yaw angle of -10°.

For **level 3**, the target was also misaligned laterally by 0.3 m, with initial yaw angle of 0°, and was **rotating** at 4°/s about its *z* axis. This high rotation represents the baseline for *DEOS* mission planning.

Participant **training** was achieved by two additional approach scenarios with the targets having both lateral and angular misalignment. Table 7-3 provides an overview of the experiment scenarios for the first pilot experiment series.

Table 7-3: Experiment scenarios for the first pilot series of ThirdEye evaluation experiments.

Scenario	ThirdEye active	Start position x [m]	Start position y [m]	Target yaw angle [°]	Target yaw rate [°/s]	Signal roundtrip delay [s]
11 Training 1	✓	-10	0.25	-15	0	~ 0.7
12 Training 2	✓	-10	-0.5	5	0	
13 Training 3	✗	-10	0.25	-15	0	
14 Training 4	✗	-10	-0.5	5	0	
21 Difficulty 1	✗	-10	0	0	0	
22 Difficulty 2	✗	-10	0.3	-10	0	
23 Difficulty 3	✗	-10	-0.3	0	4	
31 Difficulty 1	✓	-10	0	0	0	
32 Difficulty 2	✓	-10	0.3	-10	0	
33 Difficulty 3	✓	-10	-0.3	0	4	

Test Matrix

The difficulty levels and *ThirdEye* activity status are thus the **independent variables** of the experiments, while the metrics described in Section 7.4.1 define the **dependent variables**. This results in the test matrix shown in Table 7-4.

Table 7-4: ThirdEye experiments test matrix and expected qualitative experiment results. The operator performance in test case difficulty 1, ThirdEye inactive *serves as the baseline and therefore receives a medium operator performance rating in all dependent variables. All other performance ratings are given in relation to that baseline.*

		Independent variables					
	Expected Qualitative Results	Difficulty 1		Difficulty 2		Difficulty 3	
		ThirdEye inactive	ThirdEye active	ThirdEye inactive	ThirdEye active	ThirdEye inactive	ThirdEye active
Dependent variables	Approach success	o	+	−	+	− −	o
	Situation awareness (SART)	o	+	−	o	−	o
	Task load (TLX)	o	+ +	−	o	− −	o
	Axial contact velocity	o	+	−	o	− −	o
	Radial contact velocity	o	+	−	o	− −	o
	Docking angle	o	+ +	−	+	− −	o
	Velocity change	o	+	−	o	−	o
	Rate change	o	+	−	o	−	o
	Task completion time	o	+	−	+	−	o

Pilot Experiment Test Method

In the pilot experiments, each participant first viewed a **slide show** explaining the system characteristics and user interfaces. He then proceeded to complete the four **training scenarios** defined in Table 7-3. After that, he would proceed through the **test scenarios**. Half of the participants flew the active *ThirdEye* scenarios 31 through 33 first, the other half scenarios 21 through 23. The sequence of the scenarios was random. This alternation and randomization is supposed to statistically cope with the training effect during the experiment, which is always a factor in tasks that demand coordination and timing. The TLX and SART questionnaires were used after each complete set of three experiment runs with active and inactive *ThirdEye*.

Success Criteria

A docking approach was considered **successful** if the docking probe hit the target plate and the docking switch engaged. In case the docking probe hit the rim or the interior or exterior sides of the nozzle, or the target spacecraft body, the approach was considered a **failure**. The telemetry data for failed approaches was not used in the data analysis.

7.4.3 First Pilot Study

The **pilot experiment series** was aimed at identifying the final *ThirdEye* system configuration, test and training scenarios, and participant number for the *ThirdEye* evaluation experiments. In the statistical analyses of the pilot experiments, I was advised by Zarrin Chua, a doctoral student at the Cognitive Engineering Center of the Georgia Institute of Technology.

Pilot series I had six participants completing the series of scenarios provided in Table 7-3. This number was considered sufficient to determine the suitability of the test scenarios and to determine the expected effect sizes and hence the number of participants for the evaluation experiment. All participants were aerospace engineering students or research associates. Mean age was 28.3 years, with a standard deviation of 1.5 years.

Figure 7-13 shows the **docking success rates** for the different difficulty levels, both for *ThirdEye* inactive and active. In both difficulty levels 1 and 2, the success rate was 100%, whether *ThirdEye* was used or not. For difficulty 3, use of the *ThirdEye* resulted in 50% (3 of 6 approaches) success, compared to 33% (2 of 6) without the *ThirdEye*.

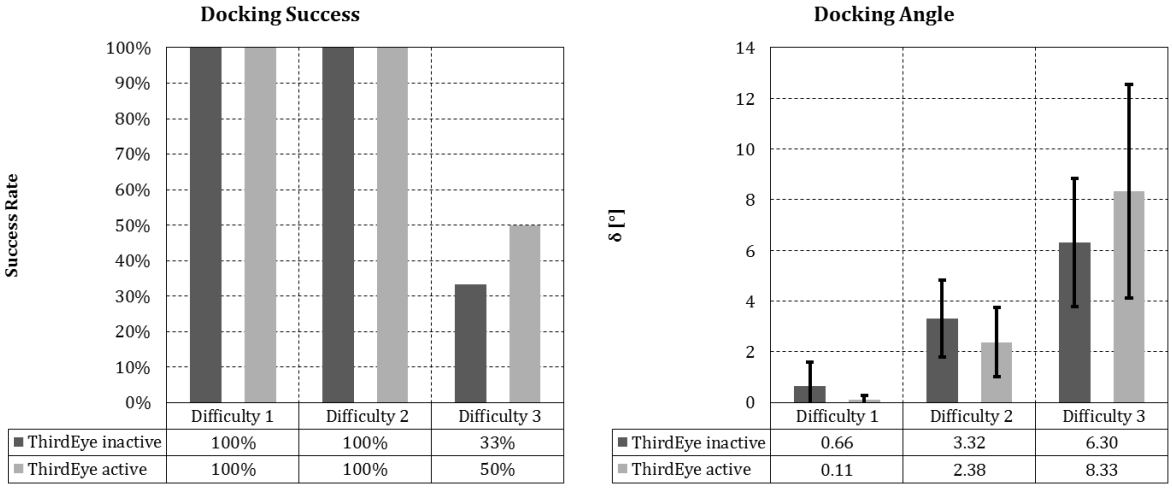

Figure 7-13: ThirdEye pilot evaluation series I docking success and docking angles. In docking success, there is no difference between difficulty levels 1 and 2. With the rotating target of level 3, the success rate was higher with the ThirdEye than without. The mean docking angles grow with difficulty level. Docking precision with ThirdEye is better at difficulty levels 1 and 2, and worse at level 3. These differences are however not statistically significant.

The **docking precision** of the *successful approaches*, measured by the combined docking angle δ_D, is also provided in Figure 7-13. It can be seen that between the perfectly aligned target in difficulty level 1 and the misaligned target in level 2, the docking angle increases significantly. The docking precision thus decreases with target angular misalignment.

The effect of *ThirdEye* usage also becomes evident. At difficulty level 1, docking precision is improved by over 80% with active *ThirdEye*. At difficulty level 2, the use of *ThirdEye* leads to 28% lower docking angle, although a t-test showed this difference is not statistically significant.

The rotating target of difficulty 3 leads to a further increase in docking angle, with the *ThirdEye* active case now showing worse performance than without the *ThirdEye*. Since for that difficulty only two approaches were successful with inactive *ThirdEye*, and three with active *ThirdEye*, the number of available data points for docking precision was small and the corresponding variances within the groups high. The comparison result for docking precision is thus not significant and also has high uncertainty.

A similar result is derived for **maneuver efficiency**, for which only the plot for translation velocity change *Δv* for successful approaches is shown in Figure 7-14. There is only a small difference between difficulty levels 1 and 2. This is understandable, since the main difference between these difficulty levels is a 0.3 m lateral offset of the target, which does not result in a big difference in approach *Δv*. In both cases, use of *ThirdEye* does not result in any significant reduction of maneuver demand. Difficulty level 3 shows higher approach *Δv*, which results from the need for aborted approaches and **collision avoidance maneuvers** due to the rotating target. *ThirdEye* use seemingly results in higher maneuver demand. This result might be due to the small number of available data points and must be confirmed in the evaluation experiment series.

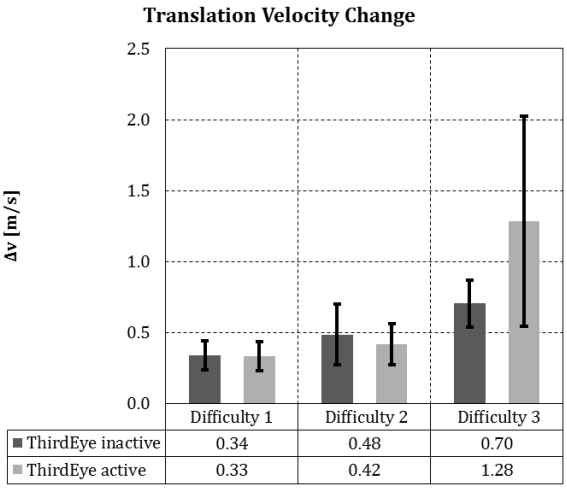

Figure 7-14: ThirdEye pilot evaluation series I velocity change. There is no significant difference between the results for difficulty levels 1 and 2. The performance with and without ThirdEye at these levels is almost identical. At difficulty 3, ThirdEye use causes higher velocity change and thus higher propellant consumption. The difference is however not significant, since with only three dockings with ThirdEye and two without, the available sample size is very small.

Figure 7-15 concludes the measurement results of the first pilot evaluation series with the **TLX scores**. It can be seen that the TLX score for active *ThirdEye* is almost 25% higher than for inactive *ThirdEye*. This reflects the increase in operator workload by having to control the robotic arm and having two video images to regard, instead of one.

No **SART score** is included in this evaluation of the first pilot experiment, because the SART data was corrupted due to errors in the score calculation formula of the computerized questionnaire. This error was not noticed until the data analysis and the correct scores could not be reconstructed.

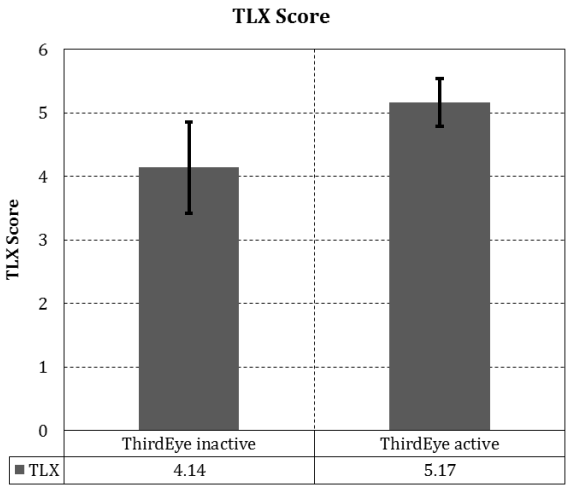

Figure 7-15: ThirdEye pilot evaluation series I TLX scores. The task load perceived by the operators with the ThirdEye is higher than without the ThirdEye. This reflects the added demand of controlling the robot arm.

Pilot Series I Conclusions

The first pilot experiment series thus showed primarily that the difference in **difficulty** between scenario levels 1 and 2 is not significant, therefore not resulting in significant differences in the experiment results. The test scenarios must therefore be changed in order to get meaningful results.

***ThirdEye* use** is furthermore shown to have effects on docking success, precision, efficiency, and task load. The differences and trends in operator performance between active and inactive *ThirdEye* are however not certain. This is attributed to the fact that especially at difficulty level 3, the number of successful approaches was too small to allow meaningful statistical analysis.

It was therefore decided to run a **second set** of pilot experiments. This set was to test **new experimental scenarios** as well as to serve to determine a **minimum number** of test subjects for the evaluation experiment campaign.

Scenario Changes

Two new scenarios were designed to have difficulty levels between the former difficulty 2 (lateral and angular misalignment, no rotation) and difficulty 3 (lateral misalignment, 4°/s rotation). The new scenarios have the target rotate by 0.5°/s and 2°/s and thus create difficulty levels which were expected to result in strong differences in operator performance between active and inactive *ThirdEye*. The targets in the new scenarios furthermore have an initial yaw angle.

In combination with the rotation rates, this created **fixed windows of opportunity** during which the target motor nozzle was in the right position to be docked to during the first rotation. At difficulty levels 2 through 4, the nozzle would be in the perfect position to dock 60 s after beginning of a

test run. Another factor contributing to difficulty level 3 was that the nozzle would appear out of the target body's **shadow** shortly before coming into docking position. This therefore required the operators to deduct the nozzle motion from the body motion and thus required spatial comprehension and modeling.

The first pilot experiment series furthermore showed that the original test scenarios had the participants spend too much time at relatively long distances from the target, where the use of the *ThirdEye* is of no relevance. Beyond a target distance of about 2 m, the target will not be within the *ThirdEye's* FOV unless the arm is fully extended. It was therefore decided to start the docking approaches at a distance of 2 m in order to focus the experiments on the flight segment in which *ThirdEye* use is of potential benefit. Table 7-5 provides an overview of the resulting set of scenarios.

This measure had the side effect of shortening the time required to complete the individual flights. This made spare time available for one more training flight, as well as one more evaluation flight per *ThirdEye* activity level.

Table 7-5: Experimental scenarios for second pilot series and evaluation experiment campaign of the ThirdEye system.

Scenario	Third Eye active	Start position x [m]	Start position y [m]	Target yaw angle [°]	Target yaw rate [°/s]	Signal roundtrip delay [s]
11 Training 1	✗	-10	-0.5	-15	0	~ 0.7
12 Training 2	✗	-5	-0.25	180	1	
13 Training 3	✗	-2	0.3	-60	1	
21 Training 4	✓	-10	-0.5	-15	0	
22 Training 5	✓	-5	-0.25	180	1	
23 Training 6	✓	-2	0.3	-60	1	
31 Difficulty 1	✗	-2	-0.3	20	0	
32 Difficulty 2	✗	-2	0.3	-30	0.5	
33 Difficulty 3	✗	-2	-0.3	120	-2	
34 Difficulty 4	✗	-2	0.3	-240	4	
41 Difficulty 1	✓	-2	-0.3	20	0	
42 Difficulty 2	✓	-2	0.3	-30	0.5	
43 Difficulty 3	✓	-2	-0.3	120	-2	
44 Difficulty 4	✓	-2	0.3	-240	4	

Test Procedure Changes

Operator training was furthermore reorganized. In the first pilot series, *all* training flights were conducted prior to *all* evaluation flights. For the second pilot series, the training flights with active *ThirdEye* were completed prior to the evaluation flights with active *ThirdEye*. Then the flights with inactive *ThirdEye* would follow. Between participants, the sequence *ThirdEye* active/inactive was alternated, while the sequence of scenarios was randomized. This measure was again intended to reduce the impact of training effects on the test results.

The error in the calculation of SART scores was corrected. It was furthermore decided to use the TLX and SART questionnaires after each evaluation run, in order to get a higher resolution of data points.

Operator Interface Changes

Besides the changes in the organization of the experiment, further changes were made in the *Third-Eye* attitude HUD. Following observations and participant comments made during the first pilot experiment series, the **positions** of the secondary video frame and the pitch and yaw rate indicators were changed to the lower left corner of the display. This moved these items into direct vicinity of the trajectory prediction display and therefore centered all important information into a small field of the screen, thereby reducing the need for display-scanning by the operator (see Figure 7-16 as compared to Figure 6-31). The attitude HUD **angle envelope** was reduced to the interval [-90°, 90°] in yaw and pitch angles. This increased display angular resolution, made it more accessible, and also represented a more practically relevant envelope for approach and docking maneuvers than the former interval [-180°, 180°].

Another change was the addition of two **pre-set postures** for the camera arm, to be activated by key presses. Key ‘1’ moved the arm into its initial position, camera pointing straight forward. Key press ‘3’ had the arm move into a close-range posture, in which the point of the docking probe was visible from above and behind. With this posture, the target became visible at a distance of 2 m.

This pre-set pose is no unjustified alteration of the experiment conditions, since it reflects the fact that operators would either have had time to position the camera for docking during the approach, or actually have a favorite arm posture for final approach and docking which would be pre-set for each operator.

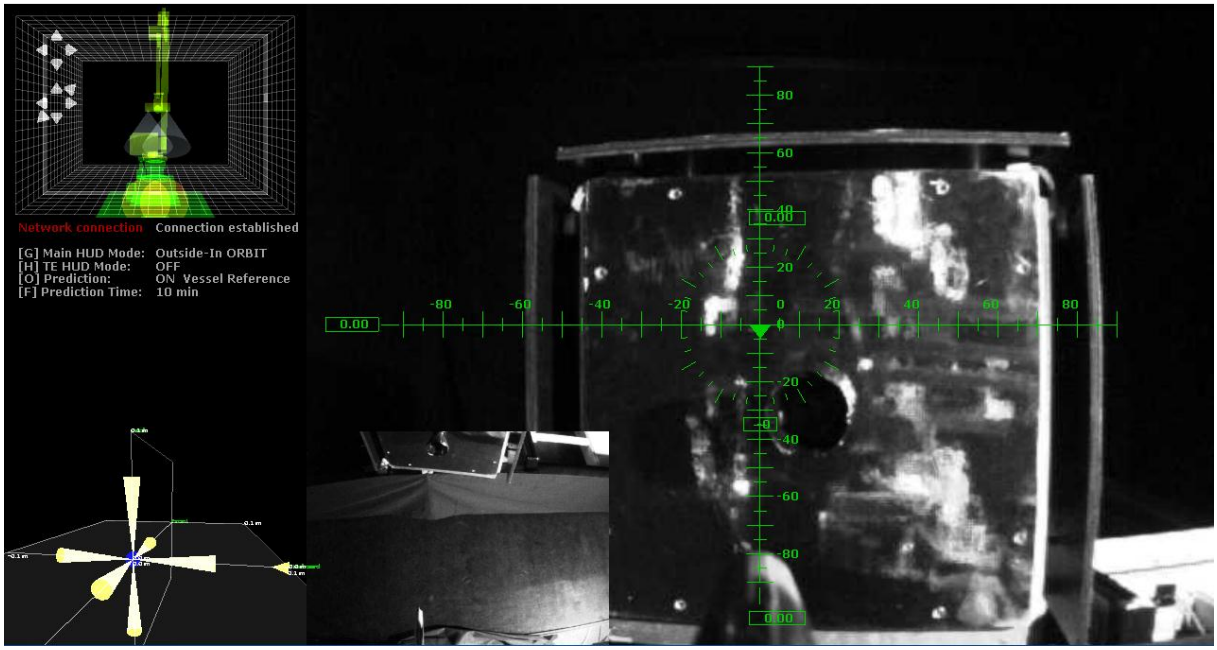

Figure 7-16: ThirdEye Proximity Operations GUI as changed after pilot experiment series I. The secondary camera view and the pitch and yaw indicators have been moved to the lower left corner, right next to the trajectory prediction display. This moves all critical information into a narrow field of regard and thereby reduces the need for visual scanning by the operator.

7.4.4 Second Pilot Study

Using the altered scenarios, test procedure and HUD layout, three participants were tested in the second pilot series. The participants of pilot series II were three male aerospace engineering students with a mean age of 23.7 years.

It must be noted that only the revised difficulty levels 2, 3 and 4 were used in this pilot series II, because no new information was considered to arise from re-testing level 1. In the statistical analysis I was again supported by Zarrin Chua of the Georgia Institute of Technology.

The second pilot experiment series was not designed to actually determine *ThirdEye* effects. The low number of data points in this experiment series does not allow statistical analysis of *ThirdEye* performance. The second pilot series nonetheless served to show that the redesigned test scenarios result in differences in task performance between the difficulty levels, as well as in differences in performance between active and inactive *ThirdEye*.

The results of the second pilot series are visualized in Figures 7-17 through 7-19. Note that the plots for docking angle, translation velocity change, and task completion time only use the data for successful docking approaches.

Without *ThirdEye*, only 33% of the runs were successful at difficulty levels 2 and 3, and none at level 4. Using the *ThirdEye*, the success rates were 100% for levels 2 and 3, and 67% for level 4. The low success rates without *ThirdEye* limit the informative value of the comparison of **docking an-**

gles. The angles with active *ThirdEye* are however significantly lower than with inactive *ThirdEye* and are almost equal over all difficulty levels.

The **translation velocity change** during the approaches with *ThirdEye* is lower than without *ThirdEye*. The data for **task completion time** is inconclusive. *ThirdEye* usage resulted in longer mean completion time in difficulty level 2, and shorter times for difficulty level 3.

The data used for TLX and SART score plots is from all approaches. This reflects the fact that while unsuccessful approaches do not generate meaningful performance data, the information about participants' perception of task load and situation awareness during failed attempts is nonetheless of interest. The TLX score is lower for *ThirdEye* use, although not significantly. The data for SART is inconclusive.

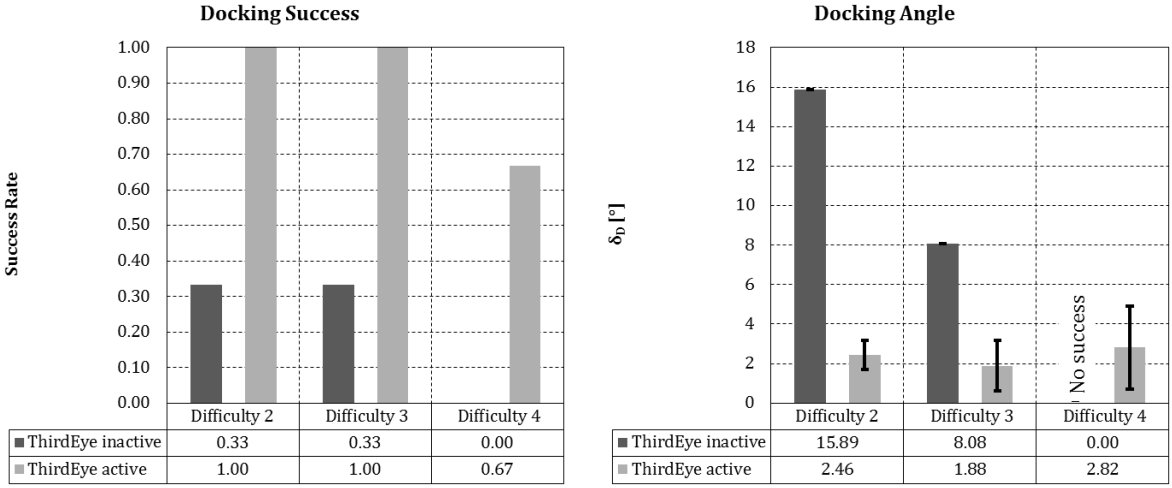

	Difficulty 2	Difficulty 3	Difficulty 4
ThirdEye inactive	0.33	0.33	0.00
ThirdEye active	1.00	1.00	0.67

	Difficulty 2	Difficulty 3	Difficulty 4
ThirdEye inactive	15.89	8.08	0.00
ThirdEye active	2.46	1.88	2.82

Figure 7-17: ThirdEye pilot evaluation series II docking success and docking angles for successful approaches. Without ThirdEye, only 1 of 3 runs was successful at difficulty levels 2 and 3, and none at level 4. Using the ThirdEye, the success rates were 3 of 3 for levels 2 and 3, and 2 of 3 for level 4. The low success rates without ThirdEye limit the informative value of the comparison of docking angles. The angles with active ThirdEye are significantly lower than with inactive ThirdEye and are almost equal over all difficulty levels.

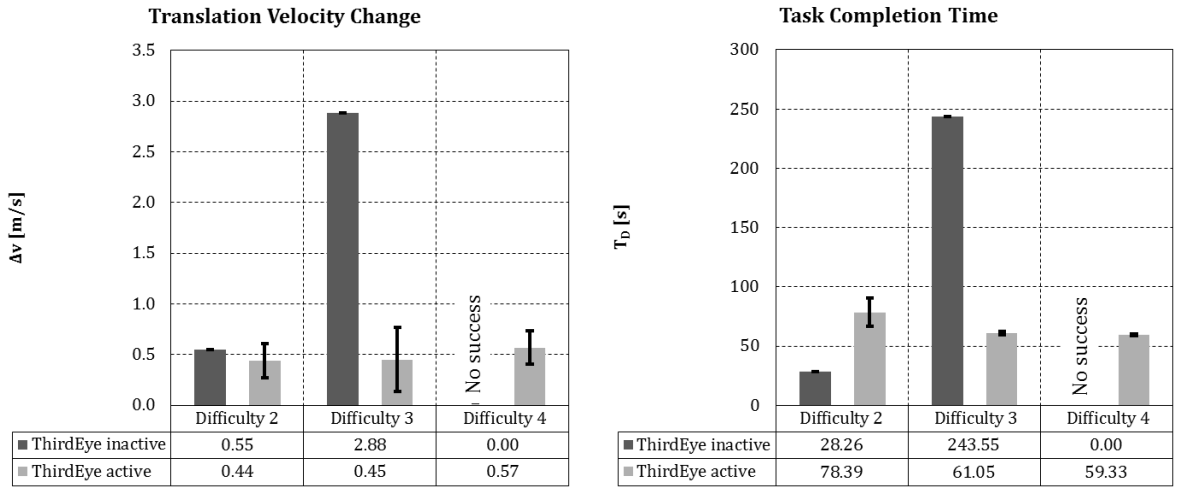

	Difficulty 2	Difficulty 3	Difficulty 4
ThirdEye inactive	0.55	2.88	0.00
ThirdEye active	0.44	0.45	0.57

	Difficulty 2	Difficulty 3	Difficulty 4
ThirdEye inactive	28.26	243.55	0.00
ThirdEye active	78.39	61.05	59.33

Figure 7-18: ThirdEye pilot evaluation series II efficiency metrics for successful approaches. The translation velocity change during the approaches with ThirdEye is lower than without ThirdEye. The data for task completion time is inconclusive. ThirdEye usage resulted in longer mean completion time in difficulty level 2, and shorter times for difficulty level 3.

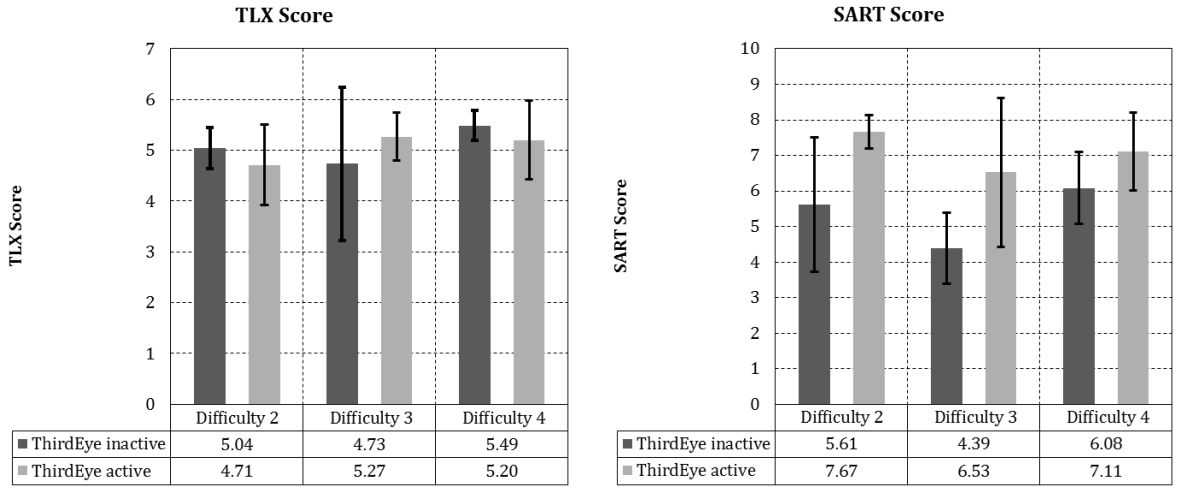

	Difficulty 2	Difficulty 3	Difficulty 4
ThirdEye inactive	5.04	4.73	5.49
ThirdEye active	4.71	5.27	5.20

	Difficulty 2	Difficulty 3	Difficulty 4
ThirdEye inactive	5.61	4.39	6.08
ThirdEye active	7.67	6.53	7.11

Figure 7-19: ThirdEye pilot evaluations series 2 user perception metrics. The TLX score is lower for ThirdEye use, although not significantly. The data for SART is inconclusive.

Based on the results of pilot series II, it was decided to proceed with the reworked scenarios and test plan. The minimum participant size for the evaluation series was determined to be 15 persons. In order to have additional data, it was decided to test 20 subjects.

7.5 Summary

The second part of the working hypothesis behind this doctoral thesis states that a flexible vantage point which can be freely positioned in relation to a spacecraft-fixed main camera, serves to improve operator performance during teleoperated final approach and docking.

In order to test this hypothesis, a **laboratory version** of the *ThirdEye* robotic camera arm system was developed and implemented. It consists of the 5DOF **robotic arm** itself, its **control software**, and **human-machine interface software** which reads user commands from various input devices and shows the current state of the arm in a 3D graphic display. Furthermore, an **automatic target pointing system** was implemented for the arm, which was however not used in the evaluation experiments.

An **evaluation study of input devices and control modes** showed that a joystick was the superior input mode for forward-kinematics control, since it allowed intuitive, one-hand control of all degrees of freedom. An inverse-kinematics control mode using a 6DOF space mouse was implemented but not used in the *ThirdEye* evaluation experiments, since the input device study showed that operator's required substantial training in order to be able to control the individual degrees of freedom of a space mouse separately and precisely. The study furthermore showed that pan and tilt stabilization for the camera head actually result in lower control performance of the operator.

The *ThirdEye* evaluation will use the **performance metrics** approach success (percentage of successful docking approaches), operator situation awareness and task load (measured by questionnaires using the SART and NASA-TLX methods), docking safety (measured by the radial and tangential docking contact velocities), docking precision (angle between chaser and target at docking contact), and docking efficiency (measured by velocity change and rotation rate change during an approach, as well as the time to complete the approach). The data for these metrics will be logged during the experiment flights and by means of computerized questionnaires between flights.

Two **pilot experiment studies** were conducted to fine-tune the test scenarios and procedures and to get user feedback for the operator interface before the actual *ThirdEye* evaluation experiments. A number of changes were made to the test scenarios in order to generate real differences in scenario difficulty and to reduce the experiments to the part of the approach in which the use of the *ThirdEye* was really expected to cause a difference in operator performance. The main difficulty in the scenarios lies in the rotation of the target object and the resulting need for precise and well-timed maneuvering. This therefore represents approaches of uncooperative and tumbling targets in OOS applications. The rotation rates featured in the reworked test scenarios are 0°/s, 0.5°/s, 2°/s and 4°/s. Operator training is achieved in scenarios with the target rotating at 1°/s.

After the second pilot experiment series it was decided that the reworked scenarios met the requirements. Based on the effects observed in the pilot experiments, the number of test participants was determined to be 15 people. It was decided to use 20 participants in order to increase the amount of available data.

8 ThirdEye Evaluation Experiment Series

During the *ThirdEye* evaluation experiment series, 20 participants were tested over a span of ten days. All participants were aerospace engineering students or research staff. Only one participant was female. Mean age was 27.1 years, with a standard deviation of 7.3 years.

Test Procedure

For the evaluation series, all scenarios specified in Table 7-5 were used. The test procedure had the participants first get basic information about the docking task, the test setup and the operator interfaces by means of a PowerPoint slide show. They then completed three training flights with one *ThirdEye* activity status, before proceeding with four evaluation flights with the same status. Training flights were repeated if the participant showed problems in understanding the sensor outputs and guidance principles of the simulated system. After each evaluation flight, the participant completed a computerized TLX and SART questionnaire. After the evaluation flights in one *ThirdEye* activity status, the series of training and evaluation flights was repeated with the other *ThirdEye* status. The sequence of *ThirdEye* active/inactive was alternated between participants. The sequence of scenarios was randomized. The test matrix showing the test sequence for each participant is provided in Appendix C.

Docking Strategy

Since any fly-around to match the rotation of the target was ruled out by the simulation setup (refer to Section 5.2.2), the participants had to adopt a wait-and-dash strategy for docking to the targets in scenarios 3 and 4. The operators positioned the chaser spacecraft at a safe holding point in front of the target's rotation axis and waited until the motor nozzle reached the right position for a final thrust. If the timing was correct, this final thrust led to successful docking. If not, it either resulted in a collision with the nozzle bell, a collision with the target satellite body, or in fuel-expensive collision avoidance maneuvers in which the operators moved the chaser back to a holding point. In two cases, the collision-avoidance maneuvers resulted in complete loss of orientation and thus control by the operator, which led to body collisions.

Success Criteria

For the evaluation docking approaches, two success criteria were used. Both must be met in order to achieve a successful approach. An approach was thus considered successful, if

a) The docking probe hit the target surface and the docking switch engaged, and
b) The docking angle δ_D was smaller than 5°. This reflects the capabilities of the *Orbital Express Capture System* [212].

The docking precision criteria resulted in different time windows for successful docking for the different scenario difficulty levels (see Table 8-1).

Table 8-1: Timing requirements for successful docking at the four scenario difficulty levels.

Scenario Difficulty	Initial target yaw angle [°]	Target yaw rate [°/s]	Time to ideal docking position [s]	Timing window for successful docking [s]
Level 1	20	0	n/a	n/a
Level 2	-30	0.5	60	20
Level 3	120	-2	60	5
Level 4	-240	4	60	2.5

The performance metrics docking angle, velocity change, rate change, task completion time, and contact velocities were only evaluated for successful approaches. The subjective measures TLX score and SART score were evaluated for all approaches, since the subjective perception of task load and situation awareness is of interest for both successful and failed docking attempts.

Analysis Scheme

Figure 8-1 shows the data analysis scheme for the evaluation of the experiment results. First, the success rates, TLX and SART scores were compared between the difficulty levels, using analysis of variance (ANOVA) [255] and Tukey's honestly significant difference (HSD) method [256]. This served to establish whether there existed real differences in operator performance and perception between the levels.

In the second step, the TLX and SART scores were analyzed, in order to determine whether there existed a correlation between these metrics and task success. This analysis determined whether TLX and SART scores were correlated to objective operator performance and whether they could be used to evaluate *ThirdEye* utility. This was achieved by comparing TLX scores and SART scores of successful and failed approaches using Student's t-test [274].

Third, performance metrics were compared between the first and second halves of the experiment runs in order to determine training effects. Since the sequence of *ThirdEye* active/inactive was alternated between participants, ten participants first completed the active *ThirdEye* runs, ten the inactive *ThirdEye* runs. The comparison of operator performance between first and second halves of experiment runs therefore yielded information about the presence of training effects. This comparison was achieved by t-tests and Mann-Whitney U-tests [274].

Student's t-test was used if the samples show normal distribution and equal variances. If these criteria were not met, the U-test was used for the analysis. Testing for normal distributions was done with the Lilliefors test [274], testing for equal variances with an F-test [255].

The final step in the experiment evaluation was the actual comparison of operator performance between active and inactive *ThirdEye*. This was also achieved by pairwise comparison of each performance metric for each difficulty level, again using t-tests and U-tests as appropriate.

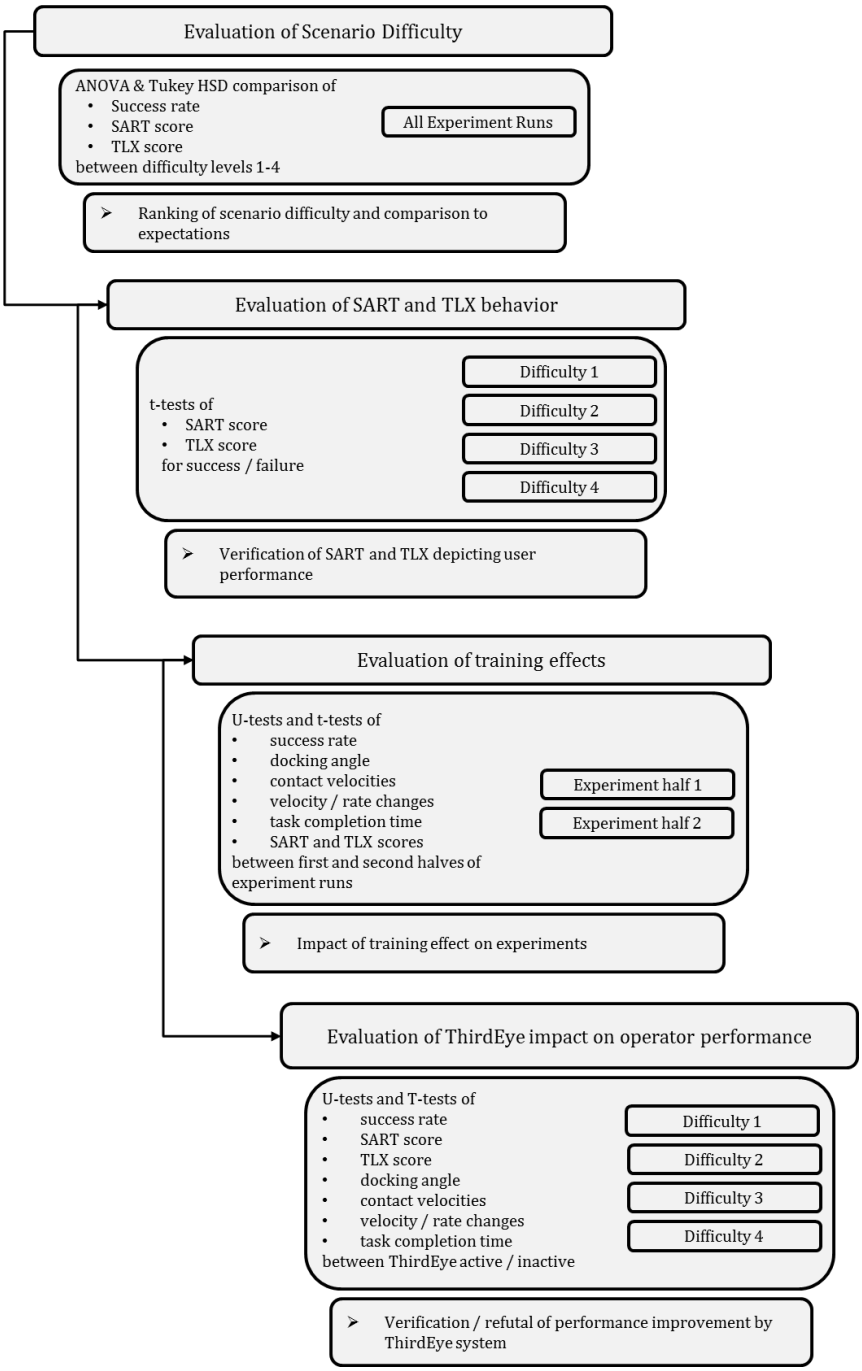

Figure 8-1: Analysis scheme for the ThirdEye evaluation experiment series. The first step of the analysis process was to compare success rates, SART scores and TLX scores between the difficulty levels. This served to determine whether the difficulty levels caused the expected differences in operator performance and perception. The second step was to determine whether TLX and SART reproduced the success rates, and whether there thus existed a correlation between task success, task load and situation awareness. In the third step, the training effects were evaluated using the statistics for the performance metrics. Finally, the ThirdEye impact on operator performance was evaluated. In this step, the individual performance metrics were compared between active and inactive ThirdEye status using T-tests and U-tests. After this evaluation step, it is possible to verify or refute the hypothesis that operator performance is improved by use of the ThirdEye system.

8.1 Evaluation of Scenario Difficulty

The **success rate** is defined as the primary objective indicator of scenario difficulty. It is therefore expected that the success rate decreases with increasing difficulty level. This expectation is met by the experiment data, as shown in Figure 8-2. There thus exists a real difference in scenario difficulty between the levels.

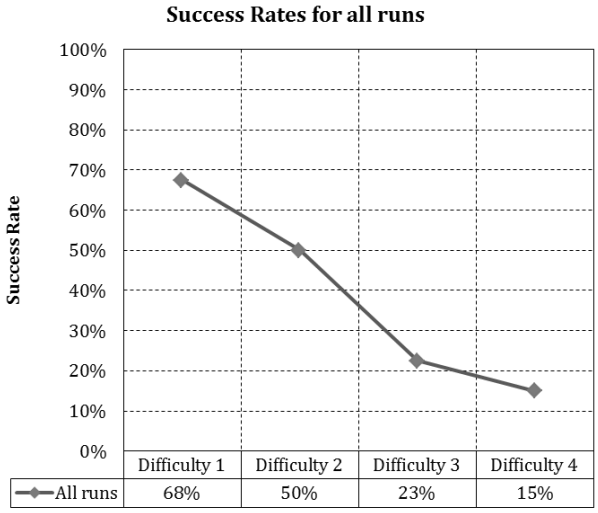

Figure 8-2: Comparison of success rates between difficulty levels. The success rate decreases with increasing difficulty level. This shows that there is a real difference between scenario difficulties.

Apart from the objective evaluation of scenario difficulty, the subjective perception by the participants is also important. The **SART and TLX scores** are therefore also compared between difficulty levels. The comparison plots are shown in Figure 8-3 and Figure 8-4. At first glance, the behavior of both scores meets expectations. The SART score, a metric for operator SA, decreases with increasing difficulty. The TLX score increases with difficulty, and thus operator task load. Since both the SART scores and TLX scores have a normal distribution, ANOVA and Tukey's HSD tests were used to compare between the difficulty levels.

The HSD comparison test results for SART scores are given in Table 8-2. They show significant differences (at $p = 0.05$ level) between difficulty levels 1 & 3, 1 & 4, as well as 2 & 4.

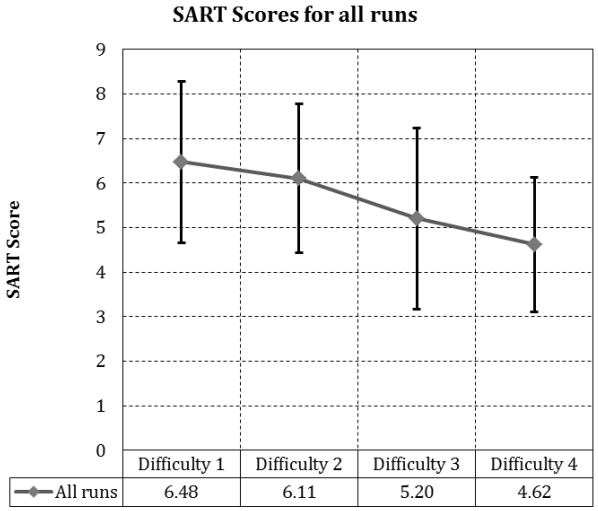

Figure 8-3: Comparison of mean SART score between difficulty levels. SART scores and thus user SA decrease steadily with rising difficulty level.

Table 8-2: Tukey HSD comparison test results for SART scores.

Compared difficulty levels	95% confidence interval	Difference in means	Difference significant
1 – 2	[-0.65 1.39]	0.37	✗
1 – 3	[0.26 2.29]	1.28	✓
1 – 4	[0.84 2.87]	1.86	✓
2 – 3	[-0.11 1.92]	0.90	✗
2 – 4	[0.47 2.50]	1.49	✓
3 – 4	[-0.44 1.60]	0.58	✗

Table 8-3 shows the corresponding test results for TLX scores. The differences between levels 1 & 3, 1 & 4, 2 & 3, 2 & 4 are significant at the p = 0.05 level. Based on the HSD tests, no significant differences in situation and task load perception can be determined between difficulty levels 1 & 2, as well as between 3 & 4. The general trend towards decreased SA and increased task load with increased difficulty level is however clear.

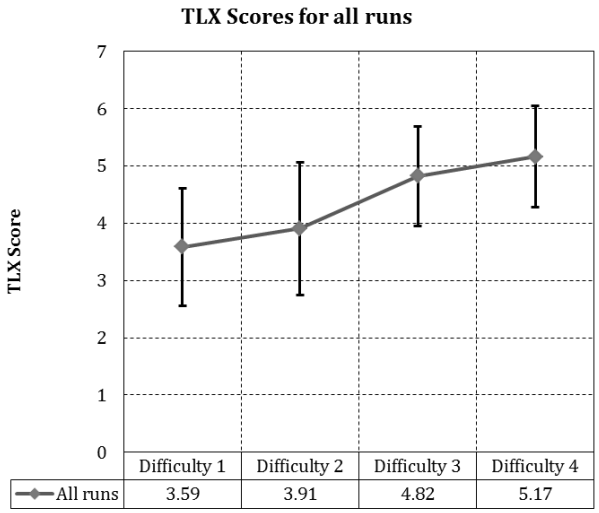

Figure 8-4: Comparison of mean TLX scores between difficulty levels. TLX scores and thus operator task load increase steadily with rising difficulty level.

Table 8-3: Tukey HSD comparison test results for TLX scores.

Compared difficulty levels	95% confidence interval	Difference in means	Difference significant
1 – 2	[-0.89 0.25]	-0.32	✗
1 – 3	[-1.81 -0.67]	-1.24	✓
1 – 4	[-2.15 -1.01]	-1.58	✓
2 – 3	[-1.49 -0.35]	-0.92	✓
2 – 4	[-1.83 -0.69]	-1.26	✓
3 – 4	[-0.91 0.23]	-0.34	✗

The scenarios used in the evaluation experiments therefore **differ in their levels of difficulty**. This difference is evident in approach success rates, as well as in the subjective situation awareness and task load perception.

8.2 Evaluation of SART and TLX Performance

In order to be able to confidently use SART and TLX as measures for *ThirdEye* performance, it must be determined whether both scores correlate with operator performance. For this purpose, the SART and TLX scores are compared between successful and failed docking attempts. It is expected that unsuccessful attempts see a decreased SART score and increased TLX score, as compared to successful attempts.

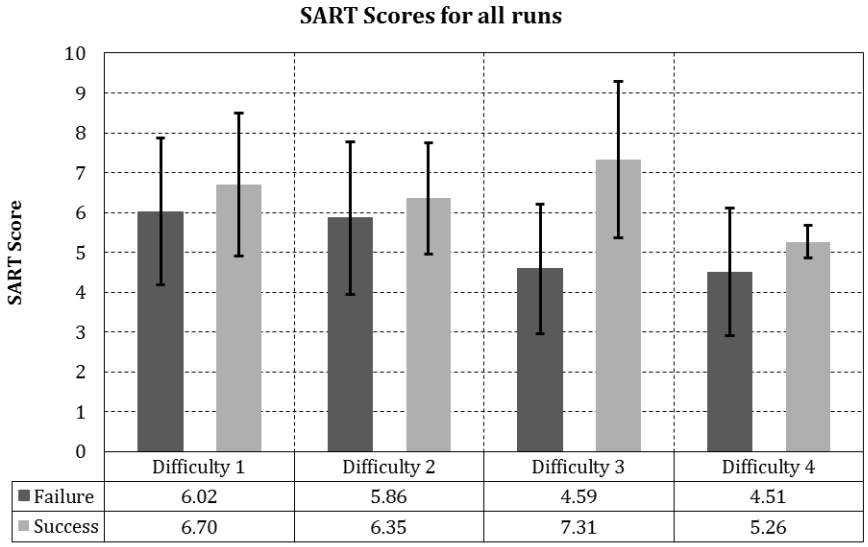

Figure 8-5: Comparison of SART scores for successful and unsuccessful approaches over all difficulty levels. The mean values for successful approaches are always higher than for failed attempts.

Figure 8-5 shows that the mean SART scores follow this expected behavior. SART was always higher for successful approaches than for failed attempts. This indicates a correlation between task success and level of operator SA. It must however be noted that the t-test and u-test comparisons for each difficulty level do not show significant differences, except for level 3 (refer to Table 8-4).

Table 8-4: SART score data for successful and unsuccessful approaches over all difficulty levels. The low number of successes at difficulty level 4 creates a negative result of the variance comparison. The u-test is thus used for comparing SART scores. The comparison between successful and failed attempts yields mostly insignificant results, except for difficulty 3, in which the difference between SART scores is highly significant.

Level	Approach status	Min	Max	Median	Mean	Standard Deviation	Distribution normal	Variances equal	Comparison test	Difference significant
Difficulty 1	success	3.3	10.6	6.5	6.7	1.79	✓	✓	t-test	×
	failure	2.7	8.7	6.3	6.0	1.84	✓			
Difficulty 2	success	3.8	8.8	6.5	6.4	1.40	✓	✓	t-test	×
	failure	0.3	8.8	5.8	5.9	1.92	✓			
Difficulty 3	success	4.8	10.0	6.8	7.3	1.96	✓	✓	t-test	✓ $p = 7.2 \times 10^{-5}$
	failure	1.3	8.7	4.5	4.6	1.63	✓			
Difficulty 4	success	4.9	6.0	5.2	5.3	0.40	✓	×	u-test	×
	failure	0.9	7.3	4.5	4.5	1.61	✓			

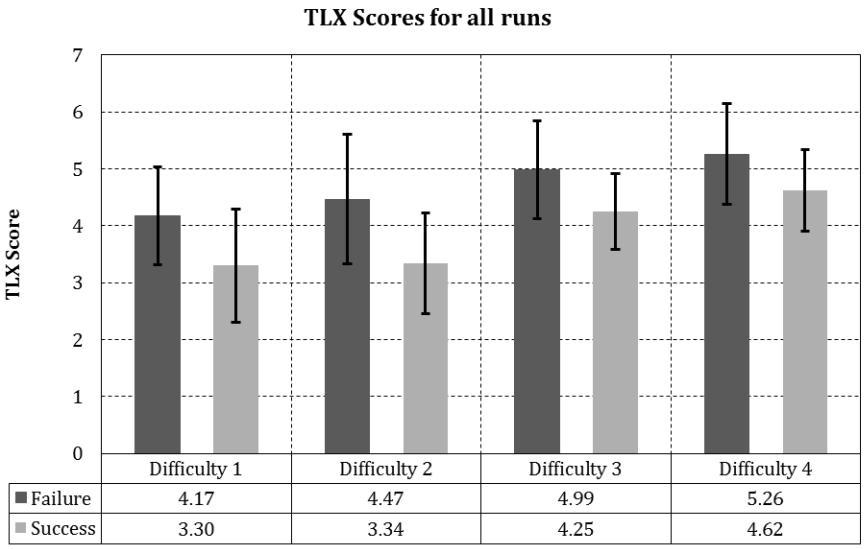

Figure 8-6: Comparison of TLX scores for successful and unsuccessful approaches over all difficulty levels. The mean values for successful approaches are always lower than for failed attempts.

The TLX scores also follow the expected pattern (see Figure 8-6). Successful attempts are accompanied by lower TLX scores and thus operator task load than failed attempts. Table 8-5 shows that this correlation is supported by the results of the t-test comparisons. The differences in TLX score between successful and failed attempts are significant for difficulty levels 1 through 3. At difficulty 4, the difference is only significant at the p = 0.1 level. This is reasoned to be due to the low number of successful docking attempts at difficulty level 4, which do not allow a confident analysis of variances.

Table 8-5: TLX score data for successful and unsuccessful approaches over all difficulty levels. All TLX score comparisons are significant at the p = 0.05 level, except for difficulty 4, which shows only a significance at the p = 0.1 level.

Level	Approach status	Min	Max	Median	Mean	Standard Deviation	Distribution normal	Variances equal	Comparison test	Difference significant
Difficulty 1	success	2.0	5.2	3.1	3.3	0.99	✓	✓	t-test	✓ p = 0.0053
	failure	3.1	5.3	4.3	4.2	0.86	✓			
Difficulty 2	success	1.3	4.6	3.4	3.3	0.89	✓	✓	t-test	✓ $p = 5.9 \times 10^{-4}$
	failure	1.1	6.5	4.8	4.5	1.14	✓			
Difficulty 3	success	3.3	5.2	4.2	4.3	0.67	✓	✓	t-test	✓ p = 0.0115
	failure	2.9	6.5	5.1	5.0	0.86	✓			
Difficulty 4	success	3.9	5.6	4.4	4.6	0.72	✓	✓	t-test	✗ p = 0.0523
	failure	3.3	6.8	5.3	5.3	0.89	✓			

While the statistics for SART scores cannot statistically prove the correlation between SA level and task success, it can be concluded based on the experiment results that **SART and TLX scores can serve as indicators for operator performance**. They therefore are a valuable metric for *ThirdEye* performance.

8.3 Evaluation of Training Effects

The experiment plan was designed to reduce or eliminate the impact of training effects on the test results by (1) providing three participant training runs per *ThirdEye* activity level, by (2) randomizing the sequence of test scenarios, and by (3) alternating the sequence of *ThirdEye* activity levels between participants. In a task such as approaching and docking to a rotating target object, which depends on coordination and timing, training effects caused by operator experience cannot be completely eliminated. This would require a more thorough training and practice program which was not possible within the *ThirdEye* evaluation campaign.

Since this limitation of the experiment campaign was known, it was decided to evaluate the training effects in order to be able to better understand the *ThirdEye* evaluation results. The evaluation of training effects is achieved by comparing operator performance in all relevant metrics between the first and second halves of the experiment runs. Since *ThirdEye* activity was alternated between participants, ten participants first used the inactive *ThirdEye*, ten the active *ThirdEye*. Each half of experiment runs therefore had equal numbers of *ThirdEye* active and inactive scenarios. Any differences in mean values of the metrics between first and second halves of the runs therefore serve as indicators for the presence of training effects.

For the objective performance metrics, only the maneuver-based data for successful docking approaches is used. For subjective metrics, SART and TLX scores are used for all experiment runs.

Table 8-6 and Figures 8-7 through 8-11 show the results of comparisons between experiment halves. While approach success is 30% higher during the second half as compared to the first half (Figure 8-7), there exist no significant differences for the other performance metrics. Moreover, there exists no continuous trend in the data showing an improvement in operator performance in the second experiment half. The difference in task success is thus probably a result of fluctuations in operator performance instead of an indicator of training effects. It is therefore concluded that in this experiment series training effect on operator performance can be neglected in the final analysis and that the measures employed to reduce training effects were successful.

Table 8-6: Comparison of operator performance metric between experiment run halves. Except for the difference in task success rate, there exist neither significant differences for any of the other metrics, nor a continuous trend over multiple metrics.

Parameter	Experiment runs	Min	Max	Median	Mean	Standard Deviation	Distribution normal	Variances equal	Comparison test	Difference significant
Approach Success Rate	1st half 2nd half	n/a	n/a	n/a	34% 44%	n/a	n/a	n/a	n/a	n/a
Docking Angle [°]	1st half 2nd half	0.0 0.0	4.8 4.6	1.7 2.1	2.0 1.9	1.40 1.24	✓ ✓	✓	t-test	✗
Axial Contact Velocity [m/s]	1st half 2nd half	0.00 0.00	0.15 0.22	0.02 0.03	0.03 0.05	0.03 0.05	✗ ✗	n/a	u-test	✗
Radial Contact Velocity [m/s]	1st half 2nd half	0.00 0.00	0.16 0.17	0.03 0.03	0.04 0.04	0.04 0.04	✗ ✗	n/a	u-test	✗
Velocity Change [m/s]	1st half 2nd half	0.12 0.11	2.55 3.87	0.50 0.36	0.71 0.68	0.62 0.82	✗ ✗	n/a	u-test	✗
Rate Change [°/s]	1st half 2nd half	0.00 0.00	23.2 52.0	1.6 1.4	3.1 4.2	4.73 9.42	✗ ✗	n/a	u-test	✗
Completion Time [s]	1st half 2nd half	49.3 45.3	915.1 431.0	82.73 74.65	142.18 115.65	166.45 84.08	✗ ✗	n/a	u-test	✗
SART Score	1st half 2nd half	0.3 1.1	10.6 10.0	5.3 5.7	5.4 5.8	1.94 1.86	✓ ✓	✓	t-test	✗
TLX Score	1st half 2nd half	1.3 1.1	6.5 6.8	4.5 4.5	4.4 4.3	1.19 1.17	✓ ✓	✓	t-test	✗

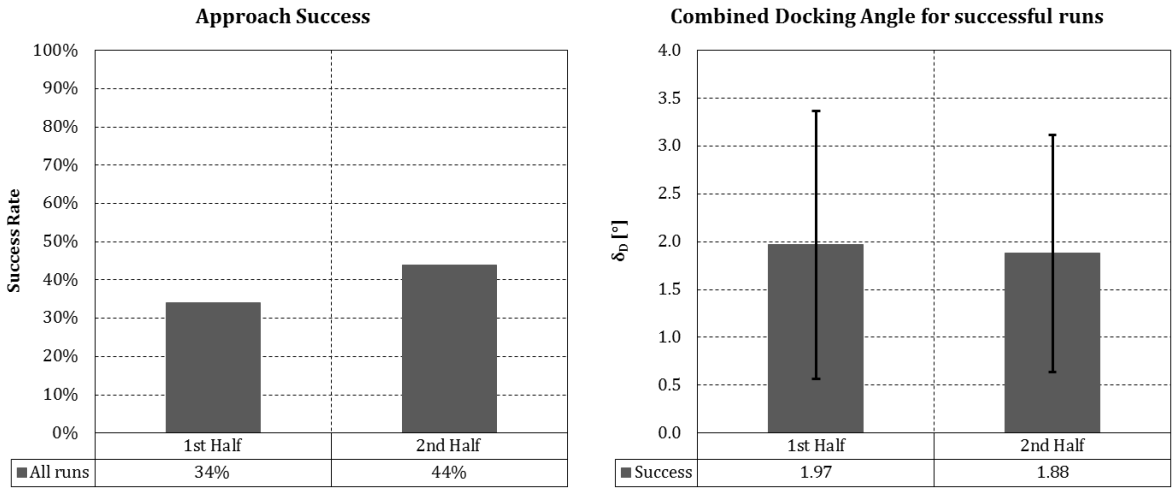

Figure 8-7: Approach success and docking angles for 1st and 2nd experiment run halves. The success rate in the second half is 30% higher than in the first half. The docking precision shows negligible difference.

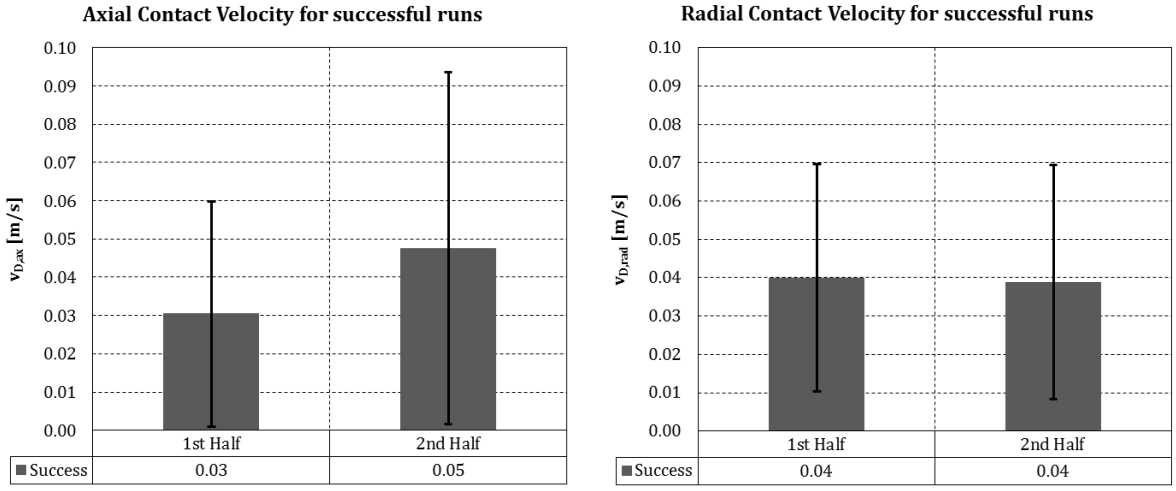

Figure 8-8: Contact velocities for 1st and 2nd halves of experiment runs. A 67% increase in axial contact velocity can be discerned. No difference exists in radial contact velocity.

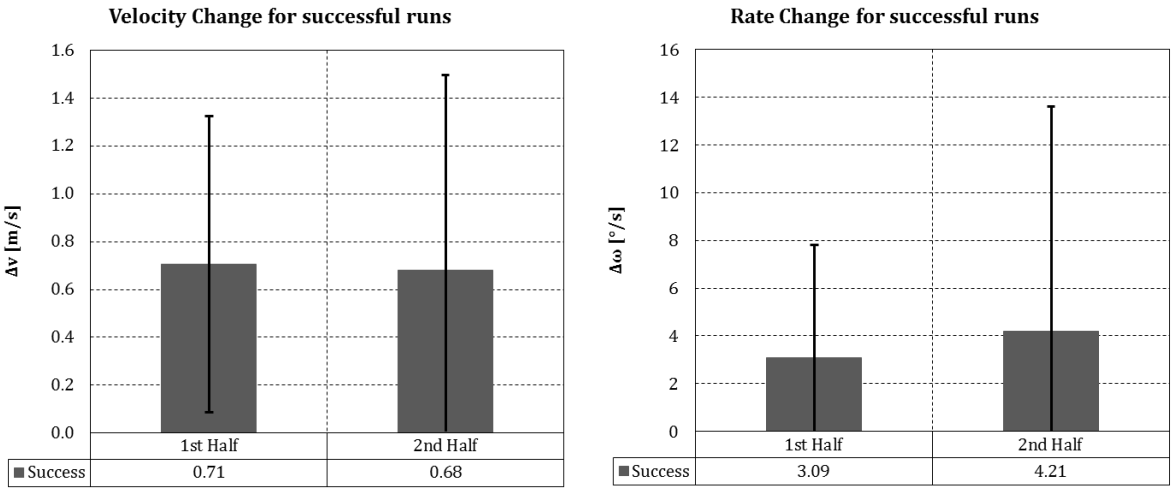

Figure 8-9: Velocity and rate changes for 1st and 2nd halves of experiment runs. The velocity change Δv shows a negligible difference, while the rate change Δω during the second half is 36% higher than during the first half.

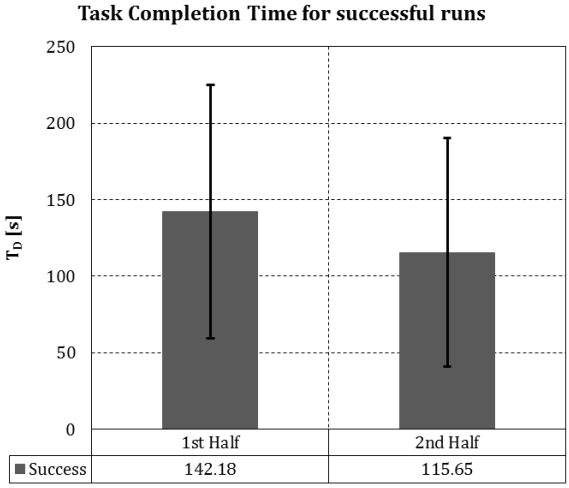

Figure 8-10: Task completion times for 1st and 2nd halves of experiment runs. During the second half, completion times are approx. 20% lower as compared to the first half.

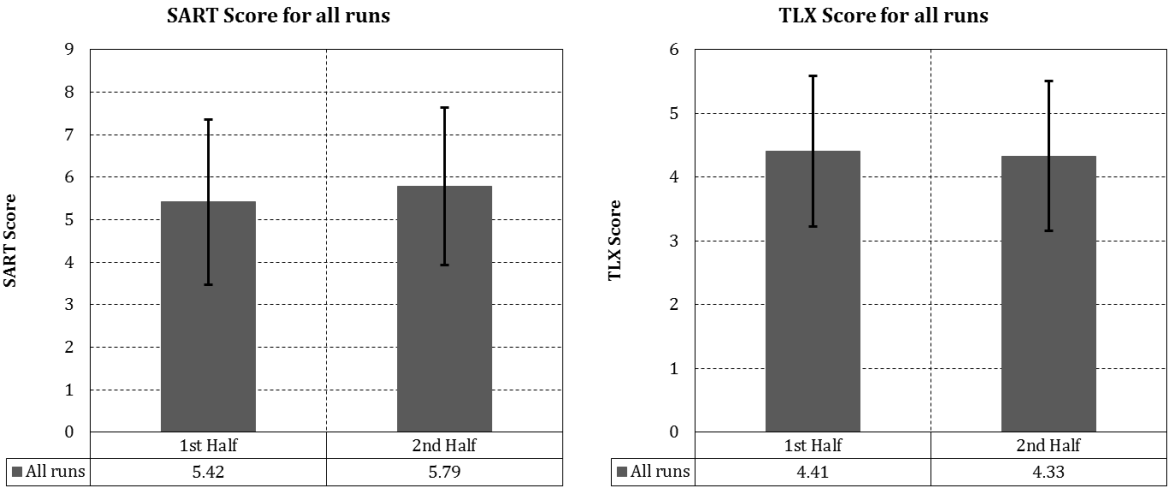

Figure 8-11: SART and TLX score for 1st and 2nd halves of experiment runs. The difference is negligible for both metrics.

8.4 Evaluation of ThirdEye Influence on Operator Performance

For evaluation of the *ThirdEye's* impact on operator performance, the performance metrics defined in Section 7.4.1 are compared between the two levels of *ThirdEye* activity, over the four levels of scenario difficulty. The analyses of test results for each metric are detailed in the following.

8.4.1 Approach Success

Figure 8-12 shows the approach success rates with inactive and active *ThirdEye* for all difficulty levels. At difficulty levels 1 through 3, the participants showed 25% - 50% higher success rates using the *ThirdEye*. At difficulty level 4, the results are reversed. It must be noted, however, that at level 4, only 2 of 20 approaches were successful with *ThirdEye*, and 4 of 20 without. At such low numbers, the higher success number without *ThirdEye* can well be due to a fluctuation in participant performance, rather than an indicator for better performance without *ThirdEye*.

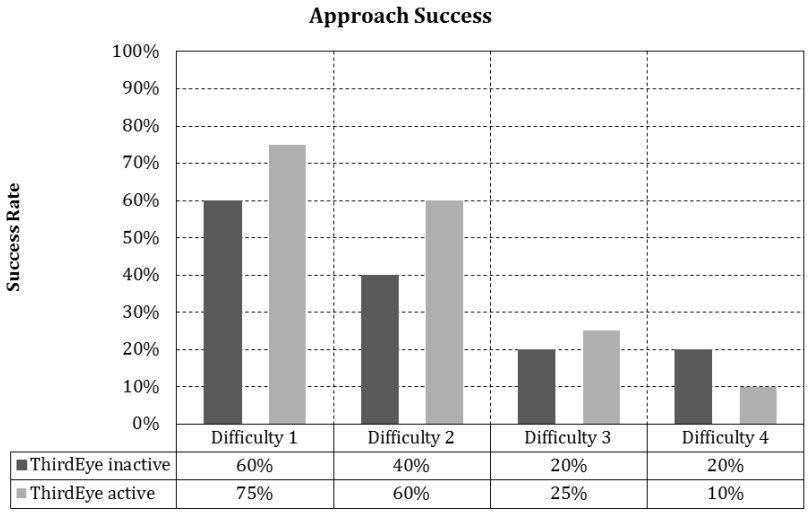

Figure 8-12: Approach success rates over ThirdEye activity. Active ThirdEye generates higher operator performance at difficulty levels 1 through 3. At level 4, operators were more successful without ThirdEye. At the low success numbers (n = 4 for ThirdEye inactive, n = 2 for ThirdEye active), this can be a result of fluctuations in operator performance, instead of a real indicator for ThirdEye performance.

The low success rates at difficulty level 4 mean that the statistical analysis of the safety, precision and efficiency metrics at that level will not yield meaningful results, since they are based on the data for successful approaches only. The low number (n = 2) of data points for approaches with active *ThirdEye* does neither allow testing for normal distribution, nor will comparisons by u-tests be conclusive.

Another fact to point out is the low success rate at difficulty level 1, in which a stationary target was approached. It was expected that close to 100% of approaches would be successful, both with and without active *ThirdEye*. The fact that only 75% were successful with active *ThirdEye* and 60% with inactive *ThirdEye* is an indicator of the unpredictable behavior of participants in a task depending on concentration and coordination.

8.4.2 Operator Situation Awareness and Task Load

The SA and task load metrics were evaluated for all approaches, both successful and unsuccessful. It was expected that SART scores would be higher with active *ThirdEye*, and TLX score higher with inactive *ThirdEye* for all difficulty levels.

Figure 8-13 shows the **mean SART scores** for all four scenarios, with the corresponding data analysis summarized in Table 8-7. The plot shows that SART scores are continuously between 9% and 25% higher with active *ThirdEye*. Due to the high variance in the data, this difference is only significant at the p = 0.05 level for difficulty level 4. The expected trend in participant SA can however be discerned.

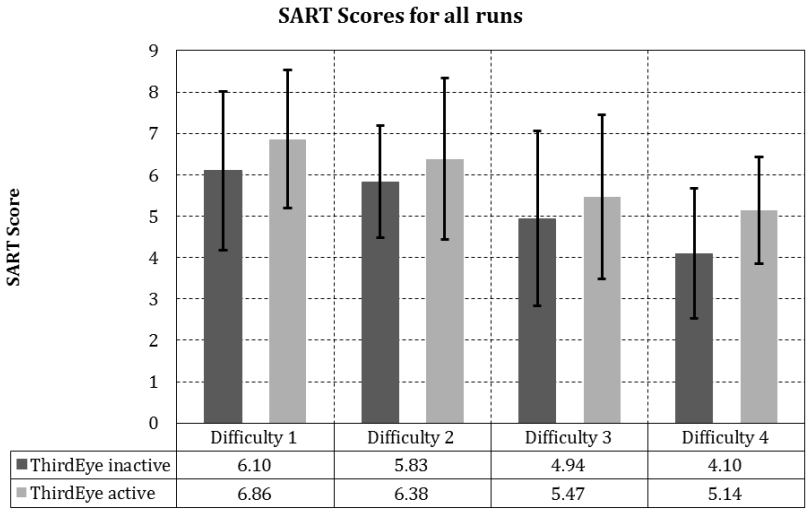

Figure 8-13: SART scores over ThirdEye activity. SART scores and thus user SA is continuously higher for active ThirdEye use.

Table 8-7: SART scores evaluation for ThirdEye activity. The comparisons between active and inactive ThirdEye is only statistically significant for difficulty level 4. This is due to the high variance in participant feedback.

Level	ThirdEye status	Min	Max	Median	Mean	Standard Deviation	Distribution normal	Variances equal	Comparison test	Difference significant
Difficulty 1	inactive	2.7	9.3	6.0	6.1	1.91	✓	✓	t-test	✗ p = 0.0936
	active	3.3	10.6	6.7	6.9	1.67	✓			
Difficulty 2	inactive	3.8	8.7	5.4	5.8	1.36	✓	✓	t-test	✗
	active	0.3	8.8	6.8	6.4	1.95	✓			
Difficulty 3	inactive	1.3	9.9	4.4	4.9	2.11	✓	n/a	u-test	✗
	active	2.7	10.0	4.9	5.5	1.98	✗			
Difficulty 4	inactive	0.9	6.5	4.5	4.1	1.56	✓	✓	t-test	✓ p = 0.0138
	active	1.9	7.3	5.3	5.1	1.30	✓			

The analysis for **TLX scores** is provided in Table 8-8 and visualized in Figure 8-14. The TLX score does not show the expected behavior. At difficulty levels 1 and 2, TLX scores are lower with active *ThirdEye* (by 11% and 3%), although not significantly. For levels 3 and 4, TLX for active *ThirdEye* is higher than without *ThirdEye*, by 5% and 7%. This difference is however also not statistically significant. While the differences in TLX scores are small, they seem to indicate that at low rotation rates of the target (ω_z = 0°/s, ω_z = 0.5°/s), the *ThirdEye* reduces operator task load, while at high rates ((ω_z = 2°/s, ω_z = 4°/s) it increases task load. A possible reason for this is that the additional visual

information available through the *ThirdEye* makes the task easier at low rotation rates, where timing requirements are not as stringent. However at higher rotation rates, where timing becomes the essential factor for docking success, the *ThirdEye* introduces an additional element of information that must be processed in the limited time available. The time required to do so is then lacking for processing of the other camera stream and the predictive display, as well as for precise spacecraft control.

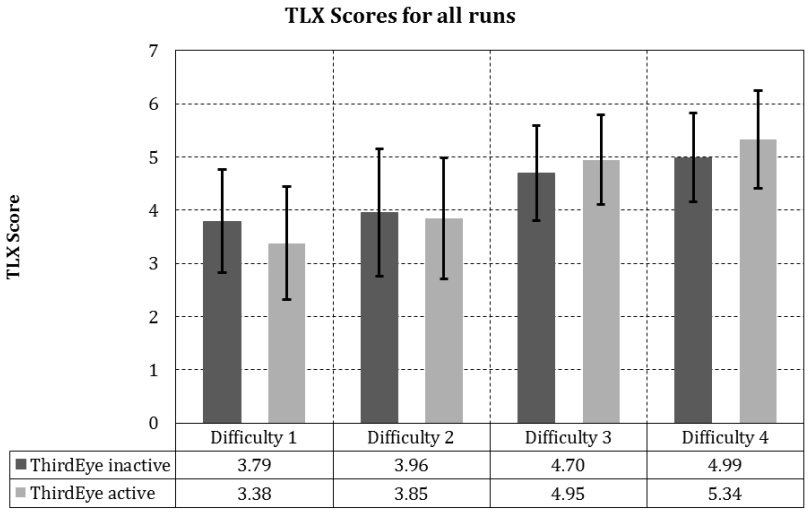

Figure 8-14: TLX scores over ThirdEye activity. While TLX scores for active ThirdEye are slightly lower at difficulty levels 1 & 2, and slightly higher at levels 3 & 4, no conclusive trend can be deducted.

Table 8-8: TLX scores evaluation for ThirdEye activity. The comparisons between active and inactive ThirdEye do not show significant differences.

Level	ThirdEye status	Min	Max	Median	Mean	Standard Deviation	Distribution normal	Variances equal	Comparison test	Difference significant
Difficulty 1	inactive	2.0	5.2	3.7	3.8	0.91	✓	✓	t-test	×
	active	2.1	5.3	3.0	3.4	1.07	✓			
Difficulty 2	inactive	1.1	5.3	4.2	4.0	1.20	✓	✓	t-test	×
	active	1.6	6.5	3.9	3.9	1.14	✓			
Difficulty 3	inactive	2.9	6.4	4.7	4.7	0.90	✓	✓	t-test	×
	active	3.3	6.5	5.0	5.0	0.84	✓			
Difficulty 4	inactive	3.3	6.3	5.1	5.0	0.84	✓	✓	t-test	×
	active	3.7	6.8	5.3	5.3	0.92	✓			

8.4.3 Docking Safety

Docking safety as expressed in **residual relative velocity** at docking contact is analyzed independently for axial and radial docking velocities. Overall, the contact velocities measured during the experiment series are within the performance envelopes of most current docking mechanisms (see Table 4-1), albeit especially the radial velocities frequently reach the limits of these envelopes.

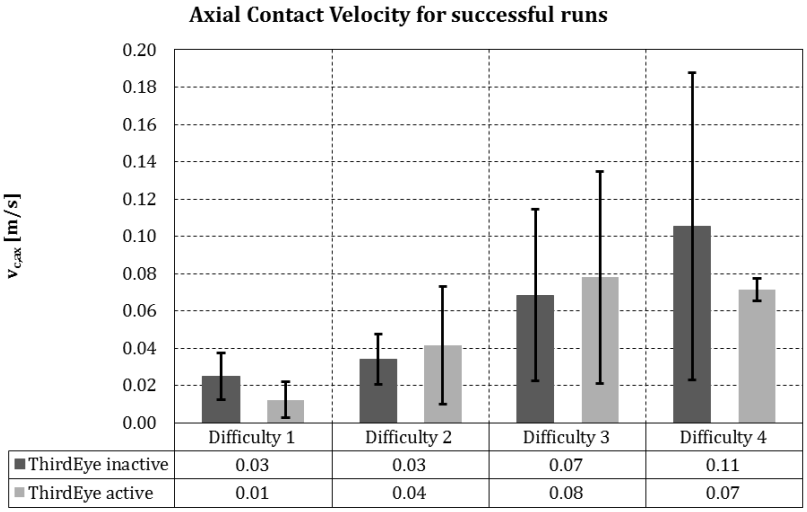

Figure 8-15: Axial contact velocity over ThirdEye activity. Contact velocity for active ThirdEye is higher at difficulty levels 1 – 3, but lower at level 4. This can be caused by the low number of data points (n = 2) at level 4.

Table 8-9: Axial contact velocity evaluation for ThirdEye activity. The low number of successful approaches using the ThirdEye at difficulty level 4 (2 of 20) does not allow testing for normal distribution. Due to the low number of data points at level 4 and the high variance, the u-test shows a non-significant difference between inactive and active ThirdEye.

Level	ThirdEye status	Min [m/s]	Max [m/s]	Median [m/s]	Mean [m/s]	Standard Deviation [m/s]	Distribution normal	Variances equal	Comparison test	Difference significant
Difficulty 1	inactive	0.01	0.05	0.02	0.03	0.01	✓	n/a	u-test	✓ p = 0.0068
	active	0.00	0.03	0.01	0.01	0.01	✗			
Difficulty 2	inactive	0.02	0.06	0.03	0.03	0.01	✗	n/a	u-test	✗
	active	0.00	0.09	0.04	0.04	0.03	✓			
Difficulty 3	inactive	0.03	0.11	0.07	0.07	0.05	✓	✓	t-test	✗
	active	0.02	0.15	0.05	0.08	0.06	✓			
Difficulty 4	inactive	0.03	0.22	0.08	0.11	0.08	✓	n/a	u-test	✗
	active	0.07	0.08	0.07	0.07	0.01	✗			

The statistics for **axial docking velocity** are provided in Figure 8-15 and Table 8-9. The plot shows no clear trend in *ThirdEye* performance. While at difficulty level 1, axial contact velocity with active *ThirdEye* is significantly lower than without, it is higher at levels 2 & 3, and again lower at level 4. Since there exists neither a continuous trend nor significant differences, it is concluded that this behavior is the result of fluctuations in operator performance, rather than an indicator for *ThirdEye* performance.

This statement also hold true for the **radial docking velocity** component (Figure 8-16 and Table 8-10).

It is however interesting to note that the data shows rising docking velocities with increasing difficulty level. This shows that in order to approach the targets with increasing rotation rate, the operators were forced to accelerate to higher relative velocities to achieve the required timing, which resulted in harder impacts upon docking. The lower axial and radial contact velocities with active *ThirdEye* at difficulty level 4 seem to indicate that the *ThirdEye* helped the operators to more confidently time the final docking thrust, which results in lower impact velocities. Since this observation is based on only two data points, it is however not conclusive and must be addressed in follow-up studies.

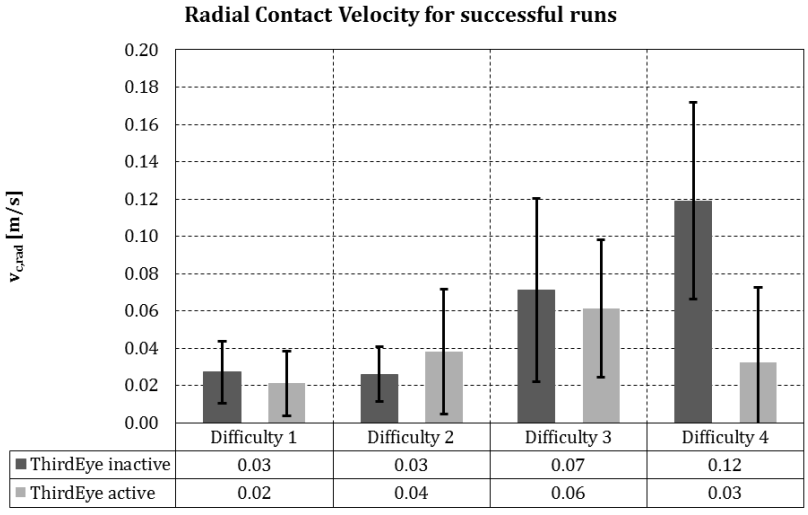

Figure 8-16: Radial contact velocity over ThirdEye activity. No clear trend for ThirdEye influence on radial contact velocity can be derived. There is however a large decrease evident for difficulty level 4. This could be due to the low number of data points (n = 2) available for that level.

Table 8-10: Radial contact velocity evaluation for ThirdEye activity. The low number of data points for active ThirdEye at difficulty level 4 does neither allow determination of normal distribution nor any meaningful comparison between performance with inactive and inactive ThirdEye.

Level	ThirdEye status	Min [m/s]	Max [m/s]	Median [m/s]	Mean [m/s]	Standard Deviation [m/s]	Distribution normal	Variances equal	Comparison test	Difference significant
Difficulty 1	inactive	0.01	0.06	0.03	0.03	0.02	✓	✓	t-test	✗
	active	0.00	0.07	0.02	0.02	0.02	✓			
Difficulty 2	inactive	0.01	0.05	0.03	0.03	0.01	✓	✗	u-test	✗
	active	0.00	0.10	0.04	0.04	0.03	✓			
Difficulty 3	inactive	0.01	0.12	0.08	0.07	0.05	✓	✓	t-test	✗
	active	0.01	0.11	0.07	0.06	0.04	✓			
Difficulty 4	inactive	0.05	0.17	0.13	0.12	0.05	✓	n/a	u-test	✗
	active	0.00	0.06	0.03	0.06	0.04	✗			

8.4.4 Docking Precision

Docking precision is measured by the **relative angle** δ_D between chaser and target at docking contact. Since $\delta_D < 5°$ is a success criteria for the docking approaches, no docking angle over 5° exists in the statistics shown in Figure 8-17 and Table 8-11. The plot shows that with *ThirdEye* the docking angle is 23% - 40% smaller in difficulty levels 1 through 3, and 6% higher in level 4. The high value in level 4 can however again be a result of the low number of data points. While the mean values thus show better performance for three difficulty levels with active *ThirdEye*, direct comparisons between inactive and active *ThirdEye* do not result in statistical significances, due to large variances. These variances are a result of the substantial fluctuations in operator performance that were observed during the experiments.

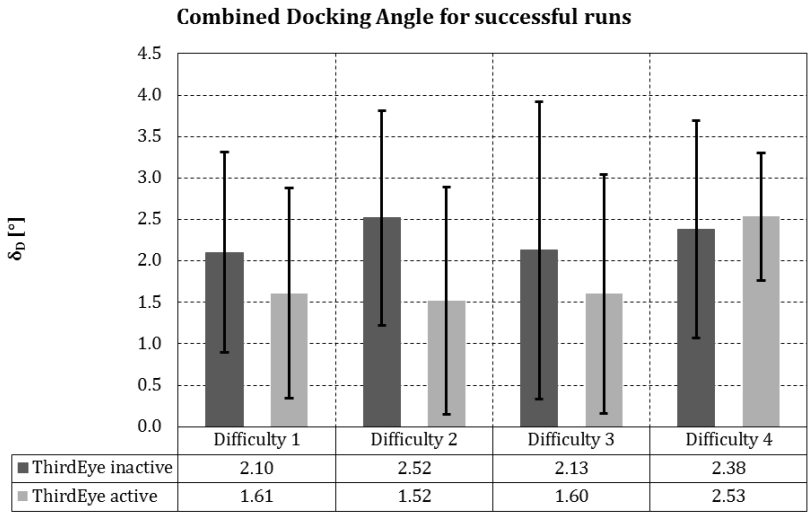

Figure 8-17: Combined docking angles over ThirdEye activity. Docking precision is better with active ThirdEye at difficulty levels 1 – 3. At level 4, the precision with active ThirdEye is slightly lower than with inactive ThirdEye. Whether this is a real effect of just result of the high uncertainties in this dynamic scenario cannot be stated with certainty, due to the small number of data points available.

Table 8-11: Combined docking angle evaluation for ThirdEye activity. The low number of data points (n = 2) for active ThirdEye at difficulty level 4 does not allow testing for normal distribution, nor meaningful comparison between operator performance with or without ThirdEye.

Level	ThirdEye status	Min [°]	Max [°]	Median [°]	Mean [°]	Standard Deviation [°]	Distribution normal	Variances equal	Comparison test	Difference significant
Difficulty 1	inactive	0.4	4.4	2.1	2.1	1.21	✓	✓	t-test	✗
	active	0.1	4.4	1.2	1.6	1.27	✓			
Difficulty 2	inactive	0.6	3.8	2.9	2.5	1.30	✓	✓	t-test	✗ p = 0.0611
	active	0.2	4.8	1.1	2.5	1.37	✓			
Difficulty 3	inactive	0.5	4.6	1.7	2.1	1.79	✓	✓	t-test	✗
	active	0.0	2.8	2.5	1.6	1.44	✓			
Difficulty 4	inactive	0.6	3.8	2.6	2.4	1.31	✓	n/a	u-test	✗
	active	2.0	3.1	2.5	2.5	0.77	✗			

8.4.5 Approach Efficiency

Docking efficiency is measured in the three metrics translation velocity change Δv, rotation rate change $\Delta\omega$, and task completion time T_D. While Δv and $\Delta\omega$ have direct influence on the propellant

and energy consumption for the docking approaches, T_D has impact on mission planning and the selection of the communication architecture.

Figure 8-18 and Table 8-12 show the **translation velocity change** data. No clear trend is visible in the data plots. The pairwise comparisons also do not yield significant differences. The peak at difficulty level 3 can be attributed to one participant requiring multiple approach and collision avoidance maneuver in order to complete the docking attempt.

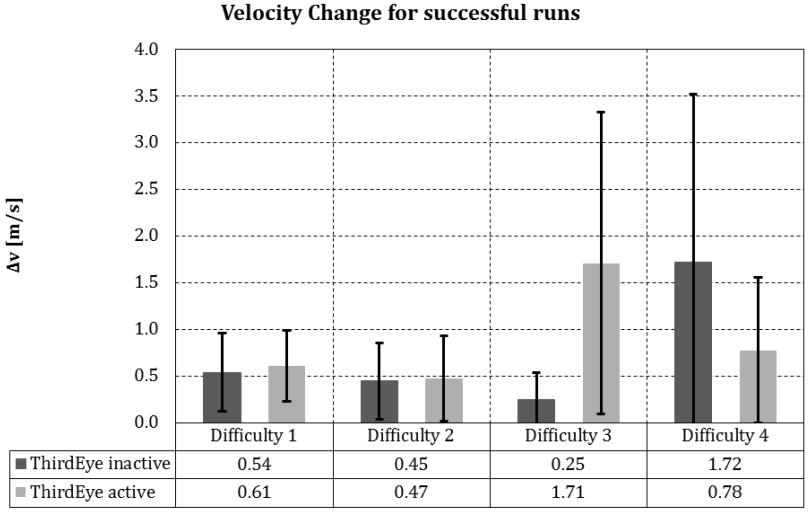

Figure 8-18: Total translation velocity change over ThirdEye activity. No clear trend in ThirdEye impact is evident. The high peak at difficulty level 3 is due to one participant requiring multiple approaches and collision avoidance maneuvers in order to complete one docking attempt.

Table 8-12: Translation velocity change evaluation for ThirdEye activity. The low number of data points (n = 2) for active ThirdEye at difficulty level 4 does not allow testing for normal distribution, nor meaningful comparison between operator performance with or without ThirdEye.

Level	ThirdEye status	Min [m/s]	Max [m/s]	Median [m/s]	Mean [m/s]	Standard Deviation [m/s]	Distribution normal	Variances equal	Comparison test	Difference significant
Difficulty 1	inactive	0.20	1.54	0.42	0.54	0.38	✓	n/a	u-test	✗
	active	0.12	2.55	0.38	0.61	0.64	✗			
Difficulty 2	inactive	0.11	0.94	0.41	0.45	0.25	✓	✓	t-test	✗
	active	0.14	0.86	0.46	0.47	0.23	✓			
Difficulty 3	inactive	0.11	0.31	0.29	0.25	0.09	✓	✗	u-test	✗ p = 0.0556
	active	0.25	3.87	1.62	1.71	1.44	✓			
Difficulty 4	inactive	0.28	3.00	1.80	1.72	1.14	✓	n/a	u-test	✗
	active	0.26	1.30	0.78	0.78	0.73	✗			

The data for **rotation rate change** (Figure 8-19 and Table 8-13) is inconclusive as well. The peak at difficulty level 3 is also the result of the multiple collision avoidance maneuvers of a single participant.

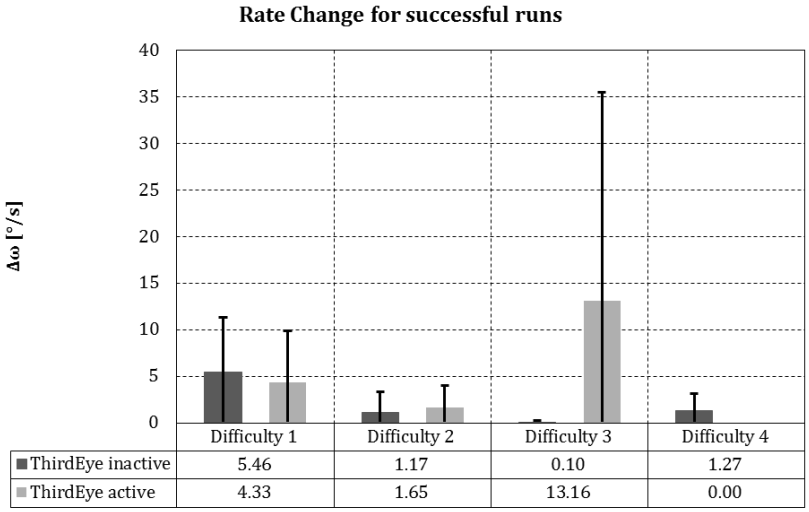

Figure 8-19: Total rotation rate change over ThirdEye activity. No conclusive trend is visible in the data. The peak at difficulty level 3 is the result of a participant requiring multiple collision avoidance and reorientation maneuvers.

Table 8-13: Rotation rate change evaluation for ThirdEye activity. The low number of data points (n = 2) for active ThirdEye at difficulty level 4 does not allow testing for normal distribution, nor meaningful comparison between operator performance with or without ThirdEye.

Level	ThirdEye status	Min [°/s]	Max [°/s]	Median [°/s]	Mean [°/s]	Standard Deviation [°/s]	Distribution normal	Variances equal	Comparison test	Difference significant
Difficulty 1	inactive	0.7	22.3	3.4	4.4	5.85	✗	n/a	u-test	✗
	active	0.7	23.2	2.9	4.3	5.57	✗			
Difficulty 2	inactive	0.0	5.8	0.0	1.2	2.19	✓	✗	u-test	✗
	active	0.0	6.8	0.0	1.7	2.42	✓			
Difficulty 3	inactive	0.0	0.3	0.1	0.1	0.12	✓	✗	u-test	✗
	active	0.0	52.0	1.0	13.2	22.40	✓			
Difficulty 4	inactive	0.0	3.9	0.6	1.3	1.84	✓	n/a	u-test	✗
	active	0.0	0.0	0.0	0.0	0.0	✗			

The data for task completion time is provided in Figure 8-20 and Table 8-14. The plot shows that with active *ThirdEye*, the operators required on average 99% - 235% longer to complete the docking approaches in difficulty levels 2 & 3, compared to inactive *ThirdEye*. This is attributed to the

additional amount of information the participants had about relative position and attitude. With active *ThirdEye*, a number of approaches were aborted by the participants when the additional video data provided by the *ThirdEye* led them to conclude that they would not be able to successfully complete the docking. However, the understanding of the situation provided by the *ThirdEye* was oftentimes flawed, meaning that participants concluded that the approach would fail and aborted, although they could have achieved successful docking. Without *ThirdEye* and the additional visual information, participants complete a higher number of approaches on the first attempt, which led to reduced precision and lower success rates.

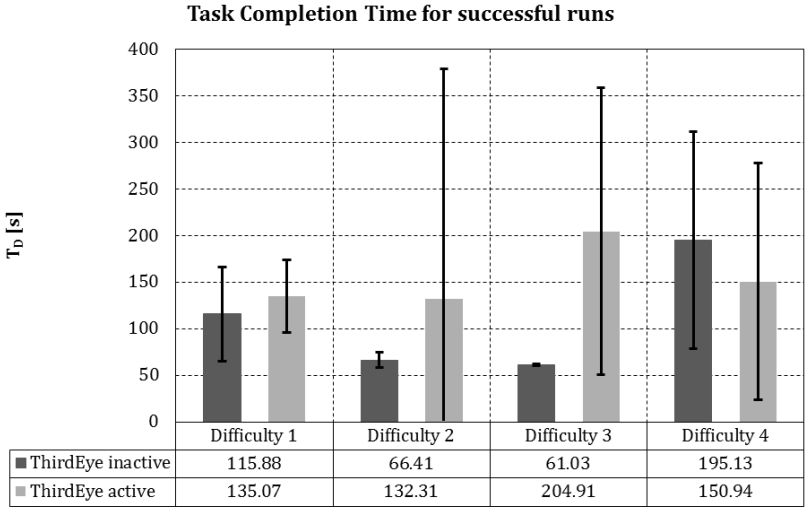

Figure 8-20: Task completion times over ThirdEye activity. ThirdEye use mostly results in increased task completion times.

Table 8-14: Task completion time evaluation for ThirdEye activity. The low number of data points (n = 2) for active ThirdEye at difficulty level 4 does not allow testing for normal distribution, nor meaningful comparison between operator performance with or without ThirdEye.

Level	ThirdEye status	Min [s]	Max [s]	Median [s]	Mean [s]	Standard Deviation [s]	Distribution normal	Variances equal	Comparison test	Difference significant
Difficulty 1	inactive	51.5	232.0	119.9	115.9	50.47	✓	✓	t-test	✗
	active	72.4	192.3	135.9	135.1	39.39	✓			
Difficulty 2	inactive	52.8	82.7	66.8	66.4	8.35	✓	n/a	u-test	✗
	active	45.3	915.1	62.5	132.3	246.73	✗			
Difficulty 3	inactive	59.8	62.4	61.0	61.0	1.08	✓	✗	u-test	✗
	active	60.0	431.0	232.1	204.9	154.23	✓			
Difficulty 4	inactive	59.5	330.0	195.5	195.1	116.25	✓	n/a	u-test	✗
	active	60.8	241.1	150.9	150.9	127.46	✗			

8.5 Learning Effects

The *ThirdEye* evaluation experiments were intentionally conducted with **inexperienced** test participants. The analysis showed in Section 8.3 showed that operator learning during the experiment runs had no effect on the results, due to the alternating sequence of *ThirdEye* active/inactive scenarios between the test participants, and the randomized sequence of scenario difficulty levels.

The high variance in the operator performance data evident in the statistical analysis discussed in Section 8.4 suggests that (1) there exist substantial performance differences between individual operators, based on their **individual skills** in perception, motion recognition and spatial modeling, as well as in their grasp of the multi degrees-of-freedom control using the joystick, and that (2) the performance of each operator is **highly variable**, resulting in substantial differences even between similar or identical simulation runs.

In order to provide an indication of the development of operator performance with growing experience and also to determine whether the use of the operator support tools *Proximity Operations HUD* and *ThirdEye* have actual impact on the learning curve of an operator, a learning curve study was run. Its details and results will be discussed in the following sections.

8.5.1 Experiment Design

In the learning curve study, three operators were tasked to repeatedly complete a set of three scenarios designed to train them in all aspects of spacecraft maneuvering during final approach and docking. The study covered a period of ten experiment days per operator, which were scheduled as consecutively as possible (see below).

Each operator had a different level of operator support available. **Operator I** was tasked to fly all approaches without any operator support system, thus relying only on the video data from the chaser primary camera. **Operator II** was using the attitude display and trajectory prediction display of the *Proximity Operations HUD*. **Operator III** had the full *ThirdEye Situation Awareness Enhancement System* available and thus the combination of the HUD and the secondary camera.

At the end of every second experiment day, each operator was confronted once with a **fourth scenario** more difficult than the training scenarios. The operators' performance in the fourth scenario indicates how well training scenarios with nominal situations and low and medium difficulty levels prepare for off-nominal and difficult situations. A fourth operator served as benchmark for the performance in this fourth scenario. **Operator IV** thus practiced this scenario on every experiment day using all three levels of operator support.

All four operators were male research associates at the Institute of Astronautics. They were all familiar with the approach and docking task, as well as with the simulation system, from the first *ThirdEye* pilot experiment series.

Experiment Schedule

The total duration of the learning curve study was 24 days. Over the course of the study, each operator ran the identical set of scenarios three times per day for a total of ten days. The plan was to have each operator fly every day, only interrupted by one weekend. Due to scheduling problems with the participants and due to limited availability of the RACOON laboratory, the final schedule covered a span of over three weeks (see Table 8-15).

Table 8-15: Experiment schedule for the learning curve study. Green shading indicates the individual participant flew one complete test series on that day. The crosses show the days on which the fourth experiment scenario was included.

Day	1	2	3	4	5	6	7	8	9	10	11	12	13	14	15	16	17	18	19	20	21	22	23	24
Operator I	■		✖						■	✖	■				✖		✖		✖					
Operator II	■	✖		■				✖	■	✖					■	✖	■	✖						
Operator III	■	✖						■	✖	■	✖			■				■				✖	■	✖
Operator IV		✖	✖					✖	✖	✖	✖			✖	✖	✖	✖							

Experiment Scenarios

The scenarios were designed to cover all aspects of spacecraft proximity maneuvering and to show a gradual increase in difficulty.

Scenario 1 included lateral and angular misalignment of the target, and non-zero initial relative velocity along the V-bar. **Scenario 2** had target lateral and angular misalignment combined with a low target yaw rotation rate, non-zero relative motion along the R-bar, and non-zero chaser pitch angle. In **scenario 3**, the target featured lateral and angular misalignment plus a medium rotation rate; the chaser had a non-zero yaw-angle, which was furthermore drifting at a low rate. In all three training scenarios, **lighting** was provided from the chaser's 4 o'clock position.

In the non-training **scenario 4**, target lateral and angular misalignment, target rotation, initial relative velocity along V-bar and R-bar, and chaser attitude drift in both pitch and yaw were combined. The position of the **simulated sun** was furthermore changed to a 1 o'clock position. The target side facing the chaser was thus in shadow, which was compensated by a small lamp, mounted on the chaser. The docking target was nonetheless difficulty to discern against the dark background. When the chaser moved far enough to the sides of the target to leave its shadow, the primary camera was largely blinded by solar lighting. The operating conditions in scenario 4 were thus substantially **more difficult** than the training scenarios.

Table 8-16 provides the characteristics of the learning curve experiment scenarios.

Table 8-16: Experimental scenarios for the learning curve study. The table provides the initial spacecraft states for chaser and target, as well as initial relative position and velocity.

Scenario	Position [m]		Relative velocity [m/s]		Chaser attitude [°]		Chaser attitude rate [°/s]		Target yaw angle [°]	Target yaw rate [°]	Signal roundtrip delay [s]
	x	y	x	y	pitch	yaw	pitch	yaw			
Difficulty 1	-5	-0.5	0.1	0	0	0	0	0	20	0	~ 0.7
Difficulty 2	-3	3	0	0.1	5	0	0	0	-80	1	
Difficulty 3	-2	0.25	0	0	0	-15	0	0.5	100	-2	
Difficulty 4	-2	-1	0.05	-0.1	0	0	0.2	0.1	-60	2	

8.5.2 Expected Learning Curves

The general development of operator performance expected to be seen in the learning curve study is shown in Figure 8-21. A learning curve in general features a **steep performance rise** at the beginning of training, followed by horizontal region of almost constant **peak performance**. These two segments of the curve can be represented by a potential function.

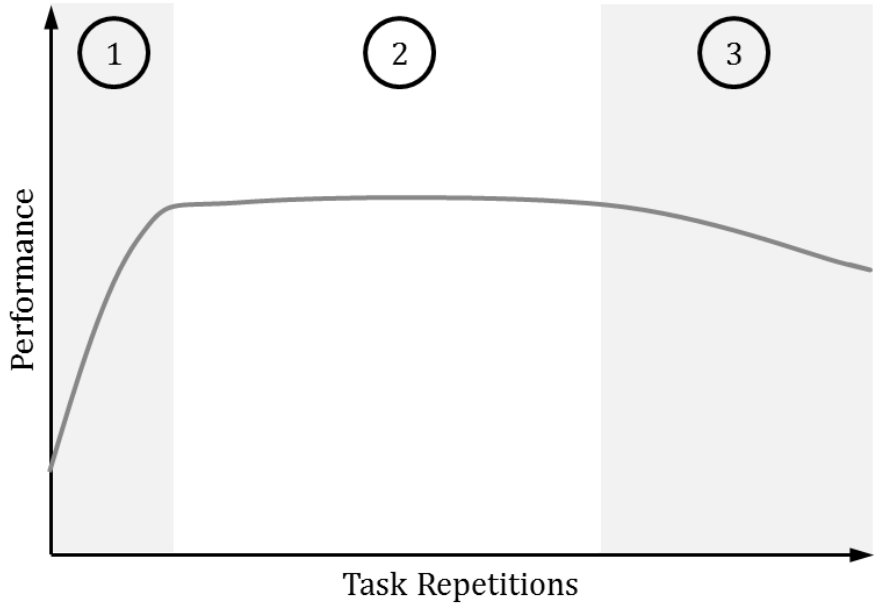

Figure 8-21: General learning curve showing the development of task performance over the number of task repetitions. At the beginning of operator training (segment 1), the performance rises steadily from its initial value until it reaches an almost constant maximum (segment 2). After a certain number of task repetitions, the operator becomes bored or annoyed by the task and the performance decreases (segment 3).

After a certain number of task repetitions, the operators grow bored or annoyed with the task, which decreases their motivation and concentration and thus also their performance. The onset of this **downward slope** of the performance curves depends on numerous factors, including the complexity of the task, and operator frustration and motivation.

The long-term performance development in the final approach and docking task is expected to follow this general learning curve. A number of **differences** between the operators and thus the levels of operator support provided to them should however become evident. These differences are expected to become evident in the **initial performance** and in the **slope** of the initial learning curve segment. With enough training, every operator should be able to reach a **similar maximum** performance level, although the initial and maximum precision, safety and efficiency of operator II (using the *Proximity Operations HUD*) is expected to be higher compared to operator I (no support system). Based on the results of *ThirdEye* performance in Section 8.4, operator III is expected to show the highest success rates and docking precision compared to the other operators, both in initial and maximum values, and the steepest slope of the learning curve. The **downward slope** of the learning curve associated with operator boredom and annoyance is not expected to be reached, due to the high complexity of the docking scenarios, and to the high motivation of the test participants.

8.5.3 Learning Curve Evaluation

The learning curves of the operators are compared in five performance criteria: (1) approach success, (2) operator situation awareness and task load, (3) docking precision, (4) docking safety, and (5) approach efficiency. As in Section 8.4, an approach was considered successful if the docking probe hit the target plate within the target rocket nozzle, and if the total relative angle at docking contact was smaller than 5°.

Since segments 1 and 2 of a learning curve can be represented by a potential function, trend lines following potential functions are laid through the data points of the individual operator performance plots. The resulting curves are considered to represent the learning curves of the individual operators in the given evaluation criteria.

Approach Success

Figure 8-22 shows the approach success rates development over the experiment days for the training scenarios 1 through 3. In all scenarios, the three performance curves approach a common maximum, which decreases with rising scenario difficulty. Operator III using the *ThirdEye* shows consistently higher performance in scenarios 1 and 3, while operator II using the HUD has better initial performance in scenario 2. The unexpected result is that operator I, working without any operator support tool, shows the biggest learning effect, which allows reaching the performance of the other operators towards the end of the experiment series. Also of note in the plot is the high fluctuation in the performance of all operators in scenarios 2 and 3. Even with increasing experience, the opera-

tors are mostly not able to hold a consistent level of performance. This fluctuation, which is also evident in the data plots for the other evaluation criteria, is an explanation for the high variances encountered in the *ThirdEye* evaluation experiment.

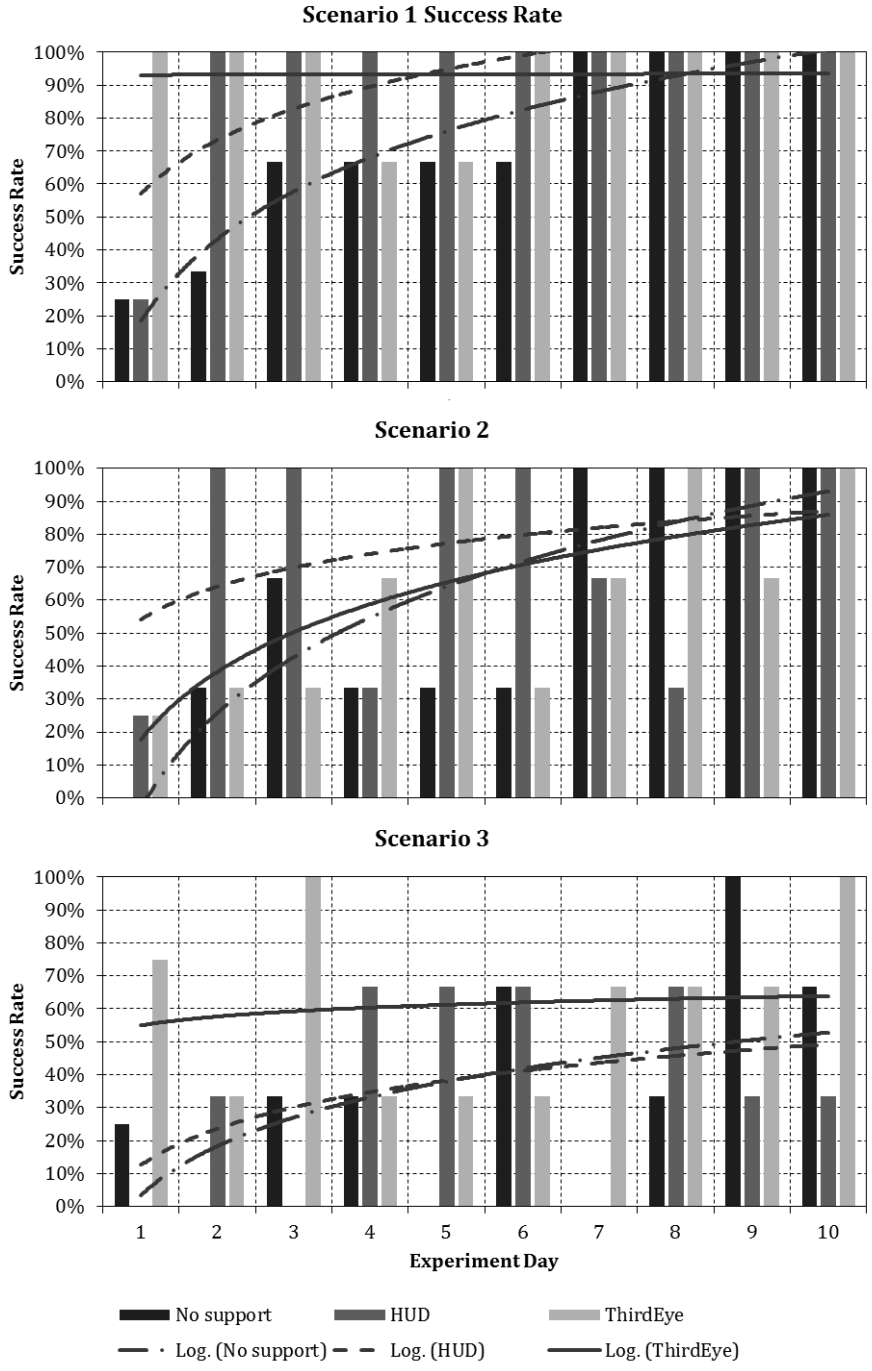

Figure 8-22: Approach success rates for learning curve scenarios 1 through 3. In all three scenarios the performance curves approach a common maximum, which decreases with rising scenario difficulty. Operator III using the ThirdEye shows consistently better performance in scenarios 1 and 3, while operator II using HUD only has better initial performance in scenario 2. Of note is the high variance in the performance of all operators in scenarios 2 and 3.

The success rates for scenario 4 are provided in Figure 8-23. The bar chart for operator I through III is overlain with the mean success rates of benchmark operator IV. Of note are the low success rates of operator I and II, who only managed to successfully complete 1 approach of 5 over the experiment series. If their learning followed the expected learning curve, both would be expected to be successful in their final approach. However, while operator I showed this behavior, operator II was successful on experiment day 6, in the middle of the series. Operator III, on the other hand, consistently showed good performance, with 80% successful approaches. The failed approach was on day 6 and thus represents a fluctuation in performance rather than an indication of learning effects. Large performance fluctuations are again evident in the data for operator IV, over which a slight learning effect can be discerned. Use of the *ThirdEye* allows the highest mean success rate.

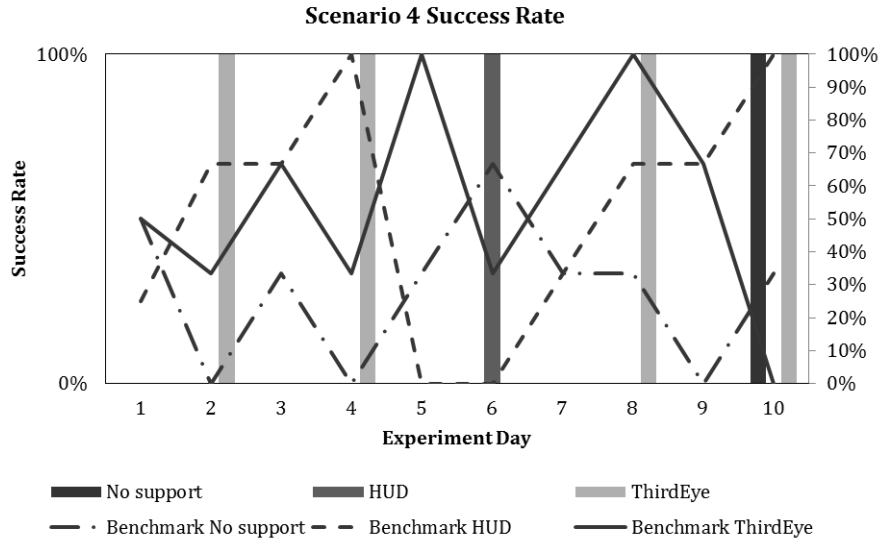

Figure 8-23: Approach success rates for learning curve scenario 4. The red lines show the development of the success rates of the benchmark operator. Of note are the low success rates of operators I and II, as well as the fluctuations in the performance of the benchmark operator. The ThirdEye allows the highest consistent success rates.

Operator Situation Awareness and Task Load

As in the *ThirdEye* evaluation experiments, operator situation awareness and task load was measured by the SART and TLX questionnaires. The questionnaires were not issued after every training flight, but only after the final flights for each scenario on each experiment day. Growing experience in the scenarios was expected to result in a steady rise in situation awareness, thus rising SART scores. Connected to the rise in operator SA, the task load and hence the TLX score was expected to decrease with time.

For the following plots and the associated learning curve trend lines, SART and TLX scores of both successful and unsuccessful approaches were used.

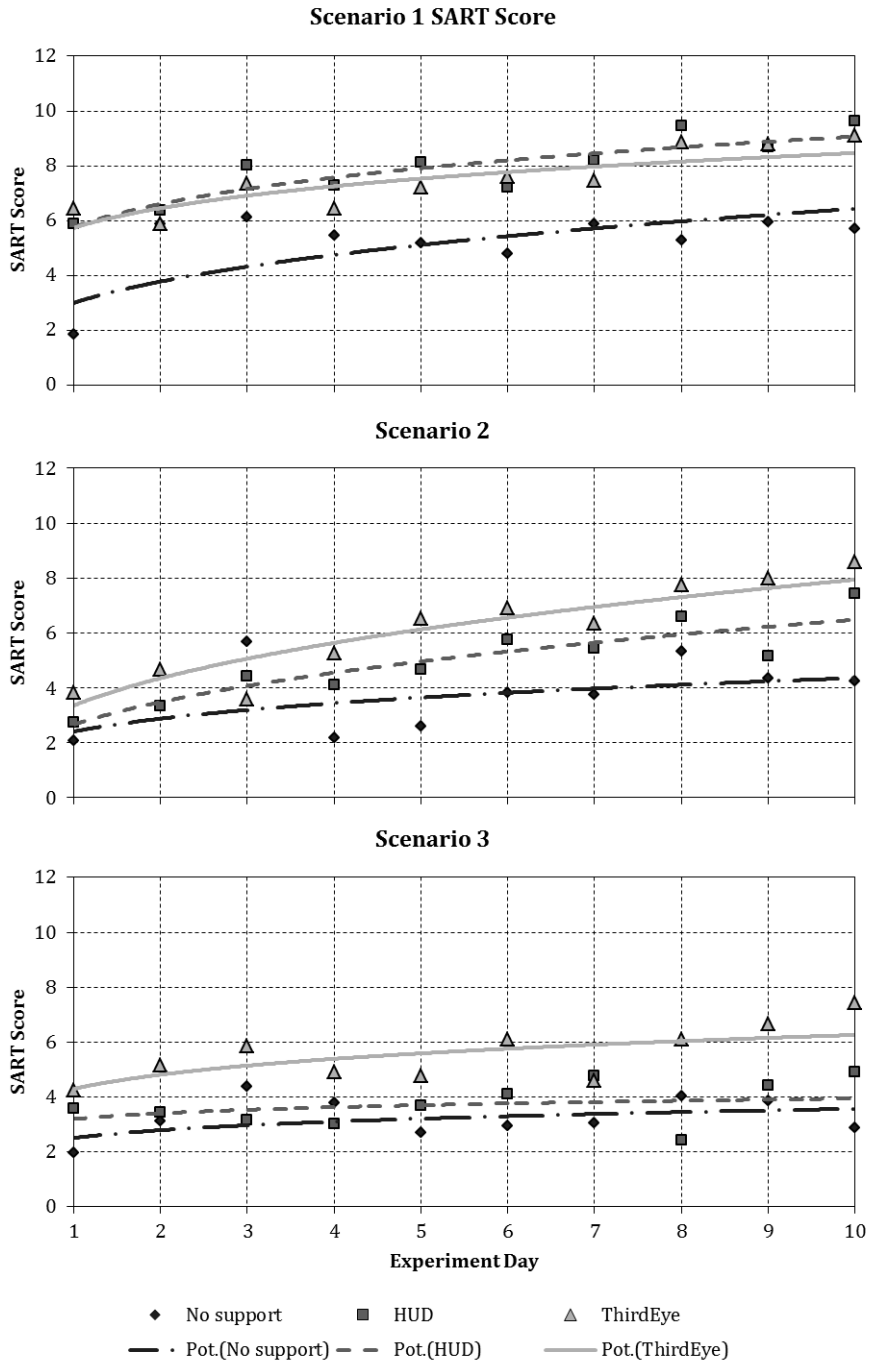

Figure 8-24: SART scores for learning curve scenarios 1 through 3. For all operators, situation awareness increases steadily with experiment time. Except for scenario 1, situation awareness with the ThirdEye is consistently highest, while the operator without support tool shows lowest SA. While the slopes of the learning curves are similar, the curves do not converge towards a common value within the time frame of the study.

The **SART scores** for scenario difficulties 1 through 3 shown in Figure 8-24 follow the expected trend. Except for scenario 1, operator situation awareness is highest for the *ThirdEye* user, and

consistently lowest for operator I without support. The SART scores for operator I also have the highest fluctuations throughout the experiment series.

In scenario 1, operators I and II show roughly the same SART scores, although the learning curve for the HUD user is slightly steeper. Overall, the learning curves for all operators show similar slopes, but they do not seem to converge within the time frame of the study. They rather appear to approach parallel maximum values or even to diverge with time, which indicates a lasting difference between the different operator support systems, with the *ThirdEye* showing the highest SART score level. This apparent trend is however not certain, since the data is only based on three participants, which does not allow secure statistics.

In scenario 4 (see Figure 8-25), the SART scores of operator II and operator III show the expected learning curves and apparently converge towards the level of operator III with *ThirdEye* support. While the nearly linear trend line for operator II does not match the approach success statistics, the fact that the highest SART score is evident for the only successful approach on day 6 shows the correlation between SART score and task success. This is not valid for operator I, whose SART trend line shows a continuous downward slope although the only successful approach occurred on day 10.

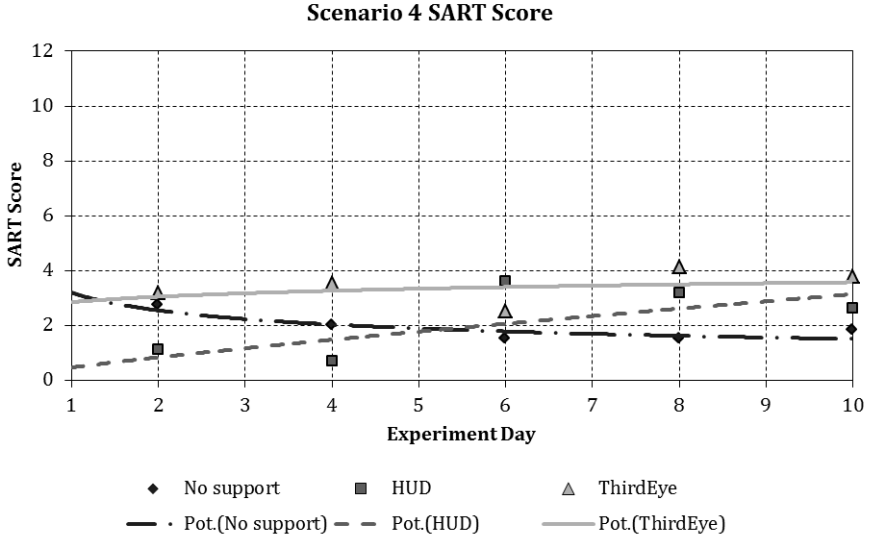

Figure 8-25: SART scores for learning curve scenario 4. The ThirdEye and HUD users show an increase of situation awareness with experience and appear to converge towards a common maximum. Their SART scores generally correlate with their approach success statistics. Operator II only was successful on day 6. Here the SART score is highest. Operator III was unsuccessful on day 6, which is accompanied by the lowest SART score. Operator I without support tools professes a decrease in situation awareness over time. The lowest SART score occurs on day 10, which coincides with the only successful approach. There therefore exists no correlation between SART score and task success for operator I.

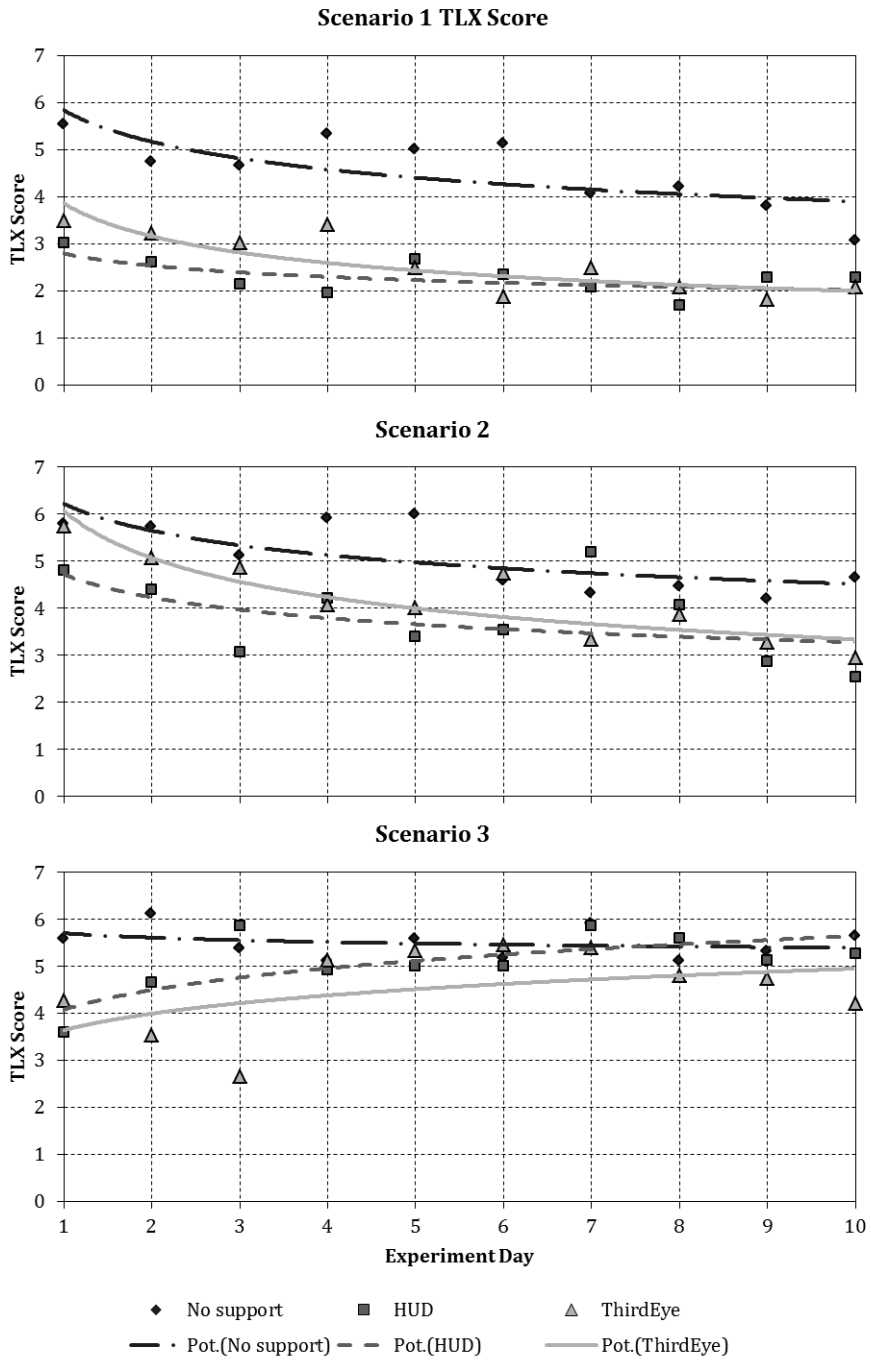

Figure 8-26: TLX scores for learning curve scenarios 1 through 3. The TLX curves in scenarios 1 and 2 follow the expected trend. The highest TLX scores and the highest fluctuation between the experiment days are evident for operator I without support tools. Operator II initially professed lower task load than operator III, their trend lines however converge towards the end of the experiment series. Different trends are visible in scenario 3. The TLX scores of operator I remain highest and show only a slight downwards tendency. Operators II and III profess a growth in task load between experiment days, although the data spread for operator III is too big to draw secure conclusions.

The **TLX score** data provided in Figure 8-26 in general shows the expected development. In scenarios 1 and 2, the trend in TLX scores is to decrease with operator experience. Operator I (no support)

consistently shows the highest task load but also the highest fluctuation between experiment days. Operator II initially starts out lowest, but the initially steeper learning curve of operator III leads the two trend lines to converge towards the end of the experiment series. The spread in the data grows with scenario difficulty. In scenario 3, the general trend of decreasing task load with growing experience is turned around. While operator I still follows this trend at a high level of TLX scores, operators II and III show rising task load with growing experience. No explanation could be found for this development. The large fluctuations evident in the data for operator III correlate closely with the fluctuating approach success rates (compare Figure 8-22).

Similar trends are visible in the data for scenario 4 (see Figure 8-27). In this scenario, operator II professed steadily decreasing TLX score, although only the approach on day 6 was successful. Operators I and III show almost constant TLX scores. The maximum for operator III occurs with his only failed approach, as would be expected.

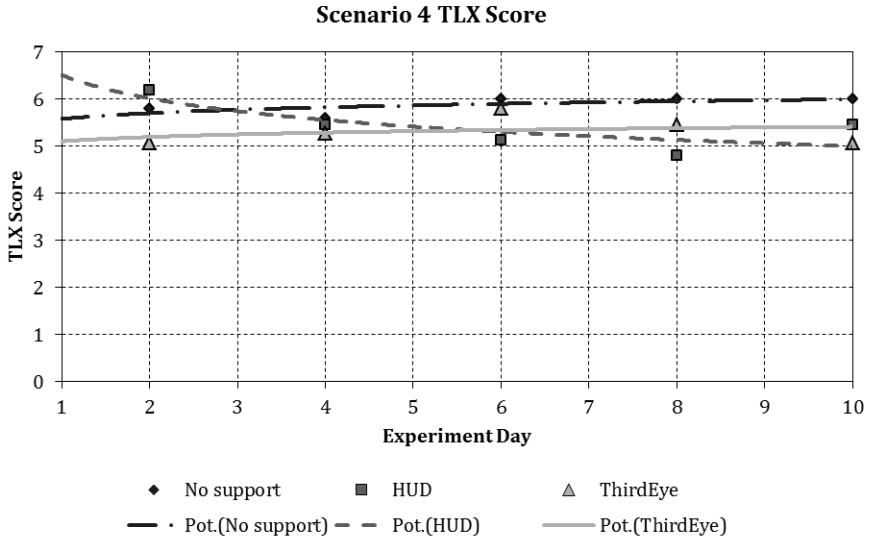

Figure 8-27: TLX scores for learning curve scenario 4. Operators I and III have almost constant TLX scores. The maximum task load of operator III occurs with the only failed approach. Operator II shows a steady decrease in TLX score, which does not correlate with approach success.

Docking Precision

The precision of the docking approaches is measured in the **combined docking angle** δ_D. The development of δ_D over the experiment series for scenarios 1 through 3 is provided in Figure 8-28, for scenario 4 in Figure 8-29.

On first glance, Figure 8-28 shows the expected behavior of docking precision increasing over time, with the *ThirdEye* operator showing superior performance over operator I and II. Of particular note, however, is the spread in the data sets for each operator. The variance between and within experiment days is often larger than the difference in mean values between first and last experiment days. Operator I shows particularly large standard deviations within experiment days, while the *ThirdEye* operator III has the biggest fluctuations between experiment days. The individual

performance of an operator therefore depends more on factors like timing, coordination and momentary concentration, than on large-scale training effects. These factors are difficult to quantify and also difficult to be addressed in operator training.

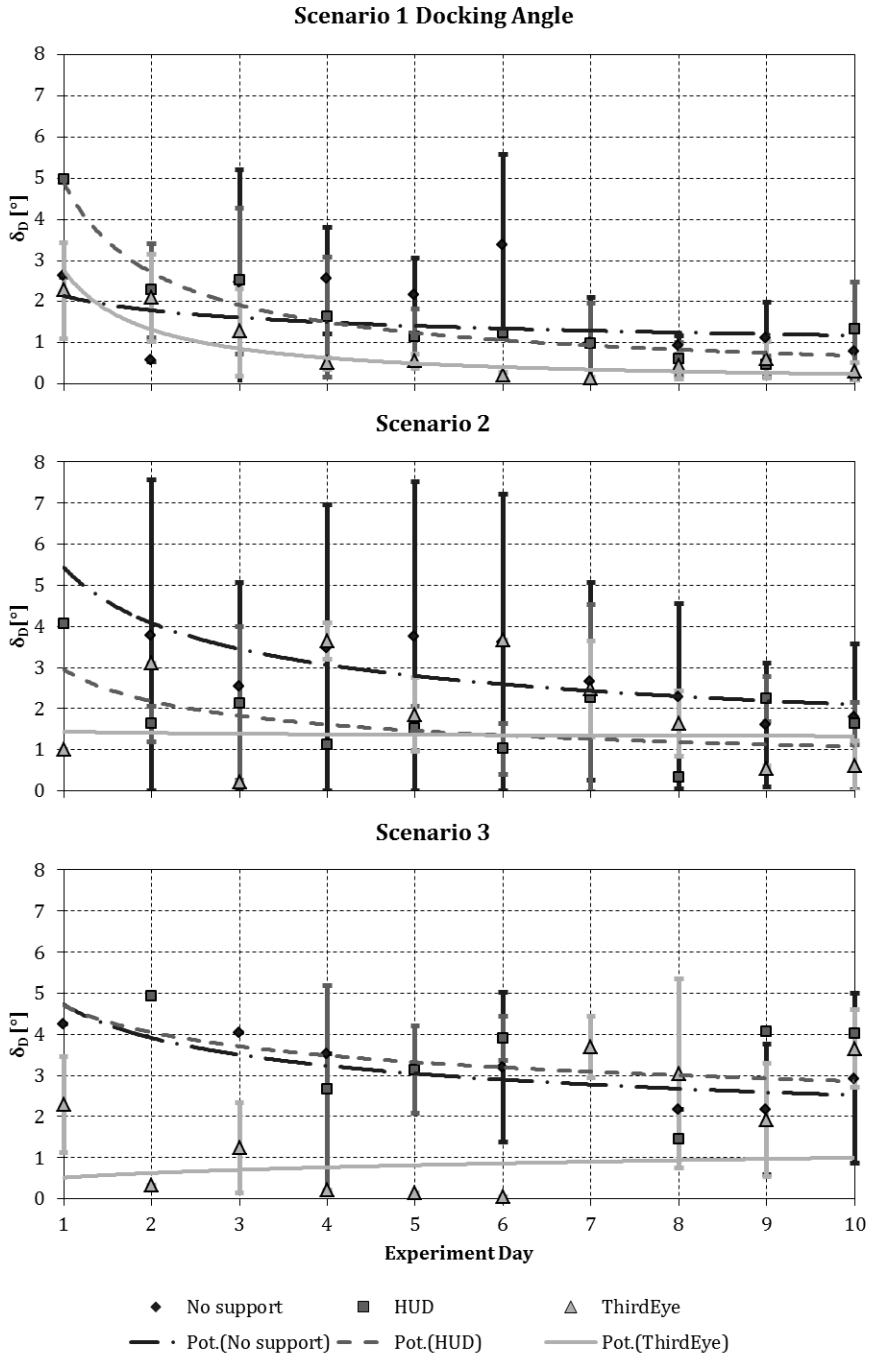

Figure 8-28: Docking angles for learning curve scenario 1 through 3. The plots confirm the expectation that operator performance increases with experience, and that the ThirdEye operator shows superior performance compared to no support and HUD only. Of particular note is the high fluctuation in the data sets of all operators, both between and within experiment days.

Large variances are also visible in the data of benchmark operator IV in Figure 8-29. The main information from this plot is that operator III was able to approach the performance of operator IV towards the end of the experiments series. This implies that the continuous training in standard situations allows an operator to reach a level of performance similar to an operator experienced in the off-nominal situation. An operator training program for any operational mission can therefore focus on training scenarios with standard situation elements and only requires occasional off-nominal situations for operator testing.

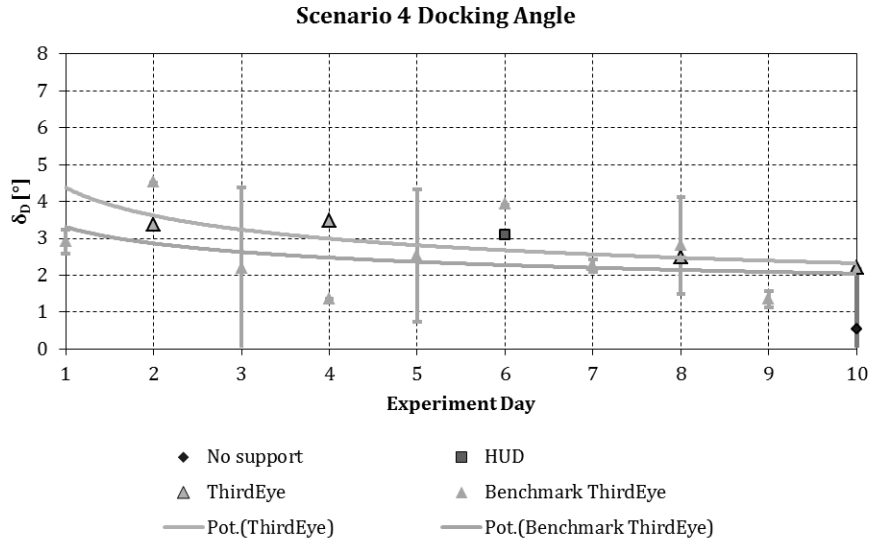

Figure 8-29: Docking angles for learning curve scenario 4. The single success each for operator I and operator II does not allow the generation of any trend line. The performance curve for operator III approaches the trend line for the benchmark operator IV. This implies that the continued training in standard situations allows the operator to increase the performance to reach similar levels to an operator experienced in the off-nominal situation. Of note is again the spread in performance, this time for the benchmark operator.

Docking Safety

The safety of the docking approaches is represented by the absolute contact velocity v_C. The lower v_C, the lower the probability of the target suffering damage at docking contact. The contact velocity furthermore serves as an indicator for the timing of the approach, as operators tend to finish an approach with high relative velocity if their timing was corrupted during the approach. The contact velocity curves for scenarios 1 through 3 (see Figure 8-30) show the expected trends in the data for operators I and III, with the contact velocity with *ThirdEye* use being substantially lower than without any support tool. The trend lines of operators I and II clearly show the expected training effects. The performance of operator II, however, decreases with growing experience. This trend cannot be explained from approach success, SART and precision data. The operator commented on the data that he felt more confident in his maneuvering with increasing experience, and that this emboldened him to approach the target with higher relative velocities. Besides the anomalous development of operator performance for operator II, the plots again serve to visualize the large spread in performance data points, both as variance within experiment days (particularly in scenario 1), and

as fluctuation between experiment days (scenario 2). These outliers highlight the dependence of total performance during an approach on timing and concentration issues.

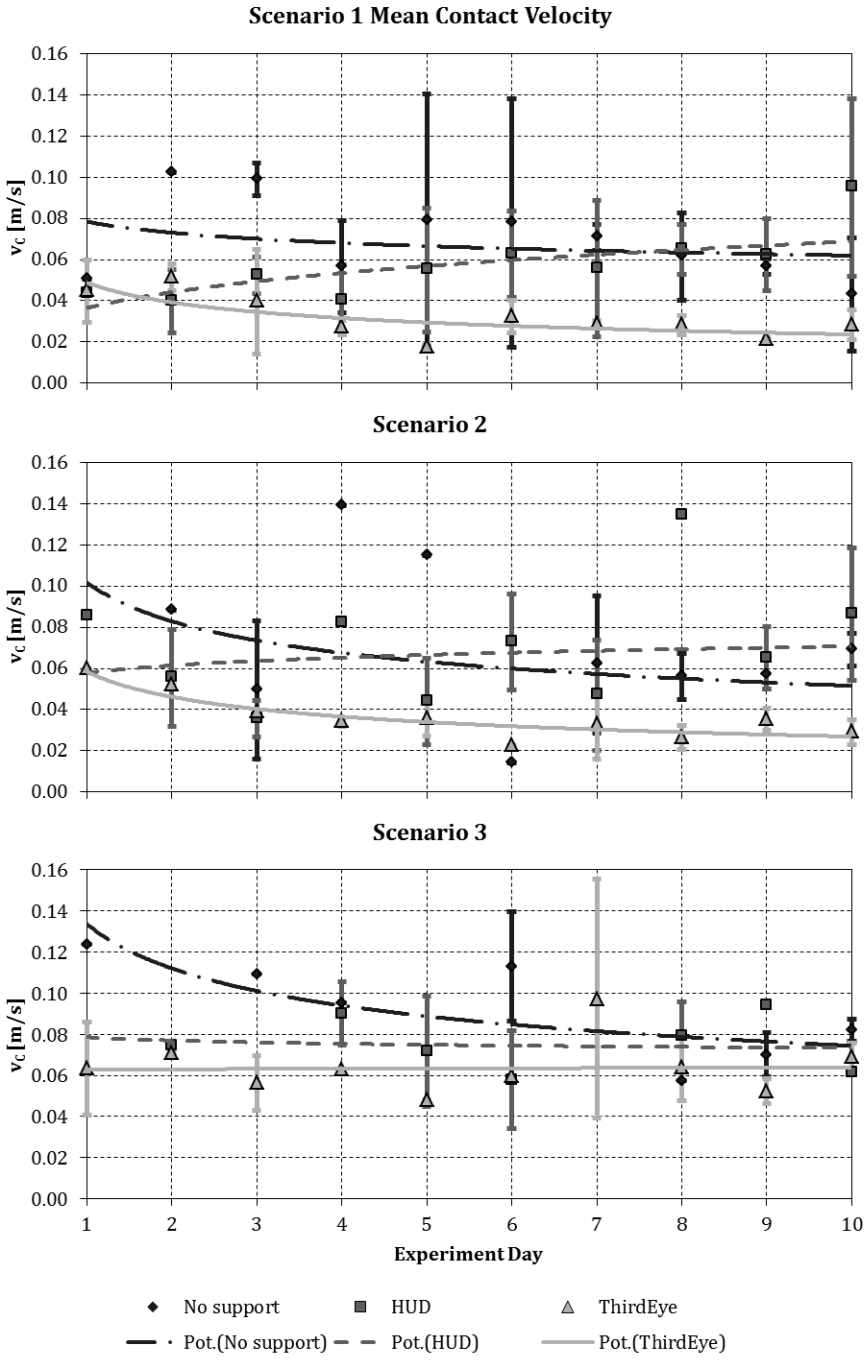

Figure 8-30: Contact velocity for learning curve scenarios 1 through 3. The general trend of performance increase with experience is again visible. The ThirdEye operator shows superior performance throughout the experiment series. The decrease of the performance of operator II cannot be explained based on the other data sets. Also note the high variance for individual experiment days in scenario 1, and the high fluctuation between experiment days in scenario 2.

The data for scenario 4 in Figure 8-31 shows that the mean contact velocities achieved by operator III using the *ThirdEye* were lower than those of the benchmark operator. It also again highlights the wide spread in data points.

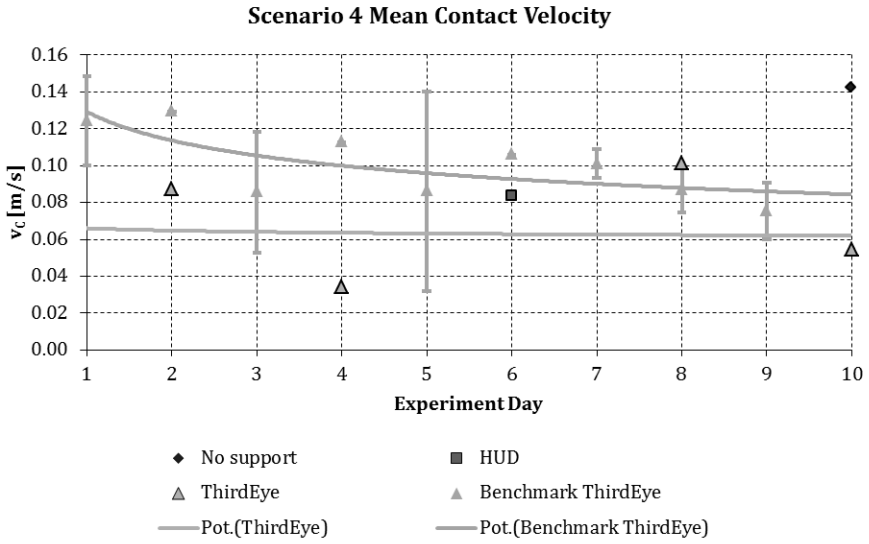

Figure 8-31: Contact velocity for learning curve scenario 4. Note the wide spread in the data points for both the ThirdEye operator and the ThirdEye benchmark operator. The performance of operator III is nonetheless consistently better than that of benchmark operator IV. Individual skills in a task are therefore more important than training effects.

Approach Efficiency

The total velocity change Δv during an approach represents the approach efficiency. While Δv depends on the distance to be bridged by the chaser from initial position to contact and on the time window created by the rotating target, it also depends largely on the number of trajectory correction maneuvers commanded by the operator. The operators using the HUD and the *ThirdEye* have more information available about the relative position and are thus incited to command more correction maneuvers than the operator without support tools. This results in the higher trend line values in Figure 8-32. Operator I, without operator support, controlled the approaches based more on intuitive understanding of the situation rather than on precise knowledge and thus with less trajectory corrections.

The level of the performance curve therefore depends largely on the individual skills of the operator. Once the scenario becomes challenging enough so as to overwhelm the operator's intuition, the HUD and *ThirdEye* operators achieve superior performance, as can be seen in the plot for scenario 3. The plots also show that the performance variance within individual experiment days can be as large as the training effect over the complete experiment series.

In scenario 4 (Figure 8-33), the development of Δv expenditure of the benchmark operator shows no training effect and very small fluctuations. Operator III manages to approach this performance

level steadily with experience. It is also of interest to note that the singular performances of operators I and II are also very close to this benchmark performance.

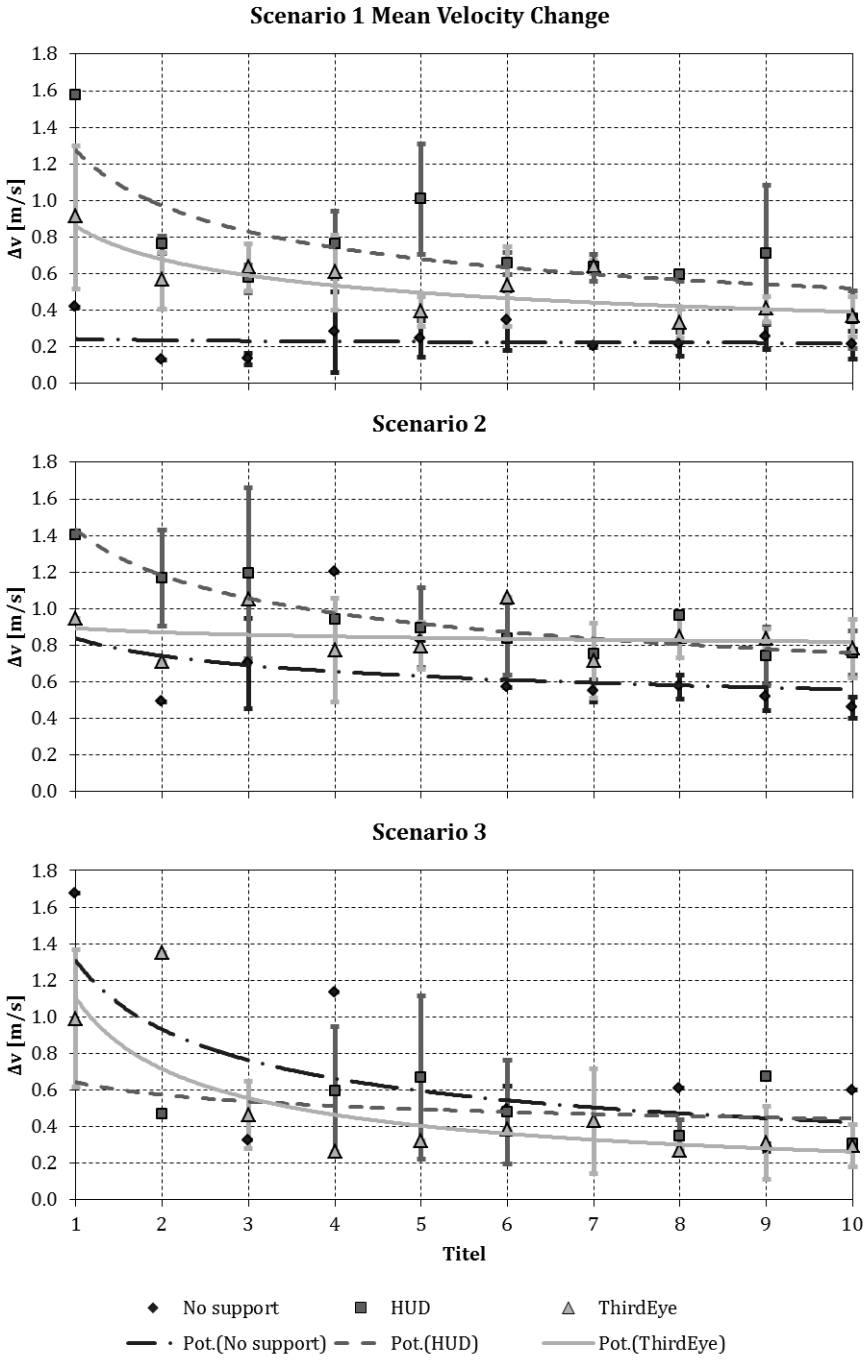

Figure 8-32: Approach velocity change for learning curve scenarios 1 through 3. In the less-challenging scenarios 2 and 3, the individual skills of operator I allowed him to control the approaches without large correction maneuvers, and hence with lower Δv than the HUD and ThirdEye operators. With rising difficulty, the scenario becomes too challenging for intuitive guidance, and the HUD and ThirdEye begin to achieve superior performance levels. The fluctuations between experiment days, as well as the variances within experiment days are substantial.

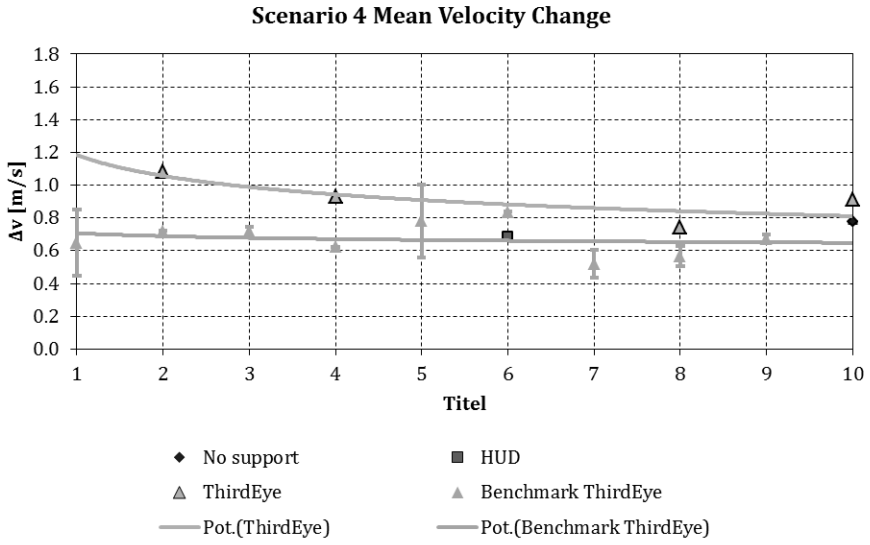

Figure 8-33: Approach velocity change for learning curve scenario 4. The commanded Δv by ThirdEye benchmark operator IV is almost constant throughout the experiment series. The learning curve of operator III approaches this benchmark level and is assumed to reach it with growing operator experience. Operator IV shows no consistent training effect.

8.5.4 Conclusions

The learning curve study confirmed the existence of differences in operator performance between no operator support, *Proximity Operations HUD*, and *ThirdEye Situation Awareness Enhancement System*. It also indicated that the magnitude of the performance differences depends on the **difficulty** of the task, on the **skills** of the individual operator, and on a number of other **internal and external factors** affecting performance. These individual factors include operator motivation and ambition, confidence levels, momentary concentration, and hand-eye coordination in translating visual information into maneuver commands. These factors are difficult to quantify even in questionnaires but can be observed during the experiment runs.

The **distinct learning curves** becoming evident in the evaluation of approach success, operator situation awareness and task load, docking precision, docking safety, and approach efficiency can ameliorate the initial performance differences over time, although not in all combinations of evaluation criteria and scenario difficulty level, and mostly not completely. The degree and also the direction of performance change over time again depend on task difficulty and individual factors. The impact of these individual factors becomes clear by the large **performance fluctuations** between experiment days, and by the substantial variances within the approaches flown during one experiment session. The performance fluctuations of an individual operator can thus be larger than differences between different operators, which is shown in the data collected and evaluated during the learning curve study. This explains the large fluctuations in the *ThirdEye* evaluation study, which in most cases prevented the experiment data from showing significant differences and thus conclusive results.

The learning curve study also showed that in being confronted with a scenario that is substantially more challenging than the training scenarios, and which is only flown every second experiment day, an operator – in this case the *ThirdEye* operator – is able to achieve a performance level similar to an operator trained in this off-nominal scenario. Repeated practice in realistic, nominal scenarios will thus prepare the operator for off-nominal situations. As the success rates in the "challenge" scenario for the operators using only the HUD or no support tool at all was significantly lower than for the *ThirdEye* operator, this suggests that the *ThirdEye* not only has impact on the performance of an operator, but also on the adaptivity in the face of off-nominal situations.

8.6 Summary

The *ThirdEye* evaluation study was conducted to **evaluate the effect of *ThirdEye* use on operator performance** and thus to confirm or refute the working hypothesis that the use of a flexible vantage point in addition to a spacecraft-fixed camera increases operator SA and thus operator performance.

During the study 20 participants completed a number of final approach and docking mission simulations, both with active and inactive *ThirdEye*.

The data accumulated during the experiment series showed that the four test scenarios have a **real difference in difficulty**, and that both **SART score and NASA-TLX score correlate with mission success/failure** and thus scenario difficulty. Further analysis also showed that the experiment **results are not blurred by training effects**. The countermeasures taken to that effect, namely alternating the sequence of *ThirdEye* active/inactive test runs between participants, and randomizing the scenario sequence between the runs, were thus proven to be effective.

The evaluation results of the *ThirdEye* system did not in all metrics meet expectations.

Approach success was higher with active *ThirdEye*, except for high (4°/s) target rotation rates. This might be due to the generally low number of successes at difficulty level 4 and thus the high impact of small fluctuations in operator performance on task success.

Operator SA was higher with active *ThirdEye* in all scenarios. Operator task load seems to be lower with active *ThirdEye* at low target rotation rates and higher at high rates. This could be due to the fact that the time required to process the additionally available visual information of the *ThirdEye* competes with the timing requirements of quickly rotating targets and thus increases task load. Why this effect not also leads to lower SA cannot be answered in this doctoral thesis.

Approach safety represented by the **contact velocity was not affected** by *ThirdEye* use.

Approach precision, on the other hand, **was improved** by the *ThirdEye*.

The data for the efficiency measures **velocity change and rotation rate change was inconclusive**. The measured approach completion times showed that **approaches with *ThirdEye* on average take longer** than without use of the system. This is reasoned to be due to operators using the additional relative position and attitude information to erroneously judge their approaches to be likely to fail. They thus abort the approach and try again after the target rotated to the right attitude, which results in longer approach times.

The **learning curve** study showed the dependency of operator performance on operator skill, scenario difficulty level, and other contributing factors. The **large fluctuations** observed in the *ThirdEye* evaluation study were also evident in the learning curve study. These fluctuations in operator performance in most cases **outweigh the beneficial effects of operator training** and experience. Operator training is therefore an important part in mission preparation, in order to achieve a consistent level of performance and a reliable and capable teleoperation system.

CHAPTER C:
RESULTS AND DISCUSSION

Results! Why, man, I have gotten a lot of results. I know several thousand things that won't work.

Thomas Alva Edison

9 Research Results

This doctoral thesis evaluated the effects of the *ThirdEye* system on operator performance in teleoperated final approach and docking of uncooperative, rotating target objects.

The *ThirdEye* system consists of two parts: (1) the *ThirdEye Proximity Operations HUD* with the attitude display and the trajectory prediction display, and (2) the *ThirdEye Robotic Camera Arm* system, consisting of the camera arm positioning the secondary camera, as well as the associated operator interface.

These components were developed and implemented in the course of the research flowing into this doctoral thesis. Furthermore, a simulation and test environment consisting of a teleoperation ground control center, a HIL proximity operations testbed and a communication signal time delay simulator was designed and implemented in cooperation with other research projects. This simulation environment was used in a number of user studies evaluating *ThirdEye* system components.

The results of these evaluation studies are summarized as follows.

1. An outside-in attitude HUD increases teleoperation performance in spacecraft attitude maneuvering tasks.

The HUD study described in Chapter 6 showed that the availability of an attitude HUD significantly increases operator performance in attitude maneuvering tasks. It furthermore showed that the outside-in attitude representation is superior to an inside-out display, both in subjective operator perception and in objective performance measures. A three-dimensional trajectory prediction display based on an egocentric reference frame facilitates maneuver planning and execution during final approach and docking.

2. Approach and docking maneuvers with uncooperative, rotating target objects can be teleoperated under the impact of time delay with the operator being only supplied a video stream, an attitude HUD and a trajectory prediction display.

The *ThirdEye* evaluation experiments showed that the combination of egocentric monoscopic camera view, attitude HUD and trajectory prediction display enables inexperienced operators to successfully accomplish docking approaches of uncooperative target objects under the impact of signal time delay. The time delay in the experiments was set to about 700 ms, which is representative of a ground-to-LEO communication chain involving a single data relay satellite. The target object was a generic satellite covered with highly reflective foil and solar array imitations, rotating at between 0°/s and 4°/s.

Using solely the *ThirdEye Proximity Operations HUD* and a single joystick for control of all orbit and attitude maneuvers, the test participants were able to dock with the rotating target at all rotation rates, albeit with the success rate decreasing with increasing rotation rate.

As shown in Figure 9-1, the success rates decrease from 60% for a motionless target to 20% for a target rotating at 4°/s. When evaluating these rates it must be considered that the test participants were inexperienced in their task. They were conducting docking maneuvers for the first time, conducting teleoperation with time delay for the first time, and encountered the situation for the first time. The low rates highlight the general difficulty of the teleoperated maneuvers. It is however expected that with adequate practice, operators are able to dock to slowly rotating targets with close to 100% success rate and with faster rotating targets at over 50% success rate. This expectation is founded on the results of the mid-term learning curve study in which consistent success rates of this magnitude were achieved towards the end of the training program.

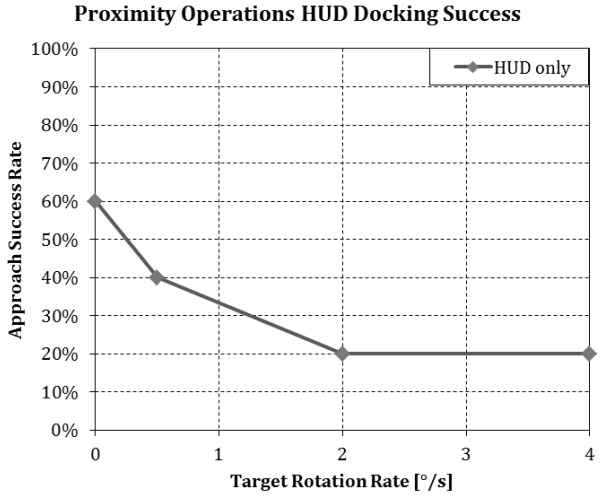

Figure 9-1: Docking success with rotating targets for use of the Proximity Operations HUD. While docking is possible under the test conditions, the success rate decreases significantly with target rotation rate.

3. The use of the *ThirdEye Robotic Camera Arm* increases operator situation awareness, approach success and docking precision at the cost of approach efficiency.

The additional use of the *ThirdEye Robotic Camera Arm* and therefore the integrated *ThirdEye Proximity Operations GUI* increased the **docking success rates** for the same inexperienced operators (see Figure 9-2), except for the 4°/s rotation case.

The bad performance at these high rotation rates is attributed to the lack of experience of the test participants and thus the high fluctuation in operator performance when it comes to coordination, precision and timing. Another factor is the low reaction time available at such high rotation rates. In order to hit the target nozzle, the operator must command the final thrust maneuver within a time

window of 2.5 s. With so little time available, it is speculated that operators are overwhelmed fusing the primary and secondary camera views, which could result in a lower approach success rate. This trend is also indicated by the higher TLX score for active *ThirdEye* at difficulty level 3 & 4.

It is nonetheless expected that more practice and experience in the use of the *ThirdEye* system would ameliorate these effects so that the approach success rate of more experienced operators with active *ThirdEye* would surpass that for inactive *ThirdEye*. It is therefore recommended that future studies focusing on approaching targets with high rotation rates investigate the apparently negative effects of the *ThirdEye* system on approach success at high target yaw rates.

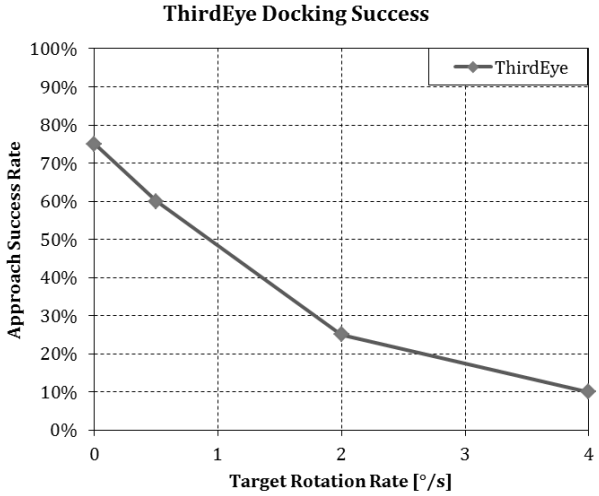

Figure 9-2: Docking success with rotating targets for use of the ThirdEye system. Compared to the HUD-only case, the success rates are increased but still drop to 10% for the fast-rotating target.

The *ThirdEye* furthermore increases **operator situation awareness** at all scenario difficulty levels by between 9% and 25%, as compared to HUD use only. The biggest increase in SA can interestingly be seen in the 4°/s target rotation rate scenario.

Docking precision is increased by between 23% and 40% for difficulty levels 1 through 3. At level 4, with 4°/s target rotation, docking precision is reduced by 6% when compared to docking attempts without *ThirdEye*.

The *ThirdEye* therefore meets its design goal of being a situation awareness enhancement and precision improvement tool.

However, the increased success and precision come at the cost of decreased **efficiency** of the docking maneuvers. Since the operators have more information about their relative position and orientation, they also tend to compensate for alignment errors or to abort approaches if they appear too risky. The results are higher velocity and rate changes, as well as higher task completion times. There therefore exists a tradeoff between probability of success and precision on the one hand, and propellant, energy and time consumption on the other (see Table 9-1).

Contrary to expectations, the *ThirdEye* does not have conclusive effects on participants' perception of their **task load**, nor on **docking safety**. The beneficial effects of the *ThirdEye* do therefore not come at the expense of increased operator task load. However, the *ThirdEye* does also not cause a reduction in relative velocities at docking contact, which would greatly decrease the probability of afflicting damages to the target object during the docking operations. Since both aspects are of interest for operator interface and mission design, they merit further investigation.

Table 9-1 summarizes the effects of the *ThirdEye* on operator performance, as compared to operators solely using the *Proximity Operations HUD*.

Table 9-1: Summary of ThirdEye effects of operator performance

Criterion	ThirdEye effect				
	No rotation	0.5°/s rotation	2°/s rotation	4°/s rotation	Overall
Approach success	++	++	+	−	+
Operator SA	+	+	+	++	+
Operator task load	+	+	−	−	o
Docking safety	+	−	o	++	o
Docking precision	+	++	+	−	+
Docking efficiency	o	−	−−	+	−

Operator Performance Comparison

For application of these research results, it is of interest to compare the finding of the individual studies conducted in this thesis. Since the metrics in the HUD evaluation study were not identical to those of the later *ThirdEye* evaluation study, this comparison can only be provided qualitatively. This comparison is provided in Table 9-2.

The operator performance benchmark is the performance shown with the *ThirdEye Proximity Operations HUD*, as measured during the *ThirdEye* evaluation campaign. Compared to this benchmark, approach success and docking efficiency were substantially lower without the support of an attitude and trajectory prediction HUD, while operator task load was also increased. As stated above, the use of the full *ThirdEye Situation Awareness Enhancement System* generated improved approach success rates, operator SA and docking precision, at the cost of reduced docking efficiency. Operator task load and approach safety were not influenced by *ThirdEye* use.

Table 9-2: Comparative qualitative summary of the study results. The operator performance with ThirdEye Proximity Operations HUD serves as the baseline. Operator SA, approach safety and docking precision were not tested in the test flights without visual support system. The operator task load rating for maneuvers without visual support was not measured by TLX but deducted from the participants' responses to questions regarding scenario difficulty and the required concentration.

Criterion	No visual support	ThirdEye Proximity Operations HUD	ThirdEye Situation Awareness Enhancement System
Approach Success	– –	o	+
Operator situation awareness	not tested	o	+
Operator task load	–	o	o
Approach safety	not tested	o	o
Docking precision	not tested	o	+
Docking efficiency	– –	o	–

In addition to the performance and perception data gathered during the individual experiment runs, it was also important to get a measure for the user acceptance of the *ThirdEye* system. For this purpose, the participants were asked to rate the quality and usability of the *ThirdEye* system in discrete steps between 1 (display confusing and not helpful) and 7 (display sufficient for needs, no revisions needed) at the end of the *ThirdEye* experiments series. The minimum participant rating of the *ThirdEye* in this scale was 5, resulting in a mean of 5.98. The *ThirdEye* system was therefore rated to be a helpful tool.

The participants were furthermore asked to describe advantages and disadvantages of the system. Without exception the test participants professed that the *ThirdEye* helped their spatial modeling by making distance and orientation in relation to the target easier accessible. The secondary camera of the *ThirdEye* also helped to compensate for adverse lighting conditions like deep shadows or glare, since one camera could have a clear view of the target while the other was affected by the lighting.

Major criticisms stated were the size and position of the secondary camera view. Some felt that the picture was too small, while others thought it obstructed too much of the main image during some phases of the approaches. The simultaneous control of spacecraft and camera arm was also an issue, although this was ameliorated by the pre-set arm postures provided in the evaluation experiment series.

It can therefore be stated that relying on video data and supported by an attitude HUD and a trajectory prediction display, a human operator is able to accomplish safe and efficient final approach and docking of an uncooperative, rotating target spacecraft under the system limitations typical for space teleoperation.

It was furthermore shown that a robotic camera arm, guided independently of other manipulators and the satellite platform, enhances the operator's awareness of the chaser satellite's position and

orientation relative to the target spacecraft sufficiently to improve his performance compared to the baseline.

The working hypotheses of this doctoral thesis have therefore been confirmed by a combination of experimental measurements and user statements.

The *ThirdEye* thus enhances operator SA and thus increases operator comfort and confidence during final approach and docking. Its use can therefore be recommended for every teleoperated approach and docking mission, regardless of whether the human operator serves as prime spacecraft controller or as a backup for an autonomous system. The use of the *ThirdEye* increases the probability of mission success and also increases the precision of the docking approach, which is an important factor for successfully capturing uncooperative target objects.

Limitations

The above statements about HUD and *ThirdEye* performance are mostly based on the trends in the measured data, instead of significant differences between sample groups.

One reason for this is that the low success rates at higher target rotation rates reduced the available data points for successful approaches to levels that prevented conclusive statistical analysis. This effect can be countered in future studies by increasing the overall sample size.

Another reason is that the performance showed by the test participants was highly variable. The final approaches and docking maneuvers of the test scenarios required high levels of concentration and coordination, not least good timing when approaching the rotating targets. While the participants went through system familiarization and training runs prior to experiment flights, it nonetheless frequently occurred that joystick axes and buttons were confused in critical situations, which resulted in unexpected approach failures. A number of perfect approaches were thus ruined in the final second. Such mishaps can only be prevented by extensive practice, which cannot be achieved in training sessions prior to test runs during an experiment campaign. The large fluctuations evident in the learning curve study showed that very intensive training is required to achieve consistent and reliable operator performance. The elimination of these rogue effects on experiment results can only be achieved by selecting a cadre of operators and having them practice various scenarios over weeks and months before running experiments. Neither the personal or financial resources nor the time for such a program were available during this doctoral research.

A third potential reason for the quality of the data could be the test scenarios. Their task complexity and difficulty were designed to create conditions that result in clear performance differences between test cases. This design however only represents a best effort by me and might not actually have resulted in perfect test conditions for the different visual support systems. Future studies into the design of final approach and docking test scenarios for teleoperation experiments are therefore recommended.

10 Technical Issues and Directions of Future Research

While the utility of the *ThirdEye* system was proven in the experiment campaign, a number of system integration issues must be addressed before a use of this principle can be considered for use on a space mission.

Data Handling and Communications

Realtime teleoperation of the final approach and docking maneuvers places stringent requirements on the teleoperation system. Above all, the use of the *ThirdEye* system places high demands on the **space communications system**. In *ETS-VII* and *Orbital Express*, the teleoperated manipulator systems were highly automated and could be represented in a VR environment in sufficient detail to allow very low video frame rates of 1-4 frames per second [153]. For tasks like docking, frame rates of 30 fps are desirable [151], while 15 fps were used throughout the *ThirdEye* experiments.

This amount of video data must be compressed, packetized and transmitted to the ground with as little latency as possible. This requires higher **computing power** than ordinarily available in space computers. The spacecraft must also be equipped with a high-performance **data bus**. For this reason, *Orbital Express ASTRO* used an IEEE 1394a interface for all computers and rendezvous sensors, which enable data exchange at up to 400 Mbps [80]. Furthermore, teleoperated proximity operations require high-rate telemetry in order to be able to update state predictions and displays. An update rate of 100 Hz was used for the experimental *ThirdEye* system.

Overall, the **data rate** transmitted via local network during the *ThirdEye* evaluation experiments has been 4.6 Mbps (megabits per second). A realtime teleoperation system therefore requires a communication link with substantially higher **bandwidth** than standard spacecraft telemetry links, which in the example of *ETS-VII* operate at data rates of about 2 Mbps [169].

Command Security and Reliability

This link must also be **secure and reliable**. Since malfunctions in the communications chain and thus a loss of contact cannot be ruled out completely, the teleoperation system must be able to compensate for that by providing **automated backup functions** should the operator lose control. In “ordinary” spacecraft operations, each command string can be checked and re-checked before being transmitted to the spacecraft and executed by the on-board computer. This approach can also be pursued for robotic missions operating in supervised autonomy, but definitely not in the more direct modes of teleoperation. In direct, realtime teleoperation all commands must be considered time critical and must hence be executed immediately.

This makes the system immensely vulnerable to garbled communications, component malfunctions, or simple human error. **Automated monitoring functions** must therefore automatically sense when ground commands are either corrupted or have paused, and then take adequate measures to prevent collisions. Similar automated systems must also monitor operator commands in real time to make sure that the operator does not inadvertently cause collisions due to wrong command

inputs. A boundary condition for these automated support functions is that they must not increase **total system latency** above the values suitable for teleoperation. To the author's knowledge, there has been only limited research into such automated monitoring and backup functionalities for the teleoperation of spacecraft, which therefore is an interesting direction for future research.

Collision Avoidance

Another issue when operating a robotic manipulator in space is collision avoidance, both between manipulators and between a manipulator and the target object. It would not be beneficent if the *ThirdEye* arm was to collide with the target object during final approach, possible damaging both the *ThirdEye* and the target.

It must also be prevented that the *ThirdEye* collides with any other manipulator or appendage of the chaser satellite. These ***intra-satellite* collisions** can easily be addressed by having an internal model of all manipulator and its appendages which is continuously updated with joint angles and velocities. Thus it can be ensured that manipulators stay safe from known obstacles.

Such an approach is not feasible for ***inter-satellite collisions***, since in the OOS context no exact model of the target object and its motion is available, hence no model-based collision avoidance can be achieved. It is therefore necessary to equip the camera arm with capacitance or IR distance sensors [275], or the combination of both in a so-called sensor skin [276]. The distance information can then be used in virtual potential field [277] or virtual spring-damper [276, 278] controllers to guide the arm around obstacles.

Representative Test Scenarios

Besides these technical issues, a number of research challenges were identified for future investigations of spacecraft teleoperation.

During the preparations of the HUD and *ThirdEye* evaluation experiments, no scenarios representative of OOS missions could be found in literature. The test scenarios were therefore based on *Space Shuttle* approach profiles and *Orion* test scenarios. It would however be interesting to compare the performance of different automated and teleoperated systems, which would be facilitated by a set of **benchmark scenarios** based on real and projected missions.

If a rendezvous & docking system is being developed for a specific mission, for example flights to the *ISS*, the set of requirements and the test cases are clear. This is the reason why the manufacturers of the current generation of RVD systems do not have a use for a wide set of different scenarios. Research institutes that look at future applications and future missions do. It is therefore recommended that future research is dedicated to a set of experiment scenarios representing the key challenges in proximity operations of satellite servicing, debris removal, and near Earth object (NEO) missions. This would allow for **comparison** and possibly **interoperability** of systems, and would also facilitate the development of sensors and controllers.

Comparison of Teleoperation and Autonomous Systems

As the basic premise of this thesis it was postulated that a teleoperated system has more flexibility than autonomous systems and that this quality is advantageous when approaching uncharacterized and uncooperative target objects. This performance advantage has however never been demonstrated. It would therefore be of interest to actually compare the performance of automated, supervised, and directly teleoperated systems in representative mission scenarios with different tasks and target characteristics. This would not only serve to actually validate the benefits of teleoperation, but also to identify areas of supreme performance for the different systems and so to arrive at an optimum combination of different control modes.

This combination of direct teleoperation and autonomy, or of multiple teleoperators working on the same system, should also be the focus of research activities in order to make operational OOS missions a reality. Autonomous system research mostly has a human operator back up a computer, but maybe the right way may be the other way round in some situations. Or maybe having a second, trained and experience operator looking over the shoulder of another human operator is the most efficient way to conduct OOS and space debris removal missions.

I expect that for many missions neither autonomy nor teleoperation will be the only ways to bliss. Both will be applicable if the mission is designed properly and if the system requirements are formulated accordingly. The question whether a computer of a human operator and a satellite link will be entrusted with success and failure of a mission does not only depend on technical considerations, but also on policy, programmatic considerations, and the gut feeling of project managers. Most people riding on the passenger seat of a car know the urge to personally assume control. It will not be different with people monitoring and supervising an autonomous spacecraft approaching a potentially expensive target satellite. It must be assured that the human operator is given the tools necessary to assume control if needs be. It must however also be assured that he knows exactly what he is doing and when he really is supposed to do so.

11 Summary and Conclusion

This doctoral thesis provided an overview of the applications for a robotic on-orbit servicing system and the research and demonstrator missions and development projects planned, completed and cancelled in this field. It then showed with a survey of other telerobotic disciplines that tasks relating to the complexity of on-orbit servicing are routinely conducted by teleoperated underwater, aerial and ground systems. The design principles for operator interfaces can therefore be adopted from these disciplines and applied to orbital teleoperation, with special considerations for the issues of space communications and the characteristics of the orbital operating environment. An introduction into rendezvous & docking systems established the need for human operator involvement in the final approach and docking of uncooperative target objects, and provided the general system requirements for such a teleoperation system.

These requirements for increased operator situation awareness were then realized in a specialized *Proximity Operations Head-Up Display*, as well as in the *ThirdEye Robotic Camera Arm* and operator interface, which combine to form the *ThirdEye Situation Awareness Enhancement System*.

It was hypothesized that final approach and docking of an uncooperative, rotating target under the impact of time delay is possible in direct realtime teleoperation using the Proximity Operations HUD and monoscopic video feedback, and that the operator performance is furthermore increased by the introduction of flexible camera vantage points by the *ThirdEye*.

The design and implementation of both the HUD and the *ThirdEye* were described, and the experimental campaigns pursued in testing and evaluating the system elements and the integrated system were detailed. After final analysis of the *ThirdEye* evaluation experiments it became evident that while statistically significant results could not be obtained due to large fluctuations in operator concentration and coordination levels during the experiments, the general trend of the experiment results indicated the confirmation of the research hypothesis.

It was therefore shown that an operator can successfully approach and dock to an uncooperative and rotating target in direct teleoperation, without the need for complex virtual reality representations or multimodal feedback devices. His success rates, precision and situation awareness are furthermore increased if he is provided with a secondary, flexible camera view integrated into the operator interface. This increase in performance however comes at the cost in system efficiency, as the operator tends to spend more propellant, energy and time in correction maneuver due to the increased knowledge of relative position and orientation.

The thesis furthermore discussed the implications on space system design that must be considered if planning a teleoperated rendezvous & docking mission. In this discussion, a number of technological challenges were identified, that should be addressed by future research.

To conclude this thesis, it must be stated that while the applications of a teleoperated rendezvous & docking capability will certainly be marginal compared to the future use of autonomous systems, the availability of this approach will allow more flexible, capable and also more ambitious missions

in the on-orbit servicing, space debris removal, and exploration contexts. It is not prudent or wise to state its usability for every mission scenario, but it certainly is a backup capability if autonomous systems fail or if the target behavior overwhelms the limited sensing, anticipation, planning and guidance capabilities of space computers. This contingency capability comes with substantial impact on system design, operations planning, operator training, and ground control equipment. However, it is better to prepare for the worst than to rely on the best.

APPENDIX

A Rendezvous and Docking Details

A.1 Plume Impingement

The term *plume impingement* covers all effects exerted on the target object if it is impacted by the chaser RCS thruster exhaust gases. One of these effects is the plume pressure force acting on the target and causing position and attitude disturbances. Another is the heat load placed on the target's structure by the hot gases, which can lead to overheating of parts of the surface and the underlying structure. The third effect is the contamination of the target's surfaces by combustion products and unburned propellant components. This can cause contamination of sensitive elements on the target's surfaces, particularly optical elements such as camera lenses, solar arrays or docking sensors, but also of sealing elements of the docking mechanism [196]. Plume impingement thus is one of mission planners' major concerns during proximity operations, apart from collision avoidance and maneuver precision. It can only be avoided if thruster activity near the target is minimized, which in turn means that the chaser's relative velocity must diminish below a threshold value as it approaches the target [203]. This risk of contamination must be considered during OOS missions like *Hubble* servicing, which impacts the design of final approach trajectories [43, 70] (see Figure 11-1).

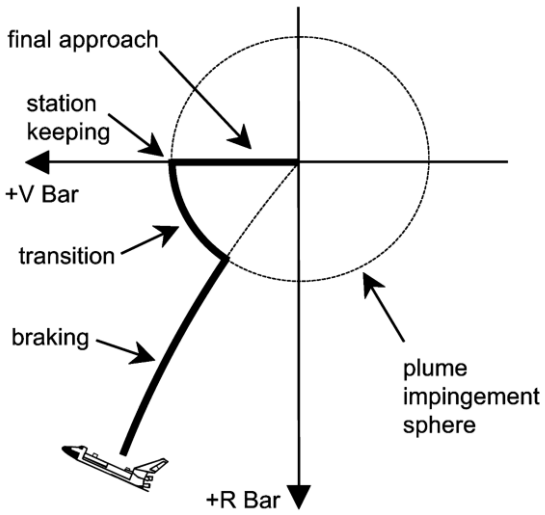

Figure 11-1: Approach profile to avoid plume impingement on target as developed for the Space Shuttle's Long Duration Exposure Facility (LDEF) retrieval mission [43, p. 947]. A minimum range was determined, at which the Shuttle's thrusters could be fired without contamination concern. At this range the orbiter transitioned from a direct approach strategy to a station-keeping point on V-bar. Simulation showed that an Apollo-type direct approach and braking would cause LDEF to tumble.

Plume impingement therefore has severe impact on any rendezvous & docking mission and will thus remain a design driver for any OOS or space debris removal systems. Plume impingement concerns must be addressed both on the technology and mission design levels. This is especially

important for OOS systems since on replenishment or repair missions, any damage caused by the servicer spacecraft can be considered a mission failure and a discredit to the whole business venture.

A.2 Docking and Capture Systems

Over the past 50 years, a number of docking mechanism systems have been developed for the *Apollo*, *Soyuz*, *Space Shuttle* and space station programs, as well as for OOS demonstrator missions. The following sections serve to highlight the most successful designs, which served as the background for the final approach positioning and orientation tolerances used during the evaluation experiments run for this doctoral thesis.

A.2.1 Probe-and-Drogue Docking Systems

Probe-and-drogue docking systems were developed in parallel for *Apollo* and *Soyuz*/*Progress*. A close derivative of the *Soyuz* probe-and-drogue system, called the Russian Docking System (RDS), is also used by the European *ATV* [208, 213]. Probe-and-drogue systems consist of an active element usually mounted on the chaser vehicle, and a passive counterpart on the target. The passive part, the drogue or cone, is a metal cone with a collar around its rim. The active part mainly consists of a telescopically extendable probe whose base is also ringed by a metal collar. During docking, the probe is extended to its full length and pushed forward by the chaser's momentum with its head guided by the cone into a socket where its latches engage. The residual relative momentum is attenuated by shock absorbers in the probe. The probe is then retracted until the collars touch and a number of latches and bolts form a tight connection. All leads for fluids, power and communications are also routed through the collars. Refer to Figure 11-2 for an overview of the probe-and-drogue systems used on *Apollo* and *Soyuz*/*Progress*.

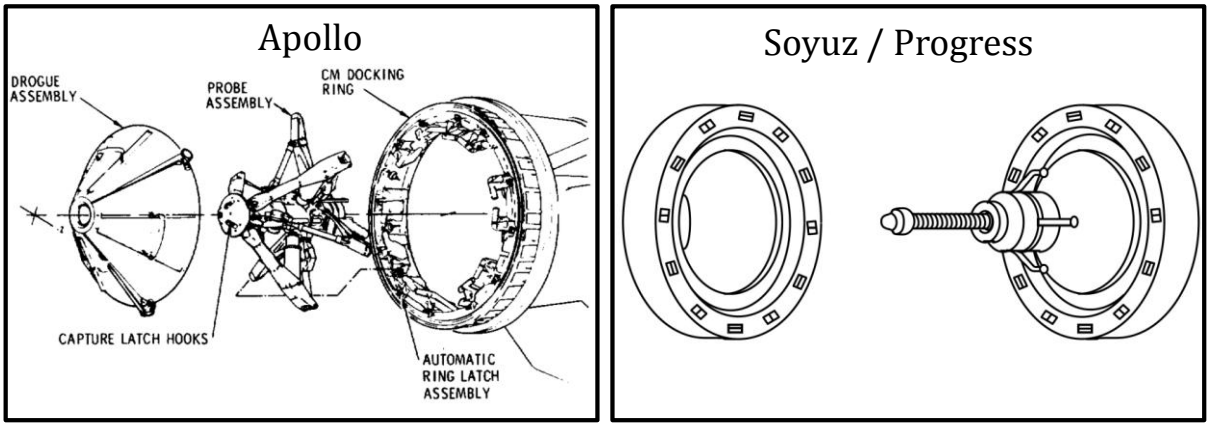

Figure 11-2: Apollo and Soyuz/Progress docking systems (adapted from [279, p. 7] and [216, p. 22]). The docking probe is pushed into the drogue by the chaser's momentum, which is attenuated by shock absorbers. Mechanisms in the probe head fixate the probe until it is retracted and latches and bolts in the collars form a rigid connection.

A.2.2 Androgynous Peripheral Attachment System (APAS)

Androgynous docking systems use two identical docking interfaces, with one spacecraft assuming the active role and one the passive. APAS is a Russian design originally developed and used for the *Apollo-Soyuz Test Program* in 1975. In the 1990s, NASA purchased APAS assemblies and installed them as the docking mechanism for the Orbiter Docking System [208]. Each side of APAS consists of a capture ring mounted on a Stewart platform (also called a hexapod). This platform makes the capture ring movable in six DOF, which extends the docking envelope, and uses its actuators for damping and attenuation. Once contact between the rings has been established, the cone-shaped segments of the capture rings interlock and guide the two mechanisms into a rigid connection [211]. The active unit is then retracted to bring the docking collars together, and guides and sockets in the collars complete alignment and connection [216]. Figure 11-3 shows the APAS-89 docking system, as developed for *Buran* and *Mir* and used by the *Space Shuttle* and *ISS*.

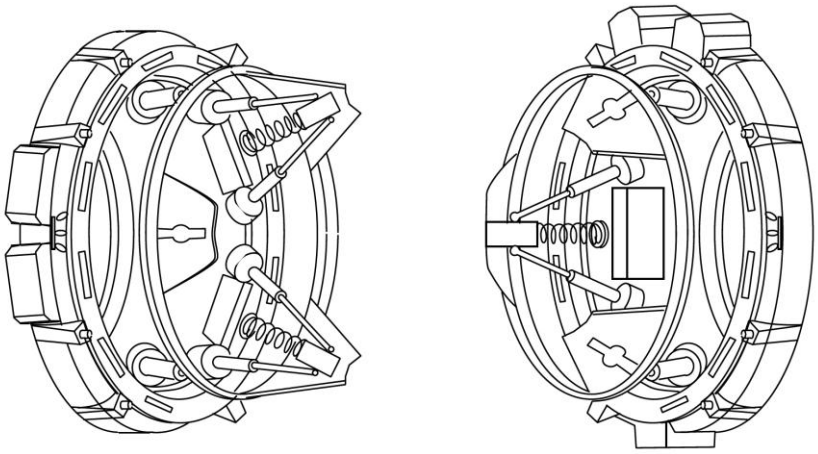

Figure 11-3: APAS-89 docking system [216, p. 166]. The docking rings are extended and actuated by hexapods. Once contact has been established, the cone-shaped segments of the rings interlock and guide the mechanisms into a rigid connection. The active ring is then retracted and the docking collars are latched together.

A.2.3 Low Impact Docking System (LIDS)

APAS is a reliable and versatile system, but still demonstrates some of the shortcomings of the heritage docking systems. Most prominently is the high relative velocity required for successful latching, which causes high shock loads upon contact. To overcome these shortcomings, NASA developed the *Low Impact Docking System* (LIDS) which uses electromagnets for initial capture and a closed-loop active attenuation system, thus reducing the impact [214]. LIDS was originally designed for the *X-38 Crew Rescue Vehicle* (CRV) and after that project was cancelled became part of the Crew Exploration Vehicle (CEV) *Orion* design [280]. In addition, a passive LIDS interface is part of the *Hubble Space Telescope* Soft Capture Mechanism (SCM) which is attached to *Hubble's* aft bulkhead. SCM will enable future rendezvous, capture and safe disposal by either a robotic or a manned mission [281]. Figure 11-4 depicts LIDS and a passive counterpart during mating tests, and the LIDS docking collar attached to *Hubble's* SCM.

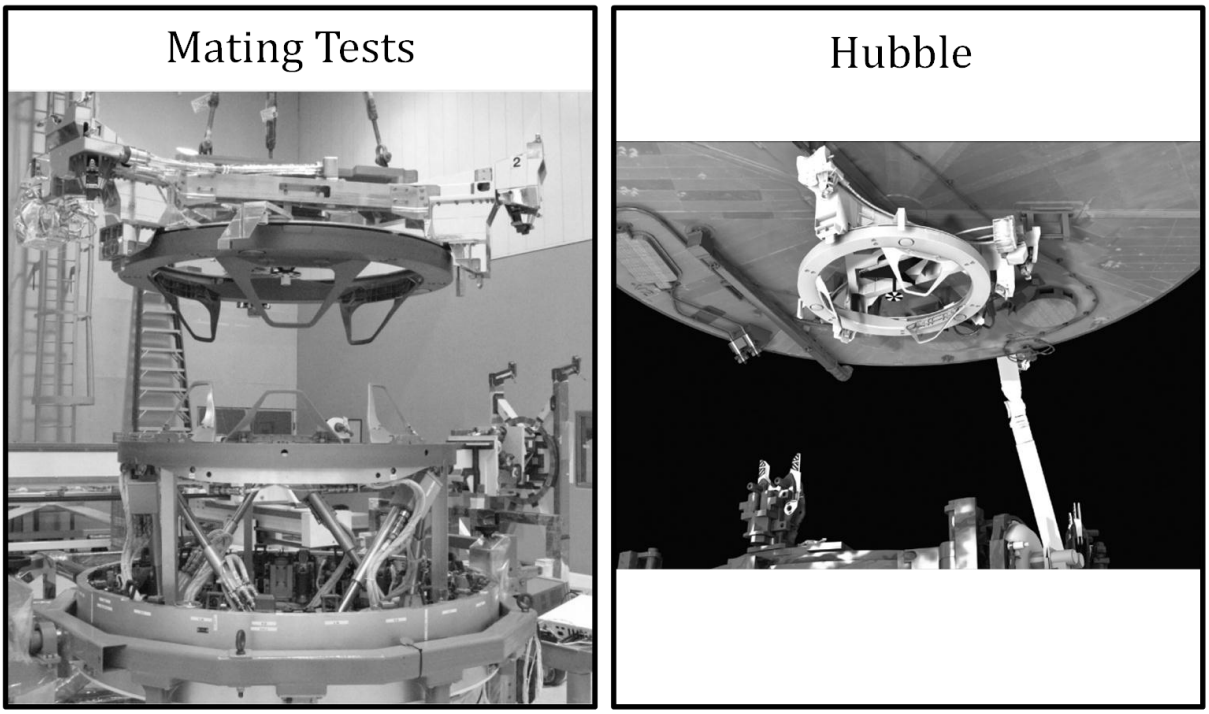

Figure 11-4: LIDS during engineering tests and as installed on Hubble (adapted from [280] and [281]. Based on the APAS principle, LIDS uses electromagnets and a closed-loop attenuation system for reduced-impact capture.

A.2.4 Common Berthing Mechanism (CBM)

The Common Berthing Mechanism (CBM) is used to provide a common attachment interface on *ISS* and thus connects all pressurized ISS modules, apart from the Russian contributions [282]. CBM relies on the SSRMS to position the two docking collars against each other (see Figure 11-5). Once within capture range, a fully automated system aligns, captures and bolts the two elements. As with the other docking systems, there exists an active and a passive half. The active half is installed on the *ISS* side of the connection, containing all static and motor actuated mechanisms as well as telemetry and control systems [282]. The passive capture ring therefore is part of the module to be installed, as with ESA's *Columbus* lab, the Japanese *Kibo* orbital laboratory or the *Multi-Purpose Logistics Modules* (MPLM). In addition to space station modules, the Japanese *H-II Transfer Vehicle* (HTV) uses the CBM [195], as will the commercial SpaceX *Dragon* and Orbital Sciences *Cygnus* supply vessels.

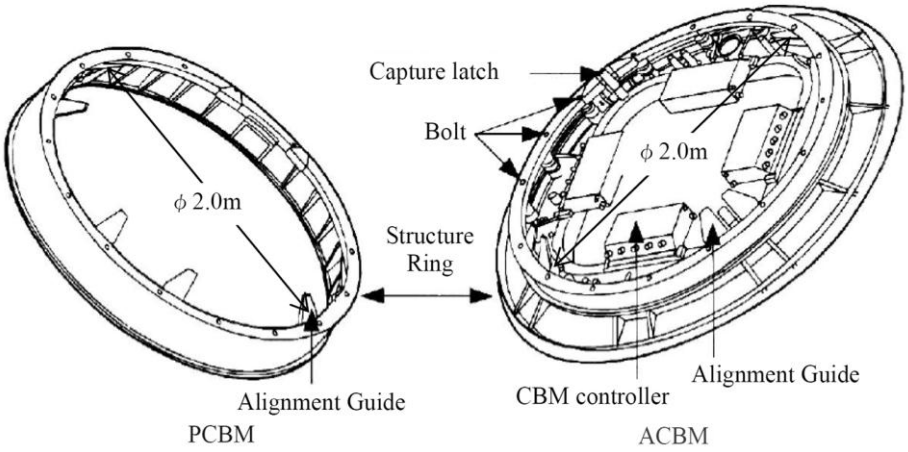

Figure 11-5: The active and passive halves of the Common Berthing Mechanism [195, p. 4-9]

A.2.5 Orbital Express Capture System (OECS)

The docking and berthing systems described to this point have all been specifically designed for crewed spaceflight. They therefore must provide means to establish pressurized passageways, which increase system complexity and mass compared to mechanisms providing only fluid, power and data couplings or maybe solely a structural connection. These systems are therefore not suitable for robotic craft designed for OOS missions. In order to fill this technology gap, DARPA developed the *Orbital Express Capture System*. The design goal was for the docking system to have low mass and support low impact docking or berthing [212]. The resulting design has an active element to be mounted on the chaser satellite. It is equipped with a mechanical claw with three talons, which are extended towards the target, open up and grasp the passive counterpart on the target, and then retract and pull the passive element into a number of pins and cones to achieve a rigid structural, electrical and data connection (refer to Figure 11-6).

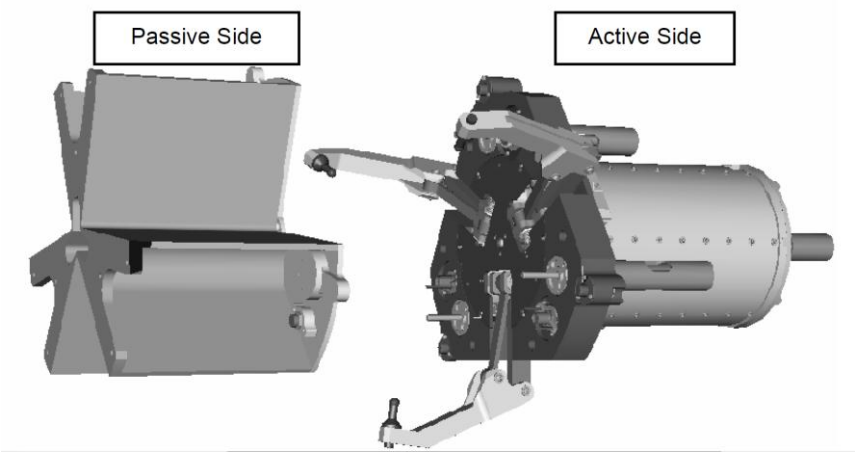

Figure 11-6: The Orbital Express Capture System [212]. The talons on the active side are opened and extended towards the target, then grasp the target and retract, thereby pulling the passive side into a rigid structural, electrical and data connection.

OECS was flown and successfully tested on the *Orbital Express* mission. Whether it will ever be employed as a standard capture interface for future generations of satellites and thus allow routine OOS servicing remains to be seen.

A.3 Sensors

Rendezvous & docking sensors must enable the chaser to acquire the target at distances of tens of kilometers and then reliably track it down to ranges of centimeters. This large distance spread cannot be covered by any single sensor, so the chaser carries an array of different sensors, referred to as a sensor suite.

In general, sensors can be classed into two categories: active and passive. Active sensors detect and track a target by actively transmitting and receiving signals. Passive sensors rely on the target's emissions to discern position and motion. Combinations of sensors using both principles are usually employed on rendezvous spacecraft. These systems are detailed in the following sections.

A.3.1 Active Sensors

Active sensors emit signals and then process the echo received from the target to determine the range and range rate as well as angular position and motion. The laser ranging systems commonly used are scanning laser range finders or lidar (light detection and ranging). Radio-based systems either use radar or radio frequency (RF) guidance principles, as with the Russian *Igla*/*Kurs* guidance system.

Lidar

Laser rangefinders transmit laser in visible or invisible wavelengths and use the light bounced back from a target's surface or dedicated reflectors to determine the distance to the target. Scanning laser rangefinders, called lidars, use an articulated sensor head in order to scan a target with multiple laser pulses. They are thus able to either generate an image of the target or track surface features or reflectors.

The systems used in spaceflight follow the principles of time-of-flight measurement or distance-determination by triangulation. Time-of-flight systems measure the time from transmission of a laser pulse to detection after reflection off the target and thus determine the distance. Triangulation systems measure the transmission and detection angles of the pulses and thus compute the distance.

A number of different lidar systems are in use aboard spacecraft, most notably on the *Space Shuttle*, *ATV*, *HTV* and some of the recent robotic rendezvous & docking demonstrators [43, 155, 215]. These systems provide distance measurement accuracies in the range of 0.1 m [155] and have a maximum range in excess of 5 km [220].

The limitation of most lidars is the dependency on retro-reflectors on the target, as well as small FOVs [215]. Another limitation of scanning lidars is their low update rates resulting from the need to scan the target line by line with the laser rangefinder. This issue is addressed by a new design of lidar systems, called the Flash Lidar. These systems use an imaging array of laser rangefinders that are engaged simultaneously (like a flash) and instantly generate range information for the whole FOV [283]. They can also be used to generate depth images in real time, which might be a valuable capability for rendezvous missions to objects with unknown or uncertain geometries, as during OOS or space debris removal.

Time-of-flight and triangulation units can also be combined into a single system, increasing accuracy and operating envelope. Such a system is TriDAR by NepTec Design Group of Canada, which has successfully been tested on multiple *Shuttle* missions [284] and is expected to be prominent in future rendezvous & docking systems.

Radar

The principle behind radar is the emission of a series of radio waves against a target, with the time-of-flight between transmission and the detection of the reflected waves being measured to determine distances. The range rate is determined by measuring the Doppler shift between outgoing and incoming waves. The range and accuracy of radar can be increased by having a transponder aboard the target actively transmit a response pulse whenever it receives a radar wave.

Radar is the original active sensor used in rendezvous & docking, seeing use during *Gemini* and *Apollo* [197]. The *Space Shuttle* uses a Ku band radar with the maximum range depending on the individual target. It is approx. 22 km for *Mir* [197] and *40* km for ISS [43]. The *Shuttle* radar can be used down to ranges of 20-30 m for small targets or 300 m for large targets like *ISS* [43][15].

Radio navigation: Igla/Kurs

Apart from radar, radio waves can also be used for another sensing approach, called RF direction finding. The basic explanation of this approach is that a radio transmitter on the target continuously broadcasts a homing beacon, and the chaser uses one or a number of antennas to determine the direction of the signal's maximum intensity and follows it to its source. This approach is common in aviation where it is used to guide aircraft between waypoints and towards airports.

The only space RF homing system in operational use is the Russian *Kurs* (course) system, with its predecessor *Igla* (needle) [202, 216]. Both systems follow the same principle. A set of antennas on the target vehicle transmit RF signals which are received by counterpart antennas on the chaser vehicle. Each set of antennas guides the chaser closer and with more precision. The general antenna layout and functionality on *Soyuz*/*Progress* and *Mir* are illustrated in Figure 11-7.

[15] This minimum range is caused by the radar beam not being as closely confined as a laser beam, and the reflected waves from different parts of the target thus creating a fuzzy range solution. This effect is called *beam wandering* [43].

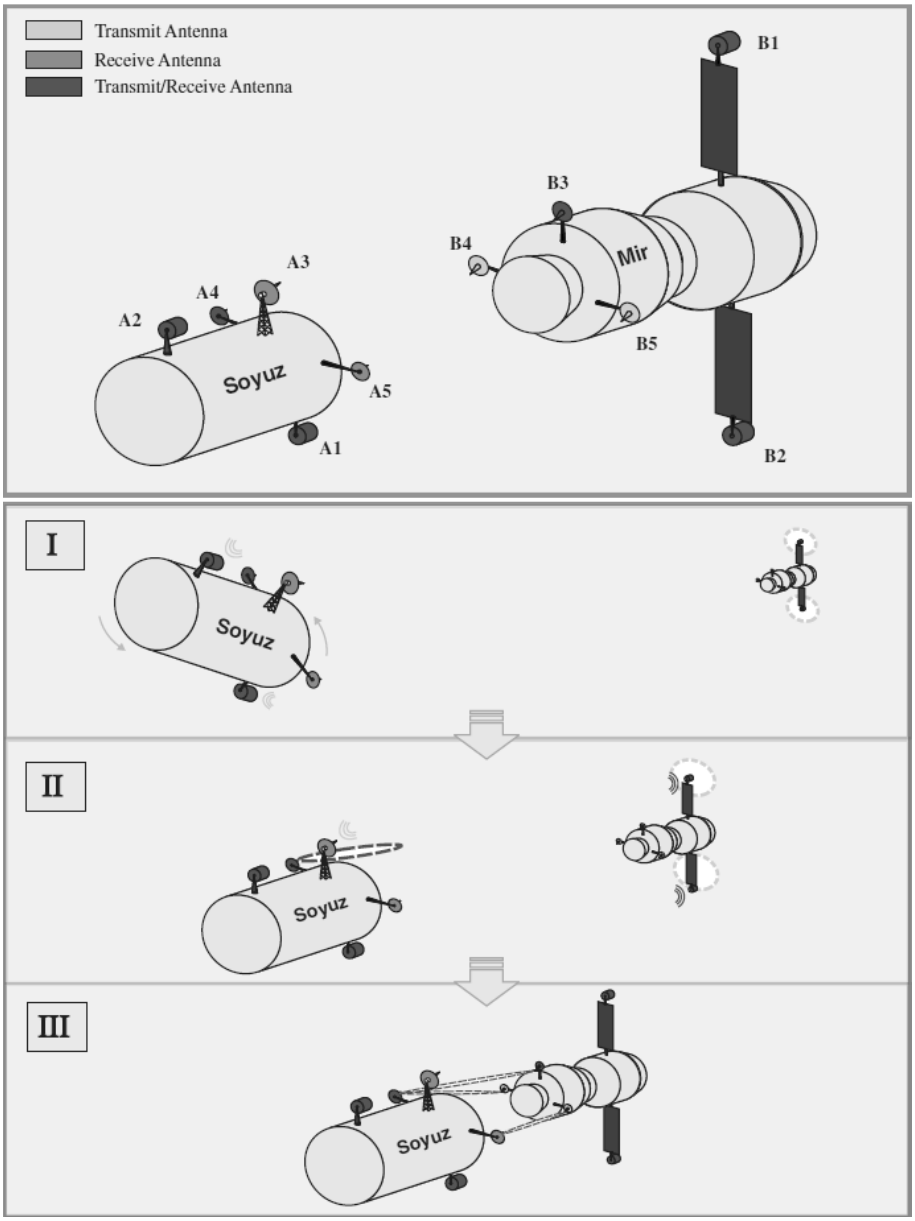

Figure 11-7: Kurs rendezvous system [202, p. 904]. Two omnidirectional transmit and receive antennas (B1, B2) broadcast a homing beacon. This is received by the omnidirectional antennas on the Soyuz/Progress' front docking port (A1) and aft bulkhead (A2) and used to determine the general direction of the target vehicle (step I). After the target has been acquired, these antennas are used to transmit and receive signals for range and range rate determination, and the wide angle gimbal antenna (A3) is used to point Soyuz at the target. A fixed electronic scanning antenna (A4) tracks the target vehicle's relative angular motion (step II). Once the chaser begins the proximity phase of the approach, B1 and B2 are turned off and the fixed antenna B3 is used to determine range and range rate. At ranges below 30 m, another fixed antenna B4 is activated to improve the range measurement quality (step III). In addition, a motor driven conical scanning antenna (B5) is rotating at 700 rpm. Its carrier signal's amplitude and phase shift is measured by the fixed narrow-beam reception antenna A5, and thus bearing angles are measured during close proximity phase, and the relative attitude is determined. Reprinted with permission of the American Institute of Aeronautics and Astronautics.

While the *Kurs* system has successfully served *Mir* and *ISS*, there are some limitations restricting its usability for OOS systems. Using automated mode only, i.e. without intervention by crew aboard chaser or target, *Kurs* has a rendezvous success rate of only 85% [4]. Apart from reliability issues, the major limitation to the use of *Kurs* in OOS systems is its high impact on both the chaser and target mass and power budgets. The total mass of the *Kurs* equipment on *Soyuz*/*Progress* is about 85 kg, while consuming 270 W of power. On the target side, total mass ranges at about 80 kg, with a power consumption of 250 W. This is far beyond the capabilities of OOS spacecraft which must be small and cheap in order to be commercially viable.

In overall, although active sensor systems make acquiring and tracking targets independent of ambient lighting conditions, provide high measurement accuracies over a wide range envelope and enable relatively simple automatic approach procedures, they share some significant limitations for their use in OOS systems. As discussed, these systems combine high power consumption with often significant mass. In addition, they also are expensive and have a rather small field of view [217], which means that the chaser spacecraft can be forced to perform sweeping motions in order to support the sensor's scanning of the sky.

These limitations render active sensors less attractive for OOS missions than passive systems.

A.3.2 Passive Sensors

Passive sensor systems use freely available emissions of the target in order to sense the target's position, attitude or even geometry. Since spacecraft usually (in the absence of the *Kurs*/*Igla* rendezvous system) do not emit omnidirectionally at radio frequencies, only optical sensors in the visual or infrared (IR) spectra are used to directly acquire and track target objects. These optical systems comprise star tracker cameras and video systems. While often spotlights or laser diodes are used to illuminate the scene in order for these systems to work in the dark, they are nonetheless classified as passive systems in this context.

The chaser can furthermore utilize a global navigation satellite system like GPS in order to determine its own position, and by means of a data link to a similarly equipped target satellite also acquire and track the target with sufficient precision to perform rendezvous maneuvers.

Optical Sensors

Optical systems, also referred to as space vision systems, in general provide three-dimensional information about the observed object's position and orientation in space [190]. These systems utilize ambient light reflected by the target's surfaces, or the IR emissions due to the target's surface temperature, to sense a bright object against the dark background of space. Therefore, space vision systems are sensitive concerning the environmental optical conditions in space, which place stringent requirements on space vision systems. Nonetheless optical systems have numerous ad-

vantages making them sensors of choice for current and future rendezvous & docking systems, especially in the context of robotic OOS.

At long ranges, optical sensors can detect and track objects before these can be acquired by radar. The *Space Shuttle* utilizes two star trackers, which are otherwise used for aligning inertial measurement units, to acquire and track the target after control handover from ground control at 74 km distance from the target [43].

During the rendezvous missions of *Gemini*, *Apollo*, the *Space Shuttle* and also *Soyuz*, the pilot's eyes have been one of the primary sensors during close-range proximity operations. Once the target gets too close for the *Space Shuttle's* rendezvous radar to give an accurate estimate of the range, the crews on the one hand use lidar systems, but also rely heavily on visual observations of the docking targets [197]. These docking targets are special geometrical features within or adjacent to the target spacecraft's docking ports, enabling the approaching pilot to judge his relative distance, radial displacement, as well as yaw, pitch and roll angles. A visual docking target basically consists of a base plate marked with linear or angular scales, and a cross mounted on a standoff above the base plate. The size of the cross as seen by the pilot is an indicator of range to target, the displacement of the cross in relation to the base plate delivers cues regarding the chaser's lateral and angular relative position. Figure 11-8 illustrates the visual docking targets' concept, as well as the view of the target installed on *Mir* as seen from a *Space Shuttle*.

In order to support the pilot to judge his position and orientation relative to the target, NASA introduced the *Crew Optical Alignment Sight* (COAS) [43]. COAS essentially is a reticle projected onto a glass plate within the pilot's field of view (see Figure 11-9). Using the angular cues provided by the reticle, the pilot can orient the vessel and fly the docking maneuver.

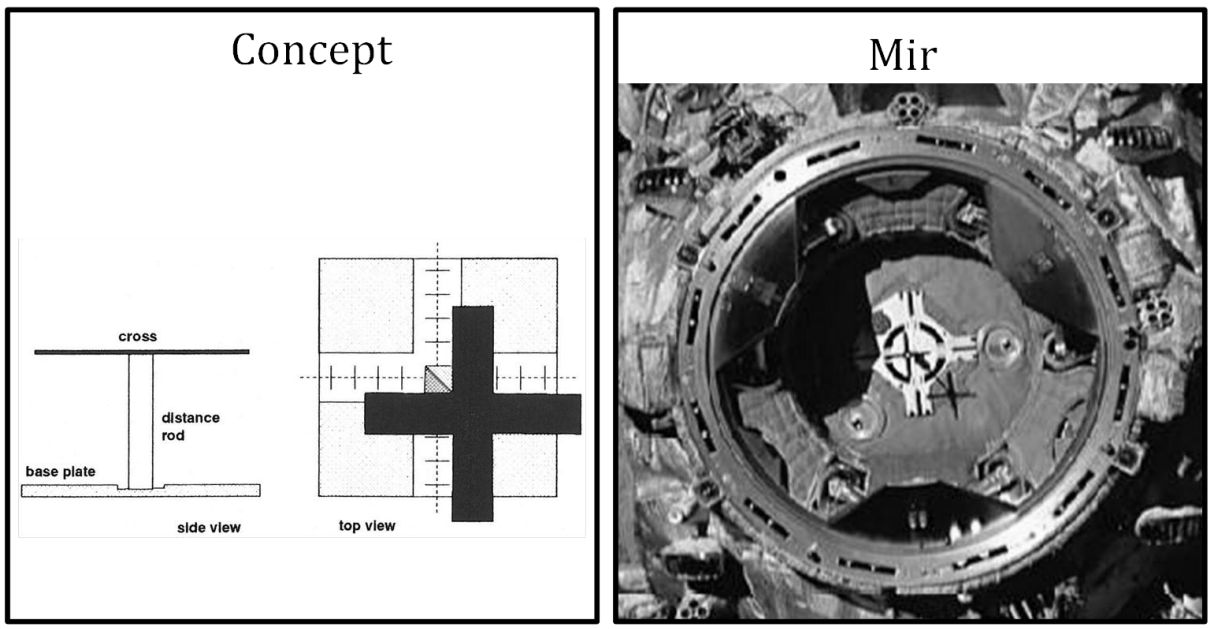

Figure 11-8: Visual docking target concept and as installed within APAS ring on Mir (adapted from [196, p. 216] and [192]). Left picture reproduced with permission of Cambridge University Press.

Figure 11-9: COAS during an approach of ISS [192]

In addition to COAS, the Shuttle crew is supported by a Closed-Circuit Television (CCTV) system. The centerline camera is positioned at the center of the orbiter's docking mechanism and pointed straight "up" [197]. Its video is displayed to the crew as a visual aid within a distance of about 90 m to the target. Another camera is pointed at the APAS from the side. Using visual rulers on the flight deck screens, the crew can accurately determine the distance to the docking targets, with the COAS used for deriving the guidance angles [43].

Apart from using camera systems simply as a means to supplement the human eyesight, they also form the center of any *machine vision system*. These systems, since long crucial to terrestrial robotics, are becoming central to unmanned space rendezvous missions, with *HTV* operationally using a system based on the *ETS-VII* experiences [218]. Machine vision systems use monoscopic or stereoscopic, visual or IR cameras to determine a target's position and pose in space. Current camera-based systems have maximum ranges of up to 100 m for target bodies illuminated by the sun [215]. This maximum range is in general limited by the size and separation of visual targets, as well as by a trade-off between image resolution and field of view.

The vision systems' operations within the maximum range can roughly be classified into three range segments. At long ranges (approx. 100 m – 20 m) the vision system must determine bearing and distance of the target, as well as its approximate orientation and motion. These parameters are to be further refined and determined accurately and with high confidence at medium ranges of 20 – 2 m. Within short range below 2 m, artificial lighting is available to illuminate the scene and well-defined features on or around the capture interfaces can be used to obtain a position and motion solution with sufficient accuracy to permit a final docking or capture maneuver [190].

Machine vision systems use the acquired video data in image processing algorithms in order to determine target distance, pose and motion. These algorithms can be broadly categorized into three approaches: *target-based*, *model-based*, and *non-model-based*.

Most current space vision systems are *target-based*, i.e. they rely on the installation of easy-to-detect and high-contrast visual targets on satellites and payloads [219]. Such targets are shaped similarly to the visual docking targets for manually guided rendezvous. Figure 11-10 provides an exemplary illustration of such a target pattern for automated rendezvous & docking.

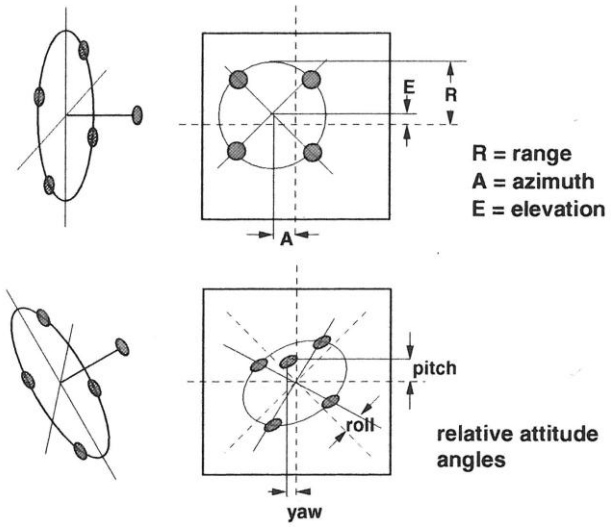

Figure 11-10: Target pattern for automated docking [196, p. 274]. The relative position between the reflector on the stand-off and the reflectors in the plane, as well as the geometry of the reflectors as observed by the sensor system, conveys information about the relative position and orientation of sensor and target. Reproduced with permission of Cambridge University Press.

Since visual targets are limited in their utility by distance and viewing angles, they can only be used in specific tasks. This requires the definition of all operations of interest concerning a satellite during the design phase and precludes any unexpected tasks [219]. Nonetheless, target-based vision systems have been fielded on operational and experimental spacecraft. The *Space Shuttle* tested the use of the *Video Guidance System* (VGS). This is an optical sensor measuring relative range, bearing and attitude of the interceptor vehicle in the terminal phase of automated rendezvous & docking [215]. The sensor head uses a camera and ten laser diodes to illuminate the target. The target has three retroreflectors mounted on the base plate in the corners of a square and a fourth middle reflector mounted on a pole [197]. The reflectors are illuminated at two separate wavelengths in order to be able to remove the background while retaining the reflector spots. The spots' relative distance and position, as well as the middle spot's position in relation to the three base plate spots are used to determine the target's relative position in space, as well as roll, pitch and yaw angles [197]. A similar system, called *Advanced Video Guidance Sensor* (AVGS) was used on NASA's *Demonstration of Autonomous Rendezvous Technology* (DART) mission and *Orbital Express* [220]. Another system working on the same principle is the *AutoTRAC Computer Vision System*. It uses Light Emitting Diodes (LEDs) to illuminate the target pattern and takes one video frame with LEDs on, the second with LEDs off, before subtracting and further processing the frames [220].

Model-based techniques do not require the a priori installation of any artificial targets, since they rely on existing geometry and structure to obtain position and orientation data. Instead, these

techniques require a priori knowledge of the target's geometry, so a CAD description containing the known structure, shape, textures, transmittance and reflectance is required [217]. While obtaining this data for any kind of *future* commercial OOS missions is assumed to be without major problems, it can be challenging for debris removal missions and close to impossible for military rendezvous missions. In addition to a geometric model of the target, the chaser spacecraft needs the capability to reliably detect natural object features for matching the model to the sensor data. This feature detection can be difficult at certain distances, viewing angles and illumination conditions encountered on orbit. In general, model-based vision systems using natural object features are most suitable for close range operations, when these features can reliably be tracked, and when an initial pose is approximately known [219]. In a three-stage process, this initial pose estimation is used to initialize pose refinement and tracking, during the course of which at first the initial estimate is updated using an iterative algorithm, and the established pose is then tracked using a known motion model in a Kalman filter [217].

A vision system using that approach is Boeing's *Vis-STAR* (Vision based Software for Track, Attitude and Ranging), flown on *Orbital Express*. At very long ranges, this software works as a point source tracker, while at short range it tracks the silhouette of the target by using reference images stored in an on-board library. Using this approach, realtime attitude determination can be achieved with accuracy below 1° in each axis of rotation. Once the target vehicle is inside the interceptor's capture corridor, an edge tracker algorithm is additionally used, and within 10 m of the target, a special target plate mounted over the capture interface is used as an aid to precisely align both vehicles [80]. Another model-based state estimation system using video images is *Natural Feature Image Recognition* (NFIR). Its operating principle is to first search the image for a bounding box of a target vehicle, then locate high-contrast target features, and finally match the target features to a 3D model and compute the pose. With perfect camera calibration, NFIR achieves accuracies of 3% in range, 6 cm/s in range rate, 2° in attitude and 0.4 °/s in attitude rate. However, it also shows performance problems when the target is moving too fast or is mostly outside the field of view, and under harsh illumination conditions [220].

Machine vision algorithms that require no a priori knowledge of the target's shape, textures or other visual attributes are referred to as *non-model-based techniques*. These techniques use arbitrary surface features of the target object and do not require establishing and maintaining direct correspondence between small numbers of high level target and model features [219]. Basically, such a technique works like the human brain. It detects and tracks prominent features on the target, establishes a pattern of the feature's motion and maps this motion onto a template in memory or a mathematical function. Examples of such algorithms can be found in [217]. The challenge in these systems lies in the frequent failure of target tracking for feature points which change shape due to perspective projection, appear and disappear due to occlusion, or move against a changing background [217]. As of late 2011, it can be stated that no non-model-based vision system matches the pattern recognition and tracking capabilities of the human eye/brain combination, making

human involvement a requirement for rendezvous & docking to unknown or unfamiliar target objects.

A limitation shared by machine vision systems is that they have difficulties when trying to identify spacecraft on orbit. While it is assumed that for many future OOS missions the target's design documents and CAD models will be available [219], a number of solar arrays and antennas will nonetheless be rotating about one or multiple axes relative to the central body of a satellite to be serviced, which can significantly alter the spacecraft's appearance from one moment to the next [209]. In addition to this, spacecraft surface characteristics and the illumination conditions discussed in Section 3.6 pose challenging problems for imaging cameras and the algorithms of vision systems [221].

Global Navigation Satellite Systems (GNSS)

Global Navigation Satellite Systems like the American GPS, Russian GLONASS, European Galileo and Chinese COMPASS-Beidou consist of large fleets of satellites in multiple orbital planes at mainly medium Earth orbit (MEO) altitudes (around 20000 km of altitude). By processing the time and position signals from at least four satellites, a GNSS receiver is able to iteratively compute its position in space and a precise time. Using GNSS, a spacecraft can determine its position and thus its orbit to within 10 cm [222]. If both target and chaser spacecraft are equipped with GNSS receivers and furthermore an intersatellite data link, they can share their position data and the interceptor can thus compute its rendezvous maneuvers. Such systems based on GPS were tested on *ETS-VII* (with GPS being used for relative navigation at ranges from 10 km to 500 m [77, 202]) and were a factor in the failure of *DART* [202]. GPS is now being operationally used for *HTV* [195], as well as *ATV* [223]. The use of GNSS for operational OOS missions is not feasible, since the current generation of target satellites is commonly neither equipped with GNSS nor the required intersatellite link systems.

Each single sensor system has its own advantages and disadvantages, as well as an optimum operational envelope. Currently no single sensor is able to provide relative position and posture data with the required precision over the complete approach from far range rendezvous down to contact. Rendezvous spacecraft therefore use a combination of different sensors, also referred to as *sensor suites*. The complex sensor suites used by the *Space Shuttle* [43, 155], *ETS-VII* [77], *Orbital Express* [80], *ATV* [224] and *HTV* [195] are good examples.

Passive rendezvous & capture sensor systems have many advantages in the areas of system mass and power consumption over active sensors. Coupled with the human brain's powerful capabilities of object and pattern recognition, they have formed the backbone of human-guided rendezvous & capture. With the growing capabilities of computer hard- and software, space vision systems, combined with GPS and some active sensor systems, will be the center of future rendezvous sensor suites. However, the current sensor and computer vision technology still requires dedicated sensor targets on target objects or extensive a priori information about target geometry. Neither of these

might be available on operational OOS mission, particularly for space debris removal scenarios. In these cases monitoring and analysis of sensor data, above all video data, by human operators will still be an essential part of teleoperation.

B ThirdEye Control Interface Definition

B.1 Packet Contents

The contents of the data packets exchanged consist generally of

- A header part
- A data part following the header

Both parts are more detailed in the following paragraphs.

B.1.1 Header

The header is a fixed structure and will contain following information:

- Length of the data packet (including the header part), in Bytes, e.g. 2 bytes in network-byte-order (big endian). Value interpreted as 16-bit unsigned integer
- Example: 0x012C == 300 bytes length of packet including the header information
- Source of packet, 1 byte, enumeration type, showing the generator of this packet; definition is given below
- Destination of packet, 1 byte, enumeration type, showing the intended destination of this data packet; enumeration is the same table as for the source
- Type of packet (packet ID) (per source), 1 byte. This value must be unique inside a specified source/destination, but it is possible to utilize same packet ID's for different data sources
- Spare Byte, reserve for future use (if necessary), currently this value is ignored and should be set to NULL.

Summary of header

Offset	0	1	2	3	4	5
Content	Length MSB	Length LSB	Source	Destination	Packet ID	Spare (reserved for future use)
Format	Unsigned Integer 16bit		Byte/Enum	Byte/Enum	Byte	NULL

Notes:

- Offset is to be understood as Byte-offset within the packet
- The "Spare Byte" is reserved for future use
- The total length of the packet header is 6 Bytes

B.1.2 Summary of Source & Destination Definition

The following table defines the meaning of source and destination for the exchanged data packets. Such a value is to be defined for each point-to-point TCP/IP communication; i.e. this table is to be extended according to future needs.

Byte Value	Meaning	Comment
0x01	ThirdEye Control	Third Eye Control monitoring and control software
0x02	Robotic Camera Arm	Robotic Camera Arm
…	…	…

Further data sources/destinations have to be defined accordingly.

B.1.3 Summary of Packet ID's

The following table shows a summary of the utilized Ids of data packets to be exchanged between the related data sources and destinations.

Please note, these Ids have to be unique related to source/destination, but it is possible to use same Ids for different sources/destinations.

The target itself is responsible to identify the "command" according to the packet ID.

Source	Destination	Packet ID	Meaning
ThirdEye Control	Robotic Camera Arm		
		0x01	Move arm to position
Robotic Camera Arm	ThirdEye Control		
		0x01	Current arm position

B.2 Packet Definition – Data Parts

The content of the data part starts directly after the header part at offset 6. The layout depends on the related ID's is specified in the following paragraphs related to these ID's.

B.2.1 Monitor Packets from Robotic Camera Arm to ThirdEye Control

The transmission of the monitoring packets (from the Robotic Camera Arm to ThirdEye Control) is performed automatically in regular intervals starting from "opening the link", except the status and settings packets which are to be generated after a reception of a command.

Packet 0x01 – Current arm position

This packet defines the transmission of the arms' current joint positions and velocities.

Header Part:

Offset	Bytes used	Format	Value	Comment
0	2	Int	0x0032	Length of packet (6+44 = 50 Bytes)
2	1	Byte/Enum	0x02	Source Robotic Camera Arm
3	1	Byte/Enum	0x01	Destination Third Eye Control
4	1	Byte/Enum	0x01	Packet ID: arm position
5	1	Byte	0x00	Spare

Data Part:

Offset	Bytes used	Format	Value / Meaning	Comment
6	4	Int	Joint 0 angular position in thousands of degrees	+720000
10	4	Int	Joint 0 angular velocity in thousands of degrees per second	+720000
14	4	Int	Joint 1 angular position in thousands of degrees	+720000
18	4	Int	Joint 1 angular velocity in thousands of degrees per second	+720000
22	4	Int	Joint 2 angular position in thousands of degrees	+720000
26	4	Int	Joint 2 angular velocity in thousands of degrees per second	+720000
30	4	Int	Joint 3 angular position in thousands of degrees	+720000
34	4	Int	Joint 3 angular velocity in thousands of degrees per second	+720000
38	4	Int	Joint 4 angular position in thousands of degrees	+720000
42	4	Int	Joint 4 angular velocity in thousands of	+720000

			degrees per second	
46	4	Int	Timestamp	

B.2.2 Control Packets from ThirdEye Control to Robotic Camera Arm

Packet 0x01 – Move arm to position

This command moves the Robotic Camera Arm to the position given in thousands of degrees

Header Part:

Offset	Bytes used	Format	Value	Comment
0	2	Int	0x0032	Length of packet (6+44 = 50 Bytes)
2	1	Byte/Enum	0x01	Source Third Eye Control
3	1	Byte/Enum	0x02	Destination Robotic Camera Arm
4	1	Byte/Enum	0x01	Packet ID: Move arm to position
5	1	Byte	0x00	Spare

Data Part:

Offset	Bytes used	Format	Value / Meaning	Comment
6	4	Int	Joint 0 angular position in thousands of degrees	+720000
10	4	Int	Joint 0 angular velocity in thousands of degrees per second	+720000
14	4	Int	Joint 1 angular position in thousands of degrees	+720000
18	4	Int	Joint 1 angular velocity in thousands of degrees per second	+720000
22	4	Int	Joint 2 angular position in thousands of degrees	+720000
26	4	Int	Joint 2 angular velocity in thousands of degrees per second	+720000
30	4	Int	Joint 3 angular position in thousands of degrees	+720000
34	4	Int	Joint 3 angular velocity in thousands of degrees per second	+720000
38	4	Int	Joint 4 angular position in thousands of degrees	+720000
42	4	Int	Joint 4 angular velocity in thousands of degrees per second	+720000
46	4	Int	Timestamp	

C ThirdEye Evaluation Experiments Participant Matrix

Participant	ThirdEye activity sequence	Test scenario sequence
101	0 – 1	33-33-31-34 | 41-44-43-42
102	1 – 0	43-41-44-42 | 34-33-32-31
103	0 – 1	33-32-31-34 | 43-41-42-44
104	1 – 0	41-43-42-44 | 34-32-31-33
105	0 – 1	34-33-32-31 | 43-42-44-41
106	1 – 0	43-41-42-44 | 34-33-31-32
107	0 – 1	33-32-34-31 | 42-43-41-44
108	1 – 0	44-41-42-43 | 32-31-33-34
109	0 – 1	34-31-33-32 | 41-42-43-44
110	1 – 0	42-43-44-41 | 34-31-32-33
111	0 – 1	33-34-32-31 | 42-44-41-43
112	1 – 0	41-44-42-43 | 31-34-32-33
113	0 – 1	33-34-31-32 | 43-42-41-44
114	1 – 0	42-44-41-43 | 34-31-33-32
115	0 – 1	32-31-34-33 | 42-43-44-41
116	1 – 0	41-44-43-42 | 31-33-34-32
117	0 – 1	34-32-33-31 | 42-41-44-43
118	1 – 0	41-43-44-42 | 32-34-33-31
119	0 – 1	34-32-31-33 | 44-42-43-41
120	1 – 0	42-44-43-41 | 33-34-32-31

D References

[1] J. L. Goodman and J. P. Brazzel, “Rendezvous Integration Complexities of NASA Human Flight Vehicles,” *32nd Annual AAS Guidance and Control Conference*, February 2009.

[2] P. Milgram and P. H. Wewerinke, *Model Analysis of Remotely Controlled Rendezvous and Docking with Display Prediction*, National Aerospace Laboratory NLR, Amsterdam N86-33003, 1986.

[3] L. M. Weeks, “Manned Rendezvous Systems,” *Proceedings of the Symposium on Space Rendezvous, Rescue and Recovery, Vol. 16, Advances in the Astronautical Sciences, Pt. 2*, pp. 161–166, 1964.

[4] NASA, *Exploration Systems Architecture Study: Final Report*, NASA, 2005.

[5] K. D. Bilimoria, E. R. Mueller, and C. R. Frost, “Handling Qualities Evaluation of Pilot Tools for Spacecraft Docking in Earth Orbit,” *AIAA Guidance, Navigation, and Control Conference*, August 2009.

[6] J. A. McDivitt, “Rendezvous, Rescue and Recovery Aspects of Space Missions,” *Proceedings of the Symposium on Space Rendezvous, Rescue and Recovery, Vol. 16, Advances in the Astronautical Sciences, Pt. 2*, pp. 12–19, 1964.

[7] E. R. Long, JR, J. E. Pennington, and P. L. Deal, *Remote Pilot-Controlled Docking with Television*, NASA Langley Research Center, Hampton, Virginia, NASA Technical Note NASA TN D-3044, October 1965.

[8] D. L. Akin, J. C. Lane, B. J. Roberts, and S. R. Weisman, “Robotic Capabilities for Complex Space Operations,” *AIAA Space 2001 Conference and Exposition, Albuquerque, NM, Aug. 28-30, 2001*, pp. 1–11, 2001.

[9] D. K. Geller, “Orbital Rendezvous: When Is Autonomy Required?,” *Journal of Guidance, Control, and Dynamics*, vol. 30, no. 4, pp. 974–981, 2007.

[10] B. P. Hine, P. Hontalas, T. Fong, L. Piguet, E. Nygren, and A. Kline, “VEVI: A Virtual Environment Teleoperations Interface for Planetary Exploration,” *SAE 25th International Conference on Environmental Systems*, vol. 25, 1995.

[11] J. H. Saleh, D. E. Hastings, and D. J. Newman, “Spacecraft Design Lifetime,” *Journal of Spacecraft and Rockets*, vol. 39, no. 2, pp. 244–257, 2002.

[12] A. M. Long, M. G. Richards, and D. E. Hastings, “On-Orbit Servicing: A New Value Proposition for Satellite Design and Operation,” *Journal of Spacecraft and Rockets*, vol. 44, no. 4, pp. 964–976, 2007.

[13] B. R. Sullivan, *Technical and Economic Feasibility of Telerobotic On-Orbit Satellite Servicing*, Dissertation, Space Systems Laboratory, University of Maryland, College Park, Maryland, 2005.

[14] A. Ellery, J. Kreisel, and B. Sommer, “The case for robotic on-orbit servicing of spacecraft: Spacecraft reliability is a myth,” *Acta Astronautica*, vol. 63, no. 5-6, pp. 632–648, 2008.

[15] J. H. Saleh, E. Lamassoure, D. E. Hastings, and D. J. Newman, “Flexibility and the Value of On-Orbit Servicing: New Customer-Centric Perspective,” *Journal of Spacecraft and Rockets*, vol. 40, no. 2, pp. 279–291, March-April 2003.

[16] J. H. Saleh, J.-P. Torres-Padilla, D. E. Hastings, and D. J. Newman, “To Reduce or to Extend a Spacecraft Design Lifetime?,” *Journal of Spacecraft and Rockets*, vol. 43, no. 1, pp. 207–217, 2006.

[17] C. Joppin, *On-Orbit Servicing For Satellite Upgrades*, Master's Thesis, Engineering Systems Division, Massachusetts Institute of Technology, Cambridge, Mass, 2004.

[18] M. Tafazoli, “A study of on-orbit spacecraft failures,” *Acta Astronautica*, vol. 64, no. 2-3, pp. 195–205, 2009.

[19] B. Wheeden, "Zombiesats and On-Orbit Servicing," *MilsatMagazine*, vol. 3, no. 5, pp. 38-, September/October 2010.
[20] J. Kreisel, "On-Orbit Servicing (OOS): Issues & Commercial Implications," *International Astronautical Congress*, 2003.
[21] C. Joppin and D. E. Hastings, "On-Orbit Upgrade and Repair: The Hubble Space Telescope Example," *Journal of Spacecraft and Rockets*, vol. 43, no. 3, pp. 614–625, 2006.
[22] M. H. Skeer, *Potential Satellite Servicing Operations and the Impact of Servicing on Satellite Design*, Bellcomm, Inc, Washington, DC 20024, Jul. 1969.
[23] D. M. Waltz, *On-orbit servicing of space systems*. Malabar, Fla.: Krieger, 1993.
[24] C. M. Reynerson, "Spacecraft Modular Architecture Design For On-Orbit Servicing," *2000 IEEE Aerospace Conference*, no. 4, pp. 227–238, 2000.
[25] A. S. Kiersarsky, *Effects of In-Orbit Servicing on Nimbus Configuration*, Bellcomm, Inc, Washington, DC 20024, Jul. 1969.
[26] G. A. P. Horsham, G. R. Schmidt, and J. H. Gilland, *Establishing a Robotic, LEO-to-GEO Satellite Servicing Infrastructure as an Economic Foundation for Exploration*, NASA Glenn Research Center, Cleveland, Ohio, USA, NASA Technical Memorandum NASA/TM-2010-216937, November 2010.
[27] B. Liang, C. Li, L. Xue, and W. Qiang, "A Chinese Small Intelligent Space Robotic System for On-Orbit Servicing," *2006 IEEE/RSJ International Conference on Intelligent Robots and Systems*, pp. 4602–4607, October 2006.
[28] G. A. P. Horsham, *Envisioning a 21st Century, National, Spacecraft Servicing and Protection Infrastructure and Demand Potential: A Logical Development of the Earth Orbit Economy*, NASA/TM-2003-212462, Glenn Research Center, Cleveland, Ohio, July 2003.
[29] R. W. Madison, "Micro-Satellite Based, On-orbit Servicing Work at the Air Force Research Laboratory," *2000 IEEE Aerospace Conference*, pp. 215–226, March 2000.
[30] M. G. Richards, *On-Orbit Serviceability of Space System Architectures*, Master's Thesis, Department of Aeronautics and Astronautics, Massachusetts Institute of Technology, Cambridge, Mass, 2006.
[31] J. H. Saleh, E. Lamassoure, and D. E. Hastings, "Space Systems Flexibility Provided by On-Orbit Servicing: Part 1," *Journal of Spacecraft and Rockets*, vol. 39, no. 4, pp. 551–560, 2002.
[32] E. Lamassoure, J. H. Saleh, and D. E. Hastings, "Space Systems Flexibility Provided by On-Orbit Servicing: Part 2," *Journal of Spacecraft and Rockets*, vol. 39, no. 4, pp. 561–570, 2002.
[33] D. A. Whelan, E. A. Adler, S. B. Wilson, and G. Roesler, "The DARPA Orbital Express Program: Effecting a Revolution in Space-Based Systems," *Proceedings of SPIE*, vol. 4136, pp. 48–56, 2000.
[34] Union of Concerned Scientists, *UCS Satellite Database: Satellite Quick Facts.* Available: http://www.ucsusa.org/nuclear_weapons_and_global_security/space_weapons/technical_issues/ucs-satellite-database.html (2011, Aug. 09).
[35] L. Pedersen, D. Kortenkamp, D. Wettergreen, and I. Nourbakhsh, "A Survey of Space Robotics," *Proceedings of the 7th International Symposium on Artificial Intelligence, Robotics and Automation in Space (i-SAIRAS-03)*, pp. 1–8, 2003.
[36] T. M. Davis and D. Melanson, "XSS-10 Micro-Satellite Flight Demonstration," *Proceedings of SPIE*, vol. 5419, no. 16, pp. 1–18, 2006.
[37] B. Wheeden, *XSS-10.* Available: http://swfound.org/media/1791/x-37b_factsheet.pdf (10 June, 2011).
[38] C. Covault, *Secret inspection satellites boost space intelligence ops.* Available: http://spaceflightnow.com/news/n0901/14dsp23/ (2011, Jul. 12).
[39] W. Doggett, "Robotic Assembly of Truss Structures for Space Systems and Future Research Plans," *2002 IEEE Aerospace Conference*, 2002.

[40] H. Ueno, T. Nishimaki, M. Oda, and N. Inaba, "Autonomous Cooperative Robots for Space Structure Assembly and Maintenance," *Proceeding of the 7th International Symposium on Artificial Intelligence, Robotics and Automation in Space (iSAIRAS 2003)*, May 2003.
[41] NASA, *Human Exploration of Mars Design Reference Architecture 5.0*, NASA Johnson Space Center, Houston, TX, USA NASA-SP-2009-566, July 2009.
[42] R. L. Werneth, "Lessons Learned from Hubble Space Telescope ExtraVehicular Activity Servicing Missions," *American Institute of Physics Conference Proceedings*, vol. 552, pp. 176–188, 2001.
[43] J. L. Goodman, "History of Space Shuttle Rendezvous and Proximity Operations," *Journal of Spacecraft and Rockets*, vol. 43, no. 5, pp. 944–959, September-October 2006.
[44] R. L. Hibbard, *Satellite On-Orbit Refueling: A Cost Effectiveness Analysis*, Master's Thesis, Naval Postgraduate School, Monterey, California, 1996.
[45] P. B. de Selding, *C band Reflector on Intelsat New Dawn Fails To Deploy.* Available: http://www.spacenews.com/satellite_telecom/110503c-band-reflector-intelsat-new-dawn-fails-deploy.html (2011, Aug. 05).
[46] P. B. de Selding, *Telesat Expects 12 Years of Service from Newest Satellite.* Available: http://www.spacenews.com/satellite_telecom/110804-telesat-expects-12yrs-service-sat.html (2011, Aug. 05).
[47] F. G. Kennedy, III, "Orbital Express: Accomplishments and Lessons Learned," *Advances in the Astronautical Sciences*, vol. 131, pp. 575–586, 2008.
[48] D. Reintsema, K. Landzettel, and G. Hirzinger, "DLR's Advanced Telerobotic Concepts and Experiments for On-Orbit Servicing," in *Springer Tracts in Advanced Robotics*, vol. 31, *Advances in Telerobotics*, M. Ferre, M. Buss, R. Aracil, C. Melchiorri, and C. Balaguer, Eds, Berlin, Heidelberg: Springer, 2007, pp. 323–345.
[49] D. R. Wingo, "Orbital Recovery's Responsive Commercial Space Tug for Life Extension Missions," *AIAA 2nd Responsive Space Conference*, April 2004.
[50] F. Morring, JR, *An End To Space Trash?* Available: http://www.aviationweek.com/aw/generic/story.jsp?id=news/awst/2011/03/21/AW_03_21_2011_p23-297586.xml&headline=An%20End%20to%20Space%20Trash?&channel=awst (2011, Aug. 03).
[51] P. B. de Selding, *Intelsat Signs Up for Satellite Refueling Service.* Available: http://www.spacenews.com/satellite_telecom/intelsat-signs-for-satellite-refueling-service.html (2011, Aug. 03).
[52] P. B. de Selding, *MDA, Intelsat Scrap In-orbit Servicing Deal.* Available: http://www.spacenews.com/satellite_telecom/120117-mda-intelsat-scrap-deal.html (2012, Apr. 04).
[53] NASA, *On-Orbit Satellite Servicing Study: Project Report*, NASA Goddard Spaceflight Center, Greenbelt, MD, USA NP-2010-08-162-GSFC, October 2010.
[54] NASA, *Robotic Refueling Mission*, NASA Goddard Spaceflight Center, Greenbelt, MD, USA, NASA Facts FS-2011-3-112-GSFC, 2011.
[55] J. Shoemaker and M. Wright, "Orbital Express Space Operations Architecture Program," *Proceedings of SPIE*, vol. 5088, pp. 1–9, August 2003.
[56] Jet Propulsion Laboratory, *Spitzer Space Telescope.* Available: http://www.spitzer.caltech.edu/uploaded_files/other_files/0000/2955/spitzer-fact-sheet1.pdf (2011, Jul. 14).
[57] R. D. Gehrz, T. L. Roellig, M. W. Werner, G. G. Fazio, J. R. Houck, F. J. Low, G. H. Rieke, B. T. Soifer, D. A. Levine, and E. A. Romana, "The NASA Spitzer Space Telescope," *Rev. Sci. Instrum*, vol. 78, no. 1, p. 11302, 2007.
[58] A. Miele, M. Ciarcià, and M. W. Weeks, "Guidance Trajectories for Spacecraft Rendezvous," *Journal of Optimization Theory Application*, no. 132, pp. 377–400, 2007.

[59] T. C. Brisibe and I. Pessoa-Lopes, "The Impact of Orbital Debris on Commercial Space Systems," *44th International Colloqium on the Law of Outer Space*, October 2001.
[60] D. Mehrholz, L. Leushacke, W. Flury, R. Jehn, H. Klinkrad, and M. Landgraf, "Detecting, Tracking and Imaging Space Debris," *ESA Bulletin*, no. 109, pp. 128–134, 2002.
[61] D. J. Kessler, N. L. Johnson, J.-C. Liou, and M. Matney, "The Kessler Syndrome: Implications to Future Space operations," *Proceeding of 33rd Annual AAS Guidance and Control Conference*, February 2010.
[62] T. Yasaka and E. W. Ashford, "GSV: An Approach Toward Space System Servicing," *Earth Space Review*, vol. 5, no. 2, pp. 9–17, 1996.
[63] A. B. Bosse, W. J. Barnds, M. A. Brown, N. G. Creamer, A. Feerst, C. G. Henshaw, A. S. Hope, B. E. Kelm, P. A. Klein, F. Pipitone, B. E. Plourde, and B. P. Whalen, "SUMO: spacecraft for the universal modification of orbits," *Proceedings of SPIE*, vol. 5419, pp. 36–46, 2004.
[64] J. R. Wilson, "Satellite hopes ride on Orbital Express," *Aerospace America*, pp. 30–35, February 2007.
[65] D. Reintsema, J. Thaeter, A. Rathke, W. Naumann, P. Rank, and B. Sommer, "DEOS - The German Robotics Approach to Secure and De-Orbit Malfunctioned Satellites from Low Earth Orbits," *Proceedings of the International Symposium on Artificial Intelligence, Robotics and Automation in Space (iSAIRAS 2010)*, August 2010.
[66] F. Riedel, *Entwicklung einer Systemarchitektur zur Entfernung von Space Debris Objekten*, unpublished student thesis (Diplomarbeit), Lehrstuhl für Raumfahrttechnik, Technische Universität München, Munich, 2009.
[67] S. Huberth, *Untersuchung von technischen Möglichkeiten zum De-Orbiting von Space Debris Objekten*, unpublished student thesis (Diplomarbeit), Lehrstuhl für Raumfahrttechnik, Technische Universität München, Munich, 2010.
[68] D. King, "Space Servicing: Past, Present and Future," *Proceeding of the 6th International Symposium on Artificial Intelligence and Robotics & Automation in Space: i-SAIRAS 2001*, 2001.
[69] NASA, *STS-103 Shuttle Mission Imagery: STS103-713-048.* Available: http://spaceflight.nasa.gov/gallery/images/shuttle/sts-103/html/sts103_713_048.html (2011, Sep. 14).
[70] J. L. Goodman and S. R. Walker, "Hubble Servicing Challenges Drive Innovation of Shuttle Rendezvous Techniques," *32nd Annual AAS Guidance and Control Conference*, pp. 1–23, February 2009.
[71] G. G. Gefke, *Mission Operations Analysis of a Telerobotic Satellite Servicer in Low Earth Orbit*, Master's Thesis, Department of Aerospace Engineering, University of Maryland, College Park, Maryland, 1994.
[72] D. L. Akin, B. Roberts, K. Pilotte, and M. Baker, "Robotic Augmentation of EVA for Hubble Space Telescope Servicing," *AIAA Space 2003*, September 2003.
[73] J. C. Parrish, "The Ranger Telerobotic Flight Experiment: A teleservicing system for on-orbit spacecraft," *Proceedings of SPIE*, vol. 2901, no. 177, 1996.
[74] J. C. Lane, C. R. Carignan, and D. L. Akin, "Advanced Operator Interface Design for Complex Space Telerobots," *Autonomous Robots*, vol. 11, pp. 49–58, 2001.
[75] University of Maryland, *Telerobotic Flight Experiment (TFX).* Available: http://robotics.ssl.umd.edu/ranger/repository/photos/RangerTFX.pdf (2011, Sep. 14).
[76] C. R. Carignan, J. C. Lane, and P. J. Churchill, "Controlling Robots On-Orbit," *Proceedings of the 2001 IEEE Sympsoium on Computational Intelligence in Robotics and Automation*, pp. 314–319, 2001.
[77] M. Oda, "ETS-VII: Achievements, Troubles and Future," *Proceeding of the 6th International Symposium on Artificial Intelligence and Robotics & Automation in Space: i-SAIRAS 2001*, 2001.
[78] Tohoku University, *Academic Experiments Carried Out on ETS-VII Japanese Flying Space Robot.* Available: http://www.astro.mech.tohoku.ac.jp/~yoshida/ETS-VII/ (2011, Sep. 14).

[79] C. R. Carignan and D. L. Akin, "The Reaction Stabilization of On-Orbit Robots: Countering the Effects of Satellite-Based Manipulators," *IEEE Control Systems Magazine*, pp. 19–33, December 2000.
[80] T. Weismuller and M. Leinz, "GN&C Technology Demonstrated by the Orbital Express Autonomous Rendezvous and Capture Sensor System," *29th Annual AAS Guidance and Control Conference*, February 2006.
[81] Boeing Image, *ASTRO and NEXTSat During Unmated Operations.* Available: http://www.boeing.com/companyoffices/gallery/images/orbital_express/oe_038.html (2011, Sep. 14).
[82] M. R. Endsley, "Situation Awareness Global Assessment Technique (SAGAT)," *Proceedings of the IEEE 1988 National Aerospace and Electronics Conference*, vol. 3, pp. 789–795, May 1988.
[83] C. J. Dennehy and J. R. Carpenter, *A Summary of the Rendezvous, Proximity Operations, Docking and Undocking (RPODU) Lessons Learned from the Defense Advanced Research Project Agency (DARPA) Orbital Express (OE) Demonstration System Mission*, NASA Langley Research Center, Hampton, Virginia, NASA Engineering and Safety Center Technical Assessment Report NESC-RP-10-00628, April 2011.
[84] S. Matsumoto, S. Jacobsen, S. Dubowsky, and Y. Ohkami, "Approach Planning and Guidance for Uncontrolled Rotating Satellite Capture Considering Collision Avoidance," *Proceedings of the 7th International Symposium on Artificial Intelligence, Robotics and Automation in Space (i-SAIRAS-03)*, May 2003.
[85] J. K. Thienel and R. Sanner, "Hubble Space Telescope Angular Velocity Estimation During the Robotic Servicing Mission," *Journal of Guidance, Control, and Dynamics*, vol. 30, no. 1, pp. 29–34, January-February 2007.
[86] J. D. Ianni, D. W. Repperger, R. W. Baker, and R. L. Williams, "Human Interfaces for Robotic Satellite Servicing," *Proceedings of SPIE*, vol. 4632, pp. 95–103, 2002.
[87] P. Milgram, *Control Loops with Human Operators in Space Operations: Part V: Executive Summary*, NLR TR 84116 U Part V, Netherland National Aerospace Laboratories, Amsterdam NLR-TR-84116-U-PartV, 1986.
[88] Union of Concerned Scientists, *UCS Satellite Database.* Available: http://www.ucsusa.org/nuclear_weapons_and_global_security/space_weapons/technical_issues/ucs-satellite-database.html (2011, Sep. 16).
[89] Arianespace, "Flight 163 - Telesat Anik F2," Arianespace, Arianespace Launch Kit, 2004.
[90] P. W. Singer and J. Polk, *Wired for war: The robotics revolution and conflict in the twenty-first century*. Washington D.C: National Library Service for the Blind and Physically Handicapped Library of Congress, 2010.
[91] Jet Propulsion Laboratory, *PIA14760: Curiosity at Work on Mars (Artist's Concept).* Available: http://photojournal.jpl.nasa.gov/catalog/PIA14760 (2012, Jun. 01).
[92] T. B. Sheridan, *Telerobotics, automation, and human supervisory control*. Cambridge, Mass.: MIT Pr, 1992.
[93] J. V. Draper, "Teleoperators for advanced manufacturing: Applications and human factors challenges," *Int. J. Hum. Factors Manuf*, vol. 5, no. 1, pp. 53–85, 1995.
[94] J. Cui, S. Tosunoglu, R. Robert, C. Moore, and D. W. Repperger, "A Review of Teleoperation System Control," *Florida Conference on Recent Advances in Robotics*, May 2003.
[95] J. M. Riley, *The Utility of Measures of Attention and Situation Awareness for Quantifying Telepresence*, Dissertation, Department of Industrial Engineering, Mississippi State University, Mississippi, 2001.
[96] M. Draper, *Advanced UMV Operator Interfaces*, NATO Research & Technology Organization RTO-TR-HFM-078, 2005.
[97] C. Stoker, "From Antarctica to Space: Use of Telepresence and Virtual Reality in Control of a Remote Underwater Vehicle," *Proceedings of SPIE*, vol. 2352, pp. 288–299, 1995.

[98] M. Ferre, S. Cobos, R. Aracil, and M. A. Sánchez Urán, "3D-Image Visualization and its Performance in Teleoperation," in *Lecture Notes in Computer Science*, vol. 4563, *Virtual Reality*, R. Shumaker, Ed, Berlin Heidelberg: Springer-Verlag, 2007, pp. 22–31.
[99] S.-L. Donovan and T. Triggs, *Investigating the Effects of Display Design on Unmanned Underwater Vehicle Pilot Performance*, DSTO-TR-1931, Maritime Platforms Division, Defence Science and Technology Division, Fishermans Bend, Victoria, Australia, October 2006.
[100] J. V. Draper, D. B. Kaber, and J. M. Usher, "Telepresence," *Human Factors*, vol. 40, no. 3, pp. 354-275, 1998.
[101] M. W. McGreevy and C. Stoker, "Telepresence for Planetary Exploration," *Proceedings of SPIE*, vol. 1387, pp. 110–123, 1990.
[102] B. P. Hine, C. Stoker, M. Sims, D. Rasmussen, P. Hontalas, T. Fong, J. Steele, D. R. Barch, D. Andersen, E. Miles, and E. Nygren, "The Application of Telepresence and Virtual Reality to Subsea Exploration," *The 2nd Workshop on Mobile Robots for Subsea Environments, Proc. ROV'94*, 1994.
[103] J. Pretlove, "Augmenting reality for telerobotics: unifying real and virtual worlds," *Industrial Robot: An International Journal*, vol. 25, no. 6, pp. 401–407, 1998.
[104] T. B. Sheridan, "Teleoperation, Telerobotics and Telepresence: A Progress Report," *Control Engineering Practice*, vol. 3, no. 2, pp. 205–214, 1995.
[105] S. Hughes, J. Manojlovich, M. Lewis, and J. Gennari, "Camera Control and Decoupled Motion for Teleoperation," *IEEE International Conference on Systems, Man and Cybernetics*, vol. 2, pp. 1339–1344, October 2003.
[106] H. G. Stassen and G. J. F. Smets, "Telemanipulation and Telepresence," *Control Engineering Practice*, vol. 5, no. 3, pp. 363–374, 1997.
[107] P. F. Hokayem and M. W. Spong, "Bilateral Teleoperation: An Historical Survey," *Automatica*, vol. 42, no. 12, pp. 2035–2057, 2006.
[108] W. Engelhardt, *Galileo, Cassini, Giotto: Raumsonden erforschen unser Planetensystem ; [mit Multiplattform-CD-ROM],* 1st ed. Frankfurt am Main: Deutsch, 2005.
[109] P. Ulivi and D. M. Harland, *Robotic exploration of the solar system*. Berlin ;, New York, Chichester UK: Springer; Published in association with Praxis Pub, 2007.
[110] T. Fong and C. Thorpe, "Vehicle Teleoperation Interfaces," *Autonomous Robots*, vol. 11, pp. 9–18, 2001.
[111] S. Lichiardopol, *A Survey on Teleoperation*, Technische Universiteit Eindhoven, Eindhoven, Netherlands, DCT Report DCT 2007.155, December, 2007.
[112] J. Yuh, "Underwater Robotics," *Proceedings of the 2000 IEEE International Conference on Robotics & Automation*, pp. 932–937, 2000.
[113] V. Iastrebov, G. Seet, T. Asokan, Y. P. Chui, and M. W. S. Lau, "Vision Enhancement Using Stereoscopic Telepresence for Remotely Operated Underwater Robotic Vehicles," *Journal of Intelligent Robotic Systems*, no. 52, pp. 139–154, 2008.
[114] Oceaneering, *Millennium ROV working subsea.* Available: http://www.oceaneering.com/wp-content/uploads/2010/05/oceaneering-millennium-rov-subsea.jpg (2011, Nov. 08).
[115] U.S. Air Force, *MQ-9 Reaper.* Available: http://www.af.mil/information/factsheets/factsheet.asp?fsID=6405 (2011, Nov. 08).
[116] iRobot, *iRobot 710 Warrior.* Available: http://www.irobot.com/gi/ground/710_Warrior//l4 (2011, Nov. 08).
[117] P. Jasiobedzki and R. Jakola, "From Space Robotics to Underwater Mining," pp. 1–9., Available: citeseerx.ist.psu.edu/viewdoc/download?doi=10.1.1.118.9489&rep=rep1&type=pdf (2012, June 15)
[118] C. F. Kottler, JR, "Underwater Systems Within the Scientific, Technological, and Economic Framework," *Journal of Hydronautics*, vol. 3, no. 1, pp. 2–11, 1969.

[119] R. D. Palamara and W. J. Bridges, "Equations of Motion of a Deep Submergence Rescue Vehicle with Active Mercury Damping Control," *Journal of Hydronautics*, vol. 2, no. 2, pp. 74–80, 1968.
[120] J. Yuh, "Design and Control of Autonomous Underwater Robots: A Survey," *Autonomous Robots*, vol. 8, pp. 7–24, 2000.
[121] C. Stoker, D. R. Barch, B. P. Hine, and J. Barry, "Antarctic Undersea Exploration Using a Robotic Submarine with a Telepresence User Interface," *IEEE Expert: Intelligent Systems and Their Applications*, vol. 10, no. 6, pp. 14–23, December 1995.
[122] M. J. Martin and C. W. Sasser, *Predator: The remote-control air war over Iraq and Afghanistan : a pilot's story*. Minneapolis, MN: Zenith Press, 2010.
[123] J. Y. C. Chen, E. C. Haas, K. Pillalamarri, and C. N. Jacobson, *Human-Robot-Interface: Issues in Operator Performance, Interface Design, and Technologies*, ARL-TR-3834, Army Research Laboratory, Aberdeen Proving Ground, MD 21005-5425, July 2006.
[124] B. Ricks, C. W. Nielsen, and M. A. Goodrich, "Ecological Displays for Robot Interaction: A New Perspective," *Proceedings of the 2004 IEEE/RSJ International Conference on Intelligent Robots and Systems*, pp. 2855–2860, 2004.
[125] G. L. Calhoun, M. H. Draper, M. F. Abernathy, F. Delgado, and M. Patzek, "Synthetic vision system for improving unmanned aerial vehicle operator situation awareness," *Proceedings of SPIE*, vol. 5802, pp. 219–230, 2005.
[126] C. W. Nielsen, M. A. Goodrich, and R. J. Rupper, "Towards Facilitating the Use of a Pan-Tilt Camera on a Mobile Robot," *2005 IEEE International Workshop on Robots and Human Interactive Communication*, pp. 568–573, 2005.
[127] N. J. Cooke, H. L. Pringle, H. K. Pedersen, and O. Connor, *Human factors of remotely operated vehicles,* 1st ed. Amsterdam: Elsevier JAI, 2006.
[128] J. E. Cutting, "How the eye measures reality and virtual reality," *Behavior Research Methods, Instruments, & Computers*, vol. 29, no. 1, pp. 27–36, 1997.
[129] C. D. Wickens, S. Todd, and K. Seidler, *Three-Dimensional Displays: Perception, Implementation, and Application*, University of Illinois, Aviation Research Laboratory, Savoy, Illinois CSERIAC-SOAR-89-001, October 1989.
[130] J. C. Lane, *Human Factors Optimization of Virtual Environment Attributes for a Space Telerobotic Control Station*, Dissertation, Department of Aerospace Engineering, University of Maryland, College Park, Maryland, 2000.
[131] B. Yamauchi and K. Massey, "Stingray: High-Speed Teleoperation of UGVs in Urban Terrain Using Driver-Assist Behaviors and Immersive Telepresence," *Proceedings of the 26th Army Science Conference, Orlando, Florida*, December 2008.
[132] M. Mouloua, R. Gilson, and P. Hancock, "Workload, Situation awareness, and Teaming Issues for UAV/UCAV Operations," *Proceedings of the Human Factors and Ergonomics Society 45th Annual Meeting*, pp. 162–165, 2001.
[133] F. DeCrescenzio, G. Miranda, F. Persiani, and T. Bombardi, "A First Implementation of an Advanced 3D Interface to Control and Supervise UAV Missions," *Presence*, vol. 18, no. 3, pp. 171–184, 2009.
[134] M. R. Endsley, "Design and evaluation for situation awareness enhancement," *Proceedings of the Human Factors Society 32nd Annual Meeting*, pp. 97–101, 1988.
[135] A. V. Gomez, C. Saracini, F. Botta, and G. Randelli, "Spatial processes in mobile robot teleoperation," *Cognitive Processes*, vol. 10, no. 2, pp. 338–341, 2009.
[136] T. Fong, D. B. Kaber, M. Lewis, J. Scholtz, A. Schultz, and A. Steinfeld, "Common Metrics for Human-Robot Interaction," *IEEE International Conference on Intelligent Robots and Systems*, pp. 1–8, 2004.
[137] C. D. Wickens, O. Olmos, A. Chudy, and C. Davenport, *Aviation Display Support for Situation Awareness*, University of Illinois, Aviation Human Factors Division, Savoy, Illinois ARL-97-10/LOGICON-97-2, July 1997.

[138] J. L. Drury, J. Richer, N. Rackliffe, and M. A. Goodrich, *Comparing Situation Awareness for Two Unmanned Aerial Vehicle Human Interface Approaches*, The MITRE Corporation, Bedford, Massachusetts, USA, 2006.
[139] H. A. Yanco and J. L. Drury, ""Where Am I?" Acquiring Situation Awareness Using Remote Robot Platform," *2004 IEEE International Conference on Systems, Man and Cybernetics*, vol. 3, pp. 2835–2840, 2004.
[140] M. L. Cummings, K. Myers, and S. D. Scott, "Modified Cooper Harper Evaluation Tool for Unmanned Vehicle Displays," *Proceedings of UVS Canada: Conference on Unmanned Vehicle Systems*, 2006.
[141] A. Steinfeld, "Interface Lessons for Fully and Semi-Autonomous Mobile Robots," *IEEE International Conference on Robotics and Automation*, pp. 1–6, 2004.
[142] Y. Nagai, S. Tsuchiya, T. Iida, and S. Kimura, "Audio Feedback System for Teleoperation Experiments on Engineering Test Satellite VII: System Design and Assessment Using Eye Mark Recorder for Capturing Task," *IEEE Transactions on Systems, Man and Cybernetics - Part A: Systems and Humans*, vol. 32, no. 2, pp. 237–247, March 2002.
[143] S. C. Martin, L. L. Whitcomb, R. Arsenault, M. Plumlee, and C. Ware, "A System for Real-Time Spatio-Temporal 3-D Data Visualization in Underwater Robotic Exploration," *Proceedings of the 2005 IEEE International Conference on Robotics and Automation*, pp. 1616–1623, 2005.
[144] S. Horton, *Predator soars to record numbers of sorties.* Available: http://www.af.mil/news/story.asp?id=123063918 (2011, Nov. 09).
[145] E. Peltzer, *2009 Pacific Northwest Expedition - Leg 1 Logbook: Day 10 - Operation Deep Probe.* Available: http://www.mbari.org/expeditions/Northern09/L1/july16.htm (2011, Nov. 09).
[146] S. R. Weisman, *The Effect of Video Configuration on Operator Control of Free-Flying Robots*, Master's Thesis, Department of Aerospace Engineering, University of Maryland, College Park, Maryland, 2000.
[147] M. Kanazawa, K. Mitani, K. Hamasaki, M. Sugawara, F. Okano, K. Doi, and M. Seino, "Ultrahigh-Definition Video System with 4000 Scanning Lines," *SMPTE Technical Conference No 144, Pasadena, CA*, vol. 112, no. 10-11, pp. 339–347, 2003.
[148] M. E. Morphew, J. R. Shively, and D. Casey, "Helmet Mounted Displays for Unmanned Aerial Vehicle Control," in *Proceedings of SPIE: Helmet- and head-mounted displays IX: Technologies and applications* (Vol. 5442), C. E. Rash and C. E. Reese, Eds, Bellingham, WA: SPIE, 2004, pp. 93–103
[149] B. P. Hunn, *The Human Factors of Sensor Fusion*, Army Research Laboratory, Aberdeen Proving Ground, MD 21005-5425, May 2008.
[150] G. Terrien, C. Thorpe, T. Fong, and C. Baur, "Remote Driving With a Multisensor User Interface," *SAE 30th International Conference on Environmental Systems. July 2000*, 2000.
[151] J. C. Lane, C. R. Carignan, and D. L. Akin, "Time delay and communication bandwidth limitation on telerobotic control," *Proceedings of SPIE*, vol. 4195, pp. 405–419, 2001.
[152] J. C. Lane, C. R. Carignan, and D. L. Akin, "Advanced Operator Interface Design for Complex Space Telerobots," *Autonomous Robots*, vol. 11, pp. 49–58, 2001.
[153] M. Oda, "Experiences and lessons learned from the ETS-VII robot satellite," *Proceedings of the 2000 IEEE International Conference on Robotics & Automation*, pp. 914–919, April 2000.
[154] Z. Milenkovic, "The Rendezvous and Proximity Operations Program Displays and Controls Capabilities as Tools for Situational Awareness," *Proceeding of the 2012 IEEE Aerospace Conference*, March 2012.
[155] D. Zimpfer and P. Spehar, "STS-71 Shuttle/Mir GNC Mission Overview," *Spaceflight Mechanics 1996*, *Advances in the Astronautical Sciences*, vol. 93, Part I, pp. 441–460, 1996.
[156] D. M. Johnson, *Introduction to and Review of Simulator Sickness Research*, U.S. Army Research Institute for the Behavioral and Social Sciences, Arlington, VA, USA Research Report 1832, April 2005.

[157] E. M. Kolasinski, *Simulator Sickness in Virtual Environments*, U.S. Army Research Institute for the Behavioral and Social Sciences, ARI Technical Report 1027, 1995.
[158] D. Hastings and H. Garrett, *Spacecraft-environment interactions*. Cambridge: Cambridge University Press, 1996.
[159] A. C. Tribble, *The space environment: Implications for spacecraft design*. Princeton, N.J: Princeton University Press, 2003.
[160] J. R. Wertz and W. J. Larson, *Space mission analysis and design,* 3rd ed. Torrance, Calif, Dordrecht ;, Boston: Microcosm; Kluwer, 1999.
[161] E. Stoll, *Ground verification of telepresence for On-Orbit Servicing*. Dissertation, München: Verl. Dr. Hut, 2009.
[162] R. Held, A. Efstathiou, and M. Greene, "Adaptation to Displaced and Delayed Visual Feedback from the Hand," *Journal of Experimental Psychology*, vol. 72, no. 6, pp. 887–891, 1966.
[163] J. C. Lane, C. R. Carignan, B. R. Sullivan, D. L. Akin, T. Hunt, and R. Cohen, "Effects of Time Delay on Telerobotic Control of Neutral Buoyancy Vehicles," *IEEE International Conference on Robotics and Automation*, 2002.
[164] R. J. Anderson and M. W. Spong, "Bilateral Control of Teleoperators with Time Delay," *Proceedings of the 27th Conference on Decision and Control*, pp. 167–173, December 1988.
[165] T. B. Sheridan, "Space Teleoperation Through Time Delay: Review and Prognosis," *IEEE Transactions on Robotics and Automation*, vol. 9, no. 5, pp. 592–606, 1993.
[166] K. Landzettel, C. Preusche, A. Albu-Schäffer, D. Reintsema, and G. Hirzinger, "Robotic On-Orbit Servicing - DLR's Experience and Perspective," *Proceedings of the 2006 IEEE/RSJ International Conference on Intelligent Robots and Systems*, pp. 4587–4594, 2006.
[167] L. Hodges and R. Woll, "Air Force Satellite Control Network (AFSCN) Support for Operational Responsive Space (ORS)," *6th Responsive Space Conference*, Los Angeles, CA, Apr. 2008.
[168] J. Teles, M. V. Samii, and C. E. Doll, "Overview of TDRSS," *Advances in Space Research*, vol. 16, no. 12, pp. 67–76, 1995.
[169] H. Anegawa and S. Furushima, "CCSDS Packet Data Handling System of ETS-VII," *AIAA 17th International Communications Satellite Systems Conference and Exhibit*, February 1998.
[170] M. Oda, "System Enigineering Approach in Designing the Teleoperation System of the ETS-VII Robot Experiment Satellite," *Proceedings of the 1997 IEEE International Conference on Robotics and Automation*, April 1997.
[171] U. Walter, *Astronautics*. 2nd Edition, Weinheim: Wiley-VCH, 2012.
[172] F. Sauceda, *Space Station Reference Coordinate Systems*, NASA, Houston, TX SSP 30219, Oct. 2001.
[173] W. H. Clohessy and R. S. Wiltshire, "Terminal Guidance System for SatelliteRendezvous," *Journal of the Aerospace Sciences*, vol. 27, pp. 653–658, 1960.
[174] A. Miele, M. W. Weeks, and M. Ciarcià, "Optimal Trajectories for Spacecraft Rendezvous," *Journal of Optimization Theory Application*, no. 132, pp. 353–376, 2007.
[175] T. Williams and S. Tanygin, "Propulsion System Sizing for Orbital Inspection Vehicles," *Journal of Guidance, Control, and Dynamics*, vol. 22, no. 2, pp. 375–378, 1999.
[176] D. A. Vallado and W. D. McClain, *Fundamentals of astrodynamics and applications,* 3rd ed. Hawthorne CA: Microcosm Press, 2007.
[177] T. Gutmann, *Manöveroptimierung im Relativsystem zweier Satelliten*, unpublished Bachelor's Thesis, Lehrstuhl für Raumfahrttechnik, Technische Universität München, Munich, 2009.
[178] C. Schiff and J. Bristow, "Formation Flying in Elliptical Orbits," *2000 IEEE Aerospace Conference*, pp. 37–47, 2000.
[179] R. A. Broucke, "Solution of the Elliptic Rendezvous Problem with the Time as Independent Variable," *Journal of Guidance, Control, and Dynamics*, vol. 26, no. 4, pp. 615–621, 2003.
[180] Y. Ichimura and A. Ichikawa, "Optimal Impulsive Relative Orbit Transfer Along a Circular Orbit," *Journal of Guidance, Control, and Dynamics*, vol. 31, no. 4, pp. 1014–1027, 2008.

[181] J. C. van der Ha, "Analytical Formulation for Finite-Thrust Rendezvous Trajectories," *39th Congress of the International Astronautical Federation*, pp. 1–17, 1988.
[182] A. Ellery, *An introduction to space robotics*. London ;, New york, Chichester: Springer; Praxis Pub, 2000.
[183] R. W. Longman, "Tutorial Overview of the Dynamics and Control of Satellite-Mounted Robots," in *Teleoperation and robotics in space*, S. B. Skaar and C. F. Ruoff, Eds, Washington, DC: American Institute of Aeronautics and Astronautics, Inc, 1994, pp. 237–258.
[184] M. Oda and Y. Ohkami, "Coordinated Control of Spacecraft Attitude and Space Manipulators," *Control Engineering Practice*, vol. 5, no. 1, pp. 11–21, 1997.
[185] J. R. Wertz, *Spacecraft attitude determination and control*. Dordrecht ;, Boston: Kluwer Academic Publishers, 1994, c1978.
[186] G. P. Beasley and J. E. Pennington, *Range Estimation of Familiar Targets Presented Against a Black Background*, NASA Langley Research Center, Hampton, Virginia, NASA Technical Note NASA TN D-2845, October 1965.
[187] R. F. Haines, *Space Vehicle Approach Velocity Judgments Under Simulated Visual Space Conditions*, NASA Ames Research Center, Moffett Field, California, NASA Technical Memorandum NASA-TM-89437, 1987.
[188] R. F. Brissenden, *A Study of Human Pilot's Ability to Detect Angular Motion with Application to Control of Space Rendezvous*, NASA Langley Research Center, Hampton, Virginia, NASA Technical Note NASA TN D-1498, December 1962.
[189] L. G. Summers, R. A. Shea, and K. Ziedman, "Unaided Visual Detection of Target Satellites," *Journal of Spacecraft and Rockets*, vol. 3, no. 1, pp. 76–79, 1966.
[190] M. Abraham, P. Jasiobedzki, and M. Umasuthan, "Robust 3D Vision for Autonomous Space Robotic Operations," *Proceeding of the 6th International Symposium on Artificial Intelligence and Robotics & Automation in Space: i-SAIRAS 2001*, 2001.
[191] K. Krishen, "Robotic Vision Technology and Algorithms for Space Applications," *Acta Astronautica*, vol. 19, no. 10, pp. 813–826, 1989.
[192] NASA, *NASA Images.* Available: http://nasaimages.org.
[193] M. M. Finckenor and D. Dooling, *Multilayer Insulation Material Guidelines*, NASA Marshall Space Flight Center, Huntsville, Alabama 35812, NASA Technical Publication NASA/TP-1999-209263, April 1999.
[194] NASA, *Cassini KSC Electronic Photo File.* Available: http://science.ksc.nasa.gov/payload/missions/cassini/images/images.html (2011, Dec. 02).
[195] JAXA, *Kibo Handbook*, JAXA Human Space Systems and Utilization Program Group, September 2007.
[196] W. Fehse, *Automated rendezvous and docking of spacecraft*. Cambridge: Cambridge University Press, 2003.
[197] M. E. Polites, *An Assessment of the Technology of Automated Rendezvous and Capture in Space*, NASA/TP-1998-208528, NASA Marshall Space Flight Center, Huntsville, Alabama 35812, July 1998.
[198] P. H. Whipple, *Some Characteristics of Coelliptic Orbits*, NASA-CR-109655, Bellcomm, Inc, Washington, DC 20024, 1970.
[199] D. C. Woffinden, M. B. Rose, and D. K. Geller, "Trigger Angle Targeting for Orbital Rendezvous," *Journal of the Astronautical Sciences*, vol. 56, no. 4, 2008.
[200] J. A. Chamberlin, "Gemini Rendezvous Program," *Journal of Spacecraft and Rockets*, vol. 1, no. 1, January 1964.
[201] K. A. Young and J. D. Alexander, "Apollo Lunar Rendezvous," *Journal of Spacecraft and Rockets*, vol. 7, no. 9, pp. 1083–1086, September 1970.
[202] D. C. Woffinden and D. K. Geller, "Navigating the Road to Autonomous Orbital Rendezvous," *Journal of Spacecraft and Rockets*, vol. 44, no. 4, pp. 898–909, July-August 2007.

[203] H. B. Hablani, M. L. Tapper, and D. J. Dana-Bashian, "Guidance and Relative Navigation for Autonomous Rendezvous in a Circular Orbit," *Journal of Guidance, Control, and Dynamics*, vol. 25, no. 3, pp. 553–562, 2002.
[204] H. Nagamatsu, T. Kubota, and I. Nakatani, "Capture Strategy for Retrieval of a Tumbling Satellite by a Space Robotic Manipulator," *IEEE International Conference on Robotics and Automation*, pp. 70–75, April 1996.
[205] P. Bond, *Jane's space recognition guide*. London: Collins, 2008.
[206] S. Stamm and P. Motaghedi, "Orbital Express Capture System: concept to reality," *Proceedings of SPIE*, no. 5419, pp. 78–91, 2994.
[207] S. Kawamoto, K. Matsumoto, and S. Wakabayashi, "Ground Experiment of Mechnical Impulse Method for Uncontrollable Satellite Capturing," *Proceeding of the 6th International Symposium on Artificial Intelligence and Robotics & Automation in Space: i-SAIRAS 2001*, pp. 1–8, June 2001.
[208] J. Ringelberg, "In-Space Assembly of the Exploration Architecture," *AIAA Space 2006 Conference*, 2006.
[209] S. Hollander, "Autonomous Space Robotics: Enabling Technologies for Advanced Space Platforms," *AIAA Space 2000 Conference & Exposition*, pp. 1–14, Sep. 2000.
[210] I. Rekleitis, E. Martin, G. Rouleau, R. L'Archevêque, K. Parsa, and E. Dupuis, "Autonomous Capture of a Tumbling Satellite," *Journal of Field Robotics*, vol. 24, no. 4, pp. 275–296, 2007.
[211] J. Ringelberg, "Docking Assembly Techniques and Challenges," *AIAA Space 2007 Conference*, 2007.
[212] S. Christiansen and T. Nilson, "Docking System Mechanism Utilized on Orbital Express Program," *39th Aerospace Mechanisms Symposium*, pp. 207–220, May 2008.
[213] Cislaghi M. and C. Santini, "The Russian Docking System and the Automated Transfer Vehicle: a safe integrated concept," *3rd IAASS Conference "Building a safer space together"*, October 2008.
[214] K. K. Timmons and J. Ringelberg, "Approach and Capture for Autonomous Rendezvous and Docking," *2008 IEEE Aerospace Conference*, March 2008.
[215] P. Jasiobedzki, S. Se, T. Pan, M. Umasuthan, and M. Greenspan, "Autonomous Satellite Rendezvous and Docking Using LIDAR and Model Based Vision," *Proceedings of SPIE*, vol. 5798, pp. 54–65, 2005.
[216] D. S. Portree, *Mir Hardware Heritage*, Johnson Space Center, Houston, TX, NASA Reference Publication NASA RP 1357, March 1995.
[217] J. M. Kelsey, J. Byrne, M. Cosgrove, S. Seereeram, and R. K. Mehra, "Vision-Based Relative Pose Estimation for Autonomous Rendezvous and Docking," *2006 IEEE Aerospace Conference*, pp. 1–20, 2006.
[218] T. Kasai, M. Oda, and T. Suzuki, "Results of the ETS-7 Mission - Rendezvous Docking and Space Robotics Experiments," *Proceedings of 5th International Symposium on Artificial Intelligence, Robotics and Automation in Space*, pp. 299–306, June 1999.
[219] P. Jasiobedzki, M. Greenspan, and G. Roth, "Pose Determination and Tracking for Autonomous Satellite Capture," *Proceeding of the 6th International Symposium on Artificial Intelligence and Robotics & Automation in Space: i-SAIRAS 2001*, pp. 1–8, June 2001.
[220] J. D. Mitchell, S. P. Cryan, D. Strack, L. L. Brewster, M. J. Williamson, R. T. Howard, and A. S. Johnston, "Automated Rendezvous and Docking Sensor Testing at the Flight Robotics Laboratory," *2007 IEEE Aerospace Conference*, March 2007.
[221] A. Ulitsky and D. King, "Enabling the Future: Lidar Space Vision Systems for Next Generation On-Orbit Servicing," *1st bilateral DLR-CSA Workshop on On-Orbit Servicing of Space Infrastructure Elements via Automation & Robotics Technologies*, pp. 1–6, November 2002.

[222] S.-C. Wu and Y. E. Bar-Sever, "Real-Time Sub-cm Differential Orbit Determination of Two Low-Earth Orbiters with GPS Bias Fixing," *ION GNSS 19th International Technical Meeting of the Satellite Division*, pp. 2515–2522, September 2006.
[223] W. Ley, *Handbuch der Raumfahrttechnik,* 3rd ed. München: Hanser, 2008.
[224] D. Pinard, S. Reynaud, P. Delaux, and S. E. Strandmoe, "Accurate and Autonomous Navigation for the ATV," *European Conference for Aerospace Sciences (EUCASS)*, pp. 1–7, 2005.
[225] J. R. Wertz and R. Bell, "Autonomous Rendezvous and Docking Technologies - Status and Prospects," *Proceedings of the Space Systems Technology and Operations Conference*, pp. 1–11, 2003.
[226] D. J. Pearson, "The glideslope approach," in *Orbital mechanics and mission design; Proceedings of the AAS/NASA International Symposium, Greenbelt, MD, Apr. 24-27, 1989 (A90-43486 19-13). San Diego, CA, Univelt, Inc, 1989, p. 109-123*, 1989, pp. 109–123.
[227] Real-Time Innovations, *RTI Data Distribution Service.* Available: http://www.rti.com/products/dds/.
[228] J. C. Lane, C. R. Carignan, and D. L. Akin, "Reconfigurable Control Station Design for Robotic Operations," *IEEE International Conference on Systems, Man and Cybernetics*, pp. 3722–3727, 1997.
[229] W. Bluethmann, R. Ambrose, M. Diftler, S. Askew, E. Huber, M. Goza, F. Rehnmark, C. Lovchik, and D. Magruder, "Robonaut: A Robot Designed to Work with Humans in Space," *Autonomous Robots*, vol. 14, pp. 179–197, 2003.
[230] M. Schweiger, "Spacecraft Simulation and Visualisation with Orbiter 2006," *3rd International Workshop on Astrodynamics Tools and Techniques*, 2006.
[231] M. Schweiger, *Orbiter Space Flight Simulator.* Available: http://www.orbitersim.com (2011, Dec. 16).
[232] J. C. Costa, *Design und Konstruktion eines 6-DOF Docking-Simulators*, unpublished student thesis (Semesterarbeit), Lehrstuhl für Raumfahrttechnik, Technische Universität München, Munich, 2010.
[233] C. L. Kössl, *Design und Aufbau der Steuerung eines 6-DOF Dockingsimulators*, unpublished student thesis (Semesterarbeit), Lehrstuhl für Raumfahrttechnik, Technische Universität München, Munich, 2010.
[234] J. L. Schwartz, M. A. Peck, and C. D. Hall, "Historical Review of Spacecraft Simulators," *Journal of Guidance, Control, and Dynamics*, vol. 26, no. 4, pp. 513–532, July-August 2003.
[235] Point Grey Research Inc, *Bumblebee Stereo Vision Camera Systems.* Available: http://www.ptgrey.com/products/bumblebee2/bumblebee2_xb3_datasheet.pdf (2012, Jun. 05).
[236] K. Peters, *Aufbau und Durchführung von Tests zum Einsatz von Laserentfernungsmessern im Weltraum*, unpublished student thesis (Semesterarbeit), Lehrstuhl für Raumfahrttechnik, Technische Universität München, Munich, 2011.
[237] M. Pfeiffer, J. Harder, and U. Walter, "Development of a compact Ka Band Antenna Pointing Mechanism for Intersatellite Links on Small Satellites," *13th European Space Mechanisms and Tribology Symposium*, 2009.
[238] M. Pfeiffer, R. Purschke, and J. Harder, "Design, construction and testing of a 2 degree of freedom Ka-band antenna pointing mechanism," *International Astronautical Congress*, vol. 2009.
[239] J. Harder, E. Stoll, M. Schiffner, M. Pfeiffer, and U. Walter, "A compact, light-weight high data-rate antenna system for remote-sensing orbiters and space exploration," *Acta Astronautica*, vol. 65, no. 11-12, pp. 1738–1744, 2009.
[240] C. Hochfellner, *Experimentelle Untersuchung des Nutzens von Lasergitterprojektion für teleprä-sentes Rendezvous und Docking*, unpublished Bachelor's Thesis, Lehrstuhl für Raumfahrttechnik, Technische Universität München, München, 2012.

[241] K. Song, *A Remote Control and Monitoring System for a 2DOF Pointing Mechanism*, unpublished Master's Thesis, Lehrstuhl für Raumfahrttechnik, Technische Universität München, Munich, 2010.
[242] E. Lindenthal, *Aufbau einer omnidirektional steuerbaren Roboterplattform*, unpublished student thesis (Semesterarbeit), Lehrstuhl für Raumfahrttechnik, Technische Universität München, Munich, 2011.
[243] D. Sekimori and F. Miyazaki, "Precise Dead-Reckoning for Mobile Robots using Multiple Optical Mouse Sensors," *Informatics in Control, Automation and Robotics II*, pp. 145–151, 2007.
[244] E. Stoll, U. Walter, J. Artigas, C. Preusche, P. Kremer, G. Hirzinger, J. Letschnik, and H. Pongrac, "Ground verification of the feasibility of telepresent on-orbit servicing," *J. Field Robotics*, vol. 26, no. 3, pp. 287–307, 2009.
[245] J. Harder and U. Walter, "Communication Architecture Evaluation for Real-Time Tele-Operated Spacecrafts," *2012 IEEE Aerospace Conference*, 2012.
[246] M. Wilde, J.-P. Hamacher, and U. Walter, "Experimental Head-Up Displays for Space Telerobotics," *Proceedings of the International Symposium on Artificial Intelligence, Robotics and Automation in Space (iSAIRAS 2010)*, August 2010.
[247] M. Wilde, S. C. Hannon, and U. Walter, "Evaluation of Head-Up Displays for Teleoperated Rendezvous & Docking," *2012 IEEE Aerospace Conference*, 2012.
[248] M. Wilde and U. Walter, "Operator Assistance for Telepresent On-Orbit Servicing," *Proceedings of the 14th IASTED International Conference Robotics and Applications (RA 2009)*, 2009.
[249] P. M. Ververs and C. D. Wickens, "Head-Up Displays: Effects of Clutter, Display Intensity, and Display Location on Pilot Performance," *The International Journal of Aviation Psychology*, vol. 8, no. 4, pp. 377–403, 1998.
[250] R. L. Newman, *Head-up displays: Designing the way ahead*. Aldershot, Hants, England, Brookfield, Vt: Avebury Aviation; Ashgate Pub. Co, 1995.
[251] M. Jukes, *Aircraft display systems*. Reston Va: American Institute of Aeronautics and Astronautics, 2004.
[252] E. Fischer, R. F. Haines, and T. A. Price, *Cognitive Issues in Head-Up Displays*, NASA Scientific and Technical Information Branch, NASA Technical Paper NASA-TP-1711, 1980.
[253] F. H. Previc and W. R. Ercoline, "The "Outside-In" Attitude Display Concept Revisited," *The International Journal of Aviation Psychology*, vol. 9, no. 4, pp. 377–401, http://www.informaworld.com/10.1207/s15327108ijap0904_5, 1999.
[254] J.-P. Hamacher, *Experimental Head-Up Display for Space Telerobotics*, unpublished student thesis (Semesterarbeit), Lehrstuhl für Raumfahrttechnik, Technische Universität München, Munich, 2010.
[255] J. Hartung, B. Elpelt, and K.-H. Klösener, *Statistik: Lehr- und Handbuch der angewandten Statistik ; mit zahlreichen, vollständig durchgerechneten Beispielen,* 9th ed. München [u.a.]: Oldenbourg, 1993.
[256] S. M. Ross, *Statistik für Ingenieure und Naturwissenschaftler,* 3rd ed. München: Elsevier Spektrum Akad. Verl, 2006.
[257] M. Wilde and U. Walter, "A Robotic Camera Arm for Increased Situational Awareness in Telepresent On-Orbit Servicing," *2010 IEEE Aerospace Conference*, March 2010.
[258] D. Hershberger, R. Burridge, D. Kortenkamp, and R. Simmons, "Distributed Visual Servoing with a Roving Eye," *Proceedings of the 2000 IEEE/RSJ International Conference on Intelligent Robots and Systems*, pp. 441–447, 2000.
[259] H. Goldberg, J. Mueller, and L. Alkalai, "Micro-Inspector Spacecraft: An Overview," *20th Annual AIAA/USU Conference on Small Satellites*, 2006.
[260] T. G. Nunez Ramirez, *Design of a Free-Flying Sensor Platform for Support of Telepresent On-Orbit Servicing*, unpublished Master's Thesis, Lehrstuhl für Raumfahrttechnik, Technische Universität München, Munich, 2009.

[261] R. D. Ballard, *The JASON Remotely Operated Vehicle System*, Woods Hole Oceanographic Institution, Woods Hole, Massachusetts, Woods Hole Oceanographic Institution Technical Report WHOI-93-34, February 1993.
[262] L. Friedmann, *Implementierung einer kabellosen Steuerung für einen Kameraarm zur Unterstützung telepräsenter Arbeiten im Weltraum*, unpublished student thesis (Semesterarbeit), Lehrstuhl für Raumfahrttechnik, Technische Universität München, Munich, 2009.
[263] D. Nedyalkov, *Design und Konstruktion eines Kameraarmes zur Unterstützung telepräsenten On-Orbit Servicings*, unpublished student thesis (Semesterarbeit), Lehrstuhl für Raumfahrttechnik, Technische Universität München, München, 2009.
[264] T. Meschede, *Zielverfolgung für einen robotischen Kameraarm*, unpublished student thesis (Diplomarbeit), Lehrstuhl für Raumfahrttechnik, Technische Universität München, Munich, 2010.
[265] M. Wilde, L. Friedmann, and U. Walter, "Intuitive One-Hand Controls for Robotic Camera Arms," *Proceedings of the 14th IASTED International Conference Robotics and Applications (RA 2009)*, 2009.
[266] M. W. Spong, *Robot Dynamics and Control*, University of Illinois at Urbana-Champaign, Lecture Notes in Computer Science, 2007.
[267] J. J. Craig, *Introduction to robotics: Mechanics and control,* 3rd ed. Upper Saddle River, N.J: Pearson/Prentice Hall, 2005.
[268] S. G. Hart, "NASA-Task Load Index (NASA-TLX): 20 Years Later," *Human Factors and Ergonomics Society Annual Meeting Proceedings*, vol. 50, no. 9, pp. 904–908, 2006.
[269] S. G. Hart and L. E. Staveland, "Development of NASA-TLX (Task Load Index): Results of Empirical and Theoretical Research," in *Human Mental Workload*, P. A. Hancock and N. Meshkati, Eds, Amsterdam: North Holland Press, 1988, pp. 239–250.
[270] N. A. Stanton, *Human factors methods: A practical guide for engineering and design*. Aldershot [u.a.]: Ashgate, 2006.
[271] M. R. Endsley and D. J. Garland, *Situation awareness: Analysis and measurement*. Mahwah, NJ: Lawrence Erlbaum Associates, 2000.
[272] M. R. Endsley, S. J. Selcon, T. D. Hardiman, and D. G. Croft, "A Comparative Analysis of SAGAT and SART for Evaluations of Situation Awareness," *42nd Annual Meeting of the Human Factors & Ergnomics Society*, pp. 1–5, 1998.
[273] R. M. Taylor, "Situational Awareness Rating Technique (SART): The Development of a Tool for Aircrew Systems Design," *AGARD Conference Proceedings No. 478*, pp. 5.1 - 5.8, 1990.
[274] L. Sachs, *Angewandte Statistik: Anwendung statistischer Methoden ; mit 317 Tabellen und 98 Übersichten,* 9th ed. Berlin [u.a.]: Springer, 1999.
[275] E. Cheung and V. J. Lumelsky, "Proximity Sensing in Robot Manipulator Motion Planning: System and Implementation Issues," *IEEE Transactions on Robotics and Automation*, vol. 5, no. 6, pp. 740–751, December 1989.
[276] H. Seraji, R. Steele, and R. Ivlev, "Experiments in Sensor-Based Collision Avoidance," *IEEE Transactions on Robotics and Automation*, 1995.
[277] O. Khatib, "Real-Time Obstacle Avoidance for Manipulators and Mobile Robots," *The International Journal of Robotics Research*, vol. 5, no. 1, pp. 90–98, 1986.
[278] B. Bon and H. Seraji, "On-Line Collision Avoidance for the Ranger Telerobotic Flight Experiment," *Proceedings of the 1996 IEEE International Conference on Robotics and Automation*, pp. 2041–2048, April 1996.
[279] K. A. Bloom and G. E. Campbell, "The Apollo Docking System," *Fifth Aerospace Mechanisms Symposium*, pp. 3–8, June 1970.
[280] T. LaBauve, *Low Impact Docking System (LIDS)*, NASA Johnson Space Center, JSC Biennial Research and Technology Development JSC-17710, February 2009.

[281] NASA, *Hubble Space Telescope Servicing Mission 4: The Soft Capture and Rendezvous System*, NASA Goddard Spaceflight Center, NASA Facts FS-2007-08-088-GSFC, 2007.
[282] R. M. Foster, J. G. Cook, P. R. Smudde, and M. A. Henry, "Space Station Berthing Mechanisms, Attaching Large Structures On-Orbit that were Never Mated on the Ground," *Proceedings of the 37th Aerospace Mechanisms Symposium*, May 2004.
[283] R. Stettner, H. Bailey, and R. Richmond, "Eye-safe laser radar 3-D imaging," *RTO SCI Symposium on Sensors and Sensor Denial by Camouflage, Concealment and Deception*, April 2004.
[284] S. Ruel and T. Luu, "STS-128 On-Orbit Demonstration of the TriDAR Targetless Rendezvous and Docking Sensor," *2010 IEEE Aerospace Conference*, pp. 1–7, March 2010.

E Supervised Student Theses

During the research for this doctoral thesis a number of student research theses were prepared at the Institute of Astronautics (LRT) under the author's supervision in the years 2008 – 2012. The author advised the students substantially in regards to scientific, technical and content matters. The student theses contributed concept studies, as well as hardware and software implementations to the research program, which have partially been included in this doctoral thesis. The following table lists the student theses contributing to this doctoral thesis, including the sections, tables, figures and equations into which their results were incorporated.

The author thanks all students for their efforts in supporting his doctoral research.

Student	Student Thesis
Costa, Joao C.	"Design und Konstruktion eines 6-DOF Docking-Simulators", Semesterarbeit, submitted July 2010, included in Section 5.2.2
Friedmann, Ludwig	"Implementierung einer kabellosen Steuerung für einen Kameraarm zur Unterstützung telepräsenter Arbeiten im Weltraum", Semesterarbeit, submitted April 2009, included in Section 7.3.2, Figure 7-6
Gutmann, Tobias	"Manöveroptimierung im Relativsystem zweier Satelliten", Bachelor's Thesis, submitted September 2009, included in Section 3.3
Hamacher, Jan-Philipp	"Experimental Head-Up Display for Space Telerobotics", Semesterarbeit, submitted August 2010, included in Sections 6.3.2 and 6.3.3, Table 6-1, Table 6-2, Eq. 6-1 to Eq. 6-19
Hochfellner, Clemens	"Experimentelle Untersuchung des Nutzens von Lasergitterprojektion für telepräsentes Rendezvous und Docking", Bachelor's Thesis, submitted February 2012, included in Section 5.2.3
Huberth, Stefan	"Untersuchung von technischen Möglichkeiten zum De-Orbiting von Space Debris Objekten", Diplomarbeit, submitted April 2010, included in Section 1.2.6
Kössl, Christoph L.	"Design und Aufbau der Steuerung eines 6-DOF Dockingsimulators", Semesterarbeit, submitted February 2010, included in Section 5.2.2
Lindenthal, Erik	"Aufbau einer omnidirektional steuerbaren Roboterplattform", Semesterarbeit, submitted November 2011, included in Section 5.2.3
Meschede, Thomas	"Zielverfolgung für einen robotischen Kameraarm", Diplomarbeit, submitted July 2010, included in Section 7.3.3, Table 7-1, Eq. 7-6 to Eq. 7-10
Nedyalkov, Danail	"Design und Konstruktion eines Kameraarmes zur Unterstützung telepräsenten On-Orbit Servicings", Semesterarbeit, submitted August 2009, included in Section 7.3.1
Nunez Ramirez, Tonatiuh G.	"Design of a Free-Flying Sensor Platform for Support of Telepresent On-Orbit Servicing", Master's Thesis, submitted December 2009, included in Section 7.3
Peters, Konrad	"Aufbau und Durchführung von Tests zum Einsatz von Laserentfernungsmessern im Weltraum", Semesterarbeit, submitted January 2011, included in Section 5.2.3

Riedel, Felix	"Entwicklung einer Systemarchitektur zur Entfernung von Space Debris Objekten", Diplom-arbeit, submitted December 2009, included in Section 1.2.6
Song, Kaijun	"A Remote Control and Monitoring System for a 2DOF Pointing Mechanism", Master's Thesis, submitted August 2010, included in Section 5.2.3.